MANIFESTATIONS OF THE MULLINS EFFECT IN FILLED ELASTOMERS

Vanessa Auxiliadora Fernandes Arruebarrena

MSc, BEng

Thesis submitted to the University of Nottingham for the degree of Doctor of Philosophy

July 2016

Abstract

This work employs five commercial carbon-black filled elastomers made from ethylene-propylene-diene, nitrile, butyl and natural rubber compounds to study different manifestations of the stress-softening phenomenon known as the Mullins effect. The structure of the materials was characterised using density, hardness, thermal analysis and microscopy.

Cyclic tensile deformations under uniaxial, constant-width and equibiaxial models were used to study the mechanical response following different strain histories. The mechanical response and the energies stored and dissipated were both dependent on the strain history. Elastomers with no strain history exhibited a relatively constant dissipated energy fraction, which reduced to a lower constant fraction when the historical maximum strain was higher than the current maximum strain. A physically based modelling approach with a simple representation of the evolution of bound rubber was proposed to account for this. The approach was able to qualitatively reproduce the energy maps observed in the experimental data.

A set of time-dependent test protocols were developed in both uniaxial and biaxial modes of deformation to investigate the effect of strain history on stress-relaxation and stress-memory following cyclic loading. All filled rubbers relaxed an approximately constant fraction of the stress after a given time when the applied strain during stress relaxation was smaller than the historical maximum. Under these circumstances the relaxed fraction was independent of both the strain history and the current strain, with important implications for scragging. An empirical function involving just five parameters was proposed to predict the fraction of unrelaxed stress for an arbitrary strain history. Stress memory was observed following unloading, with a recovered stress magnitude approximately independent of history.

Anisotropy was investigated through linear dimensional swelling measurements. A degree of anisotropy was observed specific to the manufacturing process: compression moulding led to transverse isotropy, while sheet-rolling led to full anisotropy. Following a strain history, the anisotropy was shown to evolve further.

Publications

This work has been published in the following journals and conferences

* V.A. Fernandes & D.S.A. De Focatiis, 'The role of deformation history on stress relaxation and stress memory of filled rubber', *Polymer Testing,* vol. 40, pp. 124-132, 2014.

* V.A. Fernandes, M. Durant & D.S.A. De Focatiis, 'Influence of deformation history on energy storage and dissipation in filled elastomers'. Manuscript in preparation to be submitted in the peer reviewed Journal Polymer Engineering and Science.

* V.A. Fernandes & D.S.A. De Focatiis, 'A swelling study of process-induced and deformation-induced anisotropy of filled rubbers'. Manuscript in preparation to be submitted in the peer reviewed Journal Rubber Chemistry and Technology.

Conference proceedings

* V.A. Fernandes & D.S.A. De Focatiis, 'Mechanical deformation of elastomers: a comparison between cyclic energy dissipation and stress relaxation following complex strain histories'.16th International Conference on Deformation, Yield and Fracture of Polymers, Kerkrade, 2015.

* V.A. Fernandes & D.S.A. De Focatiis, 'A swelling study of process-induced and deformation-induced anisotropy of filled rubbers'. Proceedings of European Conference on Constitutive Models for Rubber, Prague, 2015.

Oral conference presentations

* European Conference on Constitutive Models for Rubber, Prague, 2015. *A swelling study of process-induced and deformation-induced anisotropy of filled rubbers.*

* RubberCon: Advance Engineering and Materials Developments, Manchester, 2014. '*Stress relaxation, stress recovery and stress memory in filled EPDM rubber'.*

* Institute of Materials, Minerals and Mining, Young Member Conference, Loughborough University, 2014. '*The influence of deformation history on viscoelasticity of filled rubber'.*

Poster presentations

* Institute of Materials, Minerals and Mining, Rubber in Engineering Group, London, 2012. '*The Mullins effect in EPDM subjected to complex strain histories'.*

* Engineering Postgraduate Research Event, The University of Nottingham, 2013. *'Predicting the unexpected: How deformation of rubber depends on its history'.*

* 16th International Conference on Deformation, Yield and Fracture of Polymers, Kerkrade, 2015. *'Mechanical deformation of elastomers: a comparison between cyclic energy dissipation and stress relaxation following complex strain histories'.*

Acknowledgements

This project would never have been possible without the support provided by the Dean of Engineering Scholarship for International Students of The University of Nottingham.

I would like to express my deepest gratitude to my supervisor Dr Davide De Focatiis, for his excellent guidance and patience, but especially for trusting in me. I appreciate his enthusiasm to share his knowledge; he was always there to encourage me to get the best of me during this project. It has been a pleasure to work with him. Special thanks also to Prof Nicholas Warrior, for his support during my research.

Special mention to The East Midlands Materials Society, The Institute of Materials, Minerals and Mining and The Institute of Mechanical Engineers for the funding provided to attend conferences and support during my project.

I would like to thank the p.lab group: Gabriel, Olga, Magda, Mike, Andrea, David and Sam. I had the opportunity to see this group grow and I am proud to be part of such a friendly and supportive group. I would like to thank my colleagues and friends in the Polymer Composites Group, to Frank, Mikhail, Gabriel and Oliver for their advice and support, as well as for the lunch breaks. Special thanks to Gabriel and Frank for proofreading.

I wish to thank Tristan for his help on my grammar, and especially, for always being there for me in the most stressful moments. Thanks to my closest friends, that even at a distance, are ready to help and cheer when needed.

Finally, I wish to thank my family, my brothers Joao and Johann, who always believed in my geekiness, and are always there to put a smile on my face, even from a distance. To Luis, who cares about me like a father. A special mention to my father, who is dearly missed but will always be an example to follow. And most of all, thank to my mother, my hero and source of inspiration and energy. I dedicate this work to her.

'A man without education is an incomplete being'
'Un ser sin estudios, es un ser incompleto'

Simón Bolívar

Contents

Abbreviations

Abbr.	Description
BS	British Standard
CR	Chloroprene
CW	Constant width tensile deformation
DCPD	Dicyclopentadiene
DIC	Digital image correlation
DSC	Differential scanning calorimetry
EB	Equibiaxial tensile deformation
ENB	Ethylidene norbornene
EPDM1a	Ethylene propylene diene terpolymer DIK (First Batch)
EPDM1b	Ethylene propylene diene terpolymer DIK (Second Batch)
EPDM2	Ethylene propylene diene terpolymer J-Flex
FBFT	Flexible biaxial film tester
IRHD	International Rubber Hardness Degrees
MPR	Melt processable rubbers
NBR	Nitrile butadiene rubber
NR	Natural rubber
PB	Polybutadiene
PET	Polyethylene terephthalate
PVC	Polyvinyl chloride
SBR	Styrene butadiene rubber
SEM	Scanning electron microscopy
TGA	Thermogravimetry analysis
TP1	Test protocol one for tensile testing stress relaxation
TP2	Test protocol two for tensile testing stress relaxation
TP3	Test protocol three for tensile testing stress relaxation
TP4	Test protocol four for tensile testing stress relaxation
TPV	Thermoplastic vulcanised
TPE's	Thermoplastic elastomers
TPU's	Thermoplastic polyurethanes
UN	Uniaxial tensile deformation

Symbols

Symbol	Description
A	Parameter of the evolution of the fraction of unrelaxed stress with no-history
B	Parameter of the slope transition of the predicted fraction of unrelaxed stress
C	Parameter of shift point evolution of the predicted fraction of unrelaxed stress
c	Parameter of material evolution capacity in hard phase reduction (Chapter 4)
f	Flory-equation functionality of the cross-link segments
$\mathrm{d}H/\mathrm{d}T$	Heat flow derivative
$\mathrm{d}W/\mathrm{d}t$	Derivative of weight loss during time
m_i	Initial weight of specimen before swelling stage
m_s	Weight during swelling stage at T_s
m_d	Weight after swelling stage at T_d
n	Number of polymer chains
n_b	The freely oriented units along a segment of the chain between crosslink points
p	Vapour pressure
p_o	Saturation vapour pressure
t_v	Vulcanisation time
t_0	Stress relaxation start time
x	Flory's number of segments on the polymeric molecules chains
v	Density of chains in the network
A_A	Cross-sectional area of soft phase A on coupling model
A_B	Cross-sectional area of soft phase B on coupling model
A_C	Cross-sectional area of hard phase C on coupling model
A_t	Total cross-sectional area on coupling model
C_∞	Characteristic ratio (the end-to-end distance and freely oriented chain)
$E_{100\%}$	Elastic Modulus at 100% deformation
E_c	Elastic Modulus of the solid-elastic hard phase C
F_A	Force applied in soft phase A in coupling model
F_B	Force applied in soft phase B in coupling model
F_C	Force applied in hard phase C in coupling model
G	Shear Modulus
G_{aff}	Shear Modulus through Affine Theory
G_{pha}	Shear Modulus through Phantom Theory
H	Shore A Hardness

Symbols

Symbol	Description
K^{B}	Boltzmann constant
K_{eff}	Effective spring constant-Phantom network mode
K	Spring constant in phantom model
L	Total length of coupling model system
L_0	Total initial length of coupling model system
L_A	Length of soft phase A on coupling model
L_{A0}	Initial length of soft phase A on coupling model
L_B	Length of soft phase B on coupling model
L_{B0}	Initial length of soft phase B on coupling model
L_C	Length of hard phase C on coupling model
L_{C0}	Initial length of hard phase C on coupling model
M_c	Average molecular weight between cross-link points
M_0	Molecular mass of the monomeric unit
R	Gas constant
T	Temperature
T_g	Glass transition temperature
T_s	Time for swelling equilibrium
T_d	Drying time after swelling stage
T_v	Vulcanisation temperature
V	Total volume polymer-solvent
V_0	Total volume of the polymer segment
V_1	Molar volume of solvent
V_2	Molar volume of polymer
W	Weight loss content during thermogravimetry analysis
W_i	Input energy density
W_o	Output energy density
$\tilde{W}_d$	average dissipated energy density per half-cycle
$\tilde{W}_e$	average elastic recoverable energy density per half-cycle
X	Number of C-C bonds in the monomeric unit
$X\varepsilon$	Tangential evolution function of the predicted fraction of unrelaxed stress

Greek Symbols

α	Flory parameter constant
δ_1	Solubility parameter of the solvent
δ_2	Solubility parameter of the polymer
ε_1	First stage maximum strain during cyclic deformation
ε_2	Second stage maximum strain during cyclic deformation
ε_f	Deformation at failure

Symbols

Symbol	Description
ε_{end}	Final strain at the start of the stress relaxation during loading
$\varepsilon_{\text{end}}^{*}$	Final strain at the start of the stress relaxation during unloading
ε_{max}	Single loading ramp maximum strain before stress relaxation
ε_{u}	Uniaxial tensile testing deformation
ε_{EB}	Equibiaxial tensile testing deformation
ε_{CW}	Constant width tensile testing deformation
ε_{per}	Permanent set after cyclic deformation
$\varepsilon_{\text{per}}^{100\%}$	Permanent set at 100% deformation under tensile testing
$\dot{\varepsilon}$	Strain rate
η	Volume fraction parameter of the hard phase on coupling model
θ_{b}	Angle between C-C bonds
θ_{br}	Fraction of bounded rubber for filled elastomers
$\lambda_{\text{i(i=1,2,3)}}$	Dimensional elongation
λ_{l}	Dimensional length ratio
λ_{w}	Dimensional width ratio
λ_{t}	Dimensional thickness ratio
λ_{A}	Stretch of soft phase A on coupling model
λ_{A}	Stretch of soft phase B on coupling model
λ_{C}	Stretch of hard phase C on coupling model
λ_{max}	Maximum length of extensibility of the polymeric chain
ξ	Cycle rank of density of chains Phanton Model (Chapter 2)
ξ	Hard phase fraction parameter (Chapter 3-4)
ξ_0	Hard phase initial fraction parameter (Chapter 4)
ρ_1	Density of the solvent
ρ_2	Density of the polymer
σ_{a1}	Stress on axis 1 under Equibiaxial and constant with tensile tests
σ_{a2}	Stress on axis 2 under Equibiaxial and constant with tensile tests
σ_{A}	Stress on soft phase A from coupling modelling approach
σ_{B}	Stress on soft phase B from coupling modelling approach
σ_{C}	Stress on hard phase C from coupling modelling approach
σ_{Af}	Stress on soft phase A with stress flow addition
σ_{Bf}	Stress on hard phase B with stress flow addition
σ_{end}	Stress at the beginning of the stress relaxation
σ_{f}	Stress to failure
σ_{fs}	Stress flow adjustment in coupling model approach
σ_{max}	Maximum stress during loading previous to stress relaxation
$\sigma_{\text{r,600}}$	Stress at the end of 600s of stress relaxation condition

Symbols

Symbol	Description
τ_c	Average time correlation
υ_1	Volumetric fraction of solvent
υ_2	Volumetric fraction of polymer
υ_c	Apparent cross-link density
ϕ	Average junction functionality
ϕ_c	Fraction of energy dissipated during a loading cycle
ϕ_r	Fraction of stress relaxed after 600s of relaxation
ϕ_s	Swelling ratio
$\phi_{oil/plast}^{TGA}$	Fraction of content of oil/plasticiser by thermogravimetry
ϕ_{CB}^{TGA}	Fraction of content of carbon black by thermogravimetry
ϕ_{G}^{TGA}	Fraction of content of graphite by thermogravimetry
ϕ_{inor}^{TGA}	Fraction of content of inorganic materials by thermogravimetry
φ_0	Fraction of unrelaxed stress of no history material modelling parameter
φ_0'	Initial fraction of unrelaxed stress of no history material modelling parameter
φ_{lim}	Constant fraction of unrelaxed stress when $\varepsilon < \varepsilon_{max}$
φ_{pred}	Predicted fraction of unrelaxed stress as a function of strain
φ_r	Experimental fraction of unrelaxed stress
χ	Flory-Huggins solvent-polymer interaction parameter
$\Delta A_{el,phatom}$	Total elastic energy of the affine model
$\Delta A_{el,phatom}$	Total elastic energy of the phantom model
ΔG	Gibbs free energy
ΔG_{el}	Energy of elasticity of the polymer chain
ΔG_m	Modification of Gibbs free energy by Flory
ΔG_{tot}	Flory's total energy on a swollen stage
ΔH	Gibbs enthalpy of dilution
ΔS	Gibbs entropy of dilution
$\mathbf{F}$	Deformation gradient
$\perp$	Orientation perpendicular to the rubber roll sheet
$//$	Orientation parallel to the rubber roll sheet

Chapter 1   **Introduction**

Elastomers are best known for their ability to undergo large elastic deformations, although there are many elastomeric applications whose performance is dictated by the magnitude of inelastic and viscoelastic effects. In addition, deformation history plays an important role in determining the mechanical response of elastomers, principally by the manifestation of the softening phenomenon called the Mullins effect. It is necessary then to remark the influence that deformation history can have not only in the stress-strain response, but also in the energy dissipated and recovered during the stretching process. Similarly, the viscoelastic behaviour when an elastomeric product is subjected to deformations can be altered by this history. The mechanisms by which the vulcanised network evolved, are still the topic of much research and debate, due to the several compositions and polymeric structures possible. However, to understand the way an elastomer will respond under changes of modes of deformation is vital to predict product performance and future failures. This work sets out experimental data in order to contribute to a better understanding of the influence of deformation history on the mechanical response of filled-elastomers.

1.1   The first steps of rubber

Even though natural rubber applications have been reported since the 1500s, it was only in 1839 that Charles Goodyear discovered the revolutionary engineering properties of vulcanised rubber through the addition of sulphur [1]. Shortly after the start of World War II, the first synthetic rubbers such as polyisoprene and polybutadiene were produced in large scales [2]. This new discovery filled the need for greater production of materials across a broader range of properties. These new materials exhibited mechanical characteristics comparable to those of natural rubber, but also had other

advantages such as chemical resistance and manufacture at lower cost compared with natural rubber [3]. Rubber has been employed in a wide range of products such as tyres, dampers, seals and gaskets, owing to its unique properties such as large elasticity, tear and abrasion resistance, and insulation capacity, among others.

The capacity to combine these properties, and modify them depending of the requirements, make elastomers an indispensable product in modern society. The use of rubber as an engineering material has seen steady growth over the past years. This led to the introduction of another category of elastomeric materials in the 1960s, thermoplastic elastomers, with properties similar to rubber but with the added capacity of being processed as thermoplastics [4].

1.2   Composition of elastomers

Elastomers consist of very long polymeric chains capable of rearranging themselves in different spatial configurations in response to a load [5]. Long polymeric chains have large numbers of available configurations and relatively free rotation about the bond joints. However, to prevent chains form permanently slipping, they must be joined together by permanent bonds called cross-links. Uncured or unvulcanised natural rubber, for example, has weak inter-chain interactions, which results in poor mechanical properties, with low elastic recovery [3]. In chemically cross-linked rubbers, permanent bonds between the chains are formed which create a network structure as represented in Figure 1. This creates the permanent network structure that determines physical properties such as tensile and compressive strength, elongation, as well as resilience and elasticity [1].
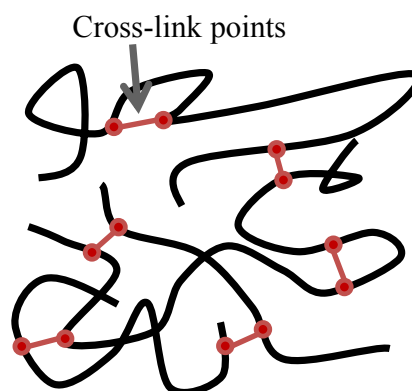
Figure 1. Diagram of a cross-linked network structure

The properties of an elastomer will therefore be controlled by the nature of its

crosslinked network, together with the composition and structure of the chains [5]. The formation of these bonds makes elastomers resistant to temperatures, and gives them the possibility to maintain their properties over a wide range of deformations. The possibility of very large, recoverable deformations without failure is the distinguishing property of elastomers. Due to the cross-links, the material is able to deform elastically under loading, while maintaining most of the original topology. After the load is removed, the drive for the material to increase its entropy directs the material to recover its original shape. This corresponds to the preferred configuration of the chains, i.e. the most disordered state [6].

The properties of rubber can be improved by the use of reinforcement fillers. The incorporation of fillers such as carbon black and silica is carried out to improve tear strength, hardness, abrasion resistance and tensile properties. In addition, these fillers can increase the energy loss (or hysteresis) of the elastomers, reduce the degradation caused by ultraviolet radiation and ozone, and decrease the liquid absorption of the material [3, 7]. Although filled elastomers are widely used and their properties extensively investigated [8-10], the exact mechanism of filler-rubber interaction remains unresolved.

1.3   Engineering applications

Because of its flexibility, elasticity and impermeability, the use of rubber is widespread in the design of engineering products. Rubber products can be processed with similar methods used for plastic processing, which makes them desirable when selecting materials for the design of commodity products. Depending on the specific performance and life cycle, a wide range of elastomers and compositions can be chosen [11]. One of the most significant applications is vehicle tyres, a product highly specialized in terms of engineering requirements. The selection of the specific elastomer needed for each part of the tyre is important to achieve specific functionality as a consequence of different requirements on each section [11].

Many other engineering products such as seals, dampers, diaphragms and gaskets are designed from filled elastomers, due to the ability to withstand loads without losing the original shape. Owing to their capacity to absorb energy, elastomers are employed as vibration-isolating materials, reducing the effects of vibrations and acting as dampers.

During service, these products are subjected to numerous strain histories and modes of deformation, including unexpected deformations during service. Regarding of this, the elastomers must keep their best performance and avoid failure.

Due to the insulating properties of many elastomers, they are the primary material in the design also of footwear and waterproof clothes. In the medical field, the flexibility and resistance to solvents is also making elastomers promising materials to manufacture long term implants.

1.4   The Mullins effect

During deformation of elastomeric products, a change in the mechanical behaviour occurs as a consequence of the deformation applied. This phenomenon was first observed in filled elastomers by Bouasse and Carrière in 1903 [12] and later investigated by Mullins and co-workers in the 1950s [13]. The phenomenon is now generally referred to as the Mullins Effect, and is defined as permanent or semi-permanent change in the response of the material after it is subjected to deformation. This leads to a difference in the mechanical response if it is unloaded and reloaded. As a consequence, a smaller amount of energy is required to generate the same deformation in any following loadings compared to the first loading. An idealized version of the Mullins effect in the stress-strain response is presented in Figure 2. During the first loading of the virgin material, the response follows path *A* until reaching point *a*. If unloading begins immediately, the material follows a different path *B*, due to changes in the network structure during the deformation. During subsequent smaller or equal loadings the stress-strain relation follows path *B* back up to point *a*. As viscoelastic effects in rubber materials are generally small, the reloading path is very similar to, but not identical to, the first unloading one. Ideal Mullins behaviour follows the same path *B* when loading and unloading. However, a real rubber will show a difference in the loading-unloading path due to viscoelasticity. If the strain of a subsequent loading step exceeds point *a*, the material will deform along path *A'*. The path *A-A'* represents the behaviour of a non-deformed material loaded all the way to point *b*. After loading the material to point *b* and releasing the stress, it unloads along a new path, *C*. Thus, in this simple example the stress-strain response (path *B* or *C*) is dependent on the load history (path *A* or *A'*) experienced by the material.
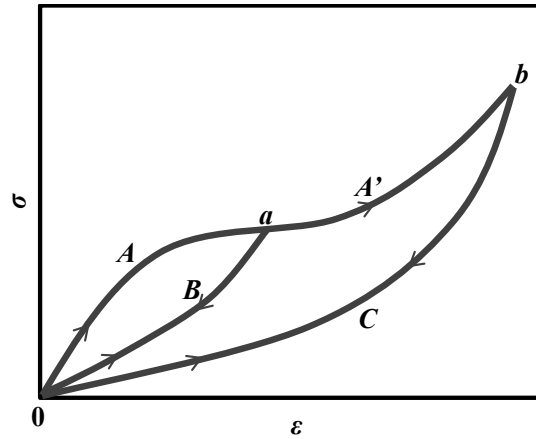
Figure 2. Diagram of stress, σ, response as function of strain, ε, showing an idealized Mullins effect under uniaxial tension.

The stress-softening phenomenon occurs after the first loading cycle. It can be thought of as a modification to the unloading-reloading path after loading path when looking at the stress-strain relation. After the first cycle, when subsequent loads are applied, the material responds in a similar way, as long as the deformation does not exceed the maximum previously reached in the first cycle. As a result of this, the material exhibits a softening effect that grows progressively with the increasing of deformation [14]. Figure 2 shows an idealised response, however, there are other effects present in the material associated to the viscoelasticity behaviour of the material such as residual strain and hysteresis.

Mullins et al. [13, 15] attributed this softening phenomenon to changes in two phases formed in the vulcanised chain network. They considered a filled elastomer as a two phase system, a soft region that allows deformation and a hard region that creates the resistance in the network. The soft region is formed mainly by the rubber matrix as the hard phase includes the filler together with rubber in direct contact with the filler. During deformation, the hard region can be broken down and incorporated into the soft region, reducing the resistance in the network. Therefore, as the fraction of the soft region increases, subsequent deformations up to the same value will require less stress.

Pre-conditioning to a specific strain, called *scragging*, is usually applied in industry, so that the service conditions will not exceed this strain [16]. This pre-conditioning avoids any changes in the constitutive response due to softening. However, under an unexpected event during service (e.g. a higher strain than the scragging strain), the deformation history can change, and hence so can the subsequent mechanical behaviour. A change in the mode of deformation applied could also lead to a modified response. If some of these events take place, the mechanical response will not be dictated by the

scragging process any more. Other properties such as hysteresis, anisotropy and the time dependent response may also be affected by deformation history. The consideration of these aspects during the design is vital to ensure the proper performance of the final product. Nevertheless, the combination of all these influences complicates the analysis of the mechanical response of filled elastomers; therefore many of them are usually neglected during rubber investigations. An improved understanding of these manifestations will allow an enhanced prediction of how an elastomer will behave under different circumstances.

1.5   Prediction of the mechanical response

Many different approaches can be found in the literature that attempt to predict the mechanical behaviour of filled elastomers under deformation, as reviewed by Diani et al. [14]. Starting from basic rubber elastic approaches as a way to describe molecular changes and rearrangements of a chain during and after deformation, many other theories can be found. The first quantitative theories were reported by Mullins and Tobin [13], using experimental data as a way to build an explanation of this phenomenon. This and similar approaches are defined as *phenomenological theories*, based on empirical observations, analysing the physics behind the experimental results and fitting the data to mathematical models [17]. Some research inspired by the lack of physical interpretation in the phenomenological approaches, presented *physical interpretations*. These are attempts to correlate changes in the mechanical behaviour after deformation to specific physical changes in the filler-rubber interactions [18]. Another type of approach that can be found in the literature is based on *macromolecular models*, incorporating parameters contained in mathematical theories based on polymer physics [19]. These could be categorised as a combination of the two previous approaches.

Many of the modelling approaches for the Mullins effect do not take into account inelastic features which are present in elastic materials, such as hysteresis and permanent strain. Other complications like time-dependent relaxation and anisotropy are seldom considered as they complicate constitutive models significantly [14]. Deformation histories in modes other than uniaxial strain have mostly been neglected by researchers. In general, models for the Mullins effect are complex and require many

parameters to be fitted, which make them challenging to apply in engineering design. Therefore, any simplifications which can arise as a result of new experimental observations are both timely and welcome. This thesis attempts to contribute on that.

1.6 Outline

The thesis consists of seven chapters. The second chapter provides a review of the fundamental properties of elastomers and their composition. A summary of the mechanical properties with emphasis in the stress softening phenomenon is also provided. In addition, rubber elasticity and the viscoelastic behaviour of elastomers are described, together with previous approaches proposed in the literature to model the softening phenomenon. The research described in this chapter allows identifying potential exploration opportunities for further contributions in the understanding and prediction of the mechanical response of filled elastomers. The final section introduces the aims and objectives of this work.

Chapters 3 to 6 present the findings of this project. Chapter 3 introduces the five elastomers chosen for this research. Physical, microscopic and mechanical characterisation is presented to identify the main differences between the materials. Chapter 4 reports the stress softening response of the filled elastomers under different modes of deformation and strain histories. The energy dissipated and recovered during loading-unloading cycles is further analysed. An energy map for each material is presented, together with the description of a simple physical model capable to describe qualitatively the variation of energy dissipations as a function of the strain history for each elastomer.

Chapter 5 is concerned with the viscoelasticity of elastomers. A new set of tests protocols is described to investigate the stress relaxation and stress memory response varying the deformation history. Based on the measured data, an empirical model to account for the fraction of unrelaxed stress as a function of strain history is generated. Chapter 6 focuses on an investigation of process and deformation induced anisotropy throughout swelling experiments. The rubber-solvent interaction is used to evaluate how the material processing technique and deformation history can induce anisotropy in the elastomeric network. Chapter 7 contains a summarising discussion and conclusions of the work presented. Recommendations for future work are presented.

Chapter 2   **Theory and literature review**

2.1 Introduction

This chapter introduces a review of the composition and properties of filled elastomers. Section 2.2 will present the different types of elastomers and the importance of the formulation and of the cross-linking processes. In Section 2.3 a description of the thermodynamics and of the entropy of swelling is provided. The most important characteristics of the mechanical properties and of the phenomenology of deformation are presented in Section 2.4.

A review of the stress softening phenomenon is presented afterwards in Section 2.5, including other properties modified after deformation such as hysteresis, time dependence and anisotropy. Section 2.7 reviews the different approaches presented in the literature to model the deformation of rubber. Special consideration is given to multi-axial deformation in Section 2.8.   Section 2.9 highlights the research opportunities. Finally, Section 2.10 presents the aims and objectives of this project.

2.2 Elastomeric materials

The main characteristics that describe a vulcanised elastomer are the ability to be subjected to large elongations without failure and the capacity to return very quickly close to their original geometry [20]. An unvulcanised rubber is sticky, easily deformable when hot and brittle at cold temperatures. This behaviour is related to the long polymer chains that can move much like a classical polymer melt. Once the vulcanisation is completed, a series of interconnections is created between chains forming a network that restricts the ability of the chains to flow, resulting in the high elasticity.

The relative freedom in the processing parameters of an elastomer and in its composition allows for a wide range of properties to be designed, depending on the final requirements. Characteristics such as material hardness, deformability, heat and chemical resistance, permanent set, resistance to abrasion, among others, can be easily modified though formulation and/or during the cross-linking process. Elastomers can be categorised depending on chain structure, processability and vulcanisation [21-23]:

* *Natural rubber* (NR) or cis 1,4-polyisoprene: this was the first natural rubber material to be discovered. It needs to be cross-linked to acquire useful elasticity and strength. Natural rubber is classified as a thermoset, as the cross-linking process is irreversible. The main properties are excellent resilience and good electrical insulation. Production depends on tree plantations, requiring years to harvest them to extract latex.

* *Synthetic rubbers*: as a result of increased rubber demand, the production of synthetic materials for mass production was needed. Their properties can be easily adapted to specific requirements, although they still require a cross-linking process (thermoset), as with NR. Some of the most important synthetic rubbers are acrylonitrile butadiene copolymers (NBR), polychloroprene (CR), ethylene propylene diene monomer (EPDM) and polybutadiene (PB). Their main use is in the automotive industry for tyres, hoses, belts, dampers and seals due to their elasticity and resistance to abrasion and tear strength.

* *Thermoplastic elastomers* (TPEs): these have replaced conventional rubbers in many areas owing to ease of manufacturing, excellent resistance to abrasion, scratching and recyclability. They exhibit elasticity similar to a cross-linked rubber with the possibility to reprocess the material. In this category are also included the *thermoplastic polyurethanes* (TPUs), used when low-temperature properties, resistance to solvents and good tear strength is needed. If resistance to heat and solvents is required, the *polyamide thermoplastics* are a good option, with the possibility to be injection moulded, extruded, blow moulded or thermoformed.

* *Melt processable rubbers* (MPR): these are amorphous polymers with hardness similar to the rest of the elastomers which can be processed in typical polymer processing machines. A common MPR is a blend of polyvinylchoride (PVC) with

a thermoplastic elastomer like a TPU. This category can be described as a subdivision of TPEs.

∗ *Thermoplastic vulcanisate* (TPV): this is one of the newest classifications, composed of a thermoplastic olefinic matrix with a discontinuous synthetic rubber phase. These are now very popular in applications requiring heat and chemical resistance.

2.2.1 Formulation and manufacturing

During the manufacturing of rubber, additives are required to facilitate the mixing process, transforming the rubber into a useful material. The main components of the formulation of a vulcanised rubber are the rubber and the vulcanising agent. The remaining additives such as fillers improve different properties of the elastomers. Table 1 shows a description of the most important additives included in an elastomer formulation and the influence they have in either the processing or the final product properties.

Selecting the right formulation is an important stage in ensuring the final performance of the elastomer, avoiding also common problems during the mixing process such as bleeding (migration of the additive) or efflorescence. The cross-linking agent, the activator and the accelerator are commonly used to establish a specific curing rate depending on the final properties requirements [23]. One of the important additives is the particle filler used for reinforcement, such as silica or carbon black. Many mechanical properties and even chemical properties have been shown to improve with the inclusion of fillers in the system [24].

Once the formulation is established the mixing process takes place, typically referred to as compounding [23]. This takes place in robust machinery, such as mixing mills or propeller mixers. During this process, each component is added to the mix, preparing a uniform compound, ensuring the proper dispersion and distribution of the additives. The batch is processed through the specific requirements of time, speed, pressure and temperature [25]. The final formulation will be in the form of pellets, sheets or ropes, depending on the manufacturing process required.

Table 1. Typical components of an elastomer formulation [23, 26].

Formulation	Influence
Elastomer	State of cure / Final cured properties
Vulcanisation system	
Agent	State of cure
Accelerator	Cure rate / Reversion resistance
Activator	Final cured properties
Fatty acids	Processing safety / Mixing process
Antiaging	
Antioxidants	Oxidation properties
Antiozonants	Ozone resistance
Reinforcements	
Inert particles	
Fillers	Final cured properties
Fabrics	
Light stabilisers	
UV absorbers	
Quenchers	Degradation resistance
Free Radicals Scavengers	
Nucleating agents	
Flame retardant	
Colorants	
Inorganic pigments	
Organic pigments	
Antistatic Agents	
Internal	Final cured properties
External	
Slip agents	
Anti-abrasion agents	
Antiblocking agents	
Processing aids	
Plasticisers	Mixing process
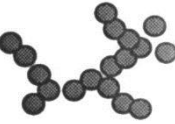
The next stage of the compound is the manufacturing process to get the final product design. The manufacturing process chosen depends on the design of the final product, as it is in this stage where the compound is shaped and vulcanised, mainly divided into three categories: moulding, extrusion and calendering. The moulding process can include compression, transfer or injection moulding, where the vulcanisation process is achieved in the mould. However, for the extrusion process, an additional step after the extrusion with screw extruders is added to vulcanise the material. For the calendering process, the compound is passed through a series of rotating rolls where the gap between them, temperature and speed can be adapted to the requirements. This process is also used to apply a coating to fabrics. Many of the product designs and specifications require the combination of two or more of these processes.

2.2.2   Filler reinforcement in elastomers

The addition of fillers to rubber compound changes the mechanical behaviour significantly in comparison with an unfilled rubber [27, 28]. Properties such as tensile and tear strength, abrasion resistance, viscoelasticity, hysteresis and modulus of elasticity can be increased [7, 29]. The most common filler is carbon black, although silica is also used when the main purpose of the reinforcement is for abrasion resistance or adhesion properties [30]. Other fillers such as silicates, clays, whitening and mineral fillers can be used when only a small reinforcement is needed [27] and are normally referred to as non-reinforcing fillers.

The primary filler particles are on the scale of angstroms and are typically bonded to other primary particles to create aggregates on the nanometre scale. These aggregates can again interact with each other through weaker bonds to create agglomerates of size ranging between 10 to 1000 μm [24]. When fillers are included in the rubber matrix, a combination of aggregates and agglomerates will be dispersed throughout the system. Table 2 shows a representation of the carbon black morphology, size and the effect it has on the filled compound. The importance of the addition of reinforcement to rubber with respect to mechanical properties will be further discussed in Section 2.4.2.

Table 2. Filler morphology and properties [24, 31].

	Morphology	Size	Effect
	Primary particle	20-50 nm	Mechanical Reinforcement
	Aggregate	100-200 nm	Hydrodynamic Occluded rubber
	Agglomerate	10-1000 μm	Filler networking Trapped rubber

2.2.3   The cross-linking process

Sulphur is the most common vulcanising agent used during the cross-linking process of elastomers. It is possible to use it when the chain contains double-bonds with which the sulphur can react in the presence of heat and catalysts. This creates a carbon-sulphur-carbon link, interconnecting the molecular chains. The popularity of

sulphur is attributed to the low cost, wide availability and minimal interference with other additives. It is still the first option for NR and for many other synthetic rubbers such as EPDM and NBR. [32, 33]

Free radical vulcanisation using organic peroxides is also a common alternative to these sulphur methods. The cross-link created is a carbon-carbon bond, which has the advantage of high temperature resistance [34]. Urethane cross-links are used for crosslinking by reaction with a suitable poly-functional reagent and metallic oxides such as zinc oxide or magnesium oxide are used to react with carboxyl groups to create bridges between the chains. The choice of a specific cross-linking agent will depend of the rubber chain chemistry and on the final properties necessary for application.

Monitoring the cross-linking process using an oscillatory rheometer can yield a good understanding of the process [35]. This technique analyses the increase in torque during the curing time, as can be observed in Figure 3, as was also explicated by Coran [35]. The process can be divided into three main phases. The initial phase is the induction and scorch, where the rubber compound is heated. In this phase the viscosity of the material decreases due to the temperature while the curing process has not started, leaving a malleable compound.
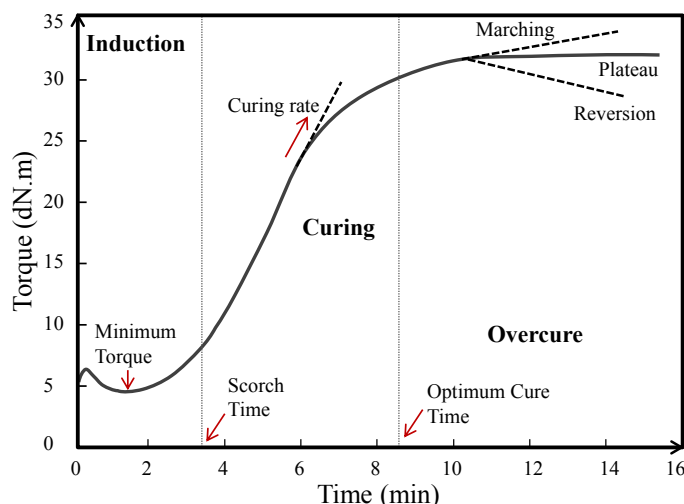
Figure 3. Torque increase during vulcanisation using a rheometer.

When the curing temperature reaches a specific value, the curing stage begins, increasing the torque resistance. The curing rate and optimum cure time of the system will depend of the nature on the rubber properties, additives, vulcanisation agent and the curing temperature. If the curing time exceeds the optimum, the degree

of vulcanisation or cross-link density can rise up to a level where an over-cure of the material is generated and a decline in many of the mechanical properties can occur.

Many properties can be altered by modifying the cross-link density, as showed in Figure 4. Only properties such as modulus and hardness will have a proportional relation with the cross-link density. A high level of vulcanisation reduces the tensile strength of the rubber. The wide range of properties can be affected by the vulcanisation process means it is a very versatile process to adjust the properties of the elastomer to the desired level. Due to this, several studies of the kinetics of vulcanization and advances in the vulcanisation process can be found in literature [36, 37].
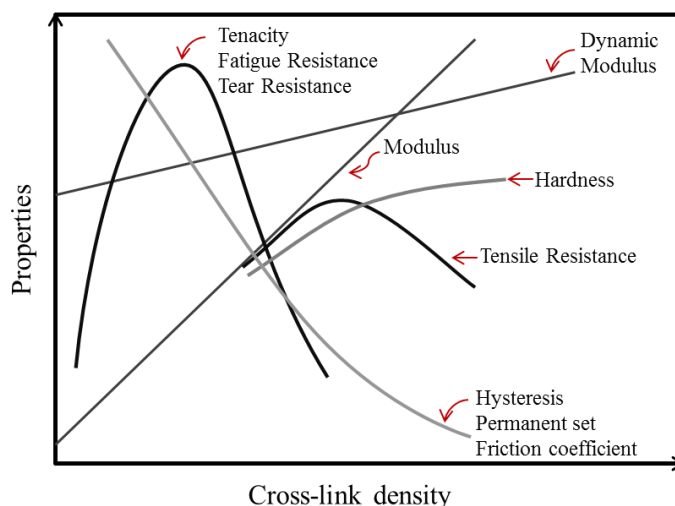
Figure 4. Dependence of properties on the final cross-link density. Adapted from Rodgers [26].

2.3 Swelling phenomena

Due to the 3D network created after the cross-linking process, if an elastomer is placed in a solvent with comparable solubility parameters, rather than being dissolved, the solvent will penetrate between the chains and the cross-links, causing the specimen to swell. During the process, the solvent interaction with the chains creates forces that separate the chains and which dilute the material. The chains are elongated through to an equilibrium state related to the density of the cross-links in the network. This generates an elastic retractive force opposed to the deformation driven by the solvent. A steady swelling equilibrium stage is reached once the two forces are balanced [38], directly associated with the cross-link density in the

network. The higher the degree of swelling, the longer the length of chains (and hence the molecular weight) between cross-links is. Flory [39] and Gee [40] first used thermodynamics to relate this phenomenon to the movement of the cross-linked network in contact with a solvent.

2.3.1   Thermodynamic principles

The basis of the swelling process and its relation with the molecular weight between cross-links can be explained using free energy theory. Equilibrium between phases, in this case between the solvent and the polymer, represents an energy exchange between the two phases. The Gibbs free energy of dilution ΔG is expressed as

$$\Delta G = \Delta H - T\Delta S \qquad \text{Eq. 2-1}$$

with ΔH as the enthalpy or heat, ΔS the entropy of dilution and T the absolute temperature [38, 41]. In terms of vapour pressure and obeying the perfect gas laws, the molar free energy of dilution is given by:

$$\Delta G = RT \ln\left(\frac{p}{p_0}\right) \qquad \text{Eq. 2-2}$$

where p is the vapour pressure, p_0 the saturation vapour pressure and R the ideal gas constant.

The mixing of solvent-rubber can be described as a physical diffusion, with an increase in entropy, and does not imply a chemical attraction [38]. In this case, the diffusion of the solvent between the polymeric chains is associated with the number of configurations available in the mixing system. This gives a good analogy with the elastic properties of the rubber, related with the configuration of the long-chains and the restriction of the cross-link points. The main difficulty then is the calculation of the number of possible configurations.

2.3.2   Entropy of swelling for cross-linked polymers: the Flory model.

The derivation of a statistical theory capable of introducing the possible configurations of the mixing system was carried out by Flory [39, 42, 43]. In order to obtain the entropy and free energy, the Boltzmann relation referring to the entropy change is employed. Using the number of liquid molecules, the possible

configurations and the total number of sites that can be filled by the polymer or the solvent during mixing, Flory introduces a more detailed description of the free energy of dilution ΔG:

$$\Delta G = RT\left\{\ln(1-v_2)+(1-1/x)v_2+(\alpha/RT)v_2^2\right\}$$
Eq. 2-3

where the volumetric fractions of solvent and polymer are v_1 and v_2 respectively, x is the number of segments on the polymer molecules in the mixing [39] and α a semi-empirical parameter associated with the heat of mixing between simple molecules [38].

The derivation of the total energy of mixing ΔG_{tot} for an isotropic elastomer immersed in a pure solvent is expressed by Flory [43] as

$$\Delta G_{tot} = \Delta G_m + \Delta G_{el}$$
Eq. 2-4

where ΔG_m is a modification of the ordinary free energy ΔG corresponding to

$$\Delta G_m = RT\left\{\ln(1-v_2)+\left(1-\frac{V_1}{V_2}\right)v_2+\chi v_2^2\right\}$$
Eq. 2-5

The main addition is the Flory-Hugging solvent-polymer interaction parameter χ, relating the chemical potential of the solvent-polymer interactions, which has a close relationship with the solubility parameter. V_1 and V_2 represent the molar volumes of the solvent and the polymer respectively.

The total free energy also includes the energy associated with the expansion of the polymer network ΔG_{el}, which is related to the elasticity of the chains [44]

$$\Delta G_{el} = \frac{1}{2}\frac{RT}{M_c}(\lambda_x^2+\lambda_y^2+\lambda_z^2-3)-\frac{2}{f}\frac{RT\ln(V/V_0)}{M_c}$$
Eq. 2-6

where M_c is the average molecular weight between cross-link points, λ_i represent the elongations in the three dimensions (x, y and z), f is the functionality of the crosslink, V the total volume of the polymer-solvent system and V_0 the volume of the polymer.

When the polymer-solvent reaches an equilibrium stage, ΔG_{tot} is equal to zero, as the polymer-solvent interaction energies are equal. The classical Flory-Rehner

expression can be then be written as

$$\ln(1 - v_2) + v_2 + \chi v_2^2 = -\frac{\rho_2}{M_c} V_1 \left(v_2^{1/3} - \frac{2v_2}{f} \right)$$

Eq. 2-7

where ρ_2 is the density of the polymer.

2.3.3 Further development of the swelling theory

These thermodynamic principles exposed by Flory were used by Gee and Treloar [45] to study the thermodynamics properties of the interaction between natural rubber and benzene, measured by different methods. Later on, Flory's thermodynamics was confirmed experimentally by Gee [40, 46] in 1946. Experimental tests using natural rubber were used to calculate the swelling in a solvent. Their initial results showed a good agreement between the theory and experimental data. Variations in the temperature and external deformations were also conducted. Results indicated some possible uncertainties in the theory, such as the inclusion of network imperfections like loose ends and looping of polymer chains.

Building on Flory's discoveries, Treloar [47, 48] investigated the equilibrium swelling of natural rubber under load using three modes of deformation: uniaxial tension, uniaxial compression and multiaxial tension, to provide a more general theory. These results showed a satisfactory interpretation of the Flory-Rehner theory under all three modes of deformation. However, some conjectures made regarding χ and the energy due to constraints in the network can bring variations in the final values of M_c. Flory [49, 50] adjusted his approach introducing the constraint due to entanglements using the phantom chain model (see section 2.7.1.2), and acknowledged the variation of χ with temperature and system concentration.

The assumptions made by Flory have also been analysed recently by Valentín et al. [44]. They described two mayor uncertainties and sources of errors in the approach. Firstly, the volumetric fraction v_2 does not include the additives of the rubber compound that can be soluble or insoluble in the solvent. Secondly, the parameter χ is assumed as a constant without consideration of the effects of heat and polymer concentration. The theory gives a qualitative description of M_c, although some approaches were presented by Valentín's research team to reduce the uncertainty.

Similar researches were presented by Saalwächter [51] , James and Guth [52] and Braden et al. [53] proposing modifications to the original Flory's equation and further considerations regarding χ. The influence of the filler was also investigated by Blanchard [54], proposing a filler fraction parameter that modifies the final M_c, including a carbon-rubber interaction fraction.

Schlögl et al. [55] studied the entanglement effect on the mechanical response and the validity of the Flory-Rehner approach. In combination with other techniques, the authors analysed the molecular weight using swelling experiments and mechanical tests, concluding that the contribution of entanglements in the polymer-solvent interaction can be contained in the cross-link contribution assumed in the theory.

2.4 Mechanical properties of filled elastomers

The mechanical properties of filled elastomer have been widely studied in relation to the structure of the network chain and formulation of the material. In order to understand the mechanical response, it is necessary to understand the microstructure of the polymer network and the filler-polymer interactions.

2.4.1 Phenomenology of the network

The structure of a rubber-like material can be represented as a series of different chain entities as shown in Figure 5, where chemical and physical linkages connect the polymer chains together [6, 21]. The physical links are referred to the entanglements and the crystal zones, creating junction points. The chemical cross-links refer to the bridges created between chains during the vulcanisation. The final structure is a 3D network with a random combination of the chain structuring, creating active junctions and chains essential for the elastic response. An active junction is one joined by at least three chains and an active chain should have a connection at both of its ends [6]. The well-known elastic performance of elastomers is the result of the elastically active chains and junctions and the small intermolecular attractions within the material. The formation of the cross-linked network permits higher elastic deformations with less stress applied, when compared to amorphous and crystalline polymers, as shown in Figure 6.
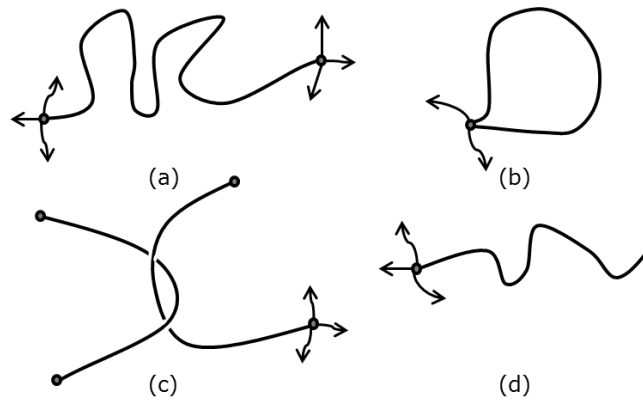
Figure 5. Representation of different entities inside a network: (a) elastically active chain, (b) loop, (c) trapped entanglement and (d) chain end [6].

An ideal scenario will imply a complete elastic response of the rubber. However, elastomers also demonstrate viscoelastic behaviour. The response to deformation will have a combination of elastic and viscous characteristics. The elastic behaviour indicates the possibility of rotation and movement of the molecular chains around skeletal bonds, allowing them to return to the initial equilibrium stage after deformation [6]. The viscous component of the response represents the loss of energy during the deformation due to inelastic rearrangements of the chains. This component also gives rise to strain rate dependence during stretching and recovery of the material. In most elastomers, the response is primarily elastic. Nonetheless, the viscous contribution generates a permanent inelastic change, altering the response in subsequent deformations.
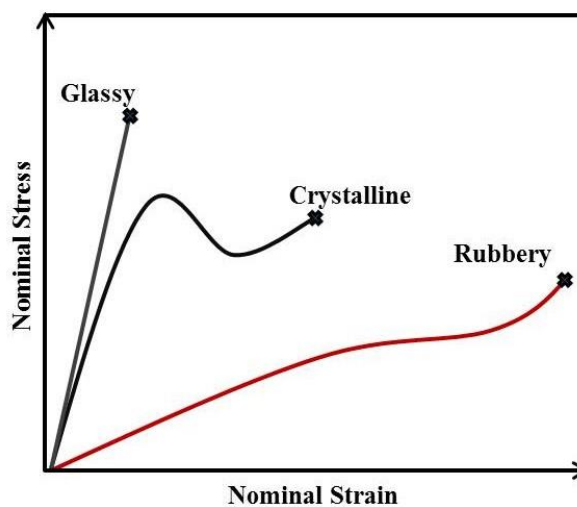
Figure 6. Comparative tensile stress-strain diagram for amorphous, crystalline and rubbery polymers [20].

2.4.2 Influence of the reinforcement in the mechanical properties

As mentioned in Section 2.2.2, it is common for rubbery polymers to be reinforced with particles, with the main purpose of changing the mechanical properties [1]. Fillers can be obtained in a range of particle sizes, with smaller sizes generally used when a higher level of reinforcement is needed. During the dispersion of the filler, a significant physicochemical interaction between rubber and filler is formed, enhancing the mechanical properties [56]. The particle morphology (i.e particle size, surface area and surface structure) is of high importance in the modification of the mechanical properties of the final compound, as shown in Table 3, where the influence of particle morphology on some properties is schematised.

Table 3. Properties influence related with the filler morphology.

Particle attribute		Strength	Modulus	Viscosity	Hysteresis
Size	↓	↑	↑	↑	↑
Structure	↑	↑	↑	↑	↑
Packing	↑	↓	-	↑	-
Surface treatment	↑	↑	↑	-	↓
Porosity	↑	↑	-	↑	-

The inclusion of fillers in the rubber matrix creates a filler-rubber interface where the mobility of the chains is lower than within the rest of the rubber matrix. Physical bonds such as Van der Waal's forces are created between the aggregates and sections of the chains located at the interface. Figure 7 shows a representation of the interface created and a correlation analysed by Litvinov et al. [57] of the average time τ_c for reorientation of a chain related in the proximity of the particle. The higher τ_c found near the interface indicates a mobility restriction, requiring more energy to move and thus increasing the resistance.
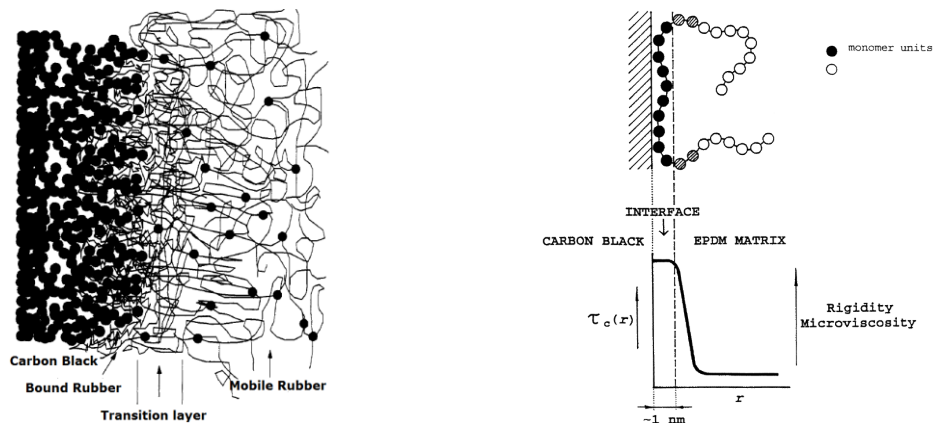
Figure 7. Representation of (a) transition layers on a filler-rubber interface [58], (b) a filler-rubber interface together with a mobility time correlation, τ_c, with respect to particle surface distance. Adapted with permission from Litvinov et al. [57].

Significant research on the mechanical properties of rubbers highlight the importance of the rubber-filler interactions [59-62]. Tunnicliffe at al. [63] exposed the possible relation with the filler content in the energy losses at small strains during oscillatory tests. As the strain is occurring in the linear viscoelastic region of the rubber, the loss is then associated with non-rubber components, attributing this modification in energy to the filler interaction in the system. Bergström [29] explained how the time dependent characteristics of a filled rubber can be affected by the filler content. The inclusion of fillers adds constraints to the structure, amplifying the stretch in the free rubber remaining. Cantournet et al. [64] analysed the mechanical response using the filler-chain slippage as the main factor of the rubber behaviour, considering additional friction energy during deformation to shift the chain between chain-filler and filler-filler interactions. Merkel et al. [65] evaluated the effect of the microstructure parameters on the softening phenomenon. Their study used rubber materials filled with carbon black subjected to cyclic uniaxial tensile tests. They found a negligible dependence on the cross-link density and the filler type, but found a linear increase in softening with filler volume fraction.

The final properties of the rubber can be modified not only with the inclusion of fillers. Li et al.[66] explained how the vulcanisation process and the curing kinetics can also be altered. When the surface area of the filler is increased, the cure rate can also be increased, requiring lower curing times. This is mainly caused by the combination of physical and chemical cross-linking related with the carbon surface area and the sulphur content respectively. The fillers around the rubber matrix allow more active junctions to be created using the filler as additional connecting points.

2.5   The Mullins effect

As shown in the previous sections, the mechanical response of rubber is influenced by many variables during manufacturing. The softening after stretching is undoubtedly one of the most important phenomena observed in filled elastomers, and clearly an important variable to consider during the design of a rubber product. This softening phenomenon, or Mullins effect, was initially studied and reported by Mullins [13, 67], although it was first observed by Bouasse and Carriere [12]. It consists of a softening in the mechanical response which, to a first approximation,

depends on the maximum loading previously encountered. When a rubber-like material is subjected to cyclic deformation, it will exhibit a lower stiffness on subsequent cycles compared with the first one, as well as lower hysteresis. If a material exceeds the previous maximum deformation, the response joins the path of the first loading stress strain path. There is, therefore, a change in the properties of the material after the application of a given strain. The stress-strain response was investigated by Mullins and Tobin [13] using filled natural rubber under uniaxial tensile deformation. As shown in Figure 8, the response during loading of subsequent cycles (increasing maximum strain history) presents a reduction in the stress when the strain applied is lower than the previous maximum.
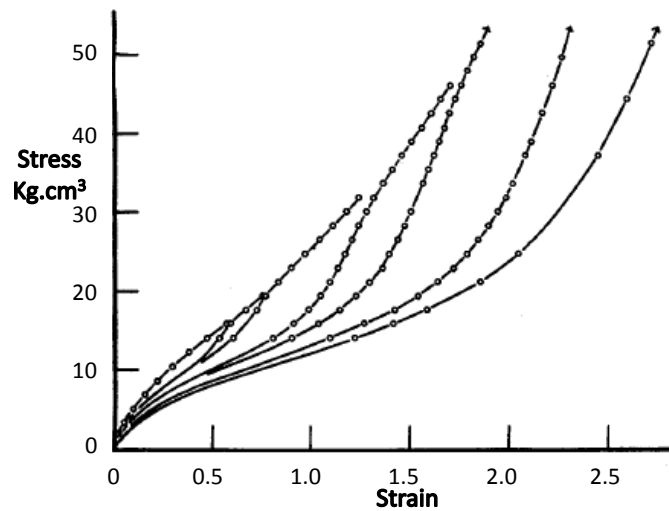
Figure 8. Stress-strain loading response of natural rubber under increasing strain history. Adapted from Mullins and Tobin [13]

The first observations made by Mullins were further evaluated together with Tobin [68], and later by Harwood and Payne [69]. They mentioned the important contribution of the filler in the softening effect. The presence of fillers, such as carbon black, increases the strain in the rubber phase by an amplification factor. Although the softening is present in elastomers with and without fillers, the effect is smaller in intensity in unfilled ones. The incorporation of reinforcements increases not only the elastic modulus and hence the stress, but also changes the mechanism of softening. An interpretation of this phenomenon was provided by Tobin [68] and is that the network is composed of two regions, one hard region, involving high volume fraction of fillers, and a soft region, mainly consisting of the rubber matrix (as presented in Figure 9). When a mechanical stress is applied, the deformation leads to a pull out effect, converting hard phase into soft phase due to breaks in the filler

agglomerates and at the rubber-filler interface [68]. Therefore, on a second stretching, the material will appear softer due to the reduction in the fraction of hard phase.

Bueche [70] also considered the filler-rubber interaction as the main cause of the Mullins effect. When the material is stretched, the fillers will deform at the same deformation scale, following the affine approach. This will require then a non-affine movement of the chains between the fillers, generating the rupture or detachment of chains between the fillers when they reach a finite extensibility
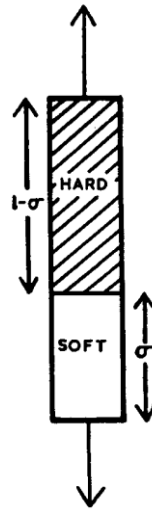
Figure 9. Mullins and Tobin's interpretation of soft and hard phase restructuring during deformation. The fraction of soft phase in represented by σ. Adapted from Mullins and Tobin [68].

The Mullins effect is controlled by the chain distribution and interactions with the filler particles. However, a detailed description of the mechanism responsible for the softening is still in debate. A combination of effects, mainly involving the fillers, will contribute to this phenomenon, that is also manifested in other aspects of the mechanical response of the elastomers, such as permanent set, hysteresis, time-dependence and induced anisotropy.

2.5.1   Permanent set

When elastomers are subjected to a deformation and released, a remaining residual extension is usually observed, referred to as the permanent set or residual stretch. In most cases, permanent set is present after unloading of elastomers. This was not considered in the initial description of the Mullins effect. However, later analysis on the simultaneous effect of the softening and permanent set showed a relationship

between the softening and the permanent set [71]. Likewise, the permanent set is dependent on the maximum strain applied, increasing when the strain subjected increases. These observations were also reported by Dorfmann and Ogden [72], who also observed an increase of permanent set with the amount of filler.

Rickaby and Scott [73] presented a diagram of the cyclic stress softening response, reproduced in Figure 10. Permanent set is observed after the first cycle (cycle *A-B*). Subsequent cycles increased gradually the permanent set and, although there is a small change in response with increasing numbers of cycles, after a few cycles the response becomes approximately constant [74, 75]. It suggests that the mechanism responsible for the softening involves more permanent changes in the network, leaving the material with a plastic deformation.
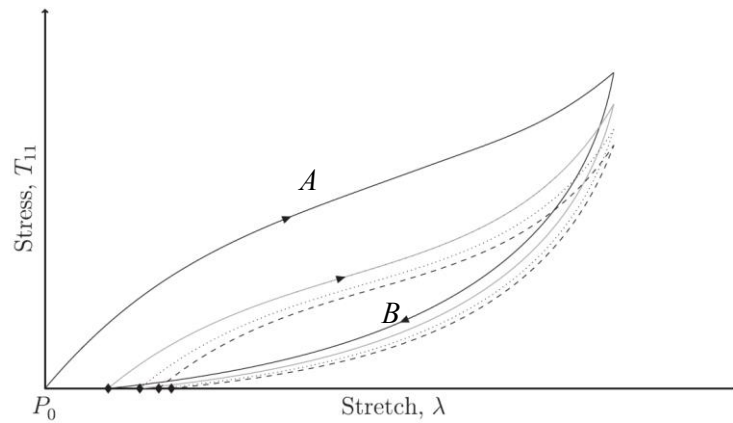
Figure 10. Cyclic stress softening with hysteresis and permanent set. First loading-unloading cycle *A-B*. Adapted from Rickaby and Scott [73]

Tobolsky and Andrews [76, 77] presented an interpretation in terms of a structural theory, explaining that the permanent set is considered to be the result of a simultaneous effect of scission and cross-linking of the chains. When the rubber is stretched the chains are moved from an equilibrium position, promoting scission events in the chains, and simultaneously generating new cross-links which are in equilibrium when the sample is deformed. As a consequence, when the load is removed, a permanent set is observed.

2.5.2   Hysteresis

Filled elastomers have the ability to dissipate a significant fraction of energy during deformation. The hysteresis is related with the dissipative capacity of the material. As well as with the softening effect, there is a noticeable reduction in the energy

dissipation due to deformation after the first cycle. As was presented by Papkov et al [78], the decrease of energy can be associated with relatively slow movements of the chains. They argue that after a first deformation, a rearrangement due to slippage of the chains at the surface of the filler is the main reason for the softening. In subsequent load-unload cycles, as long as the previous strain is not reached, the energy recovered will remain similar, showing a similar energy required in subsequent cycles.

Recently, Lorenz [79] considered that hysteresis varies as a result of a specific cluster mechanism from the filler in the network. As well as with the softening, the hysteresis increases due to the filler. This leads to a reduction of hysteresis on subsequent cycles up to the same previous strain. This theory assumes that the re-aggregation or healing process of the clusters at the end of each cycle is the main mechanism for the hysteresis observed on subsequent cycles up to the same previous strain. Although the possibility of a healing process has not been proved or disproved, there is enough evidence to convince the community that the fillers-rubber interface is an important variable in the softening mechanism and the energy variation.

2.5.3   Time-dependence

When an elastomer is subjected to a deformation, a contribution of viscous and elastic responses are involved. The elastic response is instantaneous, contributing to the elasticity and the recovery capacity after releasing the strain. The viscous contribution is a resistance of the material to flow under stress, being strain rate dependent. Therefore, a viscoelastic material has a time-dependent response under deformation. De Focatiis et al. [80] focused on cyclic uniaxial and biaxial deformation of EPDM rubber and suggested a means by which the viscous contribution to the response could be extracted from the loading and unloading parts of a cycle. Once permanent set had been accounted for, the viscous contribution during a constant rate deformation appeared relatively insensitive to both the strain level during the deformation and the maximum strain reached. This was in contrast to the elastic contribution, which varied markedly with both current and maximum strain, in accordance with the Mullins effect.

The relaxation process can be described as a process that occurs within localised regions. Smaller relaxation times can be associated with shorter distances, and intra-chain relaxations, while longer relaxation times with greater distances and inter-chain relaxation [81]. Fatt et al. [82] described the relaxation process as a combination of local scale response involving a rapid re-adjustment of chains, and a long-range response linked with more complicated configurational movements in the system. Low deformation rates can allow a simultaneous re-adjustment, reducing the relaxation response at the end of the stretching. On the other hand, high deformation rates can restrict the local scale response, requiring longer times to relax.

Miller et al [83] gave a similar description of the time-dependence, showing also that at higher strains, the amount of relaxation increases, emphasising the non-linearity of the stress as a function of time. Figure 11 shows the stress relaxation process with time at different maximum strains, after a simple loading ramp. Nevertheless, recent studies reported by Yamaguchi et al. [84] found that the stress relaxation rate is independent of the strain imposed.
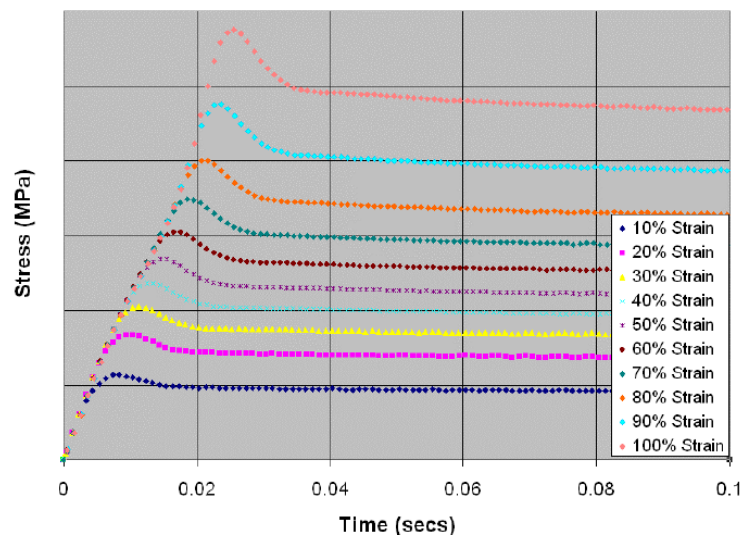
Figure 11. Stress relaxation as function of time of an elastomer at different maximum strains. Adapted from Miller [83].

Tada and co-workers [85] investigate the impact of filler on the stress relaxation of filled and unfilled styrene-butadiene rubbers. Their data indicates higher values of relaxation stress for filled rubber, although there is a similar time-dependent response between filled and unfilled. Farzaneh et al. [86] included the influence of temperature in the stress relaxation and recovery in polyurethane elastomers, with an obvious increase in the stress relaxation and relaxation rate when the temperature is increased, due to higher mobility capacity of the chains.

Many manufacturing processes take into account the Mullins effect by 'scragging' the rubber prior to it being brought into service (by subjecting them to a deformation typically greater than that expected in service) [16, 87]. This preconditioning will reduce the rubber stiffness. However, it is not obvious from the change in the mechanical response, how the viscoelastic nature of the material is affected by the scragging deformation history.

2.5.4 Anisotropy

Inducing deformation in a polymer network can bring about some alignment and reorientation of the chains, leading to anisotropy. Mullins [67] first showed that the degree of softening was not the same in all directions. After a uniaxial tensile deformation, there is a higher softening on subsequent deformations along the axis of deformation compared with the orthogonal directions. The technique used by Mullins consisted in a two phase testing, where a large specimen is stretched first, to then cut smaller specimens in orthogonal directions. This technique was further used by Machado [88], Merckel et al. [89], Hanson et al. [18], Dorfmann et al. [75], among others, to analyse the induced anisotropy under uniaxial tensile testing.

Machado [88, 90] presented clear experimental evidence of anisotropy, by pre-stretching specimens in one direction, and examining the Mullins effect in subsequent stretching at different angles compared to the pre-stretch direction. Figure 12 (a) shows the rubber specimen with the different angles where deformation is applied, after being previously stretched in the 0° direction (Figure 12 (b)). He found that after uniaxial deformation, the induced softening in the perpendicular direction was almost negligible. However, intermediate angles showed softening induced by pre-stretching, with more marked softening in the same direction of the pre-stretching. These tests are simple but clear evidence of the anisotropy that can occur in a cross-linked elastomer.
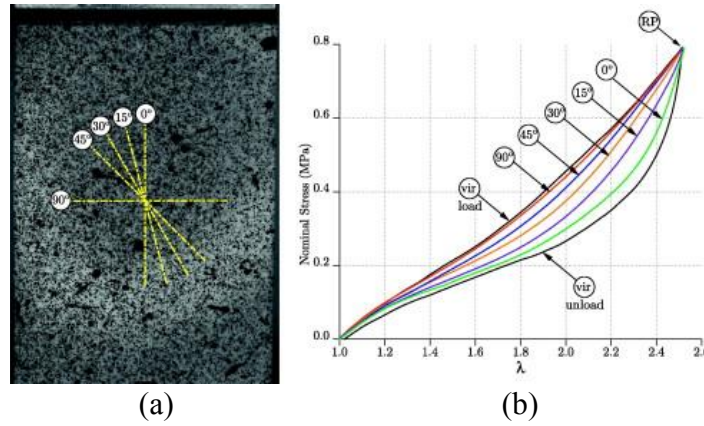
Figure 12. (a)Tensile stretched preconditioned elastomer, with 0˚ alignment as the direction of preconditioning. (b) Anisotropy of the uniaxial stress-strain response of samples stretched at different angles after precondition at 0˚. Adapted from Machado [90]

Hanson et al. [18] describes the softening and anisotropy after deformation a consequence of the movement of entanglements in the filler particle interface. The interpretation ignores the network chain crosslinking in the analysis. Depending on the direction of deformation, only those entanglements associated with the orientation of the strain will be affected and involved in the mechanism of deformation. With that statement, stress softening should not be observed if the secondary loading is transverse to the first.

During the manufacturing process, the rubber can experience deformations during the vulcanisation stage. The most common manufacturing processes found in industry are sheet rolling, compression-moulding and extrusion. All impart a compression or stretching in the material in a specific direction that can reorient the chains at the same time as it is being vulcanised. This initial induced anisotropy does not appear to have been explored in many studies. Gurney and Gough [91] presented details of the possible anisotropy present after moulding of elastomers. Blow and Demirli [92] analysed the anisotropy induced by the moulding process by studying the swelling process and variation in the swelling percentage. They found evidence of anisotropy during the moulding process related to the flow in the mould before the vulcanisation takes place.

2.6   Solvent influence in stress softening

Many industrial applications of rubbers include the direct contact with solvent during the life cycle of the product. Because of this, the interaction between rubber and

solvent has been widely studied.

The work of Treloar [47, 93] explored the anisotropy of swollen strained elastomers. The swelling ratio was examined under uniaxial and equibiaxial tension and compression. Results indicated a linear relation between the strain and the swelling ratio. The principle is based on the hydrostatic pressure; when the stress is tensile, the hydrostatic pressure becomes negative, leading to an increase in the swelling. However, compressive stresses lead to a hydrostatic pressure, reducing the degree of swelling. This was the first physical interpretation that related the stresses that occur during the swelling stage with the network properties and the anisotropy created during deformation. Nah's research team [94] reported experimental data showing the variation of the degree of swelling under simple and constrained extension, using Treloar's approach. The diffusion of the solvent and therefore the degree of swelling was shown to depend on the local stress, and also to be a time dependent process.

Chai et al. [95] focused on the analysis of the Mullins effect in the swollen state. Experimental data showed an increase in the softening during compressive deformation when the rubber was swollen, as presented in Figure 13. Compared with the stress response of a dry rubber, there is a decrease in the stress when the material is in contact with two different solvents, biodiesel BO and diesel B100. A difference in the degree of swelling was reported related with the solvent, with a higher swelling ratio with diesel B100, and the higher the swelling, the lower the stress response.
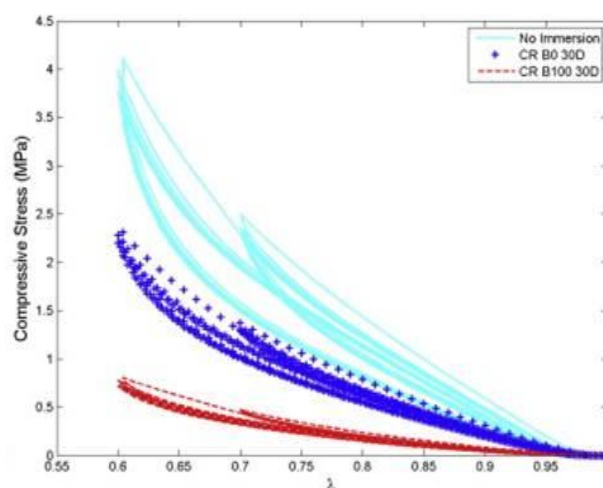
Figure 13. Comparison of stress-strain curves for CR dry and 30 days swollen in biodiesel BO and diesel B100 conditions. Taken from Chai el al.[95]

Further work by Chai and co-workers [96, 97] examined the stress relaxation behaviour in the swollen state. Data reported in Figure 14 for NBR and CR under

compressive strain using biodiesel as a solvent clearly showed the decrease in the fraction of stress relaxing with swelling time. They associated this effect with an increase in the interaction of the solvent with the rubber, reaching equilibrium and reducing the viscous contribution to the macroscopic response. Most of the studies presented focused on deformations of swollen elastomers. No literature exploring the swelling equilibrium post-deformation was found.
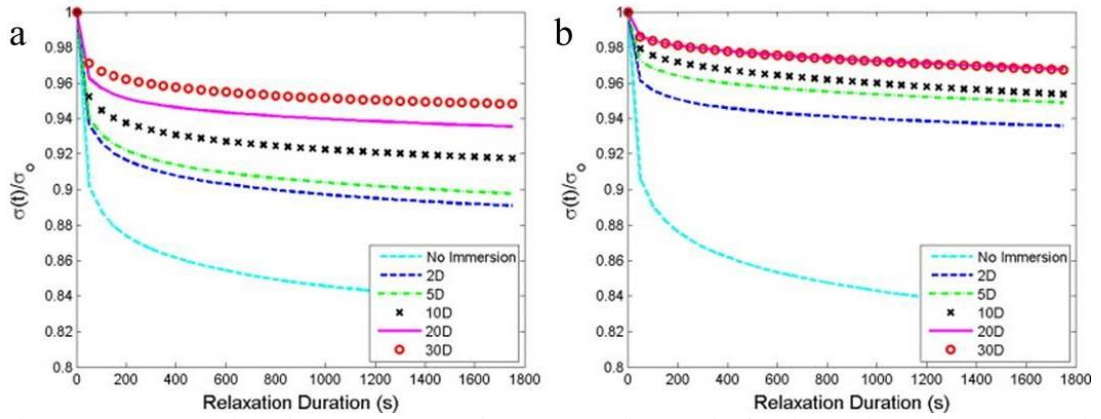
Figure 14. Stress relaxation response under compressive strain for dry and swollen NBR and CR following different immersion times. Taken from Chai et al. [96]

2.7 Constitutive Modelling

2.7.1 Rubber elasticity

To describe hyperelasticity, two standard models for rubber elasticity were introduced: the affine network model and the phantom network model. These two models describe the basic elasticity of rubbers, and are frequently used as a base for more complex models. These models are based on the assumption that polymer chains can change shape but not contour length. Therefore, a macroscopic deformation of the solid material is associated with microscopic changes in the configurations of the chains.

To quantify the change in shape of an infinitesimal solid body, a deformation gradient $\mathbf{F}$ is defined, relating the new position of a material point (x) to its original position before the deformation (X), expressed as

$$F_{ij} = \left(\frac{\partial x_i}{\partial X_j} \right)$$

Eq. 2-8

The principal stretches can be calculated from the eigenvalues of **F** [98]. For a simple case where the axes are aligned with the eigenvectors, **F** is given by

$$\boldsymbol{F} = \begin{bmatrix} \lambda_1 & 0 & 0 \\ 0 & \lambda_2 & 0 \\ 0 & 0 & \lambda_3 \end{bmatrix}$$

Eq. 2-9

Both theories use the principal stretches to describe the mechanism of deformation of the network.

2.7.1.1 Affine model

The affine model represents the simplest way to describe and relate the macromolecular deformation on a microscopic scale of the chains. It assumes that the end-to-end vectors of a length of chain between cross-links deform affinely with the macroscopic deformation, as shown in Figure 15. This means that the ends of the chains are effectively embedded in an elastic medium and attached to a non-fluctuating background. Therefore, the distance between two points in the network will change with the same deformation gradient as the macroscopic deformation [99].
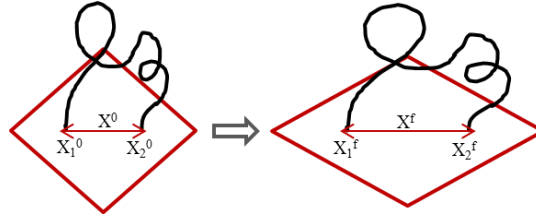
Figure 15. The Affine network model illustration of deformation of a rubber-like network.

The elastic free energy in this model is represented as the sum of the free energies of all the deformed chains. The total elastic free energy can be expressed in terms of the principal stretches of the deformation gradient tensor, λ_x, λ_y and λ_z as

$$\Delta A_{\text{el, Affine}} = \frac{1}{2} \nu k^B T \left(\lambda_x^2 + \lambda_y^2 + \lambda_z^2 - 3 \right)$$

Eq. 2-10

where ν is the density of chains in the network, k^B the Boltzmann constant and T the absolute temperature [6] [99] [21]. This theory was used by Flory [39] during his thermodynamic analysis of solvent-polymer interaction. Further investigation [44] proved that constrains in the network due to entanglements, chain-ends and fillers create a more complex response than the affine assumption.

2.7.1.2 Phantom network theory

The Phantom Network model is based on the idea that the chains of the network can cross each other and are attached to cross-links or junctions that are themselves capable of moving. The ends of the chains are linked with the surface of the network. An ideal polymer chain is described as a spring with an effective spring constant (K_{eff}). A network is formed by a series of springs connected in parallel, as shown in Figure 16 [6] [99].
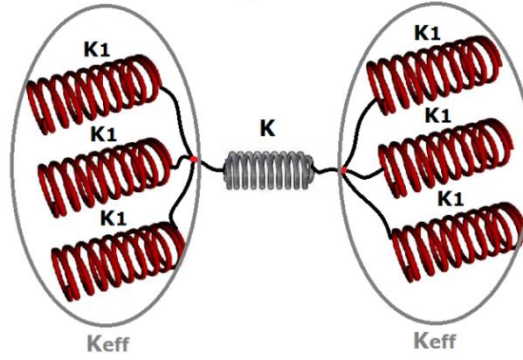
Figure 16. Representation of the rubber network in the Phantom Network Model.

If the network functionality f (i.e. the number of chains meeting at a junction point) is known, the spring constants of the chains in the network can be identified. As the springs are connected in series, the spring constant of each chain can be related to K_{eff}; and therefore, the stiffness of the network can be expressed as

$$K_{eff} = (f-1)K_1 \qquad K_1^{-1} = K^{-1} + K_{eff}^{-1}$$
$$K_{eff} = (f-2)K$$

Eq. 2-11

where K is the spring constant of the connection of springs in series, K_1. The constant K_{eff} represents how the elasticity is transmitted from a macromolecular scale to each chain involved in the network. With this model the total elastic energy of the model is expressed as

$$\Delta A_{el, \, Phantom} = \frac{1}{2}\xi k^B T \left(\lambda_x^2 + \lambda_y^2 + \lambda_z^2 - 3 \right)$$

Eq. 2-12

where ξ is the cycle rank, described as the density of chains that must be cut to reduce a network to a tree [21]. Both the Affine and Phantom Model are based on an unrestricted network. The only difference in the final equation between the Affine and Phantom Model is in the front factor. Research showed [44, 49] that the Phantom

theory approaches more closely the rubber elastic response of real elastomers. This model has become the basis of further developments in the theory of rubber elasticity, as presented by Evaraers [100]. His research combines the phantom approach and the tube model including constrained junctions modelled as coupled linear forces instead of restricting individual joints. Many other more complex theories were developed to describe the elasticity of a rubber network structure using these models as the starting point.

2.7.2 Mullins effect interpretations

Interpretations of the Mullins effect can be classified into three categories: phenomenological theories, physical interpretations and macromolecular theories. Their classification will depend on how the parameters used to describe the mechanical response are interpreted as a phenomenological point or with a physical interpretation to predict the Mullins effect.

2.7.2.1 Phenomenological theories

Phenomenological models are consistent with the observed physics behind empirical observations and phenomena of Mullins behaviour. But, they are not necessarily derived from the basic physics. The theories can be expressed mathematically but, in many cases, the fundamental connotations of the phenomena are not well described. Due to the complexity in the response of rubber involving large deformations, viscoelasticity and softening, most of the models presented in the literature are phenomenological [14].

One well known phenomenological model for the Mullins effect is the theory of Ogden and Roxburgh [17]. They developed a pseudo-elasticity theory in order to describe the Mullins effect in filled rubber-like materials. The pseudo elastic model is based on the theory of incompressible isotropic elasticity, incorporating one parameter, defined as a damage parameter. This variable is integrated into the theory in order to modify the strain-energy function. The damage parameter provides a means of changing the form of the energy function during the deformation process and hence changing the character of the material properties [101]. In essence, the

loading can be described by an elastic strain-energy function, and unloading by a different strain-energy function. A damage function serves to determine the damage parameters in terms of the state of deformation. The function is also directly related to the energy dissipated in a primary loading-unloading cycle. Ogden and Roxburgh showed numerical results for pure shear and for simple tension. They used the model to fit experimental data obtained from Mullins and Tobin [13], as shown in Figure 17. The model only deviates in the unloading stage due to the exclusion of the permanent set in the fitting analysis. They claimed that the model can be valid in multiaxial states of stress and strain [102], although they did not show data to prove this.
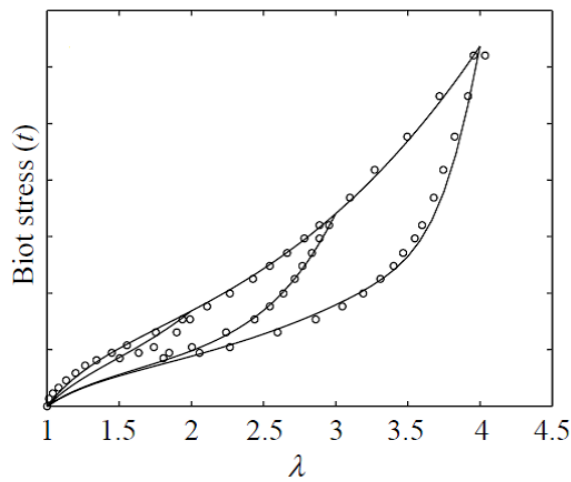
Figure 17. Ogden and Roxburgh model fit (continuous line) of the stress-strain response using Mullins and Tobin experimental data for uniaxial tests for NR. [17]

In subsequent studies, the theory was applied by Ogden [103] to a problem involving non-homogeneous deformation, allowing residual strain to be calculated and illustrating the stress softening effect with numerical calculations. The most important limitation is the assumption of isotropy. They argued that the available data was not adequate to assess the value of accommodating anisotropy into the theory. Ogden [101] demonstrated how a progressive increase in strain can be compared to the curve of a virgin filled natural rubber. This observation was the basis for preconditioning the materials at the beginning of their service life. If the material is loaded several times to a constant stretch, no further permanent set arises beyond the one generated by the initial loading.

Another example of a phenomenological model is that developed by Qi and Boyce [104]. This model is based on the Arruda-Boyce hyperelastic 8-chain macromolecular formulation [105] to model the large strain elasticity of the rubber.

The effect of filler particles is accounted for by a strain amplification factor over the macroscopic strain, which relates the macroscopic stretch with changes in the rubber network, named as the soft domain. The theory is expressed in terms of strain energy density, which originates back to Mullins and Tobin [5]. The softening is handled by considering the presence and evolution of hard and soft domains within the material. Here hard domains comprise both the filler and the bound rubber initially surrounding the filler. With increasing deformation, some of this bound rubber is freed and increases the proportion of deformable soft domains while decreasing the proportion of hard domains. The amount of softening is linked to the relative maximum amplified stretch experienced by the chains, normalized by the maximum extensibility of the chains. Five model parameters were fitted to the original uniaxial data of Mullins and Tobin, and a high quality of fit was achieved for pseudo-cyclic (load-unload with increasing strain) uniaxial loading. The model can also capture the Mullins effect under other strain states, but the formulation is based on a scalar evolution of softening and is not capable of capturing anisotropy. It also does not cater for permanent deformation or viscoelastic effects. Rickaby and Scott [73, 106, 107] later adapted the Arruda-Boyce model to create a nonlinear isotropic constitutive equation.

The concept of a two-phase material, with a fixed volume fraction of a breakable phase was introduced by D'Ambrosio and co-workers [108]. Their three-dimensional non-linear damage model describes the rate-independent hysteretic behaviour of rubber-like materials. The material is modelled by a distribution of links inside a network, with the possibility of fracture during deformation. The filler particles are represented as rigid spheres connected by two different types of chains: (1) elastic chains that allow the material to have a particular strength, and (2) breakable chains that take the responsibility for the network alteration. It is assumed that the activation and breaking events depend on the first strain, as shown in Figure 18 (a). A more complex expression of this model involves the option of reforming part of the broken links during unloading. Figure 18 shows D'Ambrosio's distribution approach of active, unloaded, broken and recross-linked (healed) chains. Figure 18 (b) shows the loading (0-A) and unloading (A-B-C) path. Figure 18 (c) and (d) illustrate the probability distribution of the chain fractions depending on the activation strain (ε_a) of the system. The damage of the chains starts during the loading until it reaches the

maximum value of the strain ε_M. During the unloading, when the strain passes the fracture strain (ε_B), part of the broken links defined as the active fraction (ε_M-Δ) return to the reference configuration and generate the recross-linked and broken region in Figure 18 (d). At the end of the unloading, the fraction of broken chains will reduce and the fraction of unloading chains will increase compared to point A, due to the possibility of healing. The model neglects viscous, inertial and thermal effects, and is focused only on the ideal Mullins effect. It also does not show permanent set or hysteresis, and the damage is isotropic.
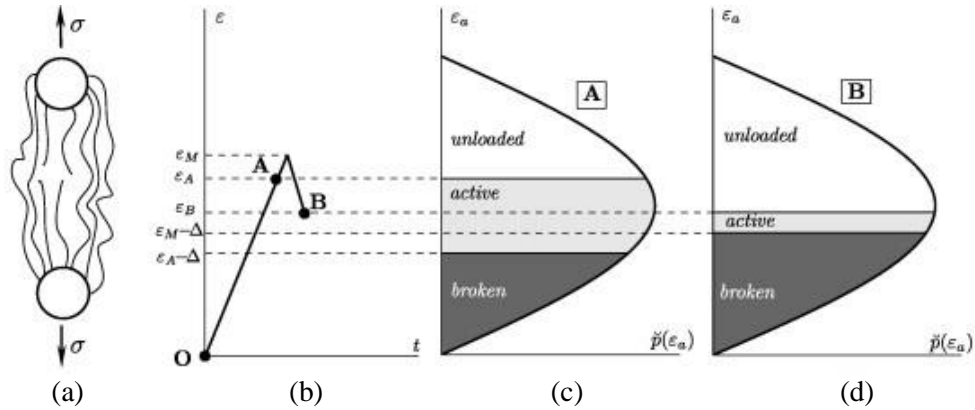
Figure 18. Scheme of the (a) prototypical model adapted from D'Ambrosio, (b), (c) and (d) evolution of the breaking and recovery of the chains related with the strain. The values of ε_M represent the maximum value of the strain, ε_a the activation strain, ε_B the fracture strain, and ε_M-Δ the active fraction [108].

A phenomenological inelastic constitutive model is that of Besdo and Ihlemann [109]. This is a model capable of reproducing several effects such as nonlinearities, hysteresis and softening. The model involves eight parameters with an optional constant (the bulk modulus) for almost incompressible formulations. The model is able to capture the response in simple shear tests, including the non-linear viscoelastic response, hysteresis, loading history and remaining deformation after unloading. Besdo and Ihlemann consider that phenomenological models are more a description of the material behaviour rather than an explanation. Considering this, they present a theory of self-organizing linkage patterns in an effort to explain the physical reasons for this complicated behaviour [110].

The majority of the theories discussed assume isotropic structure, i.e. a randomly oriented network. However, anisotropy was exhibited even by Mullins's early experiments [67]. More recent studies have attempted to incorporate material anisotropy induced by the Mullins effect. Diani el al. [111] brought to light the induced anisotropy, and sought to develop a directional model capable of capturing

the direction-dependence of pre-deformed rubber-like materials. The model has seen several iterations [89, 112] and a final approach was presented by Merkel and Diani [113]. Here they defined a Mullins softening activation criterion for filled rubbers subjected to general loadings. The final model includes a similar strain amplification factor to that from Mullins and Tobin's [13] approach. In order to predict induced anisotropy and permanent set, the model uses a phenomenological damage function. The anisotropy of the material is accounted for by considering uneven strain energy contributions according to the loading direction. Material viscoelasticity is not considered, and the focus is on the equilibrium response only. The approach made by Merkel and Diani's research represents an important advance in the incorporation of anisotropy and strain history to the creation of a relatively simple model.

Dargazany and Itskov [114, 115] presented a micro-mechanical model describing anisotropy and deformation-induced permanent set. The model is based on a physical approach considering the damage of the network as a consequence of chain sliding and/or debonding from aggregates. The final model does not introduce a phenomenological damage function, instead including seven physical parameters. The polymer-filler system presents a network evolution with two simultaneous processes, debonding and rearrangement. The model formulates the macroscopic energy as the sum of microscopic strain energies of all active chains available within the network. The model does not consider aggregates in the parameter, and treats the filler-rubber bonds in the same way as a cross-link bond. Dargazany and Itskov compare the model with uniaxial tension cycles in two orthogonal directions, capturing the anisotropy of the Mullins effect, as well as the appearance of permanent set.
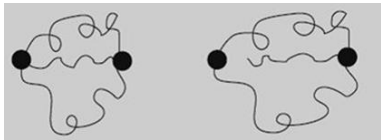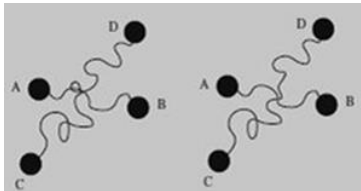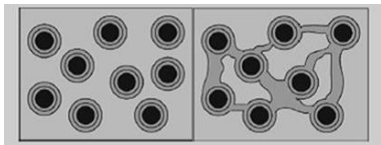
2.7.2.2 Physical interpretations

The physical mechanisms underpinning the Mullins effect were summarized by a review published by Diani [14], part of which is reproduced in Table 4. Following a phenomenological approach, Besdo and Ilhemann [110] reported a more detailed theory based on physical arguments to explain the Mullins effect. They developed a theory of self-organizing linkage patterns. It is based is a self-organizing process concerning the coexistence of chemical linkages and the destruction and recombination of physical linkages in the polymer network. Using this assumption as

a base, new properties can be calculated at the macroscopic level. The model considers that the filler particles interact with the network by way of physical linkages. They recognized that the softening exhibited by the elastomers can be described as two different processes, even though both are called the Mullins effect. The first one is cyclic softening, referring to the decrease in the reloading curve after one or more cycles until the stationary stage is reached.

Table 4. Physical mechanisms behind the Mullins effect, adapted from Diani [14].

Sketch	Physical Source
	Bond rupture
	Molecules slipping
	Filler rupture
	Disentanglement
	Double-layer model

The other process is the upper elongation bond change, referring to the decrease of stress at specific elongations, mainly during unloading. To simulate inelastic effects, some of the nodes are allowed to form physical linkages. The role of filler particles is simulated by increasing the number of active nodes. The results of this modelling show direct signs of complex processes which cause emergent effects due to an internal memory of the system. These predictions are restricted only to uniaxial tension tests. Similarly, the damage to chemical cross-links is not considered as it is assumed to be a rare behaviour. Despite the fact that they are aware that such damage occurs and has a permanent effect on the material response, it is neglected due to the complexity involved.

Another study was carried out by Suzuki et al. [116] in an attempt to find a physical interpretation for the softening phenomenon. They argued that the rubber-filler interaction in relation to chain scissions of rubber molecules during deformations is the main reason of the Mullins effect. Chain scission is related to mechanical energy applied to rubber-filled interactions. These scissions occur when the mechanical energy applied to rubber molecules exceeds the interaction energy between the filler agglomerates. This physical interpretation assumes that the mechanical performance of filled rubber is affected by the crosslink density of the rubber matrix, the size of agglomerates formed and the rubber-filler interactions. When one of these characteristics is modified, it is possible to observe a change in the mechanical behaviour. To prove this theory, they measured the density of radicals right after uniaxial testing of rubber samples with silica as filler. The increase in the density of the radicals compared with the virgin material led them to conclude that chain scission may contribute to the Mullins effect. Similarly, the modification of the interfacial bonding between the filler and the elastomer enhances the tensile stress at high deformations, as was reported by Suzuki [116]. In Figure 19, the stress-strain behaviour is illustrated for modified and unmodified silica filled elastomer. This study was mainly focused on the interaction between fillers and rubbers, and does not involve any other properties of rubbers. Experiments are only focused on uniaxial elongations and there is insufficient experimental data to verify the theory.
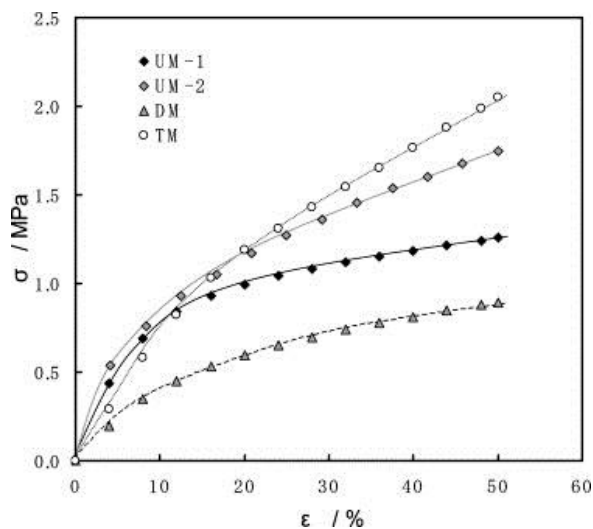
Figure 19 Stress strain curves for filled elastomers with surface modified filler: DM using mono-functional and TM a bi-functional coupling agent, and unmodified silica filler vulcanised with different sulphur content,UM-1 with 1.7phr and EM-2 with 2.9phr. Adapted from Suzuki et al. [116]

According to Fukahori [28], the softening phenomenon is associated with the

reinforcement of elastomers. In this theory, the material is presented as a two layer system around spherical filler particles. An inner glassy hard (GH) layer is within the surface of the particle and a sticky hard (SH) layer on the outside, as shown in Figure 20(a). With this premise, Fukahori explained that the increase in tensile stress is only possible when the sticky hard layer supports the stress concentration, which is then transmitted to the whole system. The model describes the creation of crazes in the sticky hard layer as a molecular behaviour in the network of carbon particles.
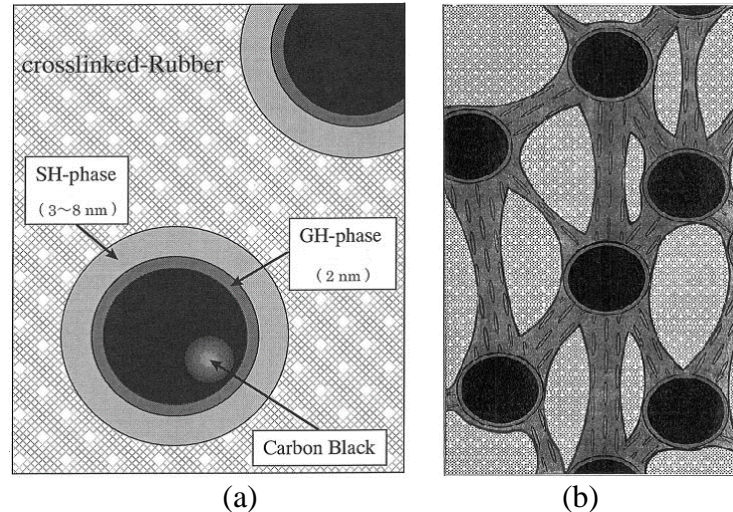
Figure 20. (a) Schematic double layer interface, and (b) super network structure interconnection Adapted from Fukahori [28].

Another assumption that Fukahori invokes is that there are very few or no crosslinks in the sticky hard layers, owing to the difficulty of the sulphur to dissolve in the bound rubber during the vulcanization process. Subsequently, the maximum stress concentration appears between the rigid particles. When the sticky hard layers surrounding two adjacent carbon particles overlap, these interconnected layers construct a superstructure that is strong enough to support the maximum stress concentration, as shown in Figure 20(b). If time and temperature are involved, the molecules can relax and a higher entropic state occurs, presenting a recovery of the system. In this research, Fukahori proposes a new concept for carbon black reinforcement in relation to the Mullins effect using experimental data of simple extension of filled rubber samples created by varying the volume fraction of the filler. The theory refers to the effect between the filler particles and does not mention any other properties evolving during the tensile test, or the elastic behaviour of the rubber.

Buckley et al. [74] investigated the mechanical response of thermoplastic elastomers

with flexible soft segments providing rubbery characteristics, and hard segments forming relatively rigid connexion points between the molecules. The mechanical response of the material is determined by the dispersed phase volume fraction, the mechanical coupling between the phases, and the mechanical properties of the individual phases. They consider the coupling between the phases as a combination of series and parallel couplings, as suggested by a Takayanagi model [117]. The approach used is based on the proposal that a significant fraction of hard domain lie in a weakly bound surface layer. Therefore, when the stress increases, the soft phase will pull off surface segments of hard phase and add it to the series coupled soft phase, thereby reducing the hard phase volume fraction.
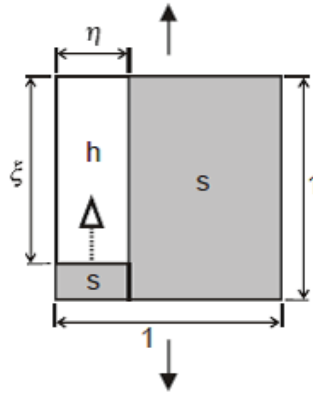
Figure 21. Series and parallel coupling representation between hard (h) and soft (s) phase for modelling tensile deformation. The arrow indicates the evolution of the hard phase to the soft phase during deformation. Adapted from Buckley [74].

A one dimensional coupling between phases for modelling tensile deformation is presented in Figure 21. The pull-out effect was represented via a linear reduction of the hard phase via an empirical material parameter. The response of the model deviates from the experimental results since other important aspects are neglected, such as soft phase hysteresis and finite extensibility, time dependence and multiaxiality of the response. Even so, this physically based constitutive model is a simple elastic and elastic-plastic representation of soft and hard phases of filled elastomers that could be adapted in order to provide a more accurate prediction of the mechanical response.

2.7.2.3   Macromolecular theories

Kluppel and Schramm [19] used a non-Gaussian tube model combined with a damage parameter to explain the phenomenon of softening from the micromechanics of hyperelasticity of filler-reinforced rubbers. Their final complex model is based on

topological constraints and packing effects and includes the effect of finite chain extensibility. They start by considering freely fluctuating chains and non-isotropic fluctuations and contemplate the idea of non-isotropic fluctuations of chains segments. Kluppel and Schramm then create a probability distribution of the space curve relative to the mean position including a constraint parameter. During the strain there is a successive breakdown of filler clusters, as represented in Figure 22. This continuous breakdown of filler clusters allows for an understanding of the softening. The cluster size (denoted as ξ by Kluppel and Schramm) will increase every time that the strain is increased, and will remain constant when the strain remains within the bound on subsequent loads. These changes in cluster size are represented with a strain amplification factor that relates the microscopic strain to the macroscopic strain. This factor changes with modification of the strain and modifies the cluster size. The final model depends of eight parameters, but not all can be associated with measurable physical quantities.
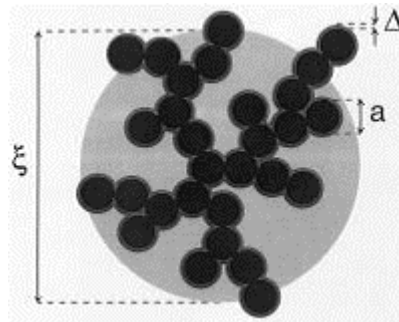
Figure 22. Structure of a filler cluster size denoted as ξ formed by filler particles of size *a* stabilised by a rubber layer Δ in a rubber matrix according to Kluppel and Schramm modelling. Taken from Kluppel and Schramm [19].

The rupture of chains linking particles, was explored by Goktepe and Miehe [118], building on the isotropic macromolecular three-chain model of Govindjee and Simo [119], using 21 different directions to discretise the induced anisotropy and the residual strain. The approach described by Meissner [120] is based on the modifications of several mathematical models and on the introduction of a new empirical parameter to represent the tensile stress-strain dependencies on filler-reinforced rubber like networks. The final equation contains eight parameters, of which six are adjustable.

2.8 Mechanical response of elastomers under multi-axial deformation.

For a more accurate simulation of the real life cycle of a rubber product it is necessary to understand the mechanical response during multi-axial deformation. Due to the lack of equipment capable of inducing biaxial strains, limited experimental data is available analysing the influence of biaxial strains on the Mullins effect. A review of some of the experimental equipment used to provide biaxial deformation can be found in Table 5. Research like those presented by Dorfmann [75] and Istkov [115] first tried to include biaxial deformation in their analysis, mainly to fit them in their modelling approaches. They used a cruciform shape to stretch sequentially using a common uniaxial tensile testing machine, first in one direction and afterwards in the perpendicular direction (see shape specimen in Table 5 (a)). In this case, it is not possible to analyse the behaviour during a simultaneous multi-axial deformation. Nevertheless, a difference in mechanical response could be observed when the material is subjected to subsequent perpendicular deformations.

The incorporation of simultaneous biaxial testing using a cross-shaped sample was presented by Merckel and Diani [89, 111] to compare constitutive models with the experimental data obtained during cyclic uniaxial and biaxial tensile tests. The method was also applied to pre-deformed samples, presenting experimental data that provides evidence of an activation criterion for the Mullins effect related not only with the maximum stretch but also with the stretch direction.

Bhatnagar et al. [121] presented a biaxial rig fixture for uniaxial tensile testing machines. The configuration provides equibiaxial stress and the possibility of different stretch ratios by adapting the fixture shown in Table 5 (b). One of the downsides is the restriction of high deformations due to the size of the rig.
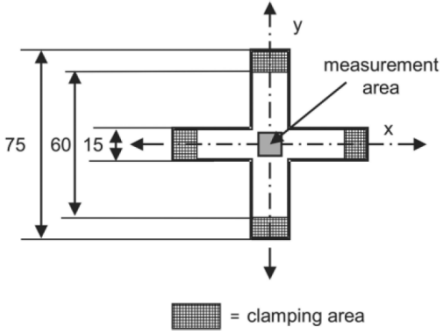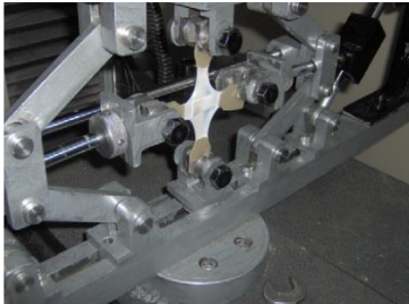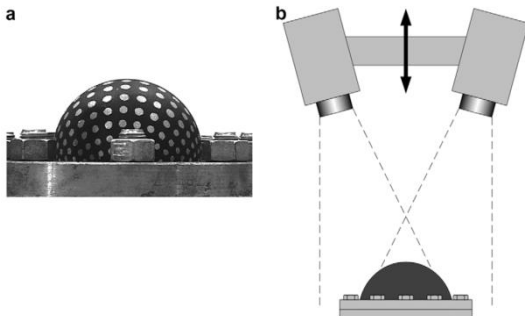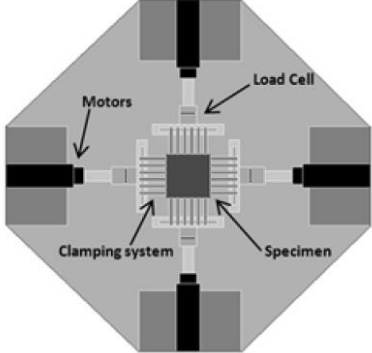
Another common test protocol used for biaxial testing is bubble inflation. Sasso and Palmieri [122, 123] carried out multiaxial tensile tests using a hydraulic balloon test rig (see Table 5 (c)). Treloar [124] also used the balloon test to include different modes of deformations in his analytical model. This method requires measurements of the radius of curvature of the balloon to calculate the tension state. This is a more tedious method with larger sources of error, such as the difficulty in the strain control and the inhomogeneity of deformation.

Li et al. [125, 126] used a thin rubber sheet inflated with water to simulate biaxial deformation in order to develop a constitutive model, and used cavity growth as the main physical explanation for the Mullins effect. Comparison of biaxial extension using cruciform and bubble inflation methods was conducted by Galliot [127]. Both techniques have advantages and limitations and similar results in the mechanical analysis were found. It is also important to acknowledge that only equibiaxial deformation can be performed with these two techniques.

A different approach was made by Axel Products, Inc. and presented by Day and Miller [128]. They used radial strain using circular specimens (presented in Table 5 (d)). This is a good approach for equibiaxial deformation, although it does not allow large deformations due to the complicated fixturing. De Focatiis and Kelly [129, 130] presented a prototype mechanism for equibiaxial testing using uniaxial tensile testing machine. The rig consist of an arrangement of single degree of freedom mechanisms in order to deform a circular specimen uniformly moving two opposite points apart using the uniaxial test machine.

More recently investigations of mechanical behaviour of elastomers were carried out using improved biaxial testing machines, such as that of by Lombardi el al. [131], as shown in Table 5 (e). Their prototype has four independent motors to generate arbitrary strain on each axis. The load cell is located behind the set of grips on each axis, giving the possibility of alteration in the load recorded due to the friction of the grip joins. Separate studies presented by Kim [132] and Tada [85] used a similar biaxial set-up to study the mechanical response of filled elastomers. They were able to clearly observe differences in the mechanical response when compared with uniaxial tests.

Table 5. Biaxial tensile testing equipment used in the literature for elastomers.

Biaxial tensile testing set up	Set up diagram
(a) *Cruciform shape.* Used by Itskov et al. [115] for biaxial deformation using a tensile testing machine. The specimen is first stretched in one direction and then clamped and deformed again in the perpendicular direction.	
(b) *Simultaneous biaxial deformation.* Using a common uniaxial tensile testing machine. Rig developed by Bhatnagar et al. [121].	
(c) *Balloon test.* Used by Sasso and Palmieri [122, 123] for biaxial deformation.	
(d) *Equibiaxial rig* Developed by Axel Physical testing Services. [128]	
(e) *Multi-axial set up.* Four independent motors allow separated movement on each axis. Presented by Lombardi et al. [131]	

2.9   Research opportunities

The literature review of this chapter showed significant research related with the mechanical response of filled elastomers and the softening phenomenon. Since the first interpretation of Mullins of the softening phenomenon, many theories have been proposed to describe the mechanism of deformation and the variables affecting their behaviour. However, there is still no general agreement to explain the softening behaviour. This is mainly due to the complexity and variability of the elastomeric network structure and the complicated interpretation of the interactions between the rubber and the filler.

Most of the models and interpretations suggested in the literature can only describe selected aspects of the mechanical behaviour of rubbery materials. Many are complicated to use and involve parameters that are not easily linked to physically measurable quantities. The use of physical interpretations are a good approach to explain the changes in the material that leads to the Mullins effect, involving microstructural ruptures and rearrangements, mainly focus on the filler-rubber interaction. However, none of the current theories are able to explain by themselves the full phenomenology and the combination of mechanisms of deformation for filled elastomers.

Other manifestations of the Mullins effect can help clarify different aspects during the mechanism of deformation, such as the influence of complex deformation history on energy dissipation, viscoelasticity and induced anisotropy. These variables are usually neglected due to the difficulty to acknowledge. Early stage research is attempting to introduce these aspects in more complex mathematical models. In order to contribute to the development of new modelling approaches, the investigation presented in this thesis is predominantly experimentally focussed, identifying new experimental techniques to analyse the manifestations of Mullins effects. Additionally, the use of five different filled vulcanised compounds will give insight of not only the effect of the compound, but also of the manufacturing process in the mechanical response.

2.10 Aim and objectives

The aims of this project are (1) to understand the influence of deformation history in the modification of the mechanical response and softening phenomenon, (2) to comprehend how the mode of deformation can alter the mechanism of deformation of vulcanised carbon-black filled elastomers and (3) to propose a simple physical approach for the prediction of the mechanical response of filled elastomers, accounting the influence of deformation history.

The main three objectives of this thesis are (1) to investigate how different modes of deformation history such as uniaxial, equibiaxial and constant width deformations can alter the mechanical response and the energy dissipated during deformation, (2) to determine the variation in the stress relaxation response when the elastomer is subjected to strain history variations, and (3) to elucidate the anisotropy induced by both the processing technique and deformation during service.

In order to understand the influence of deformation history, experimental data will explore the changes in energy during cyclic deformation, together with time-dependent response under stress relaxation experiments. It is of commercial interest to understand how the scragging process modifies the mechanical response. Together with variation in strain history conditions, experimental data can guide to general suggestions and implications for phenomenological model development. Swelling studies will be performed to elucidate how processing and deformation changes the orientation of the network. The exploration of time-dependent behaviour, energy dissipation, and induced anisotropy, are relatively unexplored aspects of the Mullins phenomenon.

Chapter 3   **Preparation and characterisation of filled elastomers**

3.1   Introduction

A description of the five filled elastomers used in this work is presented in this Chapter. Section 3.2 gives an introduction to each material, describing the chemical structure and typical commercial applications. Section 3.3 describes the vulcanisation and processing methods used for the preparation of the materials. Subsequently, the physical characterisation, such as density and hardness analysis, carried out on the materials are detailed in Section 3.4. A microscopic investigation of the elastomers using electron microscopy is described in Section 3.5. Basic mechanical properties under uniaxial and biaxial tension are presented Section 3.6. A final discussion of the principal differences in term of the physical and mechanical properties can be found in Section 3.7.

It should be noted that due to confidentiality restrictions imposed by the material suppliers, the precise formulation of some of the elastomer compounds are proprietary.

3.2   Materials

3.2.1   Ethylene Propylene Diene Rubber

Ethylene propylene diene rubber (EPDM) is a thermoplastic polyolefin that contains a copolymerisation of ethylene and propylene. When these two structures are polymerised separately, semicrystalline thermoplastic polymers with poor elastic properties are created. On the other hand, a copolymerisation using a Ziegler-Natta catalyst generates an amorphous material with rubbery properties when cross-linked. The high resilience and good resistance to abrasion, oxidation and heat [22, 66] serve commercial

applications such as jacketing systems, automotive sealing systems, electrical applications, dampers and seals.

The chemical structures of the monomers in the main chain are presented in Figure 23 (a) and (b). The final structure is a random arrangement of the monomers sequence. The addition of a third monomer, a diene such as dicyclopentadiene (DCPD), ethylidene norbornene (ENB) or 1,4-hexadiene, is added (up to 10 % weight) to include unsaturated sections in either a lateral chain or in a cyclic structure [133]. The variation of the diene selected will mainly affect the vulcanisation activation and rate, depending on the position of the double bond in the lateral chain [134]. The structures of three possible dienes that can be use are also presented in Figure 23 (c), (d) and (e).

(a) $-\left(CH_2-CH_2\right)_x-$ (b) $-\left(CH_2-CH\right)_y-$
$$|$$
$$CH_3$$

(c) $-\left(CH-CH\right)_z-$ (d) $-\left(CH-CH\right)_z-$ (e) $-\left(CH_2-CH\right)_z-$
$$CH_2 \qquad\qquad CH_2 \qquad\qquad\quad CH_2-CH=CH-CH_3$$
$$CH$$
$$CH_3$$
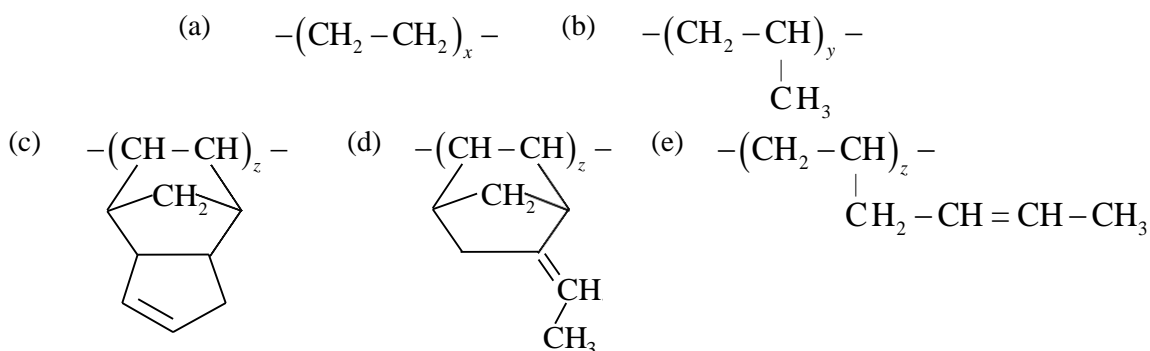
Figure 23. Chemical structures of the EPDM monomers: (a) Ethylene, (b) Propylene. Dienes: (c) Dicyclopentadiene (DCPD), (e) Ethylidene norbornene (ENB) and (f) 1,4-hexadiene.

In this work two types of EPDM were examined. The first was a sulphur cross-linked oil extended carbon black filled EPDM, denoted as EPDM1, provided unvulcanised by Dr T. Alshuth from the German Institute of Rubber Technology (DIK). A first batch was initially used, labelled as EPDM1a. This material was provided by DIK in 2008. To continue with the set of experiments, a second batch was provided in 2014, denoted as EPDM1b. As will be presented in the characterisation analysis, both are nominally identical. Nevertheless, due to ageing of EPDM1a, a small difference in the mechanical response was found. The second elastomer was a carbon black filled EPDM provided pre-vulcanised using sulphur by J-Flex Rubber Products, identified as EPDM2, and supplied in ~0.5 mm thick sheets.

3.2.2   Acrylonitrile Butadiene Rubber

Acrylonitrile-butadiene copolymer or NBR is an oil-resistant rubber with good abrasion and thermal stability. Commonly known as nitrile rubber in industry, it is widely used in packers, seals and hoses for the oil and gas industry, where chemical solutions and fuels

are transported. The oil-resistance is attributed to the nitrile segments. Although a higher content of acrylonitrile gives a better resistance to oil, hysteresis and resistance to abrasion [134], it also decreases flexibility and the glass transition temperature [22]. The content of acrylonitrile can vary between 18 % and 45 % depending on the application requirements [134]. One disadvantage of NBR is that it is susceptible to oxidation and ozone degradation due to the position of the butadiene in the main chain (see Figure 24), containing the double bond necessary to vulcanise with sulphur.

$$-\left(CH_2-CH{=}CH-CH_2\right)_x-\left(CH_2-CH\right)_y- $$
$$C \equiv N$$
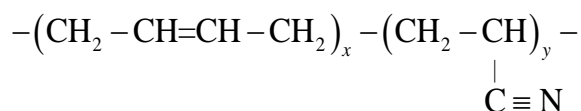
Figure 24. Chemical structure of the acrylonitrile butadiene copolymer NBR.

In this work, carbon black is used as reinforcement filler in NBR. The preparation of this material was made following the compositional and physical properties in accordance to the British Standard BS 2751 [135]. The standard stipulates that no less than 4 p.h.r. of zinc oxide (activator agent) and at least 2 p.h.r. of antioxidant should be incorporated. The vulcanisation process was carried out by J-Flex Rubber Products with sulphur and an organic accelerator. Long sheets of ~0.5 mm thick were produced using a calender.

3.2.3   Chloroprene rubber

Chloroprene rubber, CR, is commonly referred as polychloroprene or Neoprene (DuPont trade name). This homopolymer exhibits good abrasion resistance, oil resistance and mechanical strength. CR is typically used in gaskets, joint seals, hoses and cable jacketing, particularly in the aerospace and the automotive industries [133]. The initial chloroprene monomer contains two double bonds in the main chain, allowing four possible structural units during the free radical polymerisation, as illustrated in Figure 25.
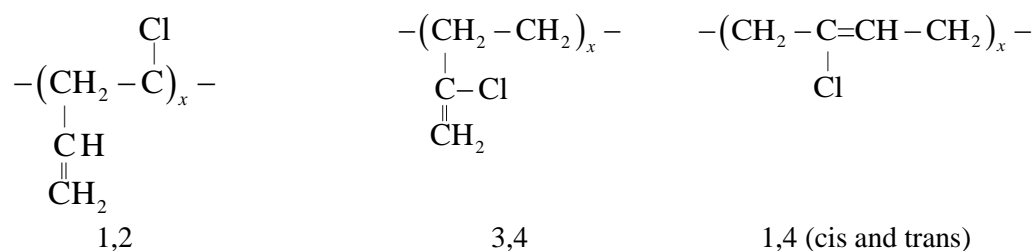
Figure 25. The four possible configuration units for the CR repetitive chain.

The different grades of commercial CR will depend on the distribution of these

structures, controlled by changing the polymerisation conditions. The inclusion of chlorine (Cl) in the chain imparts flame resistance (self-extinguishing) [134], but also stiffens the chains and reduces the chemical reactivity of the double bond. This increases the oxidation resistance and makes less probable the vulcanisation via sulphur. Following the British Standard BS 2752 [136], the material used in this work was reinforced with carbon-black and vulcanised with metallic oxides (ZnO and MgO) and with no less than 2 p.h.r. of an antioxidant. The material was provided by J-Flex Rubber, sheet rolling processed to produce long sheets of approximately 0.5 mm thickness.

3.2.4   Natural Rubber

Natural rubber, NR, is still the most common rubber chosen for multiple applications in industry. Figure 26 present the chemical structure of cis 1,4-polyisoprene. The cis configuration confers high tensile strength, fatigue and tear resistance and good dynamic properties [1, 133]. Due to these properties, the main application of NR includes automotive tires, gloves, sealants, adhesives, footwear and dampers. The vulcanization method is mainly through sulphur cross-link, using the double bonds reactivity. The carbon black filled NR compound was supplied unvulcanised by Trelleborg Industrial AVS. The vulcanisation process was carried out in-house using compression moulding, as detailed in Section 3.3.1.

$$-\left(CH_2 \quad CH_2\right)_x -$$
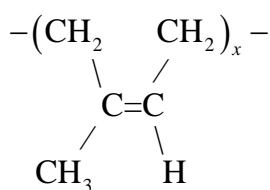
Figure 26. Chemical structure of cis 1,4 polyisoprene, or natural rubber.

3.3   Materials preparation methods

Following mixing, the final process of manufacturing rubber is the vulcanisation stage. Due to the irreversibility of the cross-links, the material should be formed into the desired specific geometry during cross-linking. In the case of EPDM1a, EPDM1b and NR, the materials were provided unvulcanised. Hence, the vulcanisation stage was carried out by in-house compression moulding. Vulcanised sheets of NBR, CR and NR,

as received from the supplier were produced using a sheet rolling process.

3.3.1   Compression moulding

Compression moulding was used to vulcanise sheets of EPDM1a, EPDM1b and NR for subsequent testing. The unvulcanised rubber was moulded using a hand operated hydraulic Daniels heated press [137]. The mould consisted of a stainless steel frame 150 mm × 150 mm × 0.7 mm, as illustrated in Figure 27. Figure 27 (a) shows the unvulcanised compound positioned in the mould prior to moulding with a slight excess of material to ensure that the cavity volume is completely filled. The dimensions of the moulded sheet are dictated by the inner cavity frame and the thickness of the mould as shown in Figure 27 (b).
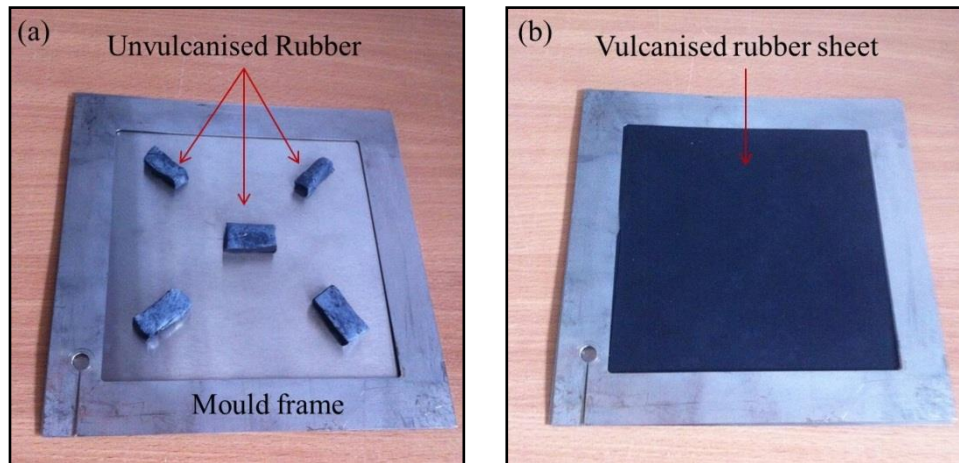
Figure 27. Mould frame to produce compressed moulded sheets. (a) Placement of the unvulcanised rubber in the frame cavity. (b) Final sheet after vulcanisation by compression moulding.

The mould was placed in a sandwich stack between sheets of stainless steel and mounted in the heated press. A detailed schematic diagram of the mould arrangement is presented in Figure 28. Prior to moulding, the stainless steel sheets were cleaned with acetone. No lubricant was needed to aid in the removal of the rubber sheets after the vulcanisation process.

The moulding time and temperature employed for each material was provided by the suppliers. In Table 6 the vulcanisation temperature, T_v, and time, t_v, suggested by the suppliers is presented. The final thickness of the sheet moulded is also reported as an average of nine measurements made across the sheet. Once the mould and the rubber are positioned between the platens, the material is then heated by conduction. At the end of the process, the specific specimen shape is cut from the sheets using a shaped cutter,

depending on the specimen profile needed.
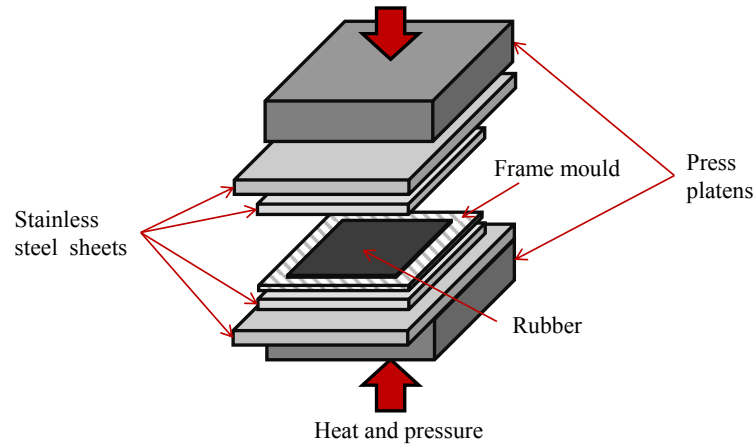
Figure 28. A schematic diagram of the compression moulding set up.

Table 6. Vulcanisation temperature T_v, and time t_v conditions during compression moulding, and final thickness for EPDM1a, EPDM1b and NR. (±2 SD)

Elastomer	Supplier	T_v (°C)	t_v (s)	Thickness (mm)
EPDM1a	DIK	160	780	0.709 ± 0.008
EPDM1b	DIK	160	470	0.683 ± 0.020
NR	Trelleborg	160	600	0.748 ± 0.045

The moulding procedure for the rubbers consisted of an initial stage of 60 seconds of pressure cycling (a total of 3 cycles) from 0 bar up to 100 bar to remove any air trapped in the cavity and ensure a better flow of the rubber. Next, the pressure is held at 150 bar for the rest of the vulcanisation time specified as reported in Table 6. After removing the moulding arrangement from the heated press, the vulcanised rubber is then carefully removed from the frame cavity mould and allowed to cool at room temperature. No mould release or cooling monitoring was used. The moulding process temperature cycle was recorder using a thermocouple and is presented in Figure 29 (a) and (b) for EPDM1b and NR respectively, with EPDM1a following a similar moulding process.
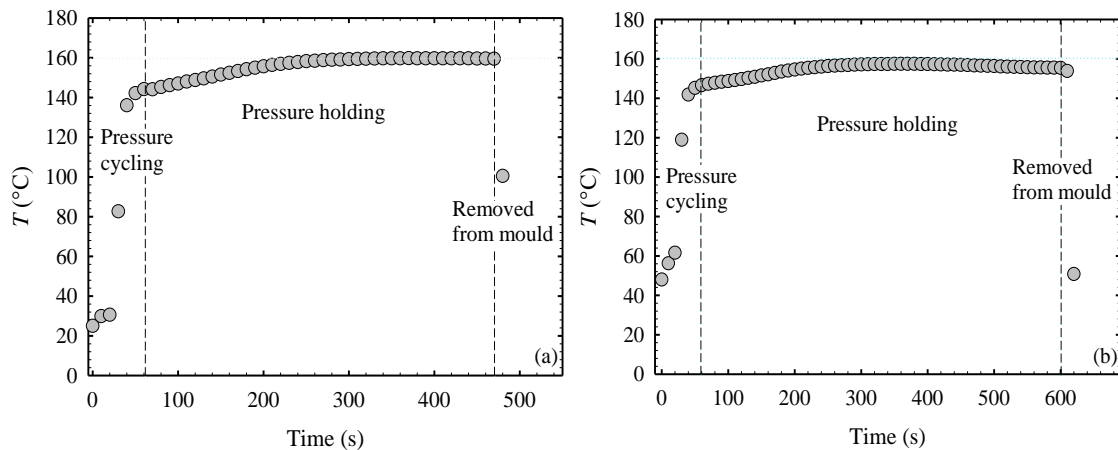
Figure 29. Moulding temperature as a function of time during vulcanisation for (a) EPDM1b and (b) NR.

3.3.2 Sheet rolling process

A very common method to create vulcanised rubber sheets is through the rolling or calendering process, as illustrated in Figure 30. After the mixing process (through a mixing mill [25]), the unvulcanised rubber is fed into a series of temperature controlled horizontal rolls. The heat is transferred to the rubber compound during the rolling process, vulcanising the rubber. The temperature, velocity and number of rolls can be modified depending on the manufacturing criteria. The final thickness of the sheets is controlled by the gap between the rolls. The rolling processed materials EPDM2, NBR and CR used in this work were provided by J-Flex Rubber Products with a fixed thickness of ~0.5 mm.
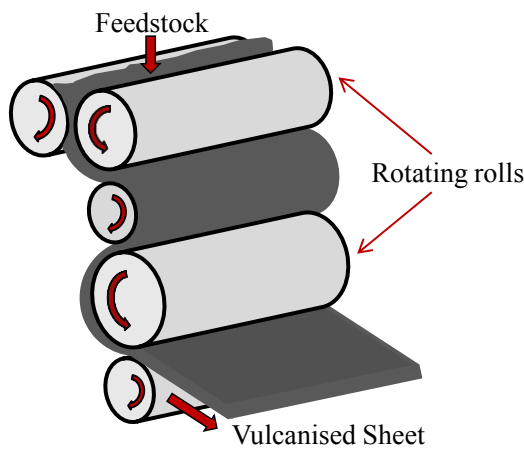
Figure 30. A schematic diagram of the final stage of the rolling process.

3.4 Physical characterization

3.4.1 Density measurement

The measurement of density ρ_2 is one of the simplest tools used in the rubber industry to identify and control rubber compounds. This intrinsic property is directly linked with the formulation and cross-linking process of the elastomers. The densities of the materials studied in this work were measured using a Mettler Toledo XS105DU analytical balance fitted with a density kit. De-ionised water was used as the fluid medium. Rectangular specimens of 20 mm × 20 mm × 0.5 mm were cut from vulcanised sheets of each material. The density kit follows the Archimedes' principle that states that every solid immersed in a known fluid will be buoyed by a force equal to the weight of the displaced fluid. The density of each specimen is determined by

weighing the specimen in air and in water. The water temperature was recorded with a precise mercury thermometer prior to the measurements. Three consecutives repeats of three different specimens were measured. The average of nine measurements of ρ_2, for each material, is reported in Table 7 with two standard errors from the mean.

Table 7. Average density measurements for the cross-linked elastomers studied. ($\pm$ 2 SD)

	Elastomers					
	EPDM1a	*EPDM1b*	*EPDM2*	*NBR*	*CR*	*NR*
ρ_2 (gr/cm^3)	1.029 ±0.003	1.026 ±0.003	1.139 ±0.005	1.215 ±0.004	1.371 ±0.007	1.072 ±0.008

3.4.2 Shore A hardness measurement

Hardness is a common physical property used in the industry to classify rubbers. This property is defined as the material resistance to indentation. A higher hardness value indicates a higher resistance to indentation. A Shore *A* durometer was employed according to BS ISO 7619-1 [138] to measure the hardness, *H*. The test is carried out by pressing the specimen at a fixed pressure using a measuring probe. The durometer records how far the measuring probe can penetrate into the rubber. The final measure is reported as Shore *A* or International Rubber Hardness Degrees (IRHD) units. According to the British Standard, the thickness recommended for this test is at least 6 mm. As all the specimens have thickness of approximately 0.5 mm, the test was carried out using layers of sheets. In order to determine the influence of the number of sheet layers on the hardness measurement, an exploratory test was performed on EPDM2. It was found that a stack of more than 7 layers (3.5 mm) had only a very limited effect on the hardness measurement as evidenced in Figure 31.
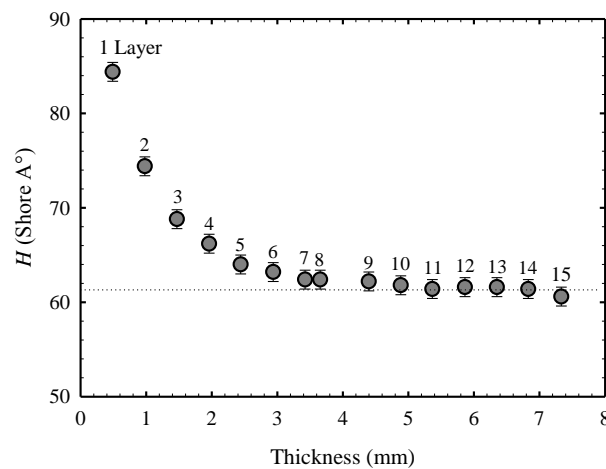
Figure 31. Hardness *H* Shore A° measurements of EPDM2 as a function of the incrementing rubber sheets thickness that was achieved by stacking the sheets.

The averages from five measurements on each material are reported in Table 8, with two standard errors from the mean. According to the specification of the British Standards followed by the manufactures, NBR can be classified as BA70 (BS 2751[135]), CR as C60 (BS 2752 [136]) and the NR studied can be classified as Z50 (BS 1154 [139]). The wide range of the hardness value reported for the materials studied indicates a noticeable difference in the physical properties, also reflected in the mechanical response that will be presented in Section 3.6.

Table 8. Hardness *H* Shore *A* average measurements for vulcanised elastomers studied (± 2 SD)

	Elastomer					
	EPDM1a	*EPDM1b*	*EPDM2*	*NBR*	*CR*	*NR*
H Shore A°	55 ± 1	54 ± 1	61 ± 1	72 ± 1	61 ± 1	55 ± 1

3.4.3   Glass transition temperature

The most important thermodynamic phase transition observed in elastomers is the glass transition, T_g. The lower the glass transition temperature, the wider the temperature window where the material behaves predominately in an elastic manner. The glass transition temperature of elastomers can be easily analysed using differential scanning calorimetry, DSC. Thermal analysis was carried out using a Thermal Analysis (TA) Instrument DSC Q10 differential scanning calorimeter (DSC). Disc samples of ~8 mg were cut from the vulcanised sheets using a punch cutter. The disc shape ensures a homogenous distribution of the material in the pan and effective heat conductivity, reducing the possibility of thermal lag [140]. Hermetic aluminium pans were used to encapsulate the specimens. A heat-cool-heat cycle between -75 °C and 140 °C was performed for all materials. In the first stage, the sample was heated to 140 °C at a rate of 20 °C.min^{-1} from room temperature to erase any thermal history, followed by cooling to -75 °C and reheating to 300 °C at the same temperature rate. Nitrogen purge gas at a flow rate of 100 ml.min^{-1} was used to prevent oxidation and any air contamination of the samples. The second heating stage was used to determine the T_g. Three specimens for each material were tested for repeatability. A baseline was determined with empty pans prior to the experiments. The baseline signal records noise level in the instrument that is commonly attributed to the residual heat flow associated with asymmetry of the heat flux or contamination in the DSC cell from previous experiments [140]. This signal is subtracted from the specimen thermogram for a more accurate signal of the specimen, as shown in Figure 32, which illustrates a typical curve of the derivative of heat flow as

a function of temperature.
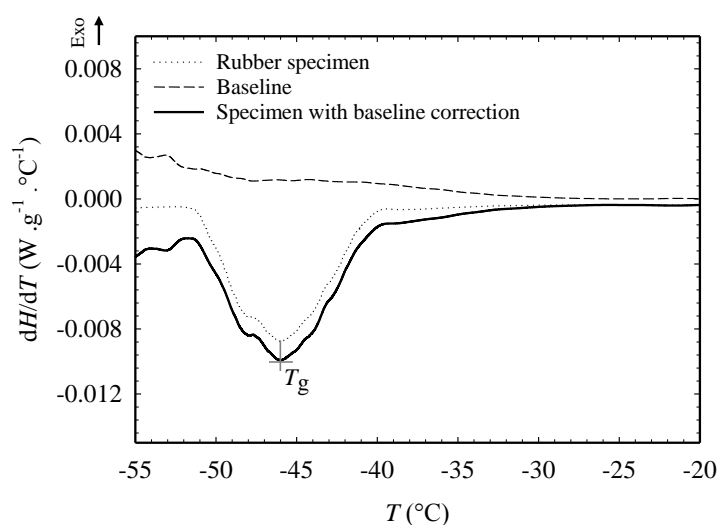
Figure 32. An illustration of the derivative of heat flow with respect to temperature of the baseline of a EPDM2 specimen and the specimen signal after subtracting the baseline.

The glass transition can be determined according to two techniques. The first one uses the temperature at the mid-point inflection between tangent lines of the heat flow temperature signal, according to the British Standard ISO 11357 [141]. The second method uses the derivative of the heat flow temperature signal, using the temperature at the peak related with the change of heat flow due to the transition. The T_g was determined using TA Universal Analysis software. Both methods were used to calculate the T_g. Figure 33 shows the thermogram in the T_g region for all vulcanised materials studied, with both the heat flow and derivative heat flow technique.

Although less than 1°C difference was observed between both measurements techniques, the first technique is more user-dependent. Therefore, the second method was selected to calculate the averages of three repeats that are reported in Table 9, with two standard errors from the mean, referring to a 95 % confidence interval. As EPDM1a and EPDM1b produced identical thermograms, only EPDM1b is shown.
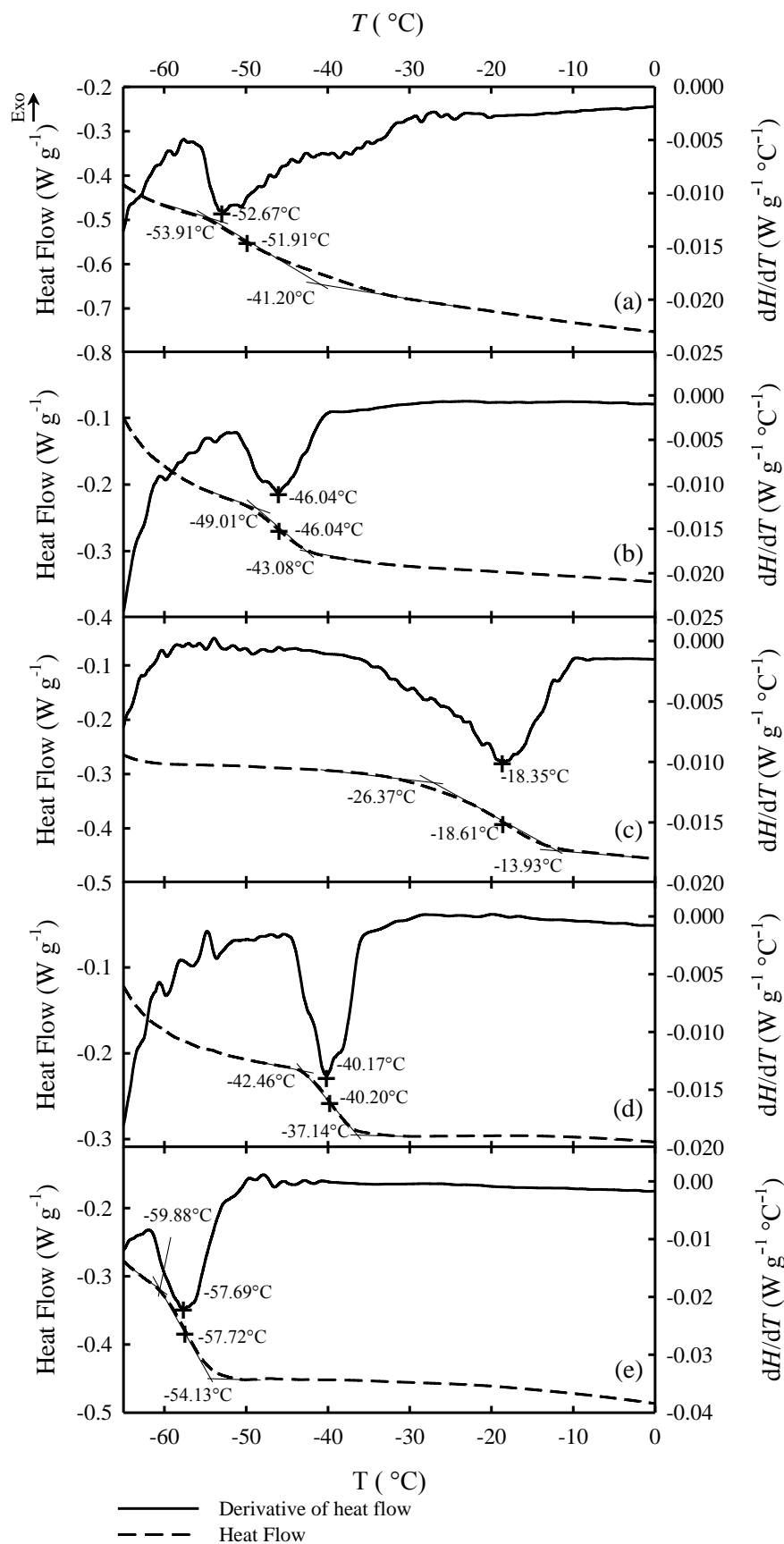
Figure 33. Determination of T_g by the peak of dH/dT and by the middle inflection point of heat flow as a function of temperature for (a) EPDM1b, (b) EPDM2, (c) NBR, (d) CR and (e) NR.

Table 9. Glass transition temperatures T_g, for the cross-linked elastomers studied using the peak of derivative heat flow method (± two standard errors from the mean)

	Elastomer					
	EPDM1a	*EPDM1b*	*EPDM2*	*NBR*	*CR*	*NR*
T_g (°C)	-51.95 ±1.77	-52.08 ±1.55	-47.35 ±1.16	-17.89 ±0.50	-39.89 ±0.47	-57.03 ±0.76

3.4.4 Determination of compound content through thermogravimetric analysis

The degradation profile of an elastomer is generally used to give an approximate percentage of the oil, polymer, filler and any organic residue of the compound [142]. As the carbon black content is unknown for all the materials, an approximation of the carbon black filler content can be determined using thermogravimetric analysis (TGA) with a TA Instrument SDT Q600. This technique monitors the change of mass in a specimen as it is heated though a specific temperature and atmosphere protocol. This method is a very common tool in analysing the composition and thermal stability of vulcanised elastomers [142-144].

Disc specimens of ~15 mg were cut from the vulcanised sheets using a punch cutter and inserted into a platinum pan that was previously cleaned using a blow torch to remove moisture and avoid any residual material. After the sample and reference pans are placed in the furnace, the system is stabilised for five minutes with flowing purge gas. Samples were first heated from room temperature to 550 °C at a rate of 10 °C min^{-1} under a nitrogen atmosphere to avoid carbon oxidation. Within this temperature range, evaporation and degradation of any oils, additives and main polymer takes place without oxidation of the polymer. The specimen is subsequently cooled to 300 °C at the same rate and then the atmosphere changed to air, followed by heating to 800 °C at a rate of 10 °C min^{-1} to measure the carbon oxidation and the ash residue.

The weight loss and rate of weight change curve as function of temperature were analysed using the TA Universal Analysis software. Typical thermograms for the decomposition of the materials are presented in Figure 34, showing the weight loss corresponding to the most important components of the formulations. During the initial stages of degradation under nitrogen atmosphere, oils and plasticizers are the first to volatise when the temperature is below 150 °C. Generally, the degradation occurs in two steps. The first step is associated to the polymer degradation whereas the second step corresponds to carbon black filler degradation. The residue obtained at ~600 °C comprises carbon black and any other filler and zinc oxide [145]. As EPDM1a and

EPDM1b present very similar thermograms, only EPDM1b is presented.

In elastomers with heteroatoms, such as CR and NBR, the protocol to analyse the thermal degradation has to be more carefully examined in the air atmosphere region due to high content of carbonaceous residues on pyrolysis [143]. For this reason, all the tests are cooled under inert conditions to 300 °C immediately after the pyrolysis of the polymer at 10 °C min^{-1}, to ensure a more distinguishable mass decrease difference between the residual carbon from the polymer and the carbon black filler. For NBR, a mass degradation is observed after 600 °C, related with carbon degradation of a filler such as graphite, commonly used as filler for NBR [146].

There are three possible methods to determine the range of weight loss for every component. The first option uses the overlay method to separate the weight loss by superposing the filled and unfilled polymer thermogram. The second method uses the extrapolation of the gradient of the curve during the weight loss, with the intercept of the tangent lines indicating the weight and temperature of separation. The third technique measures the weight loss at the derivative minimum point [143]. The last technique was used to calculate the weight loss as it gives an acceptable accuracy without the need for the pure polymer thermogram reference, and is less user dependent. Table 10 reports the average of three repeats for each material, indicating the percentage content of the weight loss peaks with two standard errors from the mean.

Table 10. Estimated oil/plasticiser, polymer, carbon black filler and residues content of vulcanised elastomers. Thermogravimetry was performed under a combination of nitrogen and air atmospheres

Composition (%)	Elastomer					
	EPDM1a	*EPDM1b*	*EPDM2*	*NBR*	*CR*	*NR*
Oil/Plasticiser	2.95 ±0.08	4.57 ±0.13	2.52 ±0.14	6.57 ±0.26	-	-
Polymer	70.22 ±0.78	68.25 ±0.69	56.70 ±0.50	55.73 ±0.33	44.36 ±0.66	72.27 ±0.24
Pyrolysis	-	-	-	2.00 ±0.01	21.10 ±0.52	-
Carbon black	24.99 ±0.30	24.59 ±0.15	34.53 ±1.08	22.59 ±0.33	31.16 ±1.14	21.88 ±0.24
Graphite	-	-	-	2.29 ±0.12	-	-
Residue	1.84 ±0.96	2.25 ±0.76	5.85 ±0.68	10.87 ±0.97	2.68 ±1.15	5.57 ±0.38
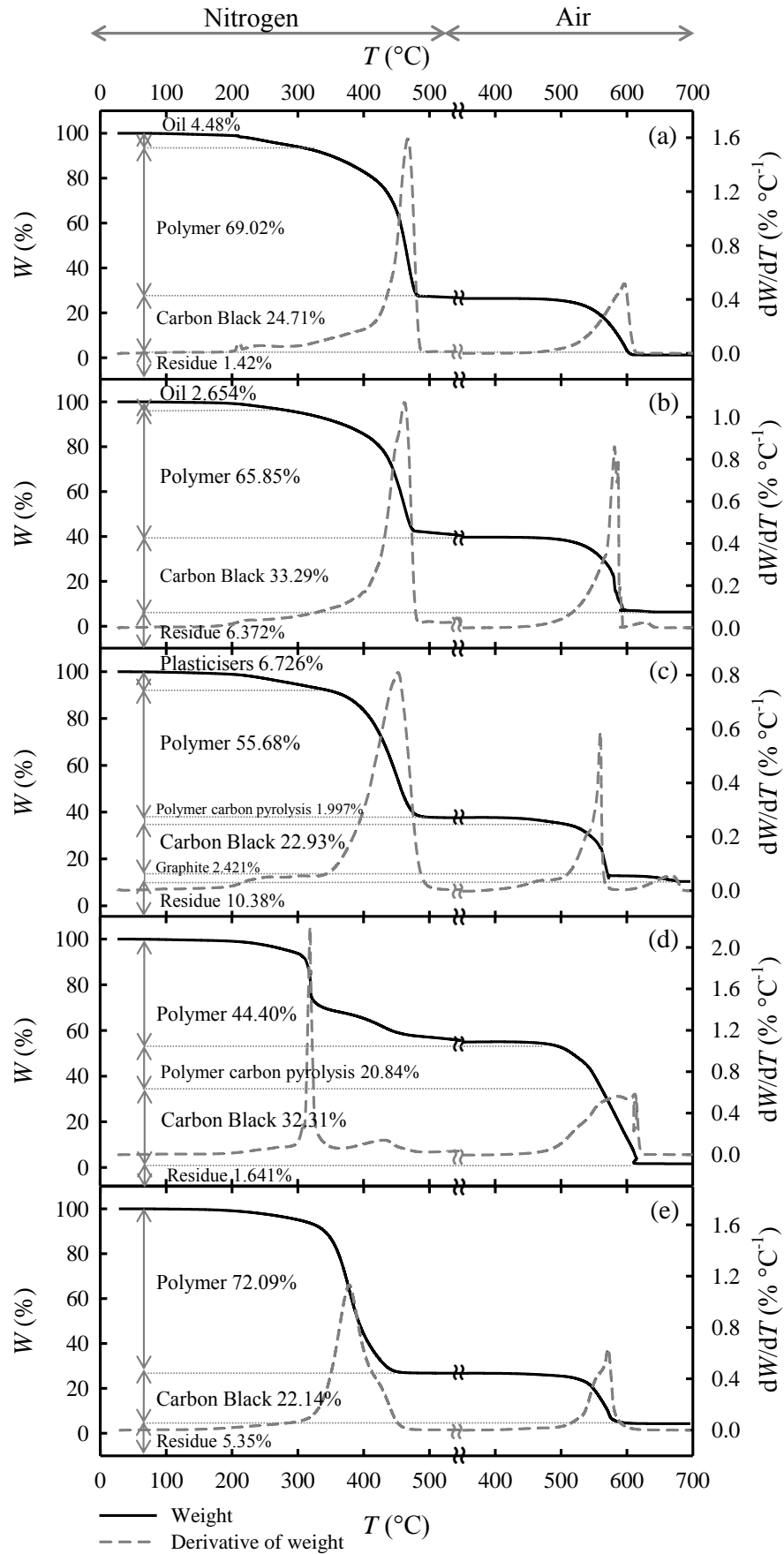
Figure 34. Thermogravimetric curves with weigh loss content description for elastomers (a) EPDM1b, (b) EPDM2, (c) NBR, (d) CR and (e) NR.

3.5   Microscopic characterisation

Industry employs microscopic techniques such as scanning electron microscopy, SEM, to analyse dispersion of polymer blends or fillers and fracture mechanisms of products [147, 148]. This is a relatively fast way to provide a description of the morphology and of the dispersion of the fillers in the rubber matrix [30]. SEM was initially explored for this work as a means of examining of the cross-section of the materials in order to define differences between the materials and as an effort to have more information about the materials compositions.

An SEM image is formed by scanning a focused electron probe across the surface under probe [149]. In order to obtain an image, a signal is selected by regulating the strength of the electron probe to display the clearest signal [143]. A magnification range between 20x and 100000x can be obtained, depending of the equipment resolution and electron signal. The specimen must be located within a vacuum system to permit the electrons to reach the specimen surface without the interfering with particles in the atmosphere [149].

3.5.1   Sample preparation and method

The elastomer sheets were cryogenically fractured with liquid nitrogen to a length of ~10 mm to fit into the SEM vacuum chamber. The specimens were mounted on a 90° angle specimen stub using a double-sided carbon tape. The fracture surface of the specimen was parallel to the stub surface to examine the fractured cross-section. The specimen surface needs to be conductive to enable the electron beam to strike the surface and transmit without charging the specimen and damaging it [149]. This is achieved by coating the specimen fractured surface with a platinum layer of approximately 10 μm thickness. SEM was performed using a Philips XL30 FEG ESEM operating at 20 kV.

3.5.2   SEM micrographs

Due to limitations of the spatial resolution of the SEM, it is not possible to analyse the filler structure within the rubber matrix. However, an interesting optical evaluation can be made on the dispersion of the filler and other additives. Figure 35 and Figure 36 shows a set of electron micrographs for each material at different levels of

magnification. For EPDM1a and EPDM1b, as both materials have the same formulation, EPDM1b was chosen to be analysed microscopically. In all the samples the presence of dispersed aggregates in the rubber matrix can be observed at resolutions higher than 5000x.

Energy dispersive spectrometry was used as an alternative tool in SEM to measure the energy and distribution of the signal generated by a focused electron beam in the specimen. The signal recorded can be related with the characteristic wavelength of the elemental composition, providing insights into the additives present in the materials.

Zinc oxide, ZnO, was found in EPDM1b, NBR, CR and NR. Figure 35 (b) shows tubes of ZnO in EPDM1b and a combination of hexagonal shapes and agglomerates are observed in NBR, CR and NR (Figure 36 (b) (d) and (f) respectively). Calcium carbonate, $CaCO_3$, agglomerates of around 10 μm, usually used as filler, was detected in EPDM2, as shown in Figure 35 (d). Traces of magnesium oxide, MgO, were detected in NBR specimens.

(a)

(b)

(c)

(d)
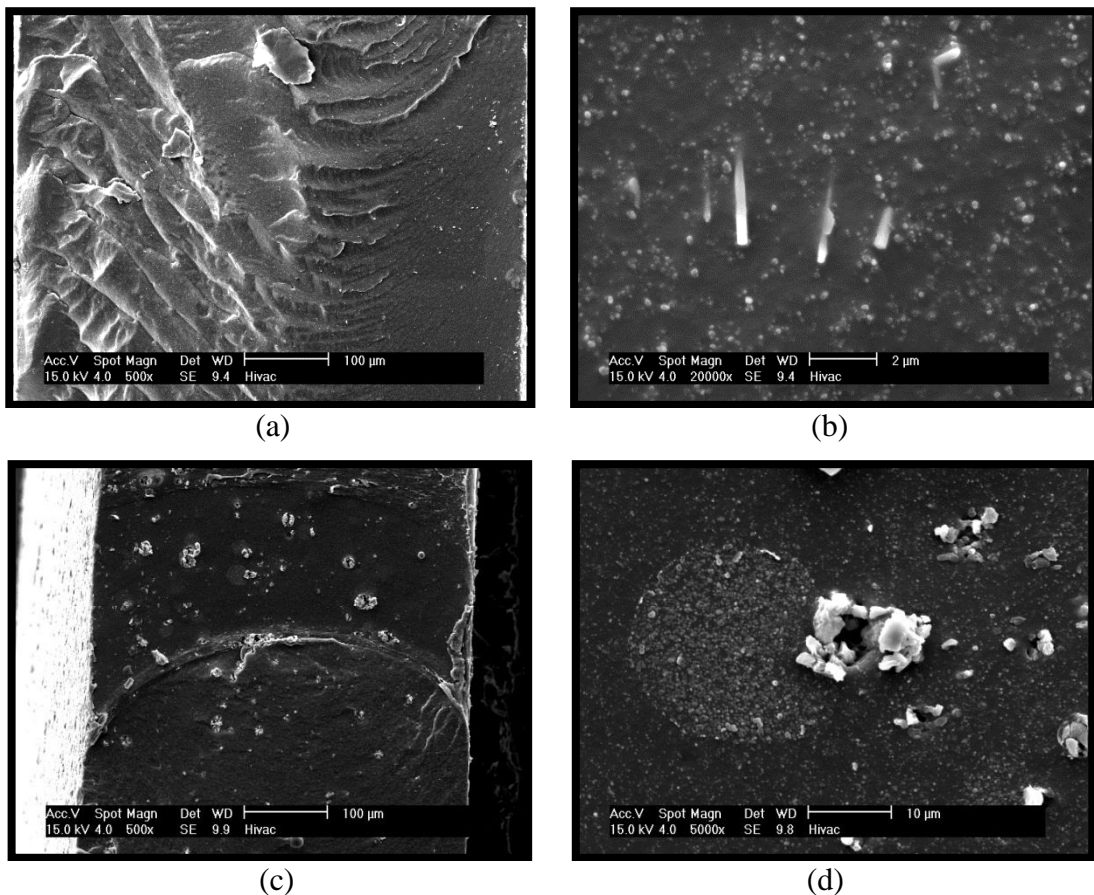
Figure 35. SEM micrographs of cryofractured (a-b) EPDM1b, (c-d) EPDM2.

(a) (b)

(c) (d)

(e) (f)
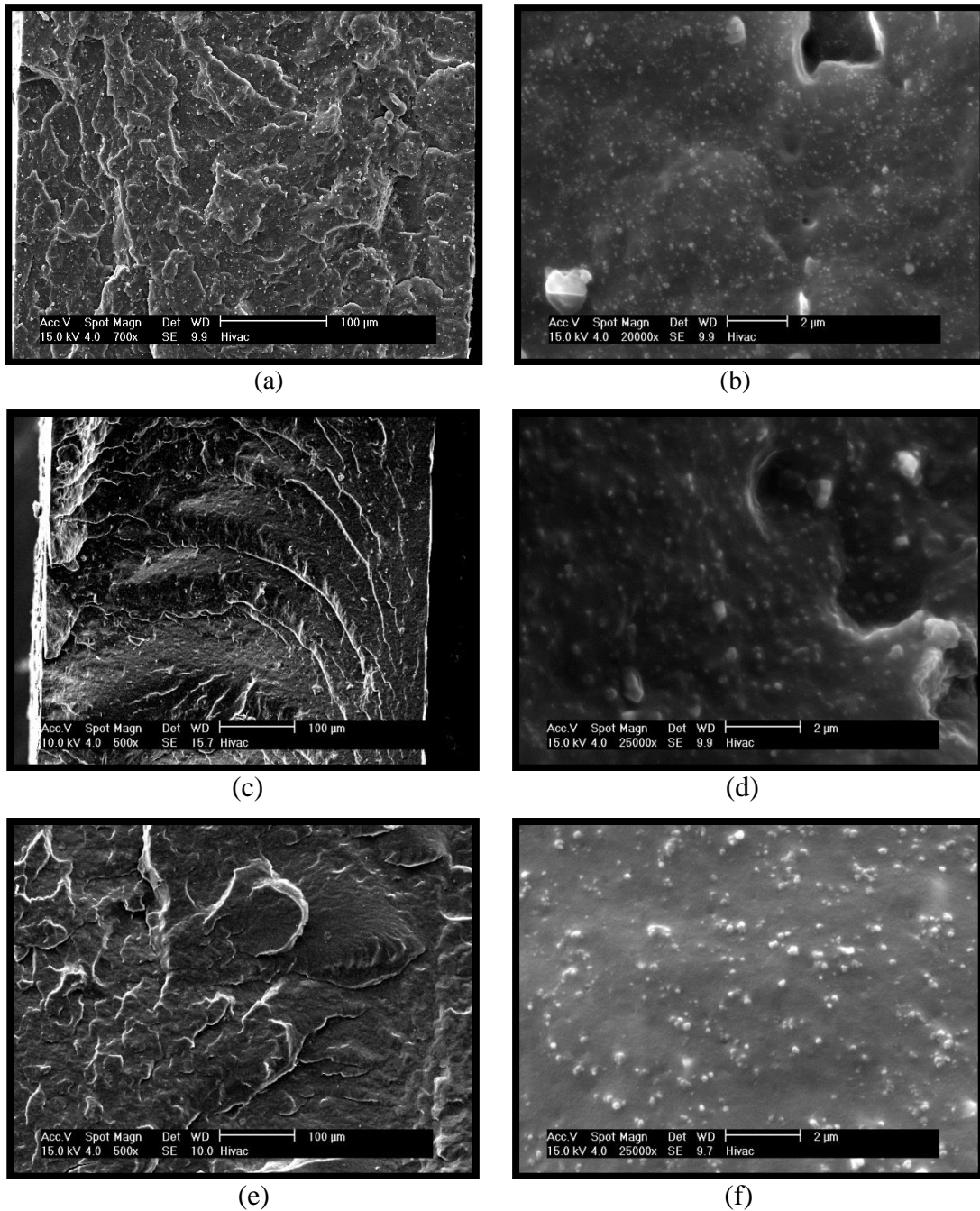
Figure 36. SEM micrographs of cryofractured (a-b) NBR, (c-d) CR, (e-f) NR.

3.6 Basic mechanical characterisation

3.6.1 Uniaxial tensile testing

Uniaxial mechanical deformation was carried out using an Instron 5969 tensile testing machine equipped with a 100 N load cell. Each specimen was mounted at the top grip and aligned vertically by visual inspection prior to gripping the bottom of the specimen. Due to the rubber flexibility, special care was taken during the gripping as a tight

adjustment can create buckling or slipping of the specimen. This effect can be minimised by visually monitoring the gripping procedure. For a more accurate recording of the axial deformation, an Instron counterbalanced travelling extensometer was connected to the uniaxial machine. The extensometer is based on a pair of counterbalanced clamps positioned to align with the centre of the specimen and fixed directly onto the specimen gauge length of 25 mm. Uniaxial tensile testing, UN, was performed to quantify the elastic modulus at 100 % elongation, $E_{100\%}$, the permanent set at 100% elongation, $\varepsilon_{per}^{100\%}$, the strain at fracture, ε_f, and stress at failure, σ_f.

3.6.1.1 Specimen preparation and methodology

Specimens were cut from vulcanised sheets using a hand-operated Wallace specimen cutting press fitted with a dumbbell shape cutter type 1BA according to BS ISO 527-2 [150]. In the case of the rubbers processed through rolling (EPDM2, NBR and CR), the specimens were cut parallel to the rolling direction. Individual specimen thicknesses were measured using a Hildebrand rubber thickness gauge according to ISO 23529 [151]. As the specimens are both flexible and thin, a measurement instrument such as a caliper is not suitable to determine the width direction due to the buckling of the material. As such, a calibrated HP Scanjet G4010 scanner system was used. Each specimen was scanned at 1200 DPI resolution, with a ruler positioned next to the specimen as shown in Figure 37. Image processing was performed using a Matlab image acquisition tool, as is described in Appendix D.1. A calibration of 47.24 pixels per millimetre was used to measure the width, providing a resolution of 0.02 mm. Tests were performed at room temperature (20 ± 1°C) and at constant cross-head speed corresponding to a nominal strain rate of 0.03 s^{-1}.
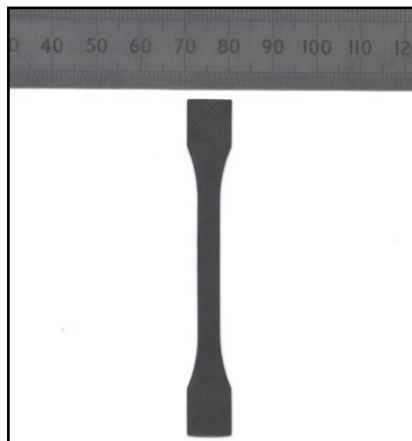
Figure 37. An illustration of the technique used to measure the dimension of a uniaxial tensile test specimen using a scanner.

Anisotropy due to material processing was also investigated cutting specimens parallel (//) and perpendicular (⊥) to the sheet role in the case of EPDM2, NBR and CR. For EPDM1 and NR, specimens were cut in perpendicular direction to each other to analyse possible anisotropy on the sheet.

3.6.2 Multiaxial tensile testing

In order to analyse the effect of different modes of deformation on filled elastomers, a special rig was used in this work, using a Flexible Biaxial Film Tester.

3.6.2.1 Flexible Biaxial Film Tester (FBFT)

Due to the need for experimental data evaluating multiaxial performance of polymeric materials, an automated horizontal biaxial tensile testing machine was developed. Buckley and Turner [152] originally developed the Flexible Biaxial Film Tester (FBFT) in order to assess multiaxial performance for elastomers and thin polymer films.

3.6.2.1.1 FBFT testing system description

The main features of this machine are: variable temperature, high test speed, complex cycles and real time video imaging of the specimen. The design of the machine allows biaxial extension along two independent axes and provides considerable flexibility in the experimental sequence. The FBFT is shown in Figure 38, illustrating all the parts that enable the movement of the motors to create a displacement on the grips, the heating system to control the temperature, the chamber with the recording camera and the National Instrument, NI, acquisition box to record the force and temperature.
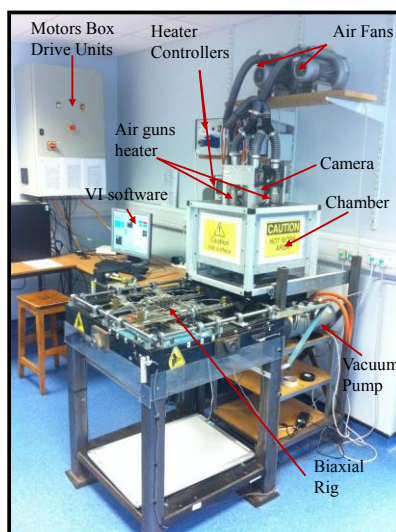
Figure 38. Flexible Biaxial Film Tester.

Each row of grips runs freely, with two independent brushless DC servo-motors on each axis, creating two independent test directions. The deformation can be applied in two axes simultaneously and independently. Each servo-motor is connected to a reverse-thread leadscrew with a load-bar, similar to a frame, as shown in Figure 39. The specimen is held around the perimeter of this frame by 24 miniature pneumatic piston grips, seven on each side. These grips are interconnected by a low friction scissor mechanism to ensure equi-spaced movement during the movement of the load-bars. The frame will move outwards when the corresponding axis landscrew rotates, leaving the centre of the specimen stationary. The use of servo-motors permits a wide range of strain rates covering up to 40 s^{-1} [152], a consequence of the high pitch of the leadscrews and the high torque and low inertia of this type of motor.
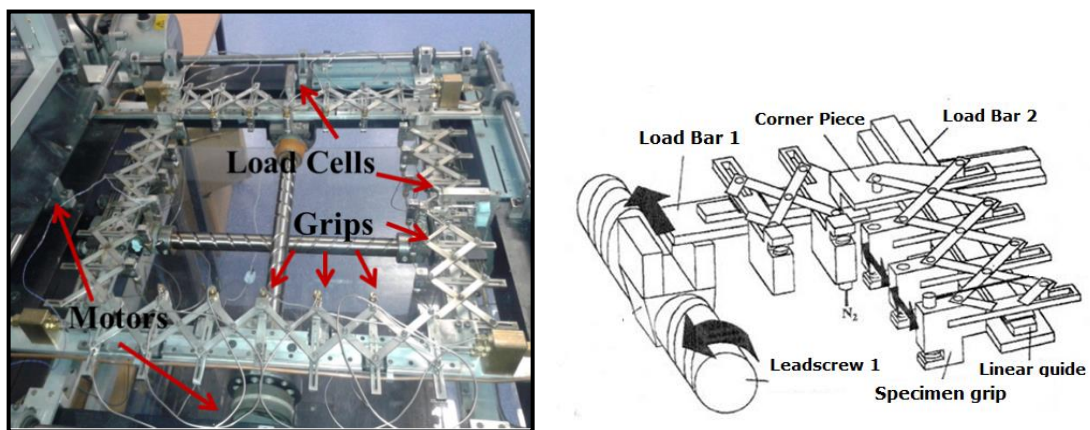
Figure 39. Grips system and schematic diagram of the load bar frames, with detail in the grips and leadscrews scheme. [56]

The temperature can be raised through a series of fan heaters in a movable chamber above the load bars frame. Air at room temperature is driven by fans located outside the chamber through four hot air guns located at the end of the air system which heat the air towards the specimen. The temperature can be controlled by the master heater controller using a thermocouple embedded at the exit of the air in the chamber. Another thermocouple is located in a grip next to the specimens to record the specimen temperature near the surface.

Typical specimens are square sheets of at least 75 mm wide with thickness between 0.3 mm and 0.6 mm. Using specimens of these dimensions, a nominal biaxial strain of 400 % is achievable. The strain measurement is made in the central region of the specimen by tracking markers using video recording, thus avoiding any effect from a non-uniform strain state in the region of the grips [56, 152]. A high-speed monochrome Mikrotron camera is located in the centre of the chamber. The camera allows a high

data rate of up to 500 fps at 1280x1024 pixels. An image acquisition board is used in the computer to record the images. Rubber specimens can be marked with plated-silver beads tracked by the camera. The separation between the beads is recorded to obtain the strain.

3.6.2.1.2 Testing software

A central grip on one side of each axis contains a 25 lb capacity load cell to measure the load during deformation. The force and temperature signals are captured by a data-logger interface via an IEEE-488 and sent to the National Instruments (NI) software in the computer. A complete outline of the control and recording system is presented in Figure 40. The servo motors are also controlled using NI software.
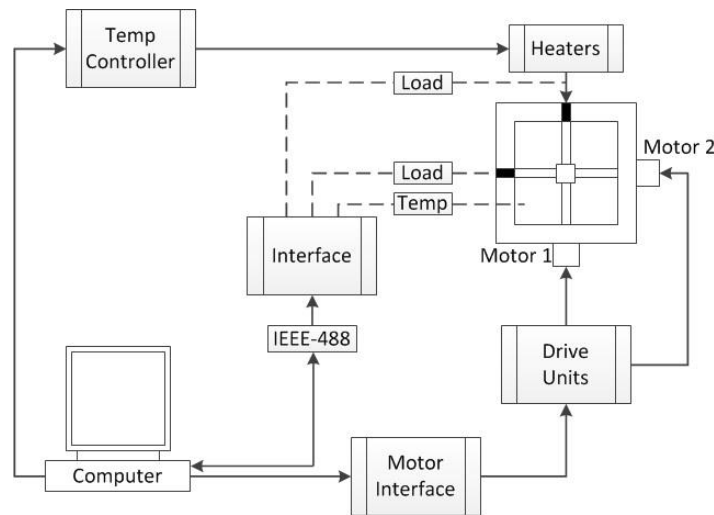
Figure 40. Schematic diagram of the system used in the FBFT.

In order to acquire and process the data, LabView software is used, including several extra modules to set up the motion profiles of the motors and camera recording. Figure 41 show the VI software interface developed, with the main features to control de machine.

The testing condition is designed by steps, where the strain and force can be controlled for both axes independently. The conditions are introduced manually on the top left of the interface, with an input sequence graph next to the steps table to illustrate the test condition of each axis. During the tests, a real time monitoring of the force and video recording during deformation allow to observe both the force and the stress (if the specimen dimensions are inserted previously in the software) as function of the strain. Likewise, a comparison between the grip displacement and the video displacement can be monitoring during deformation (not shown in the figure).
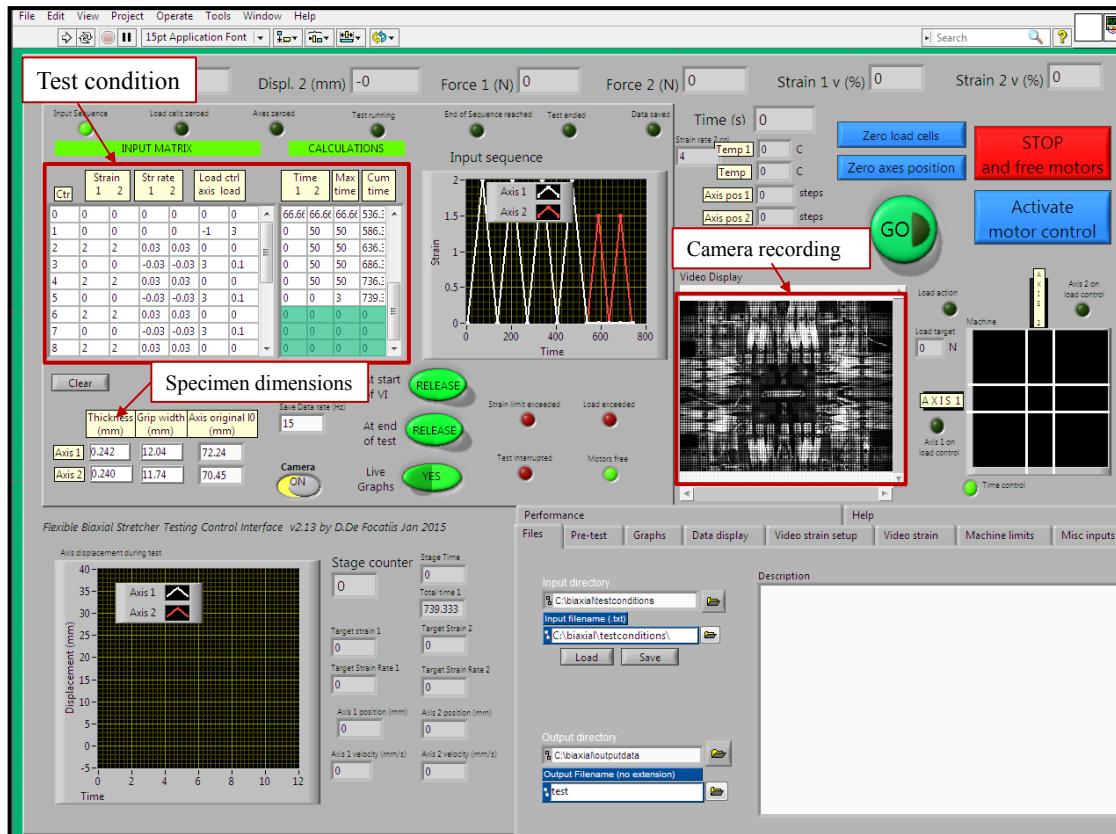
Figure 41. LabView software interface for the FBFT.

One of the main features of the machine and software is the possibility of a wide range of testing conditions as both axes can be programed independently. Figure 42 shows just a few examples of the strain conditions that can be set up to the FBFT. As each axis is programed independently, it is possible to set different strains and strain rates on each axis. Likewise, one experimental test can have several deformation combinations, depending on the study required. This work was focussed only in the analysis of the mechanical response under equibiaxial (a) and constant width (b) testing conditions.

Previous experimental data before the most recent software upgrade was presented by Buckley's research team [153-155], where a detailed description of the FBFT's capability is given [152]. Further work by De Focatiis et al. [80] extended the FBFT's use to elastomeric films. The FBFT was used in this work for both equibiaxial and constant width experiments.
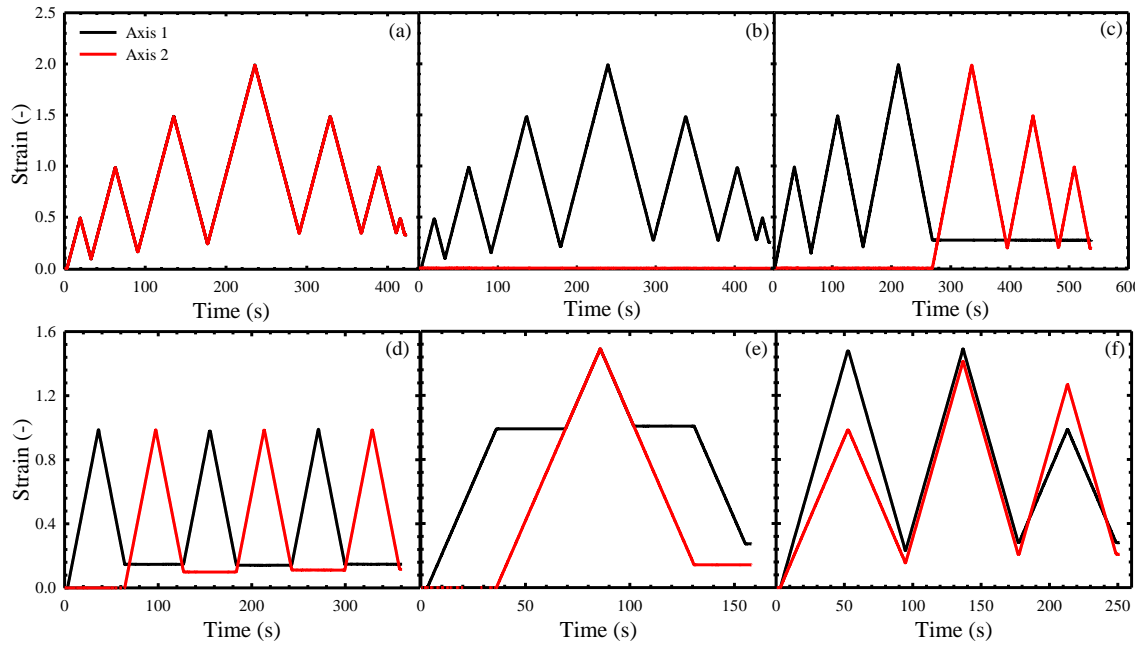
Figure 42. Examples of some tests conditions possible to perform in the FBFT. (a) Equibiaxial testing, (b) Constant width testing, (c)-(d) Alternating axes, (e) Combination of constant width and equibiaxial during one cycle, and (f) Independent strain rate variation on each axes.

3.6.2.2 Specimen preparation and methodology

Equibiaxial, EB, and constant width, CW, tensile testing was performed in tension using the flexible biaxial film stretcher FBFT [152]. Square specimens 85 mm in length were cut from the vulcanised sheet. Thicknesses were measured using a Hildebrand gauge according to the test conditions recommended on ISO 23529 [151]. The average of five measurements was taken along each axis through the centre of the specimen, as represented in Figure 43.

A detailed test protocol is made on every test to ensure the accurate acquisition of load and displacement during the test. The specimen is positioned in the grips, manually ensuring all the grips are correctly aligned with the specimen. A compressed air cylinder is used to close the grips at approximately 30 bar. Using the NI software, the specimen is adjusted moving the grips to avoid buckling or preloading. Afterwards, the initial length for both axis 1 and axis 2 are measured using a digital caliper for calculation of the initial displacement of the grips. The measurement is made from the centre of one grip to the centre of the opposite grip, as shown in Figure 43. Likewise, the distance between the grips where the load cell is located on each axis is recorded in order to calculate the nominal stress. All values are measured before the start of every test.
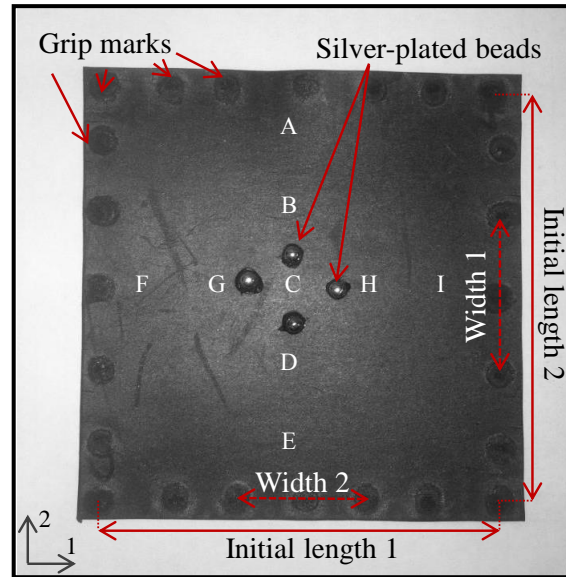
Figure 43. Rubber specimen used for biaxial tensile testing. Beads marker for video recording located in the centre of the specimen. Diagram indicates the measurements of initial width and length on each axis.

In order to use the video extensometer, four silver-plated beads are positioned in the centre of the specimen using sealant-grade wet silicone, as represented in Figure 43. The use of beads was chosen due to the large deformation subjected. If ink marks are drawn in the rubber, the large deformation leads to smearing, and the marks are not tracked on the video recorder. When the strain measured from the grips and the video strain was compared using this technique, no more than 15 % difference was found for equibiaxial and constant width deformations up to 2.0 strains. Appendix A.1 presents a comparison between the video and grip strains measurements. The video strain can also indicate any eventual slippage from the grips. An attempt using Digital Image Correlation, DIC, was used to track marks on the specimen during both equibiaxial and constant width deformation (Appendix A.2). However, most of the tracking in the specimen surface is lost after approximately 60 % strain during equibiaxial and 100 % under constant width deformation, due mainly to the deformation of the tracking points.

Once the specimen is prepared in the rig, a sequence of displacement-controlled tensile tests can be performed. EB and CW test protocols were employed to analyse the basic mechanical response under different modes of deformation. Figure 44 shows a representation of the EB and CW modes of deformation. For EB, the same deformation condition was applied for both axes simultaneously. For CW, one of the axes is keep constrained at a constant length while the other axis is deformed. Each material was tested to quantify the mechanical properties under multi-axial deformation. Tests were performed at room temperature (20 ± 1°C) and at constant cross-head speed

corresponding to a nominal strain rate of 0.03 s^{-1}. For the rolled elastomers (EPDM2, NBR and CR), the CW tests were performed deforming the axis parallel to the rolling direction, while applying constant width restriction to the perpendicular axis.
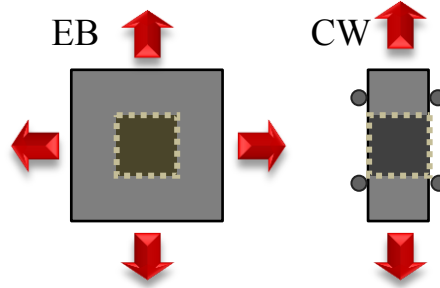
Figure 44. Schematisation of the deformation applied for equibiaxial EB and constant width CW tensile testing.

3.6.3   Mechanical test results

3.6.3.1   Uniaxial tensile testing

An initial uniaxial tensile testing was performed to the elastomers studied, finding the stress-strain response reported in Figure 45. For the material initially processed by compression moulding (EPDM1 and NR) no variation is observed between specimens cut orthogonally. In the case of the sheet rolled processed materials (EPDM2, NBR and CR) an increase in the stress is observed on specimens cut parallel (//) to the sheet role.

From the data collected from a single uniaxial UN tensile testing, the elastic modulus at 100 % elongation E$_{100\%}$, permanent set at 100 % elongation $\varepsilon_{per}^{100\%}$ after one loading-unloading cycle, the strain at fracture σ_f, and stress at failure ε_f were calculated. Three specimens for each material and mode of deformation were tested and the averages of the properties are reported in Table 11, with 95 % confidence interval. For the materials manufactured by sheet rolling (EPDM2, NBR and CR), the values presented are from the axis // to the direction of the rolling.
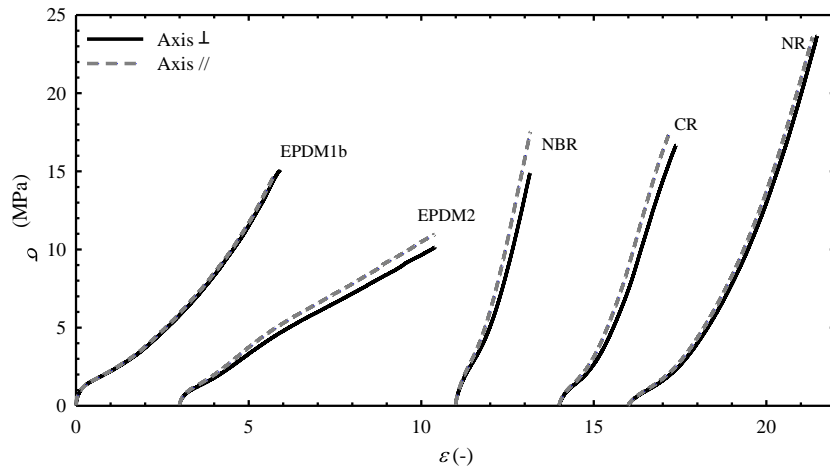
Figure 45. Stress-strain response variation under uniaxial tensile testing due to anisotropy during processing for EPDM1b, EPDM2, NBR, CR and NR. Specimens cut perpendicular to the sheet roll (Axis ⊥) and parallel to the sheet roll (Axis //).

It is clear the mechanical response differs between every material. The highest deformation tolerable for EPDM2 is above 700 %, and the lowest with less than 200 % for NBR. This gives a very wide range of mechanical behaviours in which to analyse the manifestations of Mullins effect. For the elastomers manufactured by sheet rolling, the values presented are for the specimens cut parallel to the direction of the rolling.

Table 11. Mechanical properties of elastomers studied under uniaxial tensile deformations. Elastic modulus at 100% strain, $E_{100\%}$, permanent set after loading-unloading cycle up to 100 % strain, $\varepsilon_{per}^{100\%}$,stress to failure, σ_f , strain to failure, ε_f . (± two standard errors)

	Elastomer					
	EPDM1a	*EPDM1b*	*EPDM2*	*NBR*	*CR*	*NR*
$E_{100\%}$ (MPa)	1.58 ±0.03	2.34 ±0.03	1.93 ±0.21	6.69 ±0.03	3.02 ±0.03	1.91 ±0.13
$\varepsilon_{per}^{100\%}$ (%)	4.06 ±1.33	15.04 ±0.45	20.62 ±0.70	6.96 ±0.44	5.83 ±0.47	4.45 ±0.52
σ_f (MPa)	4.17 ±0.82	14.38 ±0.85	10.90 ±0.49	16.90 ±1.42	17.84 ±0.88	26.81 ±1.73
ε_f (%)	279.38 ±8.63	511.44 ±18.75	707.81 ±16.57	194.60 ±8.05	317.95 ±12.81	506.60 ±8.91

3.6.3.2 Biaxial tensile testing

During biaxial testing, the stress-strain response of both axes can be analysed. The two materials processed by compression moulding, EPDM1a-b and NR show transversely isotropic response during equibiaxial EB deformation. On the other hand, EPDM2 shows very similar response in both axes despite of being processed by sheet rolling. NBR and CR exhibit anisotropy in the stress-strain response. When anisotropy is observed, both axis 1 (parallel to the rolling) and axis 2 (perpendicular to the rolling) values are identified.

Due to the maximum load specification of the load cell in the FBFT, it was not possible

to perform deformation up to failure. Likewise, as a result of the thickness of the specimens, after deformations above 200 % for EB and 250 % for CW, a considerable slipping on some of the grips can be observed. The mechanical properties reported in Table 12, indicate the Young's modulus at 100 % deformation, $E_{100\%\_B}$, with the exception of NBR where the EB tests could not be performed as the maximum load was exceeded. Hence, the young modulus at 50 % deformation $E_{100\%\_B}$ is reported instead. Both axes were analysed, with axis 1 parallel to the rolling (//) and axis 2 perpendicular to the rolling ($\perp$) for the sheet rolling processed materials. The data was calculated from three measurements, reporting two standard errors from the mean.

Table 12. Mechanical properties of elastomers studied under biaxial tensile deformations. Elastic modulus at 100% strain, $E_{100\%\_B}$. For NBR, the young modulus at 50% strain, $E_{50\%\_B}$ is reported instead. For sheet rolled processed materials, $^{//}$ represent parallel to the rolling and $^{\perp}$ perpendicular to the rolling.

Elastomer		$E_{100\%\_B}$ (MPa)	
		Axis 1	*Axis 2*
EPDM1a	EB	2.32 ± 0.01	2.09 ± 0.10
	CW	1.96 ± 0.14	-
EPDM1b	EB	2.75 ± 0.09	2.72 ± 0.03
	CW	2.12 ± 0.14	-
EPDM2	EB	$^{//}2.60 \pm 0.08$	$^{\perp}2.51 \pm 0.11$
	CW	$^{//}2.21 \pm 0.04$	-
CR	EB	$^{//}4.43 \pm 0.09$	$^{\perp}3.91 \pm 0.06$
	CW	$^{//}3.05 \pm 0.01$	-
NR	EB	2.41 ± 0.04	2.49 ± 0.05
	CW	1.90 ± 0.08	-
		$E_{50\%\_B}$ (MPa)	
NBR	EB	$^{//}4.16 \pm 0.06$	$^{\perp}3.96 \pm 0.17$
	CW	$^{//}3.79 \pm 0.07$	-

The constitutive response under each mode of deformation is compared between the five elastomers, showing a clear increase in the stress response when the material is subjected to EB deformation, as presented in Figure 46, with a strain offset for better comparison. For the sheet rolling processed materials, the stress response under UN and CW are for specimens deformed in the direction of the rolling (//).
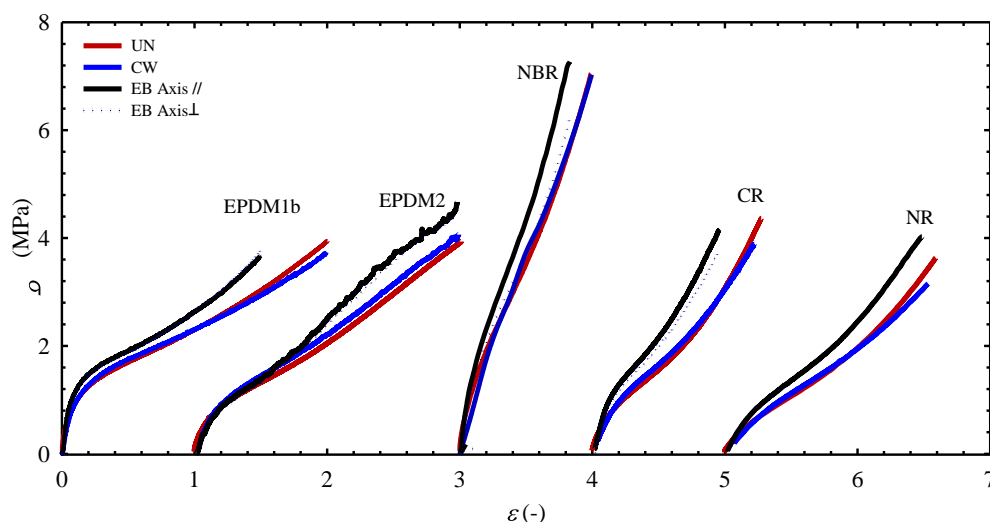
Figure 46. Stress-strain response under UN, EB and CW for EPDM1b, EPDM2 (offset by 1.0 strain), NBR (offset by 3 strain), CR (offset by 4 strain) and NR (offset by 5 strain).

3.7 Discussion

3.7.1 Elastomer composition

The thermal and optical characterisation is able to give information about the composition of the elastomers studied. Due to the lack of information about the material compositions, these techniques are a good approach to establish differences in the structure and composition between the elastomers.

From thermal analysis, it was found that T_g for EPDM1a-b, EPDM2 and NR are at temperatures below -45 °C. This is associated with higher movement capacity of the chains (free volume) which determines the mechanical properties of the materials. The thermal analysis using TGA can provide information about the content on each elastomer. Chiu [156] and Maurer [144] related the weight changes and the thermal energy during temperature degradation with the composition and content of the formulations. Both Maurer [157] and Loadman [143] showed that this technique can discern the composition of EPDM and NR, giving the confidence to employ the same technique in this work. The values of T_g have shown to give information only of the polymeric phase, as previous works have been proven that the filler content has no influence on dephasing or broadening of the T_g [158, 159].

The weight loss observed in the TGA thermogram under 200 °C for the EPDMs and NBR is related with oils used as plasticisers. The inclusion of plasticisers improves the

mixing process by reducing the viscosity and increasing the flexibility region. During degradation, oils and plasticisers are the first to migrate and evaporate [142, 144]. Among the materials analysed, only EPDM1b was reported to have oils in the formulation, corroborated by the thermogram presented in Figure 34 (a). Likewise, a small weight loss at ~200 °C is observed in EPDM2 and NBR that can be attributed to the addition of plasticiser and other cure residues that are common in EPDMs and nitrile rubber formulations. It is plausible that the weight loss change due to the addition of plasticers is masked by the degradation of the polymer, making it challenging to discern the presence of plasticers. Therefore, the determination of the addition of plasticisers in CR and NR using TGA are inconclusive. The main weight loss observed in the thermograms between 300 °C and 500 °C is associated with the polymer degradation. This occurs at ~500 °C for EPDM's and NBR, at 300 °C for CR with a steep gradient, and at 400 °C for NR, as shown in Figure 47. It was found that EPDMs have the highest heat stability. In the case of CR, the thermal degradation of the polymer chain is divided mainly in two partial degradation processes. The first step change is due to the elimination of HCl, followed by the residual polymer degradation [160, 161].
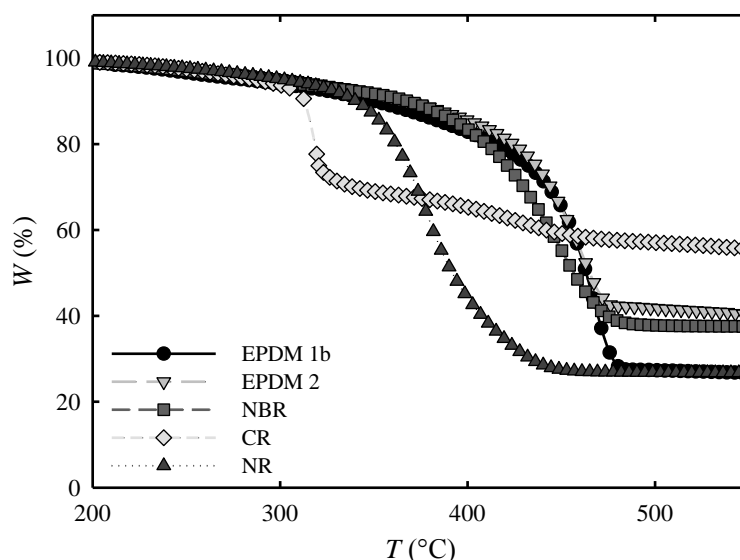
Figure 47. Weight loss associated with polymer degradation using TGA, in a nitrogen atmosphere, for different elastomers.

Once the degradation of the polymer under nitrogen atmosphere is detected, the purge gas is switched to air to promote the carbon oxidation from the carbon black filler. This is clearly visible in the last weight loss above 600 °C for both EPDM's and NR in Figure 34 (a), (b) and (e). It is noted that heteroatoms included in the NBR and CR chains produce a higher amount of carbon black residues during pyrolysis that can be confused with the carbon black filler content [145, 146, 162].

For polymers with nitrogen content such as NBR, the oxidative decomposition of the carbons in the main chain of the polymers occurs at slightly lower temperatures than the carbon black filler [145, 163]. Nevertheless, in this case, an overlapping of the weight loss is presented, making difficult to estimate the percentage related with the carbon oxidation of the chains and the filler. The derivative of the weight loss was used to calculate an approximation of the overlap of both carbon oxidative stages, as was presented in Figure 34 (c). The carbon pyrolysis is counted as part of the total amount of polymer in the formulation. The peak at the highest temperature is associated then with the carbon black filler content. Another thermal degradation was observed above 600 °C for NBR. This degradation is associated with the inclusion of graphite as reinforcement filler [146, 164]. In order to determine the nitrogen composition for NBR, the approach used by Sircar and Lamond [145] to related the T_g with content of nitrogen was employed in this work. They reported the variation of T_g with the content of nitrile for known compositions of NBR. Based on Sircar and Lamond's method, the NBR in this work with a T_g of ~-17 °C, has approximately 35 % content of nitrile.

For CR, the separation of carbonaceous residues could not be observed clearly in the thermograms (Figure 34 (d)). The oxidation of the two carbon population was identified using the peaks in dW/dT. Schwartz [163] suggested an isothermal oxidation technique to separate the carbon degradation related with the pyrolysis of the carbon black filler degradation. However, the success of this approach often requires more information about the filler particle size and polymer formulation to determine the oxidation temperature. This approach was not considered as there was insufficient information related to the filler structure. Nevertheless, from the micrographs of CR samples, a clear dispersion of fillers can be observed.

The final residue determined at 700 °C found with the TGA technique corresponds with inorganic materials that contribute to the vulcanisation reaction [163] [165]. The use of ZnO and MgO as vulcanisation agents is confirmed in the SEM spectrometry of EPDM1b, NBR, CR and NR samples. For EPDM2, there is an inclusion of calcium carbonate, $CaCO_3$, as filler, evidenced by energy dispersive spectrometry on the SEM micrographs in Figure 36 (d). The combination of fillers is a common practice in the industry to reduce costs and combine properties of the fillers [166, 167]. Narsimhan [168] found that decomposition of cylinder and spheres of $CaCO_3$ starts above 850 °C. This explains the high residue found at the end of the EPDM2 degradation.

The final relative weight loss associated with the carbon black oxidation, is used as an indicator of filler content, ϕ_{CB}^{TGA}, expressed as parts per hundred rubber (phr) in the formulation. An estimate of each material's formulation is reported using the analysis of the characterisation results (Table 13). The residue can be accounted as a combination of inorganic materials such as ZnO, MgO and $CaCO_3$ depending on the material.

Table 13. Composition of the filled elastomers in this work, based on thermogravimetric analysis. Oil/Plasticiser content, $\phi_{oil/plast}^{TGA}$, carbon black filler, ϕ_{CB}^{TGA}, graphite, ϕ_{G}^{TGA}, and inorganic materials, ϕ_{inor}^{TGA}, relative to a hundred parts of rubber (phr).

Composition (phr)	Elastomer				
	EPDM1a-b	*EPDM2*	*NBR*	*CR*	*NR*
Polymer	100	100	100	100	100
$\phi_{oil/plast}^{TGA}$	7	4	11	-	-
ϕ_{CB}^{TGA}	36	60	39	47	30
ϕ_{G}^{TGA}	-	-	4	-	-
ϕ_{inor}^{TGA}	3	10	18	4	8

3.7.2 Influence of structure on the mechanical properties

The differences founded in the chemical structure and composition of the filled elastomers can be reinforced by comparing the mechanical properties. From the thermal analysis, the T_g indicates that EPDM1b and EPDM2 present the lowest glass transition, associated with the chain flexibility and elasticity of the material. When the mechanical properties are analysed with respect to the hardness, EPDM and NR present the lowest resistance to indentation, and NBR and CR the highest values of hardness, as was reported in Table 8.

The lowest *H* reported for the EPDM's and NR is a ratification of the higher elastic response of these materials. Likewise, when the materials are subjected to UN deformations, EPDM1b, EPDM2 and NR can be subjected to deformations above 500 % before failure, more than twice the capacity of NBR which presents the highest T_g. The same tendency can be found in the $E_{100\%}$ and $E_{100\%\_B}$, for UN, EB and CW tensile testing, reporting the highest Young's modulus values measured in NBR and CR. It is clear that all the materials analysed present variations in the mechanical response, giving a wide range of mechanical behaviours to analyse for this study of the Mullins phenomenon in subsequent chapters.

3.7.3   Comparison between EPDM1a and EPDM1b

At the beginning of the experimental work, an initial batch of EPDM1a was provided by DIK in 2008. In order to continue with experimental testing, a new batch of EPDM1b was provided by the DIK in 2014, indicating to have the same processing conditions and formulation than EPDM1a. The characterisation presented of both materials clearly indicates a similar formulation between both materials. Nevertheless, the provider suggested a shorter vulcanisation time for EPDM1b to obtain the same properties as EPDM1a. This suggests that an additive (such as an accelerator or cross-link agent) could be changed between the materials. However, the filler content and polymer structure remained the same as was previously discussed in this Chapter. Regarding with the oil content, almost the double of percentage of oil was measured in the new batch EPDM1b, indication that aging of EPDM1a involves also the migration of oils.

A small difference was observed in the mechanical response. EPDM1a presented a fall in most of the mechanical properties presented in Table 11. This is directly associated with aging in the material, due to the difference in the manufacturing date between both EPDM. The aging is an irreversible modification of properties under the action of heat, oxygen, ozone, among others, creating a degradation of the chain due to chain scission and crosslink modifications. Elastomers with unsaturated bonds such as EPDM are most susceptible to aging as these are points susceptible to oxidation. Despite of the storage of the elastomers in a freezer for most of the time, aging will occur for elastomers during storage [169, 170]. The observation of this effect gives a good opportunity to show the effect of compound ageing in the mechanical properties of vulcanised elastomers.

3.8   Conclusions

Section 3.2 introduced the general characteristics and chemical structure of each material. Section 3.3 detailed the compression-moulding and sheet rolling processes used for vulcanisation and preparation of elastomeric sheets for subsequent testing. Compression moulding was employed for EPDM1a, EPDM1b and NR, and the sheet rolling technique used by the manufactures to produce EPDM2, NBR and CR.

Section 3.4 presented the physical characterisation of the filled elastomers; density and hardness of the vulcanised materials were first reported. The glass transition

temperature was determined through thermal analysis using differential scanning calorimetry. The glass transitions for EPDM1, EPDM2, NR and CR, were below -40 °C. On the other hand, the structure and composition of NBR led to a T_g of -17.89°C. Thermogravimetry provided insights into the formulation of each material. From the TGA curves, it was concluded that carbon black reinforcement was present in all materials, ranging from 22 % to 35 %. Furthermore a combination of other inorganic fillers such as $CaCO_3$ and graphite were observed in EPDM2 and NBR respectively.

Morphological studies were carried out using SEM as described in Section 3.5. Micrographs showed the dispersion of the filler in the rubber matrix as well as additional elements used in the formulation. Energy dispersive spectrometry was used in the SEM analysis to discern the elemental composition of further additives founded in the micrographs. Finally, uniaxial and biaxial tensile tests were analysed in Section 3.6. Mechanical properties such as $E_{100\%}$, $\varepsilon_{per}^{100\%}$, ε_f and σ_f for reports the main difference between the material, with EPDM1b, EPDM2 and NR the ones with higher deformation capacity (above 500% for UN). It is also clear that there is a variation of the mechanical response when the elastomer is subjected to different modes of deformation comparing the values of $E_{100\%}$ and $E_{100\%\_B}$ for UN, EB and CW.

A general discussion was presented in Section 3.7 estimating the formulation of elastomers using common techniques in polymer analysis. The variation in the five elastomers formulation was confirmed, resulting in a diverse mechanical response, essential for a more accurate analysis of the softening phenomenon described on the further chapters.

Chapter 4   **Mullins effect and energy dissipation**

One way to investigate the Mullins effect is to probe the response under cyclic deformation. A cyclic deformation analysis can be used to understand how the softening is modified as a consequence of variables such as strain history and modes of deformation. This chapter analyses the response of five different filled elastomers subjected to a series of complex cyclic deformations in order to shed light on the role of deformation history on the mechanical response by using an energy dissipation analysis.

Three modes of tensile deformation were analysed in this chapter: uniaxial UN, equibiaxial EB, and constant width CW deformation. Section 4.2 and 4.3 presents a detailed description of the specimen preparation and the test protocols used to conduct this work. The main differences in the softening effect followed a pseudo-cyclic deformation under different modes of deformation are presented in Section 4.4.1. A strain history analysis under uniaxial and biaxial cyclic deformation is presented in Section 4.4.2 and Section 4.4.3 respectively.

A detailed discussion of the influence of the deformation history in the energy dissipated and stored is presented in Section 4.5. From the data collected, and using a physical approach to describe the elastomeric network, the implications for a constitutive model are given in Section 4.6. A final summary of the most important finding are described in Section 4.7.

Aspects of this work have been presented in both the Rubber Reinforcement by Fillers, Fibres and Textiles: Latest Developments held in London on December 2012 and in 16th International Conference on Deformation, Yield and Fracture of Polymer held in Netherlands on 29th March-2nd April 2015. Parts of this work are to be submitted for publication in the peer reviewed Journal of Polymer Engineering and Science.

4.1 Introduction

The mechanical behaviour of elastomers is a complex phenomenon influenced mainly by the chemical composition and the vulcanisation process. Elastomers exhibit unique mechanical properties at large strains and relatively small energy dissipation under continuous deformations. This makes them very appealing to a wide range of applications such as seals, dampers and tyres. However, when stretched for the first time, the stress-softening phenomenon, well known as the Mullins effect, is observed. This changes the constitutive response after the first loading, reducing the stress to stretch of the material on subsequent cycles up to the previous deformation [14, 67]. A more detailed description and investigation of this phenomenon can be found in literature (Chapter 2). Though, due to the complexity of the problem, a universal model of the softening mechanism is still the subject of current researches.

The scragging process has become common practice in the rubber industry, in order to eliminate the influence of deformation history in the mechanical response [16, 87]. This process pre-conditions the elastomeric product to a certain strain, reducing the possibilities of large changes in the mechanical response due to softening. It is a good technique as long as the material does not surpass the preconditioning strain, or change its mode of deformation. If an unexpected load occurs during service, it is currently very challenging to predict the response. This makes the prediction of the mechanical response in service more challenging. The first section 4.A of this chapter explores experimentally how the strain history modifies the mechanical response as well as the energy dissipated and storage during cyclic deformations.

Many modelling approaches use strain energy density to analyse different aspects such as residual strain, stress relaxation and hysteresis [105, 106, 113, 171, 172]. However, the role of previous deformation seems to have remained relatively unexplored. Understanding the way in which pre-deformation impacts on the response of the material can contribute to improved constitutive model formulations for filled elastomers. The approach presented by Buckley et al. [74] in their study of thermoplastic polyurethanes, evaluated the relationship between hysteresis energy and energy input during tensile cyclic deformation using a model based on a hard (filler) and soft (rubber) phase conversion, initially used by Mullins [15]. The Section 4.B of this chapter uses an adaptation of this physical model together with the evolution theory proposed by Takayanagi [117] to describe the variation during the softening process.

Section 4.A   Experimental analysis

4.2   Specimen preparation

4.2.1   Specimen preparation

Five elastomers were used in this study: two types of ethylene-propylene-diene rubber (EPDM1b and EPDM2), a nitrile rubber (NBR), a chloroprene rubber (CR), and a natural rubber (NR), all chemically cross-linked and carbon-black filled. A complete characterisation of each material was presented in Chapter 3.

4.3   Mechanical testing

4.3.1   Test conditions

Tests were performed at a nominal strain rate of 0.03 s^{-1} and at room temperature (20 ± 1 °C). During the unloading stage for multicycle tests, a minimum unloading force was used of 0.1 N (the minimum resolution of the load cell) to avoid buckling of the specimen, caused by permanent set after deformation. This can occur because of permanent set after deformation.

A repeatability analysis was carried out on one condition for each material. The range of strain analysed was chosen up to 0.5 strain as this is the minimum strain analysed in many of the conditions. Strain values smaller than 0.1 are excluded due to low force vales at these strains. As the stress-strain response for each material should follow the same path when no history is present, a test was considered valid and repeatable when the deviation from the stress mean is less than 10% during the first loading stage. Appendix C describes the repeatability criteria used, using a range of strain between 0.1 and 0.5.

4.3.1.1   Uniaxial tensile test

Uniaxial mechanical deformation (UN) was carried out using an Instron 5969 tensile testing machine equipped with a 100 N load cell and an Instron counterbalanced travelling extensometer. Mechanical test specimens were cut from sheet using a hand-

operated Wallace specimen cutting press fitted with a dumbbell shape cutter type 1BA according to BS ISO 527-2[150]. The same specimen preparation protocol as described in Section 3.6.1 was used for all the uniaxial tests specimens. For materials manufactured using rolling sheet processes (EPDM2, NBR and CR), the axis parallel (//) to the rolling direction was align with the direction of deformation.

4.3.1.2   Biaxial tensile test

Equibiaxial (EB) and constant width (CW) tensile testing were performed in tension using a flexible biaxial film stretcher, FBFT [152]. Square specimens 85 mm in length were cut from a sheet. A detailed description of the FBFT machine and specimen preparation was described in Section 3.6.2. Special care was taken for materials manufactured using rolling sheet processes (EPDM2, NBR and CR) to align the axis parallel (//) to the rolling direction with axis 1 of the biaxial machine.

During the use of the FBFT, the strain measurement was made in the central region of the specimen by tracking four silver-plated beads (see Figure 43 on Chapter 3), attached using a soft silicone adhesive, using video recording; thus avoiding any non-uniform strain state in the proximity of the grips [56, 152]. Whilst the machine is controlled by the grip displacement, values of strain under EB (ε_{EB}) and CW (ε_{CW}) in the protocol details can differ from the strain measured from the video. The results are presented using the (nominal) strain measured from the video. Appendix A.1 presents the relationship between the strain according to the grip displacement and the video tracking of the beads.

4.3.2   Pseudo-cyclic deformation test

An initial analysis of the difference in the response under different modes of deformation was performed using pseudo-cyclic tests for the five elastomers studied. Pseudo-cyclic tensile tests were performed by increasing the maximum deformation on each subsequent cycle, as the test example presented in Figure 48. Three different modes of deformation were performed: uniaxial UN, equibiaxial EB, and constant width CW. Under EB deformation, the pseudo-cyclic deformation test is performed simultaneously on both axes. During CW testing, axis 1 is subjected to pseudo-cyclic deformation and axis 2 is kept under constant width conditions.
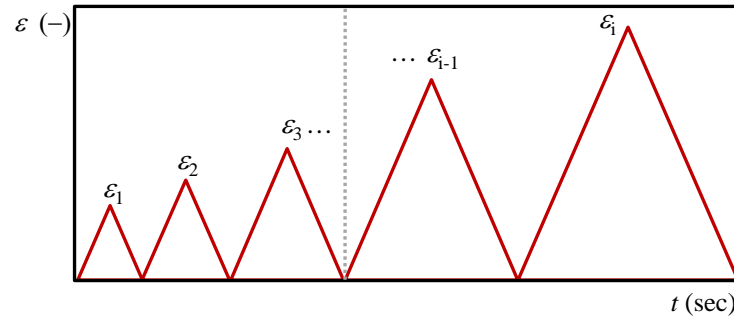
Figure 48. Strain versus time for a pseudo-cyclic tensile test diagram. The number of cycles will differ for test condition and material. *i* is denoted as the number of strain cycles per test.

The strain increment and number of cycles was adjusted depending on the deformation capacity of each material. Table 14 shows the strain values on each cycle for UN (ε_u), EB (ε_{EB}) and CW (ε_{CW}) tensile deformation. No further increments were possible during EB and CW as the load cell force limit was reached.

Table 14. Strain increment during pseudo-cyclic tensile tests under UN (ε_u), EB (ε_{EB}) and CW (ε_{CW}) conditions for EPDM1b, EPDM2, NBR, CR and NR.

	Elastomers														
	EPDM1b			*EPDM2*			*NBR*			*CR*			*NR*		
	ε_u	ε_{EB}	ε_{CW}	ε_u	ε_{EB}	ε_{CW}	ε_u	ε_{EB}	ε_{CW}	ε_u	ε_{EB}	ε_{CW}	ε_u	ε_{EB}	ε_{CW}
	0.5	0.5	0.5	0.5	0.5	0.5	0.5	0.25	0.25	0.5	0.5	0.5	0.5	0.5	0.5
	1.0	0.75	0.75	1.0	1.0	0.75	0.75	0.5	0.5	1.0	0.75	0.75	1.0	0.75	0.75
	1.5	1.0	1.0	1.5	1.5	1.0	1.0	0.75	0.75	1.5	0.85	0.85	1.5	0.85	0.85
ε (-)	2.0	1.5	1.5	2.0	-	1.5	1.5	0.85	0.85	2.0	1.0	1.0	2.0	1.0	1.0
	3.0	1.75	1.75	2.5	-	2.0	1.75	-	-	2.5	1.2	1.2	3.0	1.5	1.5
	4.0	-	-	3.0	-	-	-	-	-	3.0	-	-	-	-	-
	4.5	-	-	3.5	-	-	-	-	-	-	-	-	-	-	-
	5.0	-	-	4.0	-	-	-	-	-	-	-	-	-	-	-
	-	-	-	4.5	-	-	-	-	-	-	-	-	-	-	-
	-	-	-	5.0	-	-	-	-	-	-	-	-	-	-	-

4.3.3 Cyclic deformation with strain history tests

Multi-cycle deformations were tested as imitation of the scragging technique to examine the constitutive response and the recoverable and dissipated energies. The test methodology consisted of a first stage of four loading-unloading cycles to a maximum pre-strain ε_1 (unloading to a force of 0.1 N to avoid buckling), followed by a second additional cycle (stage two) to a specific strain ε_2. This test protocol is study followed uniaxial, UN, equibiaxial, EB, and constant width, CW, deformation.

4.3.3.1 Uniaxial tensile test

Different combinations of ε_1 and ε_2 were explored for each elastomer, including combination of $\varepsilon_1 < \varepsilon_2$ and $\varepsilon_1 \geq \varepsilon_2$ conditions for all the elastomers. Figure 49 shows a

diagram of the test protocol for UN. Due to the elastic capacity of each elastomer, different strains values were used for each material. The combination of ε_1 and ε_2 for UN tests for each elastomer are presented in Table 15.

Table 15. Combinations of ε_1 and ε_2 for UN cyclic deformation tests performed for EPDM1b, EPDM2, NBR, CR and NR.

Elastomers									
EPDM1b		*EPDM2*		*NBR*		*CR*		*NR*	
ε_1	ε_2	ε_1	ε_2	ε_1	ε_2	ε_1	ε_2	ε_1	ε_2
2.0	0.5	1.0	1.0	1.5	0.25	0.5	0.5	0.5	0.5
2.0	0.75	4.0	1.25	0.5	0.5	2.0		1.0	1.0
1.0		0.5		1.5		2.0	0.75	4.0	
2.0	1.0	0.75		1.5	0.75	1.0	1.0	4.0	1.5
3.0		1.0	1.5	1.0	1.0	2.0		0.5	
4.0		1.5		1.5		2.0	1.25	1.0	
2.0	1.25	2.0		0.5		0.5		1.25	2.0
2.0		4.0		0.75	1.25	0.75		1.5	
3.0	1.5	2.0	2.0	1.0		1.0	1.5	1.75	
4.0		4.0		1.25		1.25		2.0	
2.0	1.75	4.0	2.5	1.5		1.5		4.0	
3.0		4.0	2.75	0.5		2.0		1.0	
2.0		1.0		0.75		2.0	1.75	1.25	
3.0	2.0	1.5		1.0	1.5	0.5		1.5	2.5
4.0		2.0	3.0	1.25		0.75		2.0	
0.5		2.5		1.5		1.0	2.0	2.25	
1.0		3.0		0.5		1.5		2.5	
1.5		4.0		0.75	1.75	1.75		4.0	
2.0	2.5	4.0	3.25	1.0		2.0		1.0	
2.25		4.0	3.5	1.5		1.0		1.5	
2.5		4.0	3.75	1.75		1.25		2.0	
3.0		1.0				1.5		2.25	3.0
4.0		2.0				1.75	2.5	2.5	
3.0	2.75	3.0	4.0			2.0		3.0	
4.0		3.5				2.5		4.0	3.5
0.5		4.0				2.75	2.75	4.0	3.75
1.0		1.0							
1.5	3.0	2.0							
2.0		3.0	5.0						
2.5		4.0							
3.0		4.5							
4.0		5.0							
3.5	3.5								
4.0									
1.0									
2.0									
2.5									
3.0	4.0								
3.5									
4.0									

Figure 49. Strain as a function of time diagram for cyclic uniaxial tests. First four pre-strain cycles at ε_1 (denoted as cycles 1,1-1,2-1,3-1,4), followed by a second cycle to strain ε_2 (cycle marked in red).

4.3.3.2 Biaxial tensile test

Following the same multi-cycle testing conditions as uniaxial testing, Figure 50 and Figure 51 show the strain as function of time test protocol followed to examine equibiaxial, EB, and constant width, CW, deformation respectively. For EB, the second stage ε_2 was performed under constant width condition for axis 1, performing deformation only on axis 2. In the case of CW, ε_2 was applied in the perpendicular direction (axis 2) of the pre-strain ε_1, keeping axis 1 constrained to constant width. The modification on stage ε_2 allows a better comparison with uniaxial testing on the effect of strain history. Several ε_1 and ε_2 combinations were carried on each elastomer, with both $\varepsilon_1 < \varepsilon_2$ and $\varepsilon_1 \geq \varepsilon_2$ conditions. The deformation settings for EB and CW conditions are reported in Table 16.

Figure 50. Strain as a function of time diagram for cyclic equibiaxial tests. First four pre-strain cycles at ε_1 (denoted as cycles 1,1-1,2-1,3-1,4), followed by a second cycle to strain ε_2 (cycle marked in red).
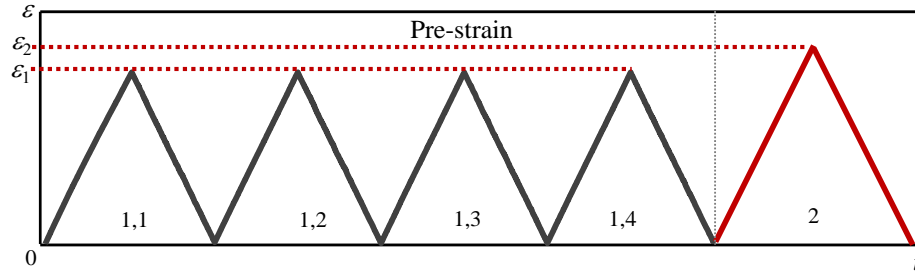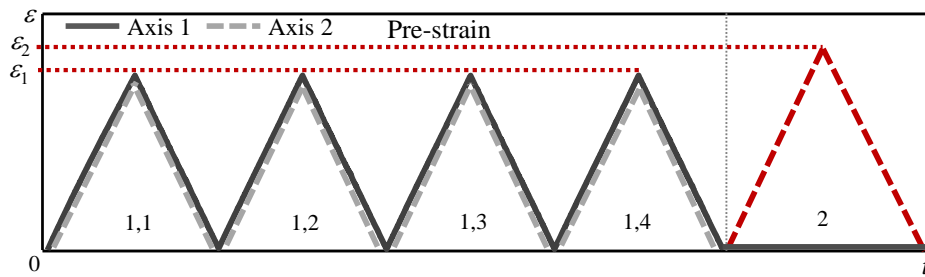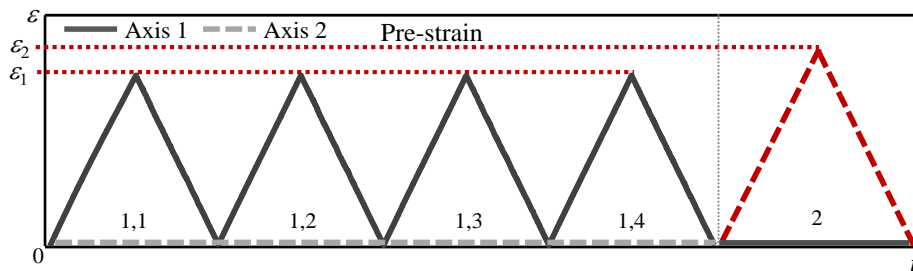

Figure 51. Strain as a function of time diagram for cyclic constant width tests. First four pre-strain cycles at ε_1 (denoted as cycles 1,1-1,2-1,3-1,4), followed by a second cycle to strain ε_2 (cycle marked in red).

Table 16. Combinations of ε_1 and ε_2 for EB and CW deformation tests for EPDM1b, EPDM2, NBR, CR and NR. The values of ε_2 correspond to CW condition on axis 1 (//). The same values of ε_2 stage are used for both EB and CW pre-strains.

Elastomers														
EPDM1b			*EPDM2*			*NBR*			*CR*			*NR*		
ε_1		ε_2	ε_1		ε_2	ε_1		ε_2	ε_1		ε_2	ε_1		ε_2
EB	CW		EB	CW		EB	CW		EB	CW		EB	CW	
0.5	0.5		0.5	0.5		0.25	0.5		0.5	0.5		0.5	0.5	
0.75	1.0		0.75	1.0		0.5	0.75		0.75	0.75		0.75	1.0	
1.0	1.5	1.5	1.0	1.25	1.5	0.75	1.0	1.0	1.0	1.0	1.0	1.0	1.5	1.5
1.5	2.0		1.5	1.5		0.85	1.25		1.2	1.25		1.5	1.75	
1.75	-		-	2.0		-	-		-	-		-	-	

4.4 Results and discussion

4.4.1 Pseudo-cyclic tensile testing

This section examines differences in the Mullins phenomenon when considering the mode of deformation during pseudo-cyclic tests. The stress-strain response for EPDM2 is presented in Figure 52 (a)-(c). A single loading test (with no previous strain history) is also included for comparison. For EB and CW testing only axis 1 (//) deformation is shown.

The data shows the dependence of the previous deformation in the stress response on subsequent cycles, with a clear variation in the constitutive response for subsequent loadings on any mode of deformation. The variation between the loading and unloading paths of EPDM2 indicates energy dissipation. Followed uniaxial deformation, UN, the Mullins effect is strongly manifested for stretches lower than, or even equal to, the maximum stretch previous applied. Once the previous strain is exceeded, the response re-joins the same loading path of an initial underformed material. The elongation capacity of EPDM2 allows uniaxial deformations of 500 % the initial length of the specimen. In the case of equibiaxial and constant width, the restriction on two axes reduces the elastic capacity to around 200 %. The same mechanical response was observed for axis 2 under equibiaxial deformation. Due to the rig and load cell capacity of the FBFT, no higher deformations were possible to examine. As well as for uniaxial testing, followed biaxial deformation the Mullins effect is observed even under relatively small deformations (0.5 strain). Similar behaviour was observed for EPDM1b (in Appendix B.1).

Figure 52. Pseudo-cyclic stress-strain response for EPDM1b, increasing maximum strain on subsequent cycles. (a) UN, (b) EB (showing only axis 1) and (c) CW restriction on axis 2.

For NBR, CR and NR the path after a first loading-unloading cycle shows a more visible variation at higher values of strain. Figure 53 (a)-(c) shows the mechanical response of NR as an example (the remaining of the materials are presented in

Appendix B.1 with similar tendency), under pseudo-cyclic deformation compared with the stress-strain response of a material subjected to a simple loading ramp.
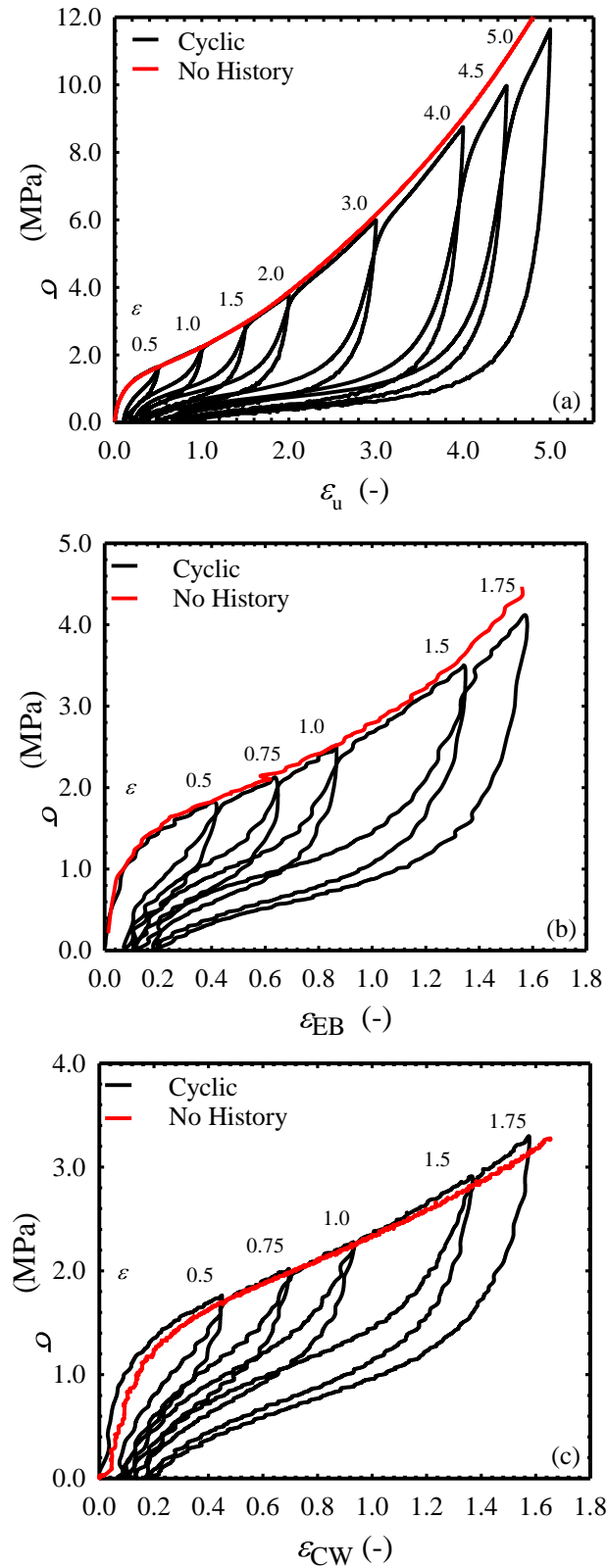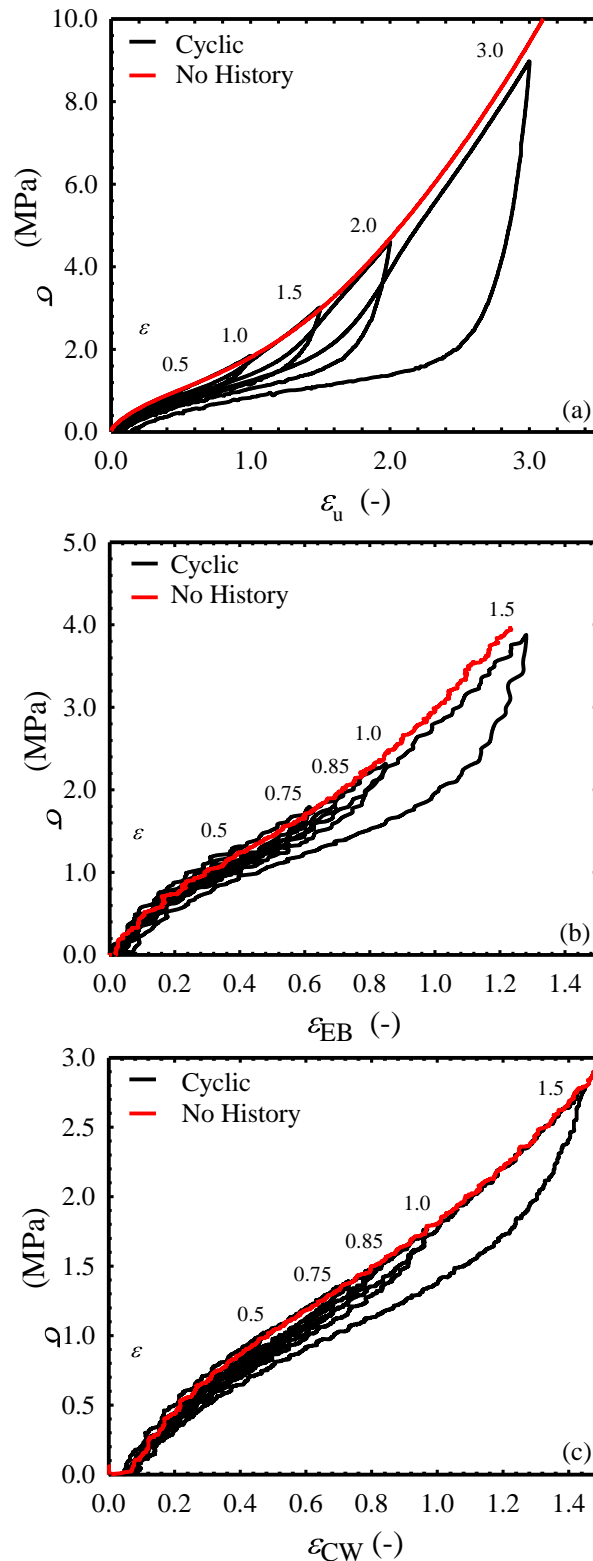

Figure 53. Pseudo-cyclic stress-strain response for NR, increasing maximum strain on subsequent cycles. (a) UN, (b) EB (showing only axis 1) and (c) CW restriction on axis 2.

When NR is exposed to small deformations (i.e. lower than 1.0) the loading and

unloading paths are not significantly different. This indicates low energy dissipation under small deformations. This behaviour is observed in the three modes of deformation. When the elastomer is subjected to UN deformation, it is possible to observe a higher softening as the maximum strain capable to deform is higher. Followed EB deformation, axis 2 presents the same mechanical response as the reported on axis 1.

4.4.1.1   Influence of mode of deformation on the mechanical response

The mechanical response and hence stress response at a specific strain is dependent of the mode of deformation for all the materials examined. When an elastomer is subjected to uniaxial deformation, the elasticity of the specimen can be almost twice what is capable to deform than when is subjected to biaxial deformations. The experimental data shows that the change in the mode of deformation is related with a limitation of the network capacity to restructure when constrains during deformation are increased. Multiaxial deformation or restriction on more than one axis, imply a higher constraint in the network, reducing the movement capacity. It is necessary then to acknowledge the stretching criteria during the life performance of an elastomeric material in order to identity the elasticity capacity.

4.4.1.2   Softening effect variation between filled elastomers

The softening response is specific to each material, making it very challenging to predict and provide a more detailed description of the parameters involved in this behaviour. It is worth reminding the reader that each material is chemically different and vulcanised and manufactured differently, as it was presented and analysed in Chapter 3. This makes it difficult to compare the materials in more details.

Literature has shown that a higher content of filler may lead to a more pronounced Mullins effect at very low stretches [14, 116]. The stress response indicates a considerable higher softening effect in EPDM2 and less softening in NR and NBR (in Appendix B). As presented in Chapter 3, EPDM2 presents the higher content of carbon black (34.53 ±1.08 %) and NR and NBR the lowest one (21.88 ±0.24 % and 24.88 ±0.33 % respectively). This could be the main factor for the phenomenon observed. Likewise, as it was analysed in Section 3.7, EPDM's and NR present a higher elastic response in comparison with the NBR and CR, due to the chemical network structure and configuration of the chains and the composition.

4.4.2   Uniaxial constitutive response under cyclic deformation

The softening effect observed previously on filled elastomers is a well-known consequence of strain history. This is the main purpose of the scragging process used on many elastomeric products [16, 87]. With a preconditioning of the final product up to a strain value above the expected service conditions, a consistent constitutive response can be expected, giving a reproducible material response. This technique is an effective way to ensure that the Mullins effect does not bring modifications to the mechanical response.

4.4.2.1   Deformation history ε_1 greater than ε_2

The mechanical response to pseudo-cyclic deformation for EPDM1b after a pre-strain of ε_1=4.0 in presented in Figure 54. Subsequent straining to strains below this value requires significantly lower stresses. When the pre-strain ε_1 is higher than the strain in the second stage, ε_2, the response is enclosed within the ε_1 stress-strain response. As long as ε_2 do not exceed ε_1, a similar loading-unloading path is found independently of strain range.
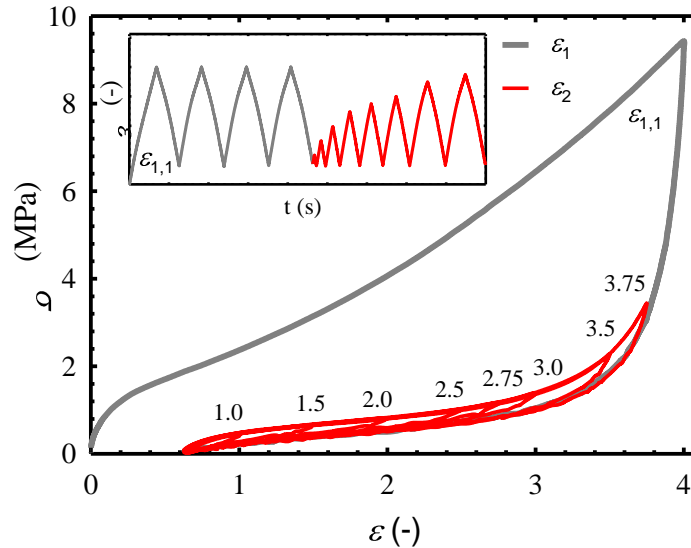
Figure 54. Uniaxial pseudo-cyclic deformation $\varepsilon_1 > \varepsilon_2$ response after pre-strain ε_1=4.0 for EPDM1b.

The softening of EPDM1b is significant, reducing around 80 % the stress required to deform to a specific strain value. The rest of the elastomers studied display similar effects in the constitutive response, as presented in Appendix B.2. The scragging is a simple method to ensure a repeatable cyclic response in the material as long as the pre-strain is not exceeded. As long as ε_2 remain below ε_1 the response can be considered

independent of ε_1.

4.4.2.2 Deformation history ε_1 lower than ε_2

A more complicated response arises when the material is subjected to a ε_1 lower than ε_2 strain history. In this case, the response is more complex and it is of practical importance to understand the behaviour and the softening criteria involved with respect to the deformation history.

The stress-strain response during cyclic deformation of one condition from Table 15 during stage ε_1 and ε_2 on each material is presented in Figure 55 (a)-(e), with an inset of the strain protocol in Figure 55 (a). In this case, the softening effect is clearly noticeable up to the value of ε_1, changing drastically the stiffness once the strain surpasses ε_1. During the four cycles at ε_1, the loading and unloading paths are considerable similar, showing the softening effect mainly between the first and second cycle. It is more clearly in the initial loading path of ε_2 (until the value of ε_1) where the stress response is the same as in the previous stage.

When ε_2 reaches ε_1, EPDM1b and EPDM2 show the steepest re-joining towards the virgin loading paths. For CR and NR it takes longer to rejoin, with a smoother stress response. The movement of the polymer network could cause a retarded effect in the strain response. For NR, a more gradual return to the no-history path is observed. Another interesting response is the permanent set after unloading on ε_2, presenting a significantly higher permanent set in EPDM1b and EPDM2 in comparison with NBR, CR and NR. This response is an important effect during deformation in order to analyse the strain history effect.
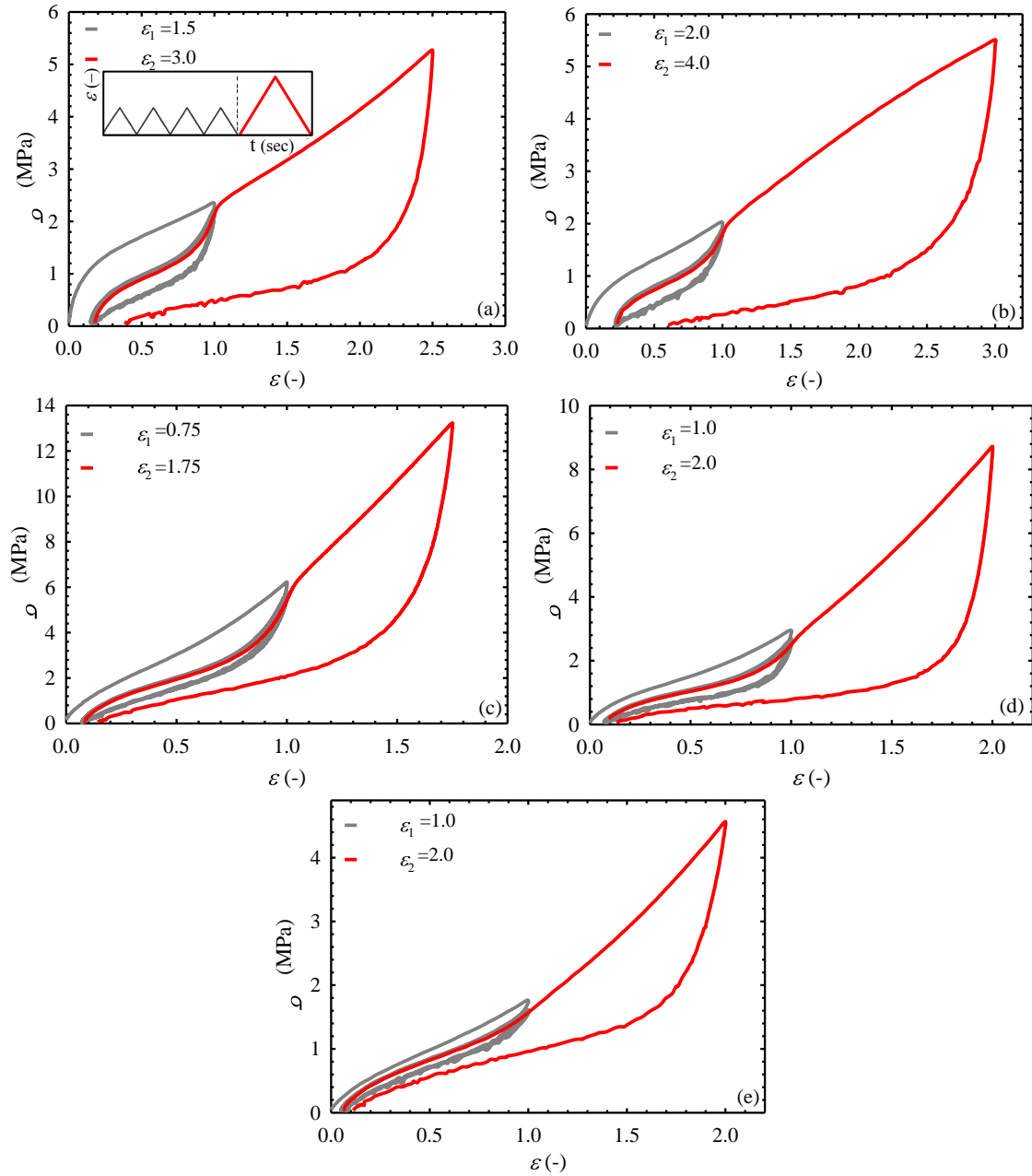
Figure 55. Uniaxial cyclic deformation response under pre-strain deformation ε_1 and second stage ε_2 for (a) EPDM1b (with an exemplary inset of the strain as a function of time test protocol), (b) EPDM2, (c) NBR, (d) CR and (e) NR.

The loading response followed different pre-strain tests where $\varepsilon_1 < \varepsilon_2$ is described in more detail in Figure 56 (a) to (e). A range of ε_1 values examined at a specific ε_2 is presented to differentiate the effect of strain history in the mechanical response of each elastomer after the first stage ε_1. The response of a material with no history is presented for comparison.
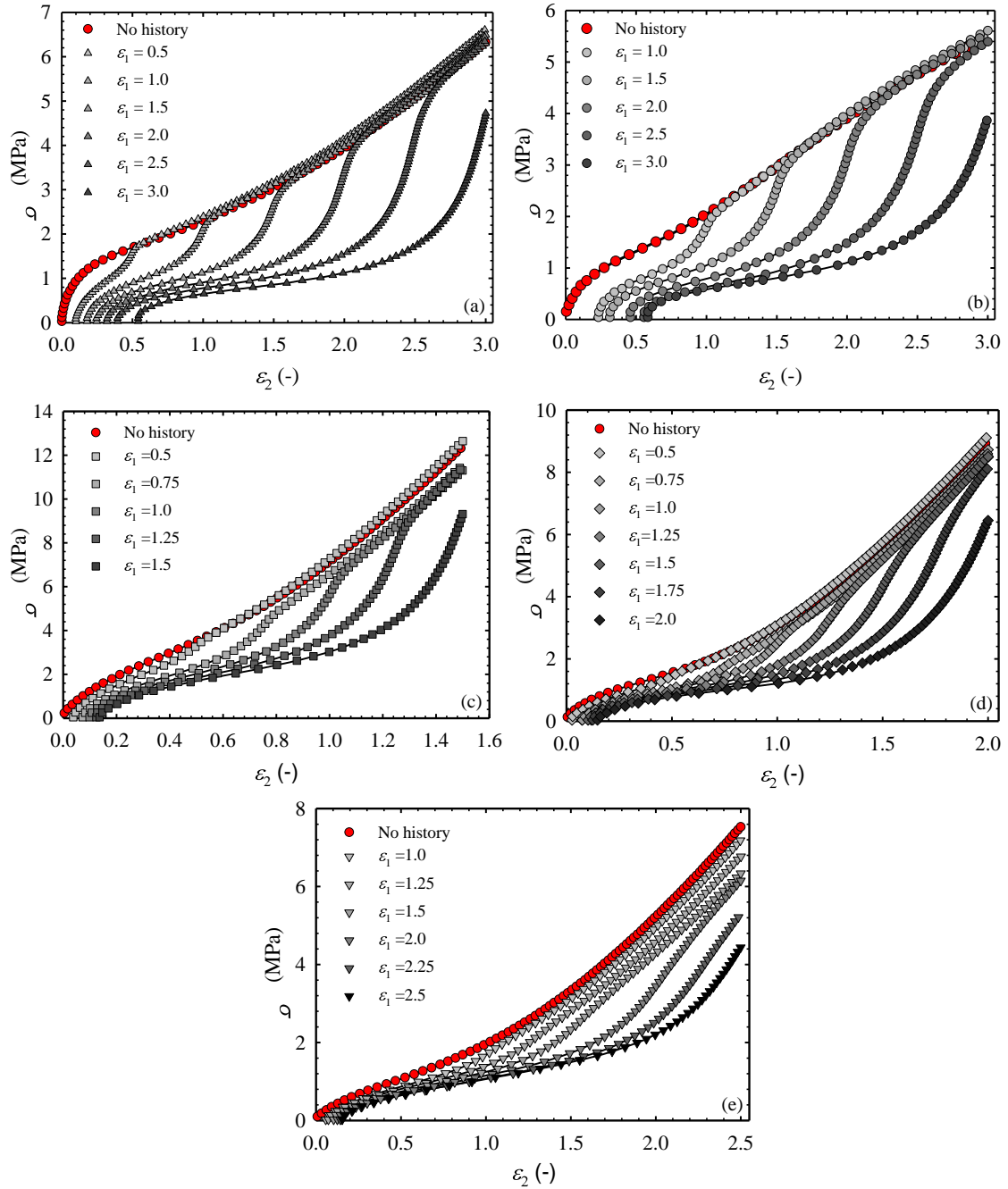
Figure 56. Nominal stress measured as a function of UN strain after different values of pre-strain ε_1 for (a) EPDM1 with ε_2 =3, (b) EPDM2 with ε_2 =3, (c) NBR with ε_2 =1.5, (d) CR with ε_2 =2.0 and (e) NR with ε_2 =2.5.

In this condition, the mechanical response is more directly conditioned to ε_1. The softening due to pre-strain, and the hence constitutive response, increases with the increase of ε_1. This is observed in the less stress required to stretch the specimen to a specific strain. Both EPDM1b and EPDM2 show a more pronounced softening and permanent set effect, even at small values of ε_1. The noticeable variation in the initial strain is due to the permanent set from the pre-stretching ε_1. In general, there is a reduction in the stress of between 50 % and 70 %, with the highest reduction observed

in EPDM1b and EPDM2. The reduction in the stress response for the rest of the materials is more noticeable after $\varepsilon > 0.5$ for NBR, 0.75 for CR and 1.0 for NR.

The non-linearity of the constitutive response of the filled elastomers is clear in the experiments. In a low deformation range ($\varepsilon < 0.1$) approximately linear elastic behaviour can be observed; however, the focus of this work is on large deformations. For EPDM1b and EPDM2, pre-strain alters the stiffness in a similar way along the deformation magnitudes studied. Figure 56 (a) and (b) show a similar slope in the section when the strain is just below the pre-strain ε_1. However, for NBR, CR and NR (Figure 56 (c) (d) and (e)) modulus at a specific strain is more conditioned to the pre-strain value, increasing with higher elongation history.

4.4.2.3 Mechanical response between filled elastomers

The restructuring mechanism of the network and the filler-rubber interaction is an inherent property of the rubber structure and filler combination. This makes even more challenging to comprehend the process in a general statement. The stress required to deform is sensitive to the chemical composition of the filled elastomer. Although the materials studied present different manufacturing processes and formulation, assumptions regarding to their characterisation can be made.

In the case of EPDM1b and EPDM2 the response is very similar as both have the same polymeric structure. The difference arises mainly from variations in the compound, such as filler content and/or crosslink density. The high elasticity capacity of EPDM2 allows elongations of the material above 700 % strain before failure. As a result, there is more plastic deformation of the network, with higher levels of permanent set. On the other side, NBR and CR have the highest T_g's (-17.89 ±0.50 °C and -39.89 ±0.47 °C respectively) between the elastomers analysed. This is associated with more configurational restrictions of the polymeric structure, the filler inclusion and the crosslink density. As a consequence, the deformation is more restricted, requiring more stress to deform than for EPDM1b, EPDM2 and NR, with T_g's of -52.08 ±1.55 °C, -47.35 ±1.16 °C and -57.03 ±0.76 °C respectively.

The filler content acts as a stiffening additive in filled elastomers. The stress softening is usually attributed to an incomplete recovery of the crosslink network combined with filler-filler and filler-rubber networks breakdown. Therefore, EPDM2, with the higher content of filler (60 pph), exhibits a higher drop in the stress during unloading than the

rest of the materials. This behaviour is related with the capacity of the material to dissipate and recover energy during a cycle (hysteresis).

Unfilled EPDM's, CR and NR are known to exhibit strain-induced crystallisation [173-175]. However, the capacity to create a regular structure and form crystals is reduced and even eliminated with the inclusion of particulate reinforcements [176]. No sign of sudden increase in stiffness was observed during the first loading in the range of deformation studied. Hence, the effect of possible crystallisation in the mechanical response during deformation is not considered in this work.

4.4.2.4 Permanent set after ε_1

Another observation from the data is the difference in the permanent set ε_{per}, or residual stretch of each of the materials. The residual strain is defined in the tests carried out as the remaining strain when specimen is unloaded to 0.1N. This can be observed in the strain gap of the samples at the beginning of ε_2, compared with the no history path in Figure 56. For all the elastomers, the gap increases when the pre-strain ε_1 increases. EPDM1b and EPDM2 have a permanent set noticeably higher than the rest of the materials. This is coherent with the previous observations. The elasticity of these two materials is linked with a high residual strain during the mobility and rearrangement of the polymer chains. The capacity of EPDM1b and EPDM2 to deform more with less stress occurs simultaneously with more permanent deformation to the material. Nevertheless, permanent set is observed in all the elastomers.

Figure 57 shows ε_{per} as a function of ε_1 for the elastomers evaluated. The permanent set and material softening usually occur simultaneously, as both effects can be attributed to physical mechanisms occurring in the material during deformation. Residual strain is an indication of permanent damage or plastic deformation in the system, related with the breakdown of cross-link joints, disentanglements and even ruptures of carbon-carbon links in the polymeric chain. The stress required to deform to a specific strain then depends not only on the rubber's composition, but also on the deformation history. The next section focuses on how the response is modified under simultaneous biaxial deformation.
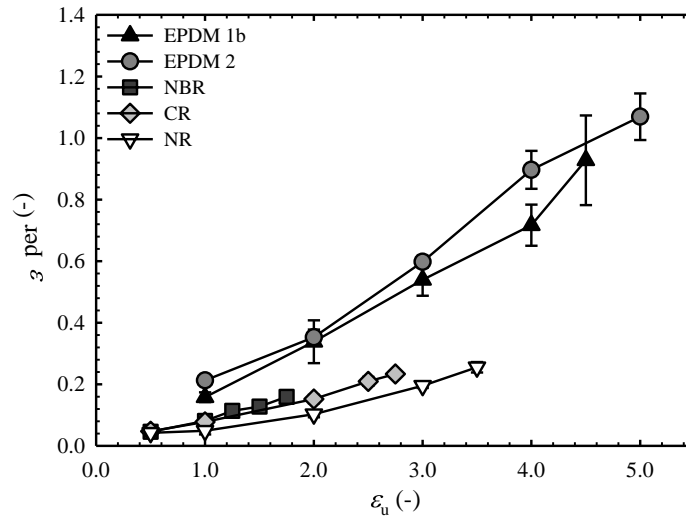
Figure 57. Permanent set ε_{per} as a function of uniaxial deformation ε_u at the end pre-strain ε_1 stage on filled elastomers.

4.4.3 Biaxial and constitutive response under cyclic deformation

4.4.3.1 Equibiaxial strain history

The variation of stress during CW loading in the two directions as a function of ε_2, after an initial equibiaxial pre-strain ε_1 is presented Figure 58 (a) to (e). The values are compared with the first loading (no previous cyclic history) under the same test conditions. A schematic inset of the test protocol is showed on Figure 58 (a) for EPDM1b as guide. The stresses in the axis 1 (//) and axis 2 ($\perp$) are symbolized as σ_{a1} and σ_{a2} respectively. Even though during ε_2 there is no movement on axis 1, the stress response on both axes can be analysed with respect to ε_2. As expected, the values of σ_{a1} are considerable lower than in the axis 2 subjected to the strain ε_2. An evident decrease of stress σ_{a2} (softening effect) is present in all the elastomers when ε_1 increases, compared with the mechanical response with no previous deformation.

At small values of ε_1, the stress response during ε_2 is closer to the *no history* path. The slight rise above the *no history* path for EPDM1b and NR for σ_{a2}, are within the expected error, considering variations in the set-up of the specimens; as such, they can be considered to re-joining the initial path. Likewise, these two materials are the initially isotropic materials. In the case of the initially anisotropic elastomers (EPDM2, NBR and NR) this effect is not present, even at conditions with ε_1 considerable lower than ε_2. It is possible that the equibiaxial pre-strain *diminishes* the initial anisotropy of these elastomers, modifying also the stress path making it more difficult to compare

with a *no history* path.

Figure 58. Nominal stress measured as a function of strain ε_2 on axis 2 and CW on axis 1, with variation in EB pre-strain ε_1. (a) EPDM1b (inset in the strain as a function of time test protocol) and (b) EPDM2 up to ε_2=1.5. (c) NBR and (d) CR up to ε_2=1.0, and (e) NR up to ε_2=1.5.

The force of compression in the axis orthogonal to the force is represented by σ_{a1}. Only EPDM1b and EPDM2 show a clear decrease in the stress σ_{a1}, mainly due to the higher permanent set from previous deformation, creating an offset of the stress-strain path. EPDM1b and EPDM2 exhibit a permanent set of around 0.30 with ε_1=1.5. A considerably smaller permanent set can be seen in NBR, CR and NR, as well as a less dependence of ε_1 on the response of σ_{a1}. Even though axis 1 was already deformed in

the pre-strain ε_1, and hence the softening phenomenon occurred, the smaller stress on the constrained axis during stage ε_2, does not show major variation in the response of the axis under constant width.

4.4.3.2 Constant width strain history along a perpendicular axis

The possibility to restrict the movement on one axis allows measuring both the stress along the deformed axis and the stress arising along the axis perpendicular to the deformation to be measured. In this test, the deformation ε_1 was applied first along axis 1, keeping the axis 2 under constant width, and then the deformation switched to constant width on axis 1. Figure 59 (a) to (b) shows the stress response σ_{a1} (axis 1) and σ_{a2} (axis 2) during the ε_2 stage with CW along axis 1 for each elastomer. Figure 59 (a) presents an inset of the strain protocol as guide.

EPDM1b, EPDM2 and NBR exhibit different levels of softening in σ_{a2} when ε_1 increases, indicating a dependence of the pre-strain, even when the deformation history was on the perpendicular direction. On the other hand, for CR and NR the constitutive response follows the same behaviour as with a *no history* material on σ_{a2}. This shows that when the previous deformation is applied orthogonally, the Mullins effect is not manifested in σ_{a2} for these two materials.

On the axis with constant width condition, the stress σ_{a1} response is considerable lower than in σ_{a2} as expected. The dependence of the pre-strain is similar to the observed for σ_{a2}. EPDM1b, EPDM2 and NBR show a variation of the stress response with pre-strain, as CR and NR present the same stress response independently of the pre-strain.

A slight exceeding from the *no history* stress σ_{a2} is again present in the two initially isotropic materials (EPDM1b and NR), as it was observed for equibiaxial deformation history. At the stress σ_{a1} on the axis 1 in the virgin loading, curves tent to be exceeded by that of the pre-stretched system in the perpendicular direction under constant width for most of the elastomers. During pre-strain ε_1, this axis was subjected to deformation, suggesting a possible reorganisation of the network in this direction, such that, when the material is stretched in the perpendicular direction, a higher stress is required. This is evidence of possible strain-induced anisotropy, and will be discussed in more detail in Chapter 6.
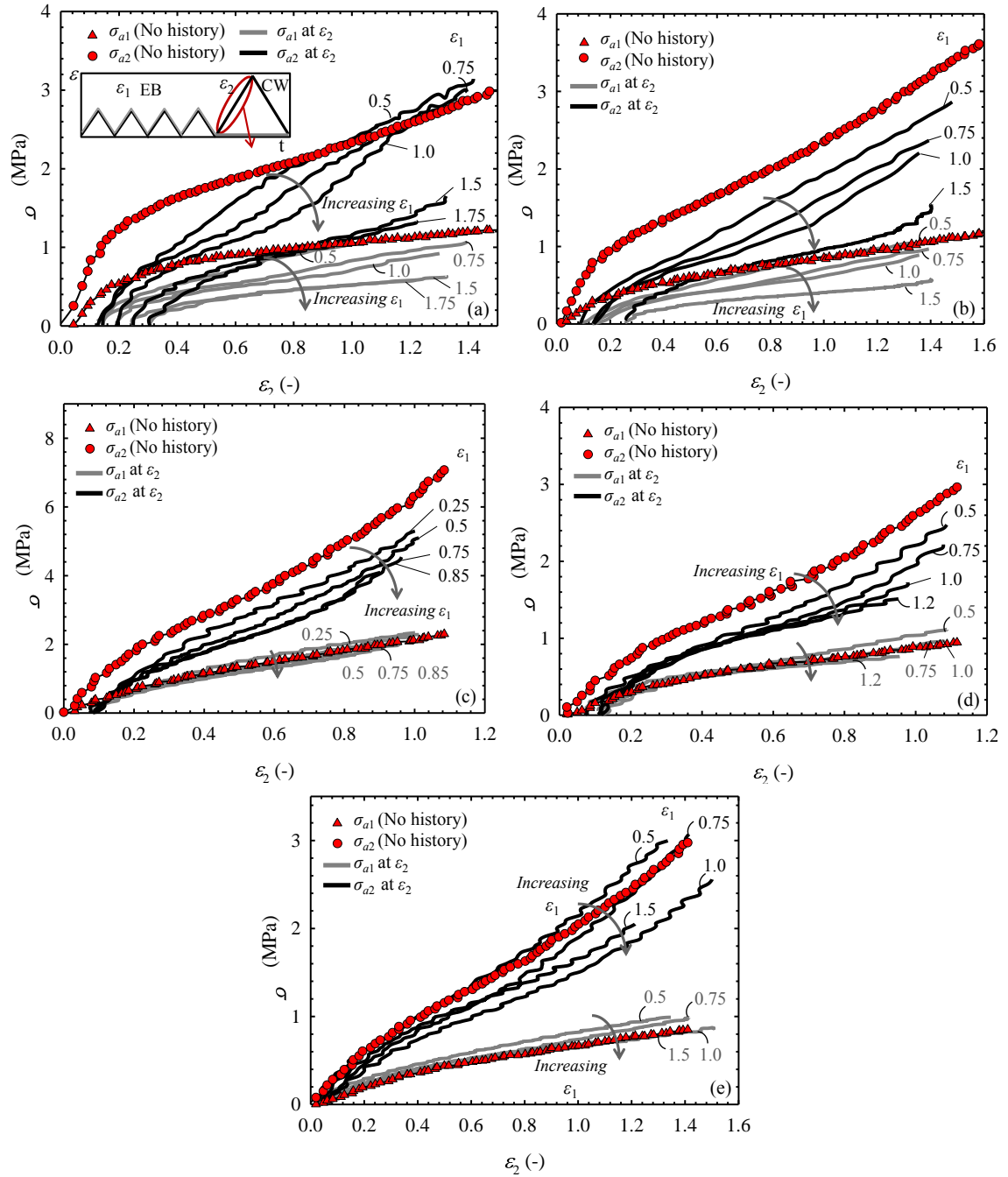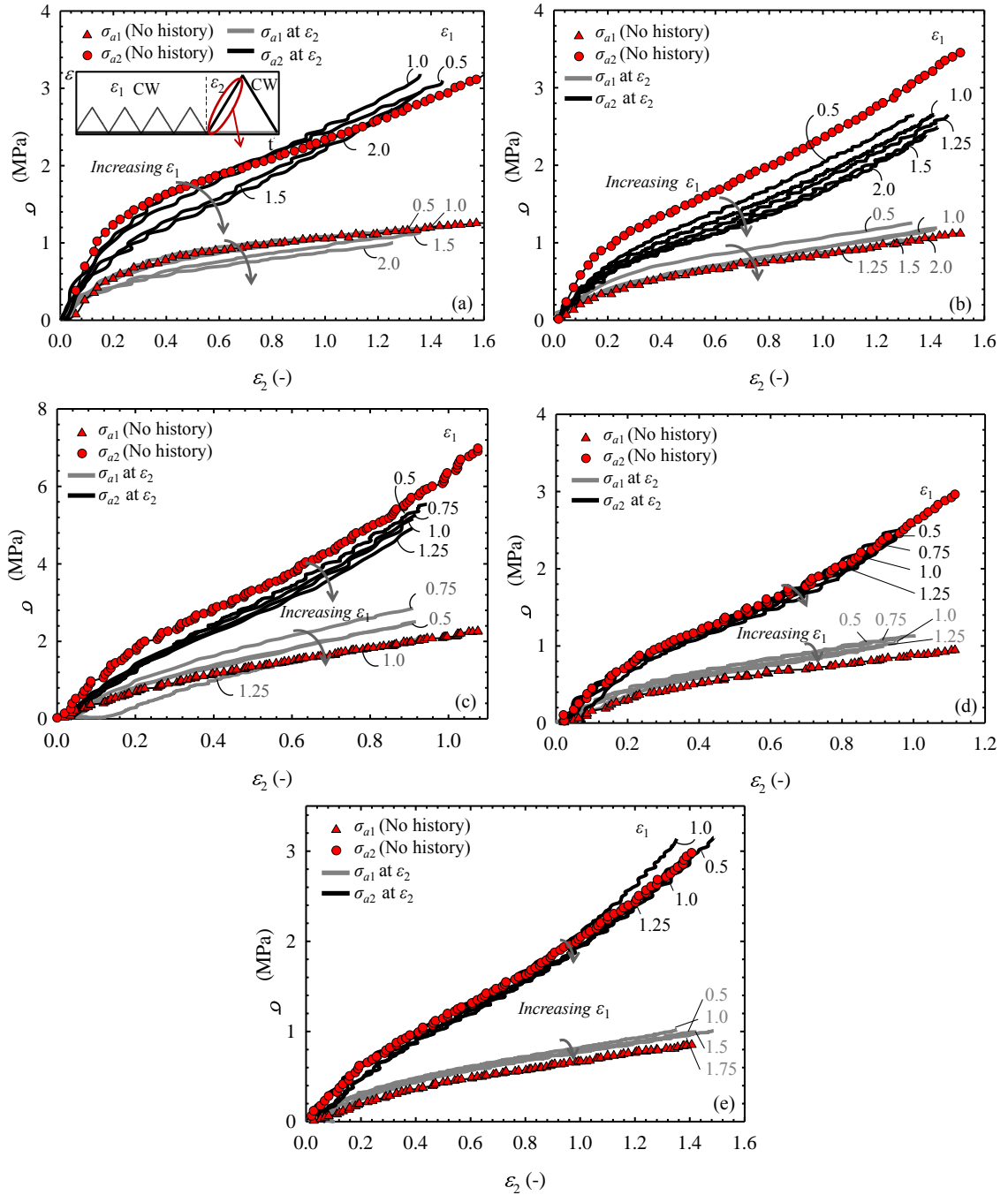
Figure 59. Nominal stress measured as a function of strain ε_2 on axis 2 and CW on axis 1, with variation in pre-strain ε_1 on axis 1 and CW on axis 2. (a) EPDM1b (with an exemplary inset of the strain as a function of time test protocol), and (b) EPDM2 up to ε_2=1.5. (c) NBR and (d) CR up to ε_2=1.0, and (e) NR up to ε_2=1.5.

4.4.3.3   Mechanical response variation followed different modes of deformation

When comparing the mechanical responses in Figure 56, Figure 58 and Figure 59 for uniaxial, equibiaxial and constant width tensile testing deformation respectively, it is clear that the performance is affected by the pre-strain condition. Mullins suggested that the degree of softening is not the same in all directions [67]. Later, Machado el al. [88,

90] presented experimental evidence of the variation of the softening at different orientations after a uniaxial stretching on silicone rubber, with hardly any difference of stress softening found in the perpendicular direction. Figure 59 suggested that some filled elastomers, such as EPDMs and NBR do exhibit directional dependency, even in the orthogonal direction. Deformation along one direction can therefore affect the response in the whole structure. On the other hand, filled elastomers such as CR and NR do not exhibit any dependence when the strain history in the orthogonal direction. It is difficult to state the cause of this effect, as there is no direct similarity in the mechanical properties of these materials.

4.5 Energy dissipation

4.5.1 Computation of energies

Following the approach of Buckley et al. [74, 177], the input energy density W_i (energy required for loading) and output energy density W_o (energy recovered during unloading) during each cycle were calculated. The shaded areas in plots of stress vs strain in Figure 60 (a) and (b) show the W_i and W_o determination from the stress-strain response. W_i is obtained by the integration of the stress-strain loading response, while the unloading path integration represents W_o. The hysteresis (W_i-W_o) was calculated as shown in Figure 60 (c).
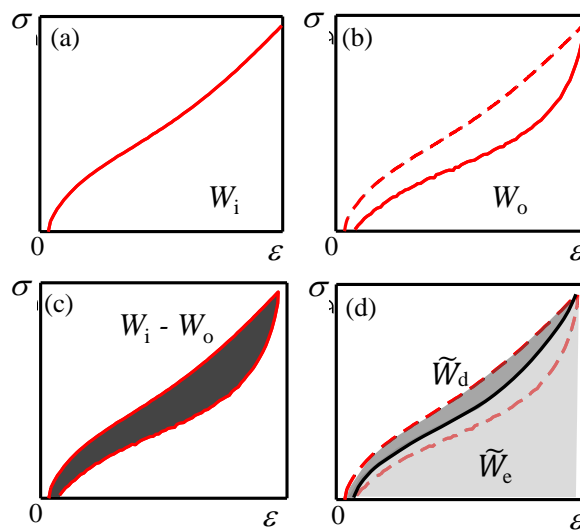
Figure 60. Schematic representation of integrals carried out for energy determination from stress-strain response. (a) Work input W_i of the loading response. (b) Work output W_o of unloading response. (c) Hysteresis W_i -W_o over one loading-unloading cycle. (d) Energy dissipated $\tilde{W}_d$ and recovered $\tilde{W}_e$ for the loading segment response.

Two further quantities are introduced on the basis of the full load-unload cycle: an average dissipated energy density per half-cycle, $\tilde{w}_d$, and an average elastic recoverable energy density per half-cycle, $\tilde{w}_e$, both defined as:

$$\tilde{W}_d = \left(W_i - W_o\right)/2 \qquad \text{Eq. 4-1}$$

$$\tilde{W}_e = \left(W_i + W_o\right)/2 \qquad \text{Eq. 4-2}$$

A 32 cycle test for EPDM2 was carried out using a maximum uniaxial strain of 1.5 to observe the change in energy (W_i-W_0) as a function of the number of cycles. In Figure 61 the drop in energy dissipated between the initial and successive loading cycles can be observed. The major drop in energy occurs between the first and second cycle, with a reduction of around 67 %. The energy converges rapidly to a steady state. The fourth cycle is used in this work as a time-efficient approximation to the steady state value.
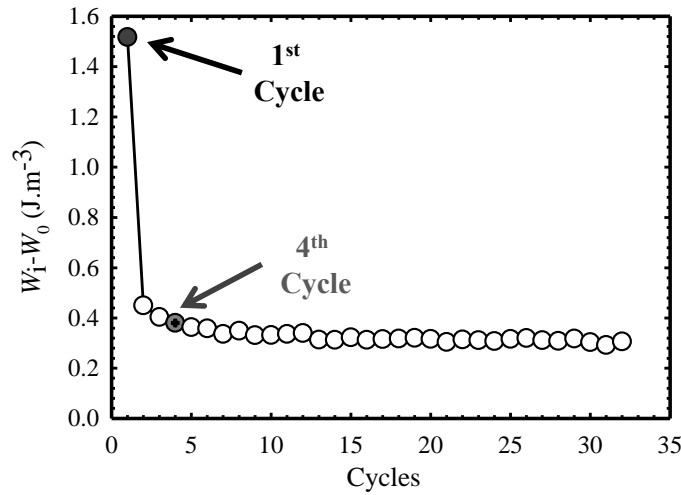
Figure 61. Variation in hysteresis W_i-W_o during 32 successive cycles for EPDM2 up to 1.5 uniaxial strain.

4.5.2 Energy dissipation following uniaxial deformation

Measurements of the constitutive response of the filled elastomers under uniaxial deformation can be further examined in terms of energy dissipation. The data is used to compute the work input W_i and output W_o during a loading-unloading cycle, as explained in Section 4.5.1. The work input $W_{i,2}$ at ε_2 stage after pre-strain ε_1 is presented in Figure 62 using EPDM1b as an example. A linear relation is observed with the strain applied when $\varepsilon_1 = \varepsilon_2$. As expected, more energy is required when ε_2 increases; however, when $\varepsilon_1 < \varepsilon_2$ is analysed, the path follows a more complex response, with $W_{i,2}$ decreasing with the increase in ε_1. This is a general observation applicable also to the rest of the elastomers, whose energy maps are presented in Appendix B.3. The energy dissipated

during a loading cycle is not only dependent on the current stretch, but also on the previous deformation history.
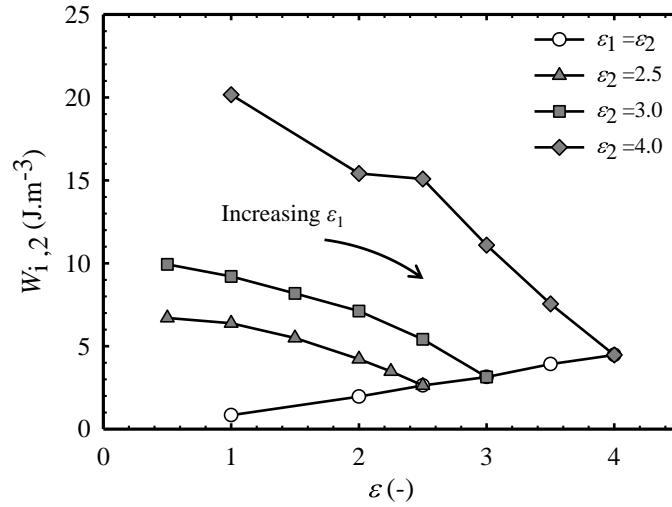
Figure 62. Work input $W_{i,2}$ as a function of ε_2, after $\varepsilon_1 < \varepsilon_2$ uniaxial pre-strain variation for EPDM1b.

The energy dissipated $\tilde{W}_d$ can also be calculated as a function of pre-strain during the stage ε_2. The dissipated energy $\tilde{W}_d$ is presented in Figure 63 as a function of W_i. The difference between the first $\varepsilon_{1,1}$ and fourth $\varepsilon_{1,4}$ cycle during pre-strain is also shown. After the first loading stage (with no previous deformation), the softening phenomenon takes place. During the first cycle, nearly all the materials follow a very similar, linear response. There is a linear correlation between the energy input required during loading and the total energy dissipated $\tilde{W}_d$ in that stage; however, the fourth cycle energies do highlight differences in the response between materials. This is presented in more detail in the figure inset.
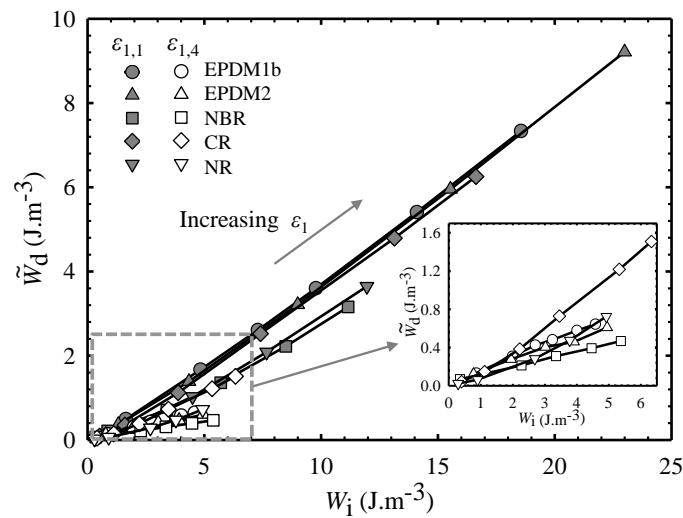
Figure 63. Energy dissipated $\tilde{W}_d$ as a function of work input W_i during first $\varepsilon_{1,1}$ and fourth $\varepsilon_{1,4}$ pre-strain cycles for filled elastomers.

Each material was analysed independently, plotting the energy $\tilde{W}_d$ at stage ε_2 in Figure 64 (a)-(e) as a function of the work input W_i during loading. The energy maps are presented for all materials, for the full range of ε_1 and ε_2 explored under uniaxial deformation (Table 14). With no previous deformation (i.e. denoted as cycle $\varepsilon_{1,1}$), dissipated energy is approximately a linear function of the input energy for all strain amplitudes.
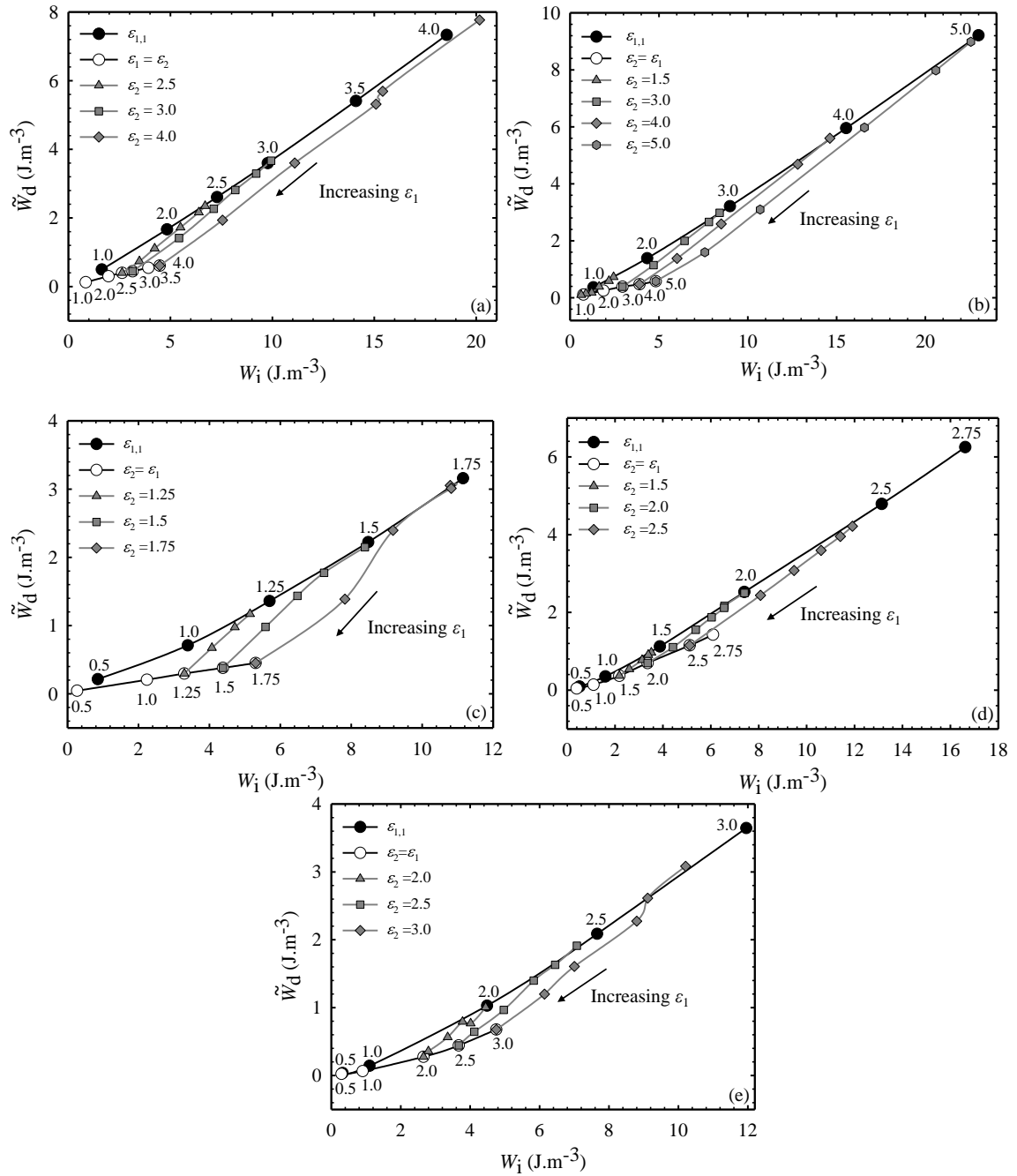
Figure 64. Energy dissipated $\tilde{W}_d$ as a function of work input W_i at different pre-strains ε_1 and ε_2 combinations for (a) EPDM1b (b) EPDM 2, (c) NBR, (d) CR, (e) NR.

After a pre-strain, two patterns of behaviour can be observed. When $\varepsilon_2 = \varepsilon_1$, the energy dissipated is again a linear function of the input energy for all strain amplitudes; however, there is a considerable decrease in the slope when compared with $\varepsilon_{1,1}$. In cases where $\varepsilon_1 < \varepsilon_2$ (pre-strain amplitude smaller than the cycle considered), an intermediate level of dissipation can be observed, transitioning from these two limits as ε_1 increases.

From the energy dissipated during the loading $\tilde{W}_d$, the cyclic dissipated fraction of energy, ϕ_c, in relation with the work input during the loading, can be calculated as

$$\phi_c = \tilde{W}_d / W_i \qquad \text{Eq. 4-3}$$

The values are presented in Figure 65 (a)-(e), showing the variation in ϕ_c as a function of W_i for the ε_1 and ε_2 combinations explored in Figure 64. The energy during the first cycle (no history) of the pre-strain is denoted as $\varepsilon_{1,1}$.

When varying the pre-strain ε_1, the dissipated fraction during the ε_2 stage goes from a higher value when $\varepsilon_1 < \varepsilon_2$, and decreases as ε_1 is increased, reaching a minimum at the condition $\varepsilon_2 = \varepsilon_1$. The range of fraction lies within the values of $\varepsilon_{1,1}$ and $\varepsilon_2 = \varepsilon_1$ when the strain is modified. For the conditions where $\varepsilon_1 \geq \varepsilon_2$, the fraction response is approximately constant for EPDM1b, EPDM2 and NBR, being independent of the current or previous strain. For CR and NR a similar increase trend is observed compared with the fraction of energy during the first loading ($\varepsilon_{1,1}$). The experimental findings give an insight into the restructuring ability of each material, with a characteristic parameter related also with the material composition. The transition observed in the fraction of energy ϕ_c maps, seems to indicate an evolution of the network where the restrictions in the network such as cross-links, entanglements and filler interaction evolve to a less restricted configuration after the material experiences a first deformation.

After the softening process, a structural equilibrium is quickly reached, and although the constitutive response differs substantially as a function of pre-strain, the dissipated energy fraction is relatively insensitive to this (for EPDM1, EPDM2 and NBR it is effectively independent of ε_1). This indicates that the dissipated energy occurring during deformation below the maximum strain is proportional to the stored energy. This lower dissipation is associated with viscoelastic processes within the material, such as rotation of bonds, frictional chain-chain, chain-filler and filler-filler sliding [29]. The energy necessary in subsequent deformations could be then associated with simple movements

inside the network such as freely rotating links (also called secondary forces) and frictions due to sliding between chain-chain and chain-filler.
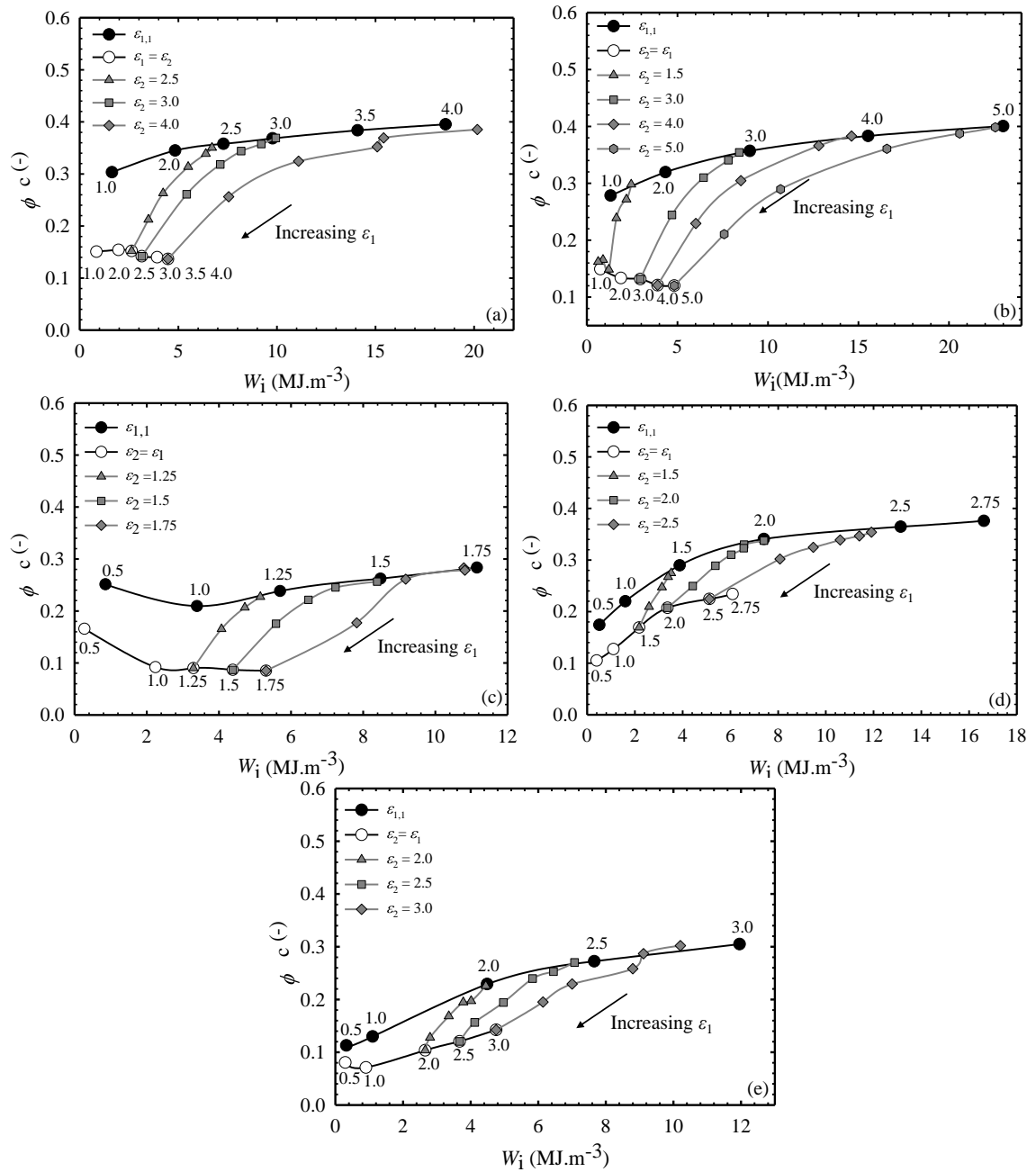
Figure 65. Fraction of energy dissipated, ϕ_c, during cyclic reloading to ε_2 as a function of work input W_i for different pre-strains of ε_1 for (a) EPDM1b (b) EPDM2, (c) NBR, (d) CR, (e) NR.

The mechanism of deformation, and hence the energy involved is observed to be characteristic for each elastomer evaluated. This offers a physical picture of a two-phase system where part of the rubber is able to deform elastically and to dissipate energy, and part is instead bounded to the surface of the filler. The act of scragging essentially frees an amount of elastomer from the surface of the filler, allowing it to deform and dissipate in the same way as the rest of the 'unbound' elastomer. This trend is consistent with the

observed effect of varying filler fractions on the mechanical response [29, 167, 178].

4.5.3 Energy dissipation under biaxial deformation

The energies stored and dissipated are also computed for elastomers subjected to EB and CW stretching. The dissipated energy fraction ϕ_c is shown for UN, EB and CW tensile testing deformations in Figure 66 with EPDM1b as an example. The inset shows the strain cycle protocol. For EB testing, the total energy in the system is considered as the sum of the energy dissipated on both axes. As for CW testing only one of the axes is deformed, hence only the energy related to the deformed axis is considered. During the first cycle $\varepsilon_{1,1}$, the fraction of energy dissipated ϕ_c for each mode of deformation starts at the same value, increasing slightly with increasing ε_1. A similar behaviour is observed for $\varepsilon_{1,4}$, with a decrease in ϕ_c due to softening. The energy dissipated in the intermediate conditions lie within the two ranges and is very similar for the three modes of deformation. All materials present a similar response; with exception of CR and NR with a slight increase in the fractions values of UN with respect of biaxial deformation (see Appendix B.4).
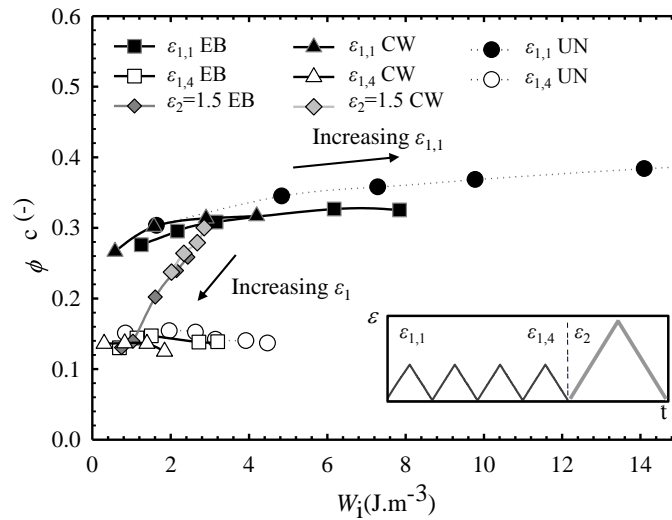
Figure 66. Comparison of the fraction of energy dissipated ϕ_c as function of work input W_i for EPDM1b under UN, EB and CW tensile testing. Several of ε_1 and ε_2 is presented. Inset describe the strain cycles protocol.

During the second stage ε_2, the deformation history dependence also presents an energy map transition as ε_1 increases. It is interesting that independently of the mode of deformation, each material exhibit a nearly constant value of ϕ_c for $\varepsilon_2 \geq \varepsilon_1$. The energy in the system seems to be an intrinsic property of the material, related with the structuring

of the network during deformation. However, the mode of deformation does not modify the relation between W_i and the fraction of energy dissipated ϕ_c . Independently of the mode of deformation, the elastomer has a fixed range of energy storage and dissipated.

Section 4.B   Modelling analysis

4.6   Constitutive model for mechanical and energy response

Mullins and Tobin [13, 15] initially suggested analysing a filled elastomer as a two-phase system to represent the softening, with a soft phase related with the elastomeric matrix and a hard phase associated with the filler and bound rubber. The phases are coupled in series to allow the reduction of the hard phase fraction with strain, highlighting the importance of the amount of reinforcement particles in the system in the mechanical response and Mullins effect [29, 167, 178]. Further approaches such as those presented by Qi and Boyce [104], De Tommasi el al. [179] and D'Ambrosio et al. [108] followed this early concept as a phenomenological path. A damage criterion was presented to explain the softening in the network, leading to no residual strain and an ideal Mullins response (reloading response coincides with previous unloading).

During the first investigations by Flory [39], the consideration of these two phase system was also presented. A predominantly elastic phase is called the soft phase and includes the rubber matrix. A secondary phase (the hard phase) with a viscous behaviour is composed of the filler combined with rubber in direct contact with the filler (bound rubber). This first approach can be integrated with coupled series and parallel phases, as suggested by Takayanagi [117] in his research on semicrystalline polymers. The approach has a soft phase (A), in parallel with a series-coupled soft phase (B) and hard phase (C), as shown schematically in Figure 67. In the original formulation of Takayanagi, the soft phases related to amorphous polymer and the hard to crystalline regions. In this work, the soft phase (A) is used to represent rubber that is free to deform and dissipates energy independently of the filler. The soft phase (B) represents rubber that is in the proximity of the filler but unbounded, and the hard phase (C) represents the combination of filler and filler-bound rubber that creates a relatively stiff inclusion. Phases (A) and (B) are intended to be the same material. This model captures the Mullins effect if the volume of soft phase (B) can increase at the expense of

the volume of hard phase (C) (i.e. bound rubber can become unbound). This transition is shown with the black arrows in Figure 67. A similar transition approach was used by Buckley et al. [74] to model the deformation of thermoplastic polyurethane elastomers in which a similar transition from hard phase to soft phase could be observed.
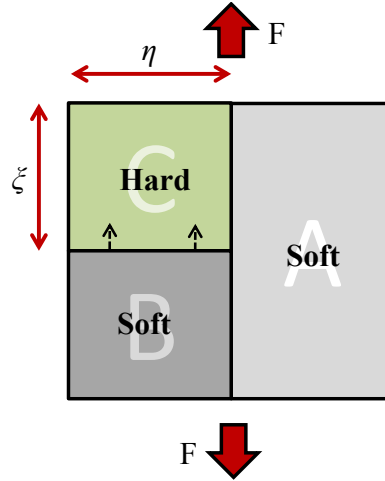
Figure 67. Representation of series and parallel coupling of the phases within the elastomer: soft phase (A) representing rubber free to deform and dissipate independently of the filler during an applied force F; soft phase (B) representing rubber coupled to the filler but free to deform; hard phase (C) representing the combination of filler and filler-bound rubber creating stiff inclusions. ξ and η are the parameters of the fraction of phase (C) in the network.

4.6.1 Physical model description

The model presented in this work defines the volume fraction of the hard phase as $\theta_{br} = \xi.\eta$. The parameter η is taken as a constant, assuming that only phase (B) is subjected to evolution from the hard phase during deformation. Due to the parallel coupling, η can be defined as a function of the cross-sectional area of phase (B), A_B, as well as of the area of phase (A), A_A, as

$$\eta = \frac{A_B}{A_t} \, ,$$

$$1 - \eta = \frac{A_A}{A_t}$$

Eq. 4-4

The ratio of areas is assumed to be proportional to the ratio of the volumes of the system. As the phases (B) and (C) are combined in series as

$$\sigma_B = \sigma_C$$

Eq. 4-5

When considering the parallel phases, the total stress is defined as the sum of forces of phase (A) and (B), acting on the relevant areas A_A for phase (A) and $A_C = A_B$ for phases

(C) and (B). Hence, the nominal stress can be expressed as

$$\sigma = \frac{F}{A_t} = \frac{F_A + F_B}{A_t} = \frac{F_A}{A_t}\frac{A_A}{A_A} + \frac{F_B}{A_t}\frac{A_B}{A_B}$$

Eq. 4-6

Combining Eq. 4-4 and Eq. 4-6, the total stress can be defined as

$$\sigma = \sigma_A(1-\eta) + \sigma_B\eta$$

Eq. 4-7

Figure 68 shows the coupling of the three phases of a filled elastomer system, identifying the lengths as well as the area distributions of each phase according with the volumetric fraction.
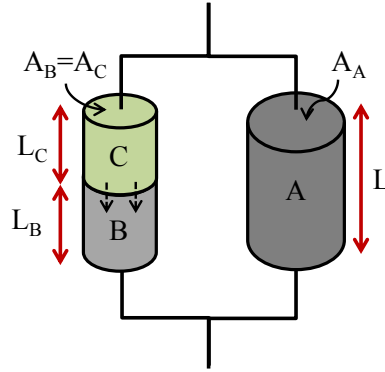
Figure 68. Distribution of lengths and areas in the phases coupling arrangement for filled elastomers.

The initial and final values of the length for each phase can then be represented as L_{B0} and L_B for phase (B), and L_{C0} and L_C for phase (C). The stretches can be expressed as

$$\lambda_C = \frac{L_C}{L_{C0}} \quad,$$

$$\lambda_B = \frac{L_B}{L_{B0}}$$

Eq. 4-8

The parameter ξ is used to describe the length fraction of distribution for (C) as

$$\xi = \frac{L_{C0}}{L_0}$$

Eq. 4-9

To relate the total stretch in the system, λ, to the stretch suffered on each phase, the total stretch in the phase (A) is considered $\lambda = \lambda_A$. Rearranging λ using L_0 and L as the initial and current length of the system

$$\lambda = \frac{L}{L_0} = \frac{L_C + L_B}{L_0} = \frac{L_B}{L_0}\frac{L_{B0}}{L_{B0}} + \frac{L_C}{L_0}\frac{L_{C0}}{L_{C0}}$$

Eq. 4-10

By combining Eq. 4-9 with Eq. 4-10, the stretch λ can be expresses in terms of the volume fraction parameter ξ, as

$$\lambda = \lambda_A = \lambda_C \xi + \lambda_B (1-\xi)$$

<div align="right">Eq. 4-11</div>

4.6.2   Gaussian rubber response.

In order to explore whether this type of model is able to produce energy maps similar to those presented in Figure 65, the following constitutive relationships to the material phases are attributed: a linear elastic behaviour to the hard filler phase (C), with modulus E_c, and the same Gaussian hyperelastic behaviour to the soft phases (A) and (B), with shear modulus G. The stresses in the three phases can therefore be expressed as

$$\sigma_A = G(\lambda - 1/\lambda^2)$$

<div align="right">Eq. 4-12</div>

$$\sigma_B = G(\lambda_B - 1/\lambda_B^2)$$

<div align="right">Eq. 4-13</div>

$$\sigma_C = E_c(\lambda_C - 1)$$

<div align="right">Eq. 4-14</div>

It should be noted that although phases (A) and (B) have the same constitutive law, they experience a different stretch due to the coupling of phase (B) to the hard phase (C).

4.6.2.1   Evolution of the hard phase by finite extensibility interpretation

As a way of representing the freeing of rubber from the surface of the filler that takes place during first stretching, the fraction ξ is allowed to vary as the strain increases, by limiting it to the finite extensibility of a single chain, λ_{max}. As the hard phase has the filler and hence the higher stiffness, when deformation is applied, due to the series coupling the majority of the stretch will be focused on the soft phase λ_B. Once λ_B reaches λ_{max}, the soft phase is not able to deform any further. The condition $\lambda_B > \lambda_{max}$ is physically impossible, and would result in a break of the chains. To be able to continue with deformation, material is extracted from the hard phase to compensate for the stretching, reducing the fraction ξ. In reality, the value considered for λ_{max} should be smaller than the maximum extensibility of the chain, as the chain is never completely stretched due to entanglements and cross-links. In this first approach, this consideration is neglected for simplification of the model.

Figure 69 shows a physical representation during the stretching of the phases, with a

section of the hard phase $d\xi$ added to the soft phase (B) when λ_{max} is reached during deformation. Further reduction of ξ occurs when the subsequent strain surpasses the previous deformation and the condition $\lambda_B = \lambda_{max}$ is reached again.
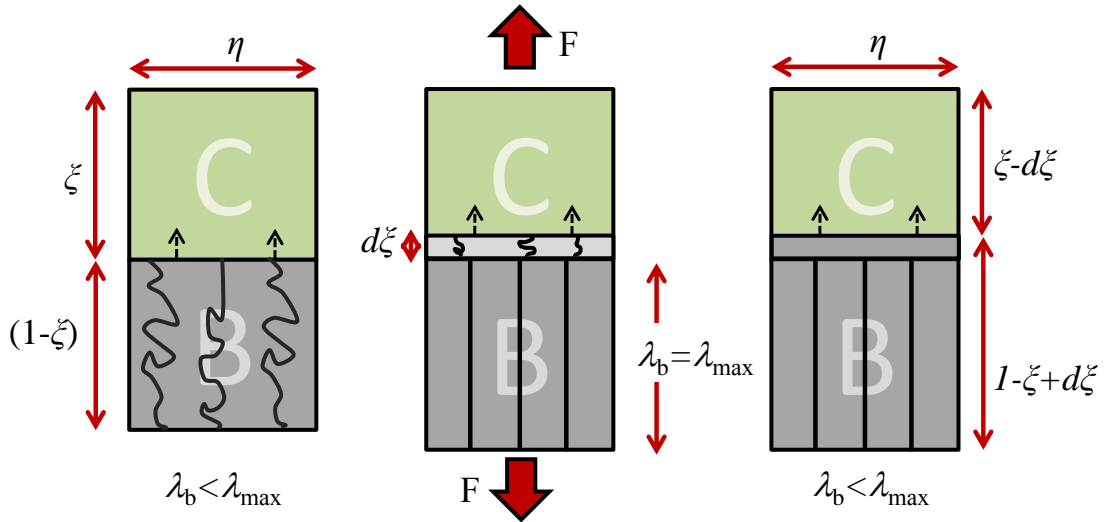
Figure 69. Representation of the evolution of the fraction ξ on the hard phase (C) into soft phase (B) during stretching.

As the stresses in phases (B) and (C) are equal ($\sigma_B = \sigma_C$), Eq. 4-13 and Eq. 4-14 are combined together, substituting λ_C from Eq. 4-11, with the condition $\lambda_B = \lambda_{max}$. The evolution of ξ can be expressed as

$$\xi = \frac{\lambda_{max} - \lambda}{\lambda_{max} - k}$$

Eq. 4-15

where *k* is a constant defined as

$$k = \frac{G}{E_c}\left(\lambda_{max} - \frac{1}{\lambda_{max}^2}\right) + 1$$

Eq. 4-16

4.6.2.2 Experimental Parameters

4.6.2.2.1 Volume fraction of the hard phase

In this first implementation, the fraction of free rubber (A) is assumed to remain constant at $(1-\eta)$, and the remaining material fraction η is apportioned into the evolving phases (B) and (C). The total volume fraction of the hard phase (C) is given then by $\theta_{br} = \xi.\eta$, with the remaining fraction $(1-\xi).\eta$ on the soft phase (B) (Figure 69). Phase (C) is intended not as the volume fraction of the filler itself but rather as the total

volume of the filler and the filler-bound rubber (the surrounding rubber interacting with the filler).

As a way to define the total fraction of the hard phase (C), the amount of bound rubber (including the filler) is estimated experimentally. In order to determine the amount of rubber that is bound to the carbon black filler an unvulcanised compound is needed. The technique lies on the solubility of the unvulcanised and unbounded rubber in a good solvent. As the rubber is not cross-linked, the polymer chains interact with the solvent, dissolving the fraction that is not bound to the filler (insoluble in the solvent). This is a suitable technique to approximate the amount of elastomer interacting with the surface of the filler. Meissener [180] defines the bound rubber as a random adsorption of polymer by reactive sites of the filler particles. The amount of bound material will depend mainly on the chemical structure of the polymer and on the surface and dispersion of the filler. Leblanc [181, 182] analysed the interaction between the filler and the rubber, describing the main theories reported for the bound rubber. He explained that the surface of the filler traps the chains of polymers in direct contact, interpreting this as a topological constraint on the elastomer, preventing this fraction of polymer from being dissolved if it is in contact with a solvent. The determination of the bound rubber is not only related with the filler surface area and surface activity, but also with other factors such as filler dispersion and extraction solvent and temperature [8]. Leblanc [9] reviewed different techniques where the bound rubber is determined on different filled elastomers.

In the present work, the filled elastomers EPDM1b and NR are used as they are the only compounds available unvulcanised. Toluene was chosen as solvent due to their similarity in the solubility parameter with the elastomers analysed, making it a good solvent for the polymeric chains of the elastomers [41] [183]. Three samples per elastomer were used to calculate an average of the bound rubber. The mass of each sample was initially recorded using a Mettler Toledo XS105 analytical balance [184], and afterwards placed in approximately 50ml of toluene for five days at room temperature (20˚C ±1˚C). The solvent was replaced twice during the immersion time. The extraction of the bounded rubber was made using vacuum filtration. The final sample was dried at 40 °C for the first 2 hours, and left for another 48 hours at room temperature to ensure the complete evaporation of the Toluene. The final weight was recorded. The mass fraction which could not be dissolved is considered the fraction of

bound rubber and can be used to define the initial fraction of the hard phase (C), θ_{br}, as presented in Table 17. In the case of the NR, the sample turned gel-like, showing also an obvious release of filler as the solvent become black. It is important to acknowledge that the content of oil in the compound is assumed to be dissolved in the solvent too. Hence, the total amount of bound rubber defined through this technique should include only the filler and the rubber in direct contact with the filler.

Table 17. Fraction of bound rubber θ_{br} for EPDM1b and NR using toluene as solvent. Fraction of carbon black content ϕ_{CB}^{TGA} .

Elastomer	θ_{br} (-)	ϕ_{CB}^{TGA} (-)
EPDM1b	0.45 ± 0.27	0.25 ± 0.01
NR	0.68 ± 0.15	0.21 ± 0.01

From the characterisation presented in Section 3.4.4 using thermogravimetry, the percentage of filler in the compound, ϕ_{CB}^{TGA}, can be assumed as the minimum value of θ_{br} assuming an extreme condition when all the rubber becomes unbounded during the deformation evolution. The value of ϕ_{CB}^{TGA} for both elastomers is also reported in Table 17. However, the specific fraction of η and initial value ξ_0 is difficult to establish. As a simple first consideration, η is assumed as 0.55 and ξ_0 as 0.85 using θ_{br} from EPDM1b

4.6.2.2.2 Modulus values

As the properties of the unfilled elastomers were not available directly, three options to determine the Modulus of the elastomer, *G*, are initially proposed. The first method is using the theory of hydrodynamics initially proposed by Einstein that describes the increase in viscosity of a fluid combined with rigid particles [185-187]. By this theory, it is possible to relate the viscosity of the compound with the viscosity of the unfilled elastomers, depending of the fraction of filler in the compound. Further research has related this theory with reinforced elastomers (Smallwood [188], and Guth and Gold [189]) expanding the equation to associated theory with the modulus of the filled and unfilled material, and to account the particle packing and interaction between filler-filler. A number of assumptions are involved in the development of these theories, such as the spherical morphology of the filler, the filler being considerably stiffer than the matrix and that there is no slip between the filler and the rubber matrix. For this work, the expansion of the theory presented by Chen and Acrivos [190] is used to determine G_0 of the unfilled elastomer as

$$G_0 = G_{100\%}(1 + 2.5\phi_{CB}^{TGA} + 5.0(\phi_{CB}^{TGA})^2)$$

<div align="right">Eq. 4-17</div>

with the coefficient values of 2.5 and 5.0 obtained by Chen and Acrivos through a fitting process. Using the fraction of carbon black ϕ_{CB}^{TGA} showed in Table 17, determined in Section 3.4.4, the shear modulus $G_{100\%}$ can be calculated from the experimental value of the Young's Modulus at 100 % deformation, $E_{100\%}$, of the filled elastomer (Section 3.6.3) assuming incompressibility of the material.

The other two approaches to calculate G are through the Affine G_{aff} and Phantom G_{pha} theory described in Section 2.7.1. The modulus for each theory can be calculated as

<div align="right">Eq. 4-18</div>

$$G_{aff} = \frac{\rho_2 RT}{M_c}$$

$$G_{pha} = \frac{\rho_2 RT}{2M_c}$$

<div align="right">Eq. 4-19</div>

where R is the gas constant, T the absolute temperature, ρ_2 the density of the polymer, and M_c the average molecular weight between cross-links [191, 192]. The values of density for each material were determined in Section 3.4.1. The values of M_c are determined in Chapter 6 using the swelling technique.

The three values of G calculated using the different methods are reported in Table 18 for the unfilled EPDM1b and NR. As the bound rubber was determined for EPDM1b and NR, only these two materials are chosen to determine the experimental parameters for the model. It is worth acknowledging that the experimental values used in these two last approaches are from the filled elastomers, giving a higher magnitude of the modulus than G_0. However, the phantom approach gives magnitudes of the modulus very similar to G_0. A lower value of G_{pha} compared with G_{aff} is a consequence of the assumption that fluctuations of the junctions in the phantom model are unaffected by deformation [192]. As the values of G_0 and G_{pha} are very similar, G_{pha} is chosen for the analysis of the model in further simulations.

Table 18. Shear modulus calculated through Hydrodynamic Theory, G_0, Affine Model , G_{aff} , and Phantom Theory, G_{pha}.

Elastomer	G_0 (MPa)	G_{aff} (MPa)	G_{pha} (MPa)
EPDM1b	0.3161	0.7859	0.3929
NR	0.2852	0.6737	0.3368

In the case of the carbon black filler Young's Modulus, E_c, the specific value of particles and aggregates is it difficult to obtain experimentally, so the modulus of graphite is considered instead. Table 19 shows ranges of values of E_c reported in the literature. In the present work, the value of E_c=10 GPa is chosen for future analysis on the model.

Table 19. Young's Modulus E_c (GPa) for graphite reported in the literature.

	E_c **(GPa)**	**Reference**
Graphite	10	Omnes [193]
	10-21	Boylan [194]
	4.1-27.6	AZom Limited/Granta Design[195]
	10.34-12.41	Marlowe [196]

4.6.2.2.3 Finite extensibility

In order to obtain the maximum extensibility of a single chain between two crosslinks, λ_{max}, an average length of the elastomeric chain can be calculated using the relation of the spatial configuration of the unperturbed end-to-end chain distance with the limiting extension of a freely jointed chain [197, 198]. The freely oriented units along a segment of the chain between crosslink points (or entanglements), n_b, can be expressed as

$$n_b = \frac{XM_c}{M_0}$$

Eq. 4-20

where X is the number of C-C bonds in a monomer main chain (EPDM X= 6, and NR X=4) and M_0 is the molar mass of the monomer unit. The values of M_c are determined in Chapter 6 using the swelling technique. As a way to relate the unperturbed end to end distance and the freely jointed chain, Flory [199] defined a constant parameter for a given monomeric unit named the characteristic ratio, C_∞. This parameter relates the number of freely jointed chains in the length segment with the total length of the chain between two constraints points, associated with λ_{max}, with the final expression as

$$\lambda_{max} = \sqrt{\frac{n_b}{C_\infty}} \sin\left(\theta_b / 2\right)$$

Eq. 4-21

The last term of the equation includes the effect of bond angles, accounting for the fact that the chains are more rigid than the freely configurational links. The chains are assumed in this section with a zig-zag (all trans) configuration, where θ_b is the angle between C-C bonds ($\theta = 109.28°$) [197, 200].Table 20 reports the values of n_b and the

values of C_∞ reported in the literature for EPDM and NR [133, 183].

Table 20. Values of freely jointed units between entanglements n_b, characteristic ratio C_∞, and finite extensibility of a chain λ_{max} of EPDM1b and NR.

Elastomer	n_b	C_∞	λ_{max}
EPDM1b	300.8	6.9	17.8
NR	225.7	5.0	18.4

4.6.2.3 Simulation

With the parameters described previously, the evolution of ξ is used to describe the effect of deformation in the stress response under pseudo-cyclic deformations for stretches between 2.0 and 6.0. The simulation was generated using the programming software Matlab®. The description of the stress and the phase distribution is used to calculate the stretch in the soft phase (B) and hard phase (C) in order to satisfy the conditions presented in Section 4.6.2. The stretch in the soft phase (B) is shown in Figure 70 (a). The stretch in the soft phase (B) is considerably higher than the macroscopic stretch, as it is in series with the hard phase (C), whose stretch is considerably lower due to the stiffness. The stretch in the soft phase (B) λ_B reaches $\lambda_{max} = 17.8$ during the third cycle. As it is not possible to reach a higher stretch, the evolution starts in this stage, pulling material from the hard phase (C) into the soft phase. The evolution of ξ is presented in Figure 70 (b), where the fraction of the hard phase is reduced through the increase on deformation. At the end of the test, the final value of $\xi = 0.70$ is reached, giving a total final fraction of the hard phase *of* $\theta_{br} = 0.39$, still higher that the carbon black content of EPDM1b (Table 17), which could indicate that the hard phase still maintains some bound rubber.
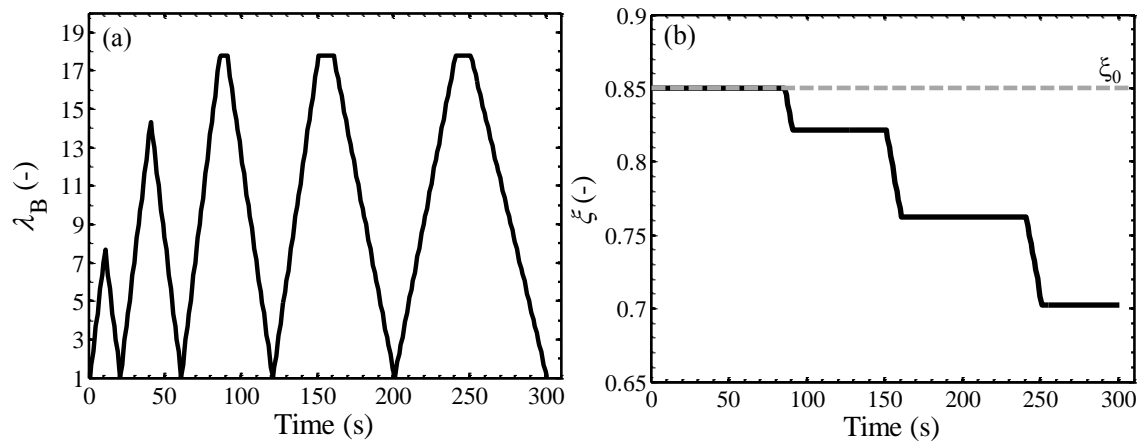
Figure 70. (a) Stretch in the soft phase (B) λ_B, and (b) Prediction of the evolution of ξ, during pseudo-cyclic deformation according to the modelling of rubber Gaussian approach.

The model is capable of describing the variation in the stresses on each phase, as presented in Figure 71. The stress in phases (B) and (C) are the same, as they are connected in series. However, the soft phase (A) experienced a smaller stress during the same total stretching. The total stress of the system will be then the combination of the three phases as defined in Eq. 4-7.
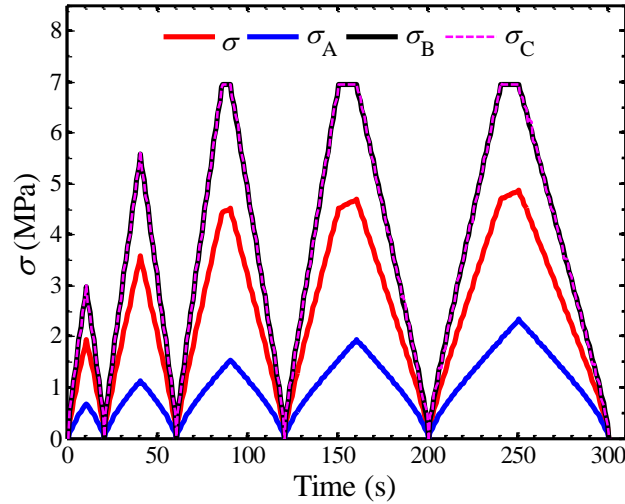
Figure 71. Stresses generated by the rubber Gaussian model approach for each phase of the network. σ is the total stress in the system, σ_A the stress suffered in the soft phase (A), σ_B the stress suffered in the soft phase (B), and σ_C the stress suffered in the hard phase (C).

The total stress-strain response generated by this model using the parameters of EPDM1b is shown in Figure 72 for the pseudo-cyclic deformation shown in the inset. The same trend is observed when the parameters values for NR are used in the model (not shown). As during the first two cycles the evolution has not started the stress-strain response follows the same loading-unloading path, without any softening or permanent modification of the system. In reality, the material suffers modification even at smaller deformations.

Figure 72. Cyclic stress response through pseudo-cyclic stretches λ from 2.5 to 6.0, using rubber Gaussian approach modelling using EPDM1b parameters.

4.6.3 Gaussian rubber model with flow stress

The first approach presented can capture the essence of the stress softening through the phase evolution of ξ. However it lacks any dissipation mechanism beyond that produced by the evolution of ξ. To account for this, the inclusion of a constant flow stress, σ_f is either added during a loading cycle or subtracted during an unloading cycle to both rubber phases (A) and (B).

$$\sigma_A = G(\lambda - 1/\lambda^2) \pm \sigma_f \qquad \text{Eq. 4-22}$$

$$\sigma_B = G(\lambda_B - 1/\lambda_B^2) \pm \sigma_f \qquad \text{Eq. 4-23}$$

As the stresses in phases (B) and (C) are equal ($\sigma_B = \sigma_C$), the new stress condition of the soft phase (B) in Eq. 4-23 and Eq. 4-14 can be combined together with the condition of $\lambda_B = \lambda_{max}$ to get the evolution of ξ, with a new constant value of k defined as

$$k = \frac{G}{E_c} \left(\lambda_{max} - \frac{1}{\lambda_{max}^2} \right) + \frac{\sigma_{flow}}{E_c} + 1 \qquad \text{Eq. 4-24}$$

Previous work presented by De Focatiis et al. [80] on EPDM, separated the rubbery and viscous contribution in the stress response during a cyclic deformation using the Edward-Vilgis strain energy function [201]. The Figure 73 (a) is an adaption of the data presented by De Focatiis et al., showing the extraction of the rubbery and viscous contribution from a stress-strain cycle. From this analysis, the magnitude of the flow stress can be estimated with the viscoelastic contribution to the stress during the first unloading-reloading, accounting the strain rate used in the experimental testing. The contribution of the stress flow σ_f from the viscoelastic response is presented in Figure 73 (b) for uniaxial tests up to different values of previous maximum strain.
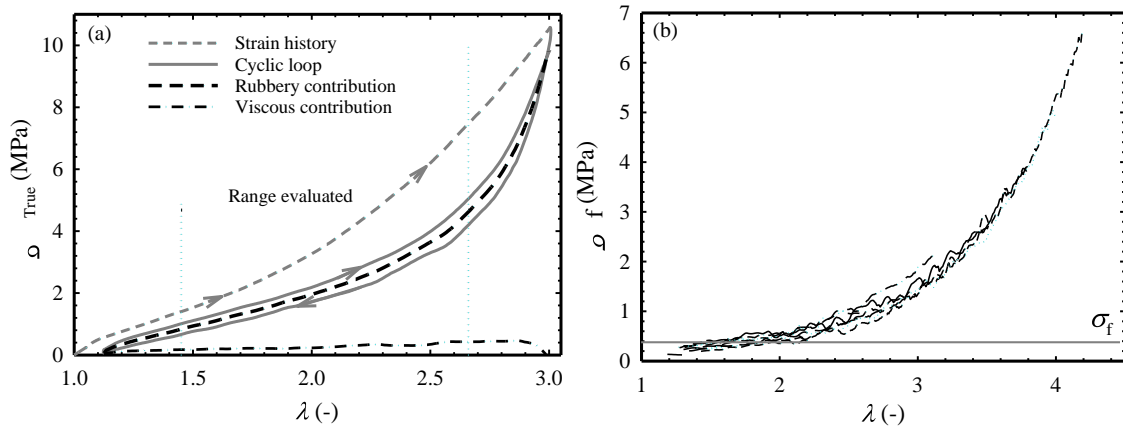
Figure 73. (a) Extraction of rubbery and viscous contribution of EPDM, based in Edwards-Vilgis strain energy function (b) Stress flow σ_f as a function of the stretch. Data adapted from [80].

It is recognised that the simplistic treatment of the σ_f contribution in Eq. 4-22 and Eq. 4-23, lacks proper stretch dependence, and also that the strain rate in phases (A) and (B) will differ. The σ_f values from the experimental data shows a clear exponential dependence with the stretch; however, the assumption of a constant value (independent of the stretch) is sufficient at this stage to illustrate the basic principle. As illustrated in Figure 73 , the value of $\sigma_f = 0.4$ MPa is chosen for the development of the model.

4.6.3.1   Simulation

The model described in Section 4.6.2 is modified to account for σ_f in the soft phases due to the viscoelastic behaviour of the elastomer. The stress-strain response produced with the added flow stress σ_f is show in Figure 74. The response illustrated is qualitatively similar to the stress-strain curves shown in where the reloading and the unloading responses differ. Through the constant σ_f assumption during the entire range of stretch, it is possible to represent the softening effect as the stretch is increased, together with the evolution of ξ, as presented in Figure 70.
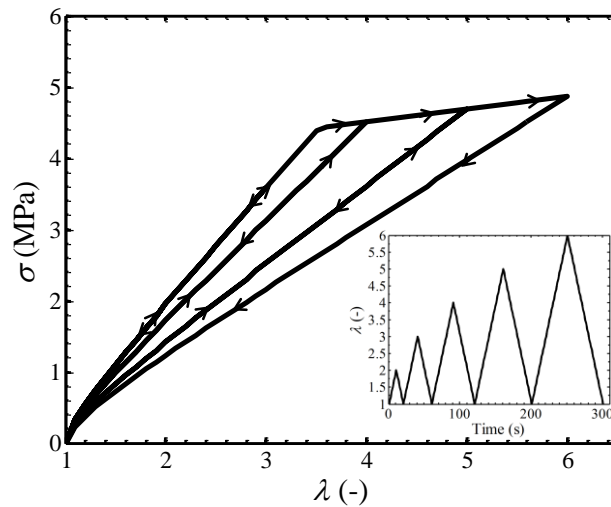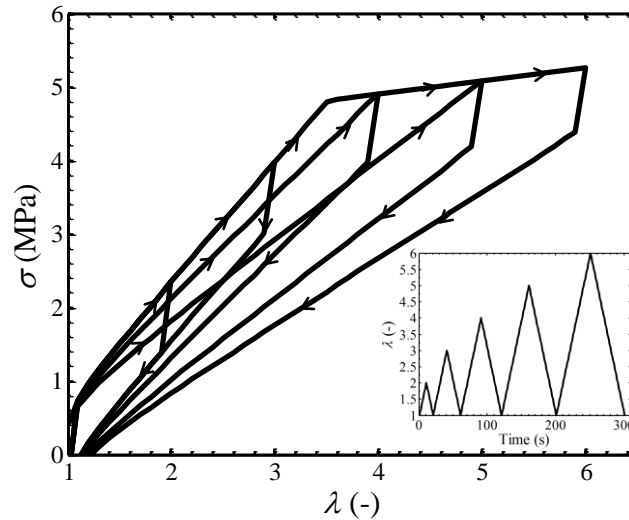

Figure 74. Cyclic stress response through pseudo-cyclic stretches λ from 2.5 to 6.0, using rubber Gaussian approach modelling with stress flow σ_f.

Once the flow stress condition is included in the viscoelastic behaviour of the elastomer, the stress-response follows a path more characteristic of the real response of filled elastomers. As the deformation in phase (B) reaches $\lambda_B = \lambda_{max}$, the evolution of ξ starts, modifying the distribution of stresses, as presented in Figure 75.
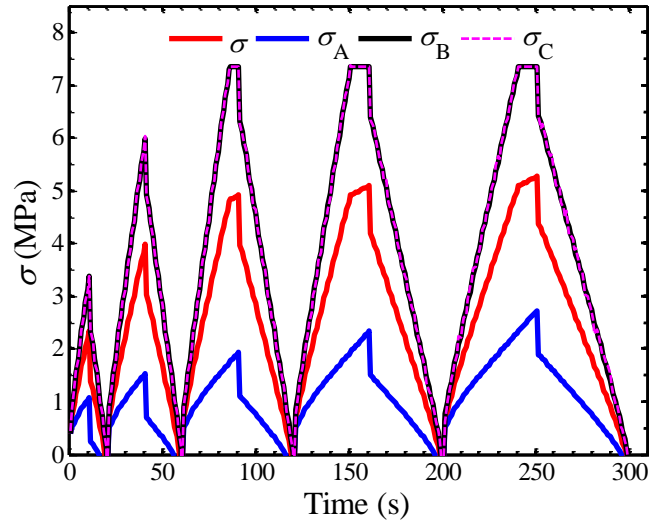
Figure 75. Stresses generated by the rubber Gaussian with stress flow model approach for each phase of the network. σ is the total stress in the system, σ_A the stress suffered in the soft phase (A), σ_B the stress suffered in the soft phase (B), and σ_C the stress suffered in the hard phase (C).

To estimate the strain energy variation, the model is evaluated at strain protocols with and without strain-history, as for the experimental data in Section 4.5. Evaluating the energy during the first cycle (no strain history) and following strain-history, it is possible to qualitatively replicate the energy map described for the experimental data in Section 4.5.2, as presented in Figure 76. The inset schematise the strain cycles, with the first cycle (no history) as $\varepsilon_{1,1}$, the subsequent cycle at the same strain as $\varepsilon_{1,4}$ and the second stage as ε_2, reproducing the experimental test in Section 4.5.

The model can reproduce qualitatively the energy map as function of the strain history and the strain applied. The main shortcoming observed in the modelling is that, at lower values of strain, there is no variation in the energy dissipated between cycles. This is due to the conditioning of the evolution of ξ with the finite extensibility of the chain, λ_{max}. When the stretch is lower than λ_{max}, no evolution and hence, no softening of the material is observed.

The approach does not account for any constrains from entanglements, ramifications and cross-link points in the chain as the softening is set to start when the stretch in one of the phases reaches λ_{max}. The following section introduces a modification in the model for a more accurate representation of the behaviour of the elastomeric phases.
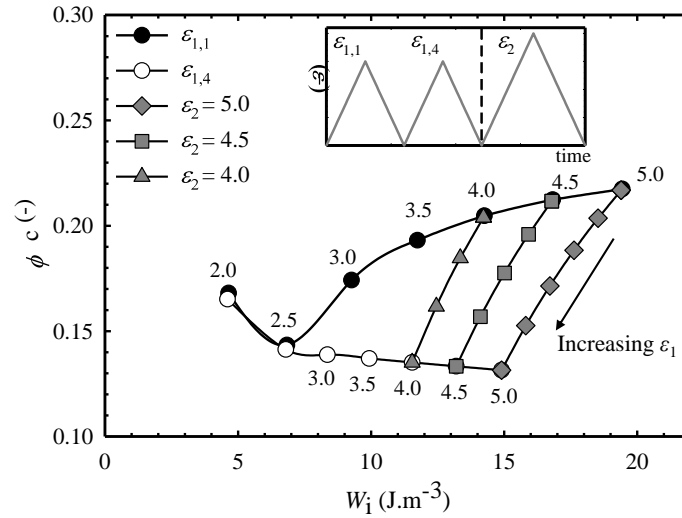
Figure 76. Modelling of the fraction of energy dissipated, ϕ_c, during cyclic reloading to ε_2 as a function of work input W_i for different pre-strains of ε_1 for EPDM1b using the Gaussian approach with flow stress.

4.6.4 Rubber behaviour according to Edwards-Vilgis theory with flow stress

The tube confinement theory presented by Edwards and Vilgis [201, 202] introduces the concept of entanglements and topological constraints in the theory of rubber elasticity (Appendix E). These entanglements are arranged in the network pictured as a tube formed by the neighbouring chains around one single chain. The displacement of these chains during deformation twist the chain in a motion called as reptation [202, 203]. The model predicts the behaviour of the material by including in the strain energy function the effect of slip-links and cross-links in the tube model, giving a good approximation in the analysis of the response of elastomers [19, 60, 80].

The theory describes the total strain energy function as the sum of the energy related with the density of the cross-links and with the slip-links present in the system. Assuming that the network is highly cross-linked, the total energy can be related only with the cross-link density. The final stress in the soft phases will depend then of the shear modulus of the elastomers and the chain extensibility.

The parameter for λ_{max} calculated in Section 4.6.2.2.3 can be used to determine the chain extensibility as $1/\lambda_{max}$. The stresses in the soft phases will again include a flow stress σ_f as an additional constant as presented in Section 4.6.3. The total stress remains as presented in Eq. 4-7, as well as the stress experienced by the hard phase (C) in Eq. 4-14.

4.6.4.1 Stress flow evolution condition

Due to the chain extensibility inclusion in the stress response of the soft phases, the condition of $\lambda_B = \lambda_{max}$ cannot be satisfied, as the stress tends to infinity as λ_B approaches λ_{max}. The condition of stress flow σ_f, also complicates the initial conditions of $\sigma_B = \sigma_C$ at $\lambda_B = \lambda_{max}$, as presented in Figure 75. It is necessary to set a new condition for the evolution of ξ. One approach is to set the boundary of ξ as a function of a flow stress limitation in the network. This introduces a new parameter σ_{Cflow} to establish the limit at which the evolution of ξ starts, instead of λ_{max}. When the condition $\sigma_B = \sigma_C = \sigma_{Cflow}$ is reached, the evolution of the hard phase (C) in to the soft phase (B) begins, as shown in Figure 69. In order to keep $\sigma_B = \sigma_C \leq \sigma_{Cflow}$, the assumption of $\sigma_C = \sigma_{Cflow}$ is combined together with Eq. 4-11 and Eq. 4-14 to give

$$\lambda_B = \frac{\lambda - \dfrac{\xi \sigma_{Cflow}}{E_c} - \xi}{(1 - \xi)} \qquad \text{Eq. 4-25}$$

to calculate the evolution of ξ that satisfies the statements. The magnitude of σ_{Cflow} is set to 7MPa from the stress when $\lambda_{max} = 17.8$ in the Gaussian approach.

4.6.4.2 Simulation

The Edwards-Vilgis tube theory modification of the soft phases is simulated using the same physical model described in Section 4.6.1, using the experimental parameters of EPDM1b defined in Section 4.6.2.2. The simulation is generated using the programming software Matlab®. From the condition of $\sigma_B = \sigma_C \leq \sigma_{Cflow}$, λ_B can be determined. As presented in Figure 77 (a), the maximum stretch in the soft phase (B), λ_B, is lower than in the previous approach with Gaussian behaviour, as the stress is now calculated from the Edwards-Vilgis function. Due to this, the evolution the ξ now starts at lower values of the stretch applied to the network, hence with a higher reduction of the fraction of the soft phase. At the end of this simulation, the final value of approximately ξ=0.38, giving a total θ_{br}=0.21, is just below the content of carbon black (Table 17).
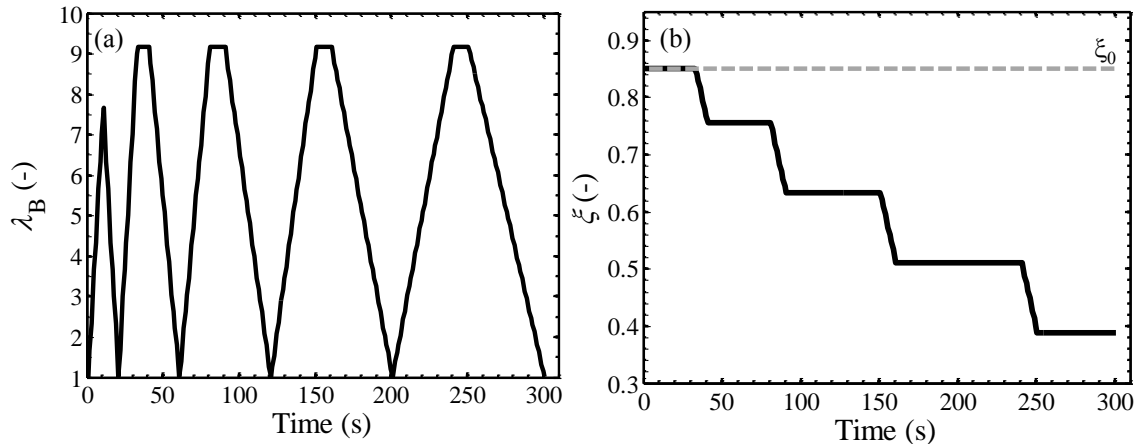
Figure 77. (a) Stretch in the soft phase (B) λ_B , and (b) Prediction of the evolution of ξ, during pseudo-cyclic deformation according to the modelling of filled rubber using Edwards-Vilgis approach.

It is worth acknowledging that the maximum strain before failure was measured in Section 3.6.1, as ε_f =511.44 ±18.75 % for EPDM1b, and hence a stretch of 6 used in this simulation would imply a failure of the material.

The stresses in each phase are reported in Figure 78. The stress in the soft phase (B) and hard phase (C) are considerably higher than the stress in the soft phase (A), as presented previously with the Gaussian approach in Figure 71. In this case, the condition of $\sigma_B = \sigma_C = \sigma_{Cflow}$ is already reached when the network is subjected to $\lambda=3$, due to the Edwards-Vilgis function.
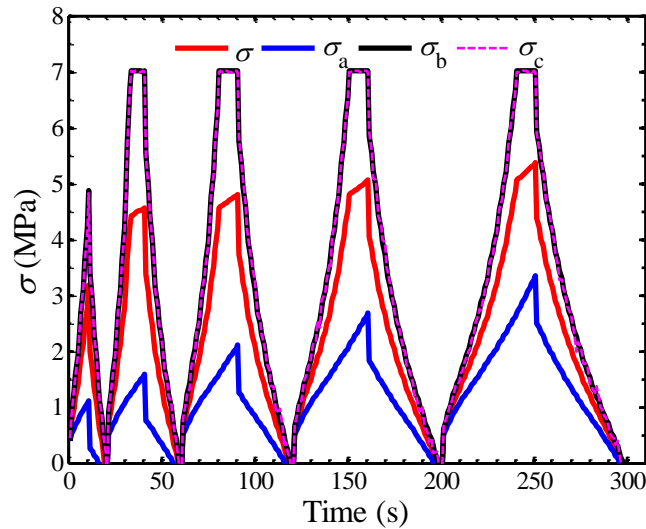
Figure 78. Stresses generated by the Edwards-Vilgis model approach for each phase of the network. σ is the total stress in the system, σ_A the stress suffered in the soft phase (A), σ_B the stress suffered in the soft phase (B), and σ_C the stress suffered in the hard phase (C).

The total stress in the network as a function of the stretch is plotted in Figure 79. In this case, the loading–unloading path follows a more realistic behaviour of a filled

elastomer. The non-linearity of the stress-strain dependence is accounted for in the Edwards-Vilgis approach. Though there is a strong change in the gradient during loading (when the condition $\sigma_B = \sigma_C = \sigma_{Cflow}$ is reached), the model is capable of qualitatively describing the behaviour of the material, showing the softening effect and the influence of strain history.
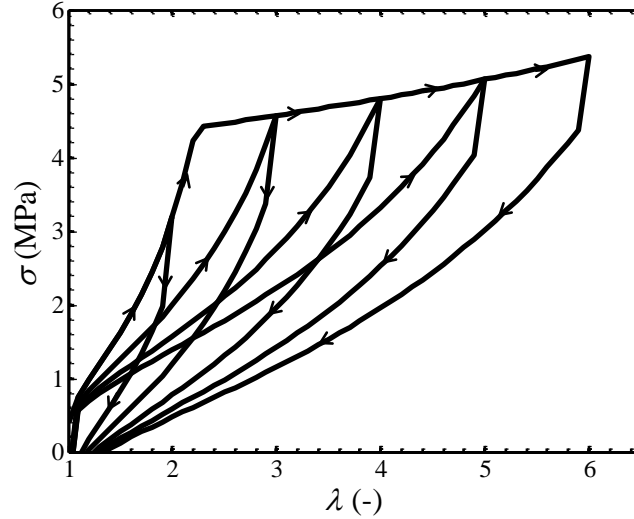
Figure 79. Cyclic stress response through pseudo-cyclic stretches λ from 2.5 to 6.0, using Edwards-Vilgis approach modelling.

With the modelling developed in the previous section, the energy dissipation can be calculated under uniaxial tensile deformation, as presented experimentally in Section 4.5.2. The modelled energy map for EPDM1b is presented in Figure 80.
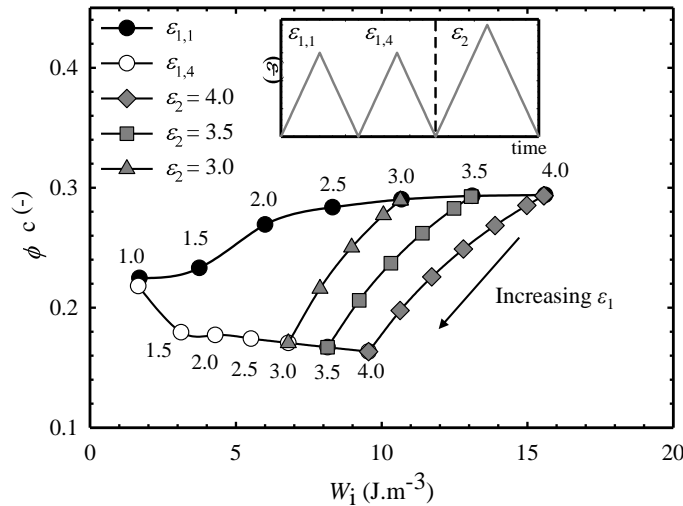
Figure 80. Modelling of the fraction of energy dissipated, ϕ_c , during cyclic reloading to ε_2 as a function of work input W_i for different pre-strains of ε_1 for EPDM1b using Edwards-Vilgis modelling.

4.6.5   Discussion

The approach presented is a simple way to describe the mechanism of a filled elastomer network structure. It has the capacity to qualitatively predict the constitutive response accounting for the influence of strain history. However, it is clear that the model cannot in its present form quantitatively reproduce the experimental data due to many simplifying assumptions.

With the Gaussian approach, the nominal stress is considered to be proportional to the extension ratio. For small deformations, the free energy of each segment of the network will follow the path with the minimum free energy for a given end-to-end chain location. Whilst this provides a good estimate of the response, under real network conditions, the constraints on the stretching of the polymer chains limit this maximum distance. This indicates that the assumption of the use of λ_{max} as the finite extensibility of the chain in the Gaussian approach is realistically impossible, as assumes no entanglements or any other constraint. At the limit of strong forces, e.g when the chains of the network become highly extended, the end-to-end distance becomes an appreciable fraction and the constraints will be more influential on the deformation mechanism. To compute this, a finite extensibility description must be considered to include the influence of constraints. The non-linear effects present additional challenges that should be presented as an extension to the work presented.

This was accounted for by invoking a non-Gaussian strain-energy function like the Edwards-Vilgis tube theory, describing the configurational movements of the network and the constraints present due to the cross-links points [201, 202, 204]. The modification using this approach gives a better response, closer to that observed in real filled elastomers. However, as the σ_{cflow} is set as a constant, an abrupt evolution is observed when σ_{cflow} is reached (Figure 79). It is clear that a more gradual evolution is needed. Also, the flow stress σ_{flow} was assumed as a constant for initial simplification, while was shown in the experimental data presented by De Focatiis et al. [74] that the flow stress is a function of the strain applied. This should also be included in further development of this model.

4.7   Summary

The mechanical response, presented in Section 4.4.1 for each material, demonstrated the

variation in the mechanical response of elastomers subjected to uniaxial, equibiaxial and constant width deformations. The use of the flexible biaxial film stretcher FBFT in the present work allowed acquisition of the simultaneous response of both axes, without the need for multiple specimen preparation and testing. Further analysis was focused on the changes in the constitutive response, as a result of different pre-strain histories, for both uniaxial and biaxial deformations, presented in Section 4.4.2 and Section 4.4.3. It is apparent from this data that the softening mechanism is influenced by both the history and mode of deformation.

The energies stored and dissipated during cyclic deformation were investigated in this chapter to shed light on the influence of strain history on energy dissipation. The test sequences were intended to simulate the scragging process commonly used in the industry. The experimental data shown in Section 4.5 revealed a clear influence of strain history on energy. An energy 'map' was generated for each material describing the influence of both the current cyclic strain amplitude and the strain history. They showed that, more energy is dissipated during the first cyclic strain, compared with subsequent cycles. If the current strain amplitude, ε_2, is below the historical maximum, ε_1, the dissipated fraction remains relatively constant, independent of both current and historical strain amplitude. In the condition when the ε_2 exceeds ε_1, the fraction of energy lies somewhere in between these two cases.

A series of simple constitutive models were presented in Section 4.6 to attempt to describe the Mullins effect and the energy map behaviour observed. The physical approach used is based on the model suggested by Takayanagi [117], together with a description of soft (rubber) and hard (bound rubber and filler) phases, as proposed by Mullins [15]. A parameter consisting of the fraction of bound rubber was used to describe the softening as a transition of rubber from hard phase to soft phase during deformation, attributing the softening effect to this process. A series of enhancements in the model are presented, using the first Gaussian rubber behaviour and then the Edwards-Vilgis Theory. The final model describes the energy trend and mechanical response as function of current strain and strain history.

Chapter 5 Role of strain history on stress relaxation and stress memory

Elastomers are frequently employed in the production of seals and gaskets being subjected to cyclic deformations. Their performance is usually evaluated in terms of compression set, defined as the degree to which a rubber remains permanently deformed when unloaded following an extended period of loading [205, 206]. A reduced recovery can lead to failure in seals, and or, for example, having an adverse effect in the functionality of dampers. It is inappropriate to talk about permanent deformation without knowledge their response over longer timescales than those for which the material was observed. In fact, what is critical in both sealing and damping applications is precisely the time-dependence of the elastic recovery, although the timescales of interest may differ dramatically across different applications. It is widely recognised that both the constitutive response and the viscoelastic behaviour of a rubber product are influenced by aspects such as choice of formulation, curing time and curing agents, and filler type [24, 165]. Especially the influence of the filler content on the relaxation response needs to be highlighted [207].

The deformation history plays an important role in the mechanical response of elastomers, as it was analysed in Chapter 4. Hence, in product applications such as dampers and seals where performance is strongly dependent on the inelastic response, it is important to consider how the degree of inelasticity is affected by the deformation history. Rubber products are regularly *scragged* prior to being brought into service, by subjecting them to a deformation typically greater than that expected in practice [16, 87]. This process is usually applied to regulate the stiffness of rubber products. However, if the in-service load is higher than expected, this will affect the mechanical properties in the same way as the pre-conditioning. The resulting

stiffness may fall outside the acceptable bounds and the rubber product may need to be replaced. It is not obvious whether and how the viscoelastic nature of the material is affected by scragging or unexpected loads. The answer to this question lies in the relationship between the viscoelastic response and the deformation history. Studies focusing on the time dependence of elastomeric materials were reviewed in Section 2.5.3. Although several provide useful time-dependent experimental data related to the influence of lubricants, temperature, strain rate [83, 84, 86, 208, 209], and even the variation of the mode of deformation [85], none of these explored the role of deformation history on the time-dependent response. In filled elastomers, the question if the time-dependent response during stress-relaxation and recovery also depends on deformation history appears to have remained unanswered to date. Even though the viscoelastic effects in rubbers are small in comparison to their elastic response, the magnitude of these effects can be critical in applications such as seals, gaskets and dampers. With this in mind, the present chapter investigates the experimental response of short term stress-relaxation and recovery tests on rubbers subjected to a wide array of prior deformation histories, including uniaxial, equibiaxial and constant width stretching.

An interesting experimental approach was presented by Caruthers and co-workers [17] studying stress relaxation and memory effects on polymer glasses. They analysed the non-linear viscoelastic relaxation process by monitoring the stress response after a series of multi-step conditions, including a previous loading-unloading stage. They introduced the stress response as a combination of multiple relaxation times effects. Their test method was used as a starting point to structure the tests protocols used in this chapter. The influence of strain history, and hence of the Mullins effect on the time dependent response of elastomers is investigated. The stress response under constant strain of five filled elastomers is studied using four different test protocols in order to probe stress relaxation and stress memory with respect to deformation history.

The experimental analysis is focus on uniaxial tensile deformations, with a limited subset of experiments carried out under biaxial tension. Specimen preparation and tests conditions are described in Section 5.1. The results and discussion are divided by the observed stress behaviours, starting with the stress relaxation in Section 5.2. Empirical curve fitting to the data and the more relevant differences between the

materials are shown in Section 5.2.4. A comparison of the time-dependent behaviour between the elastomers is presented in Section 5.3. The stress memory response is analysed in Section 5.4 and the transitions between relaxation and memory effect during partial unloading in Section 5.5. The influence of biaxial modes of deformation (equibiaxial and constant width deformation) prior to the stress relaxation was investigated using EPDM2. The experimental results and discussion are presented in Section 5.6. In addition, the experimental results from the fraction of stress relaxation are related to the fraction of energy dissipated in Section 5.7.

The experimental methodology and results for uniaxial deformation in this chapter have been presented at the '*Rubber Conference 2014; Advanced Engineering and Materials Development*' at Manchester, UK. Aspects of this work have been also published in: V.A Fernandes and D.S.A De Focatiis '*The role of deformation history on stress relaxation and stress memory of filled rubber*', '*Journal of Polymer Testing*', p-124-132. DOI: 10.1016/j.polymertesting.2014.08.018 [210].

5.1 Specimen preparation and mechanical testing

5.1.1 Uniaxial tensile testing

Uniaxial mechanical deformation was carried out using an Instron 5969 tensile testing machine equipped with a 100 N load cell. An Instron counterbalanced travelling extensometer was used for measurement of the strain. Mechanical test specimens were cut from sheet using a hand-operated Wallace specimen cutting press fitted with a dumbbell shape cutter type 1BA according to BS ISO 527-2[150]. The same specimen preparation protocol as described in Section 3.6.1 was used for all uniaxial tests specimens, made from the five materials characterised previously (Chapter 3).

EPDM1a (first batch, recalling Section 3.2.1) was used in all the tests of this chapter. For the rubbers processed by sheet rolling (EPDM2, NBR and CR), all specimens were cut parallel to the rolling direction. No special consideration of the cut direction was taken for the materials processed by compression moulded (EPDM1a and NR). One specimen was tested per strain value on each test condition. A detailed description of the sheet preparation through sheet rolling and compression moulded

was presented in Section 3.3.

5.1.2 Biaxial tensile testing

The variation of the mode of deformation, under equibiaxial (EB) and constant width (CW) tensile testing was performed on EPDM2, using a flexible biaxial film stretcher FBFT [152]. Square specimens of 85 mm x 85 mm were cut from an approximately 0.5 mm thick sheet. A detailed description of the FBFT machine and specimen preparation protocol was provided in Section 3.6.2. One specimen per strain condition was tested on each test protocol analysed. As EPDM2 was manufactured by a sheet rolling process, special care was taken to consistently align the axis parallel to the rolling direction to axis 1 of the biaxial testing machine. The strain measurement can be made using a non-contact image particle tracking method during grip displacement (see Appendix A). A verification of the difference between strains measures was made, showing a difference of no more than 10 %. The results presented in this chapter are obtained from the grip displacement data, due to less noise recorded.

5.1.3 Test conditions

In order to explore the influence of deformation history on stress relaxation, four test protocols (TP) were applied prior to recording stress relaxation at fixed displacement for 600 s. The four test protocols were used for uniaxial, equibiaxial and constant width deformations. All tests were performed at room temperature (20 °C $\pm$ 1 °C) and at constant cross-head speed corresponding to a nominal strain rate of 0.1 s^{-1}.

A repeatability analysis was performed to ensure the validity of each test as only one specimen per strain condition was tested. Appendix C describes in detail the selection criteria used. The mean of a set of stress-strain response tests was determined for deformations between 0.1 and 0.5 strain during the first loading stage. The mean includes all the specimens tested for each test protocol condition. As the stress-strain response is expected to follow the same path when no-history is present, a test was considered valid and repeatable when the deviation from the stress mean was less than 10% during the first loading stage (on each test protocol) up to 0.5 strain. Strain values lower than 0.1 are not considered due to noise on the load data

measured at the beginning of each test due to limited accuracy of the load cells at low forces. Each material and mode of deformation was analysed separately as different mechanical response is expected between the modes of deformation investigated.

5.2 Stress relaxation under uniaxial deformation

5.2.1 TP1: Single loading ramp history

5.2.1.1 Test protocol

For the first test protocol, TP1, the specimens were subjected to a single loading ramp up to a strain of ε_{max}. This strain was held and the stress-relaxation was monitored for a further 600s. Figure 81 shows a diagram of the strain history imposed, indicating the start of the stress-relaxation stage at time t_0. Table 21 indicates the values of uniaxial, UN, strains, ε_{max}, explored for each rubber. The set of strains analysed for each material was selected with respect of the deformation ability before failure reported in Chapter 3.
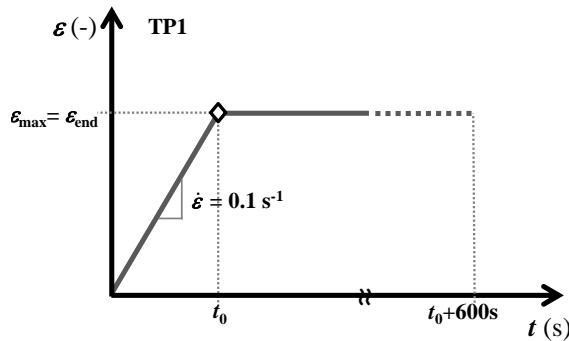
Figure 81. Strain history imposed on specimens according to stress relaxation protocol TP1. The diamond symbol indicates the start of the stress-relaxation stage at time t_0. The maximum strain reached during the test is denoted as ε_{max}, equal to the final strain at the start of the stress relaxation, denoted as ε_{end}.

Table 21. Maximum strains $\varepsilon_{max} = \varepsilon_{end}$ evaluated during stress relaxation protocol TP1 protocol for the elastomers studied.

	Elastomers				
	EPDM1a	*EPDM2*	*NBR*	*CR*	*NR*
TP1 ε_{end}	0.5	1.0	0.25	0.5	0.25
	0.75	2.0	0.5	0.75	0.5
	1.0	3.0	0.75	1.0	0.75
	1.25	4.0	1.0	1.5	1.0
	1.5	5.0	1.5	2.0	1.5
	1.75	-	1.75	2.5	2.0
	2.0	-	-	3.0	2.5
	2.5	-	-	-	

5.2.1.2 Results

When the virgin material is subjected to a first tensile deformation, the first restructuring of the chain network structure due to deformation is taken place. The nominal stress-strain response of EPDM1a in Figure 82 (a) is presented as an example. The diamonds indicate the start points of the stress relaxation test for each ε_{end}. The corresponding stress responses as a function of time are presented in Figure 82(b). In order to compare the stress relaxation fraction for ε_{end}, the measured stresses were normalised with respect to the stress measured at the end of the loading ramp σ_{end} (at ε_{end}). This is presented in Figure 83 showing $\sigma(t)/\sigma_{end}$ as a function of time. Here, the relaxation time is corrected to starting time at $t_0=0$ for each test.
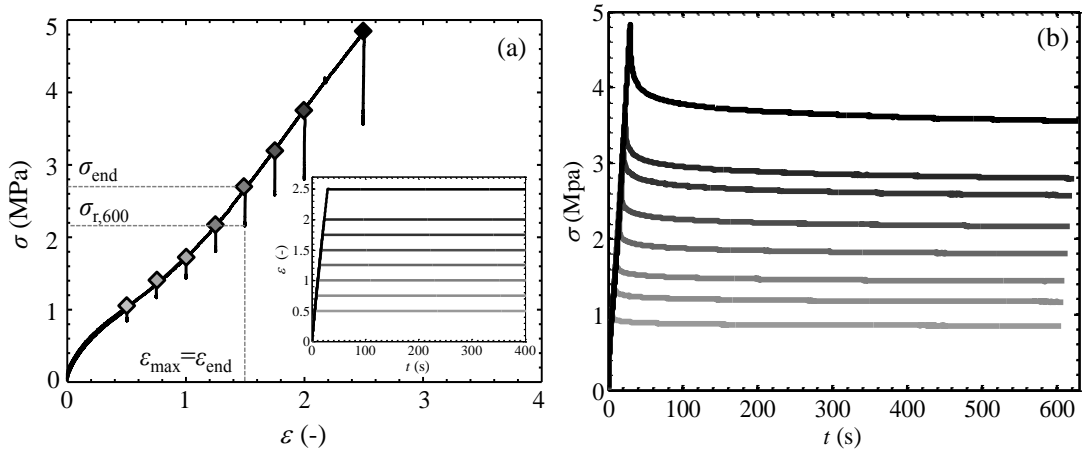
Figure 82. (a) Stress-strain curve for EPDM1a during TP1. The diamonds indicate the start points of the relaxation stage for each ε_{end} tested, shown as an inset. (b) Stress as a function of time measured for each ε_{end} tested.
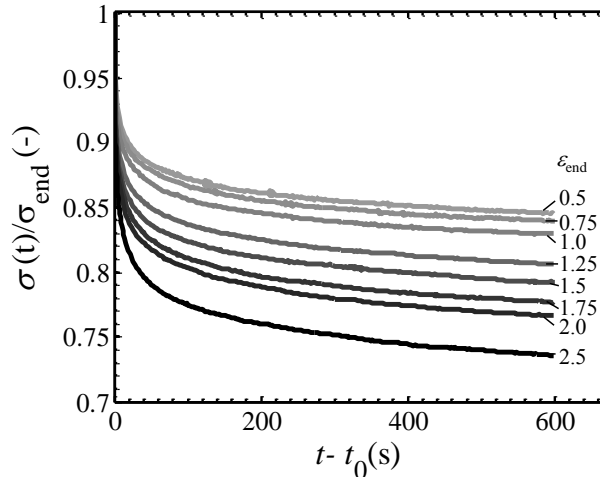
Figure 83. Stress normalised with respect to the stress σ_{end} at ε_{end} for specimens deformed according to TP1 under UN testing for EPDM1a.

The procedure described for EPDM1a above was also carried out for the other elastomers studied. The normalised stress relaxation responses for different values of

ε_{end} are presented in Figure 84. The stress relaxation response is significantly dependent on the strain history, i.e. on the amount of ε_{max}. The fraction of stress relaxation shows a steady increase with increasing strain for all materials and strain levels tested. Each elastomer analysed presents a different response of the stress relaxing. EPDM1a and EPDM2 show a continuous increase in the relaxation with increasing the strain up to values of 4.0 and 5.0 respectively. For NBR and NR, values of strain of 0.75 and lower, does not present any variation of the fraction of stress relaxing. The same response is shown at the higher values evaluated for NBR and CR. As NBR cannot be deformed to values of strain above 1.75 without failure, the range of study is limited. The stress response of CR shows a higher increase of the stress relaxing at values lower than 1.5, showing a less marked difference with strains between 1.5 and 3.0. There is a dependency of the strain subjected during the stress relaxation stage in the response over a fixed time (600s). The five elastomers have a characteristic behaviour.
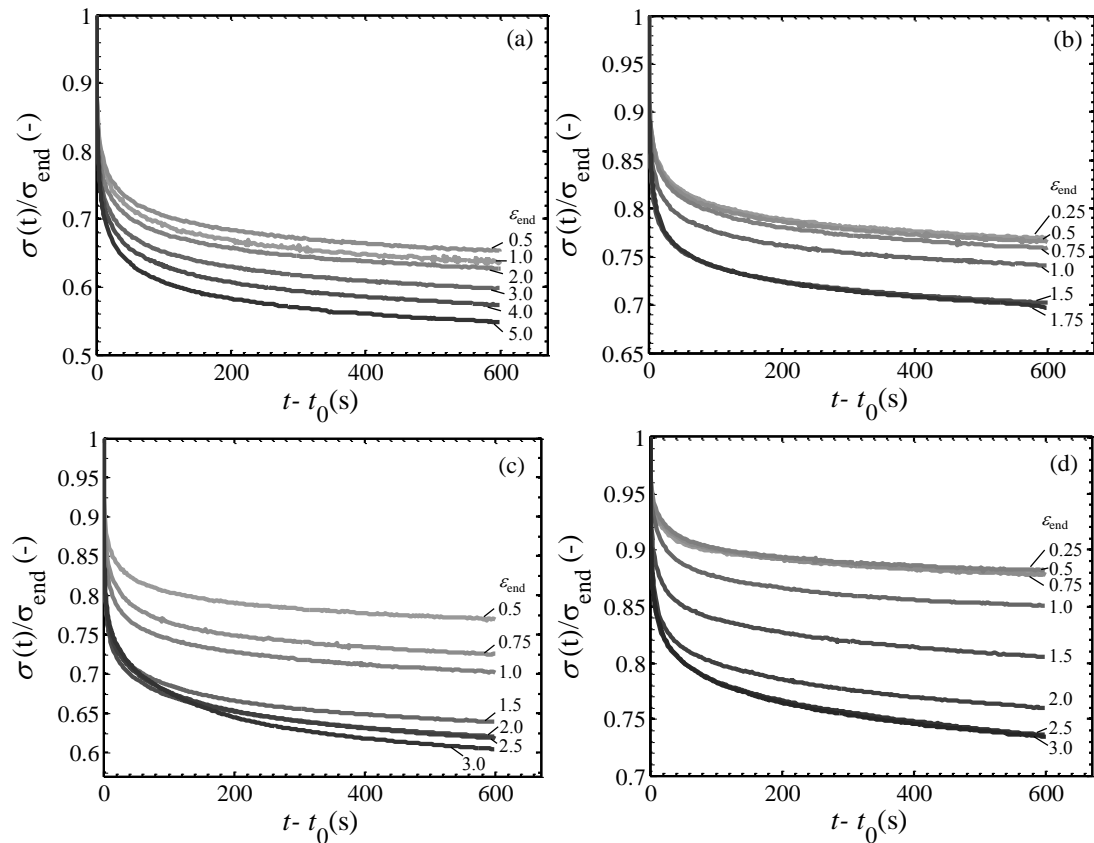
Figure 84. Normalised stress relaxation σ/σ_{end} as function of time of (a) EPDM2, (b) NBR, (c) CR and (d) NR specimens subjected to a single strain ramp to various strain levels ε_{end} (as indicated in the figure), according to TP1 under UN testing.

5.2.2 TP2: Load-unload-reload history

5.2.2.1 Test protocol

To study the effect of pre-strain on the stress relaxation response, a complete load-unload cycle was included in the protocol TP2 before the stress relaxation test is performed. Specimens were subjected to a single load-unload cycle to a maximum strain ε_{max}, at a constant strain rate (0.1 s^{-1}). The samples were unloaded to a small tensile force of 0.1 N ($\sigma \sim 0.04$ MPa) to prevent buckling of the specimen. This sample pre-conditioning was followed by a single loading ramp (as TP1) to the final strain ε_{end}. ε_{max} indicates the maximum strain to which the sample was exposed prior to the final ramp, and is not necessarily larger or equal than ε_{end}. The stress relaxation was then measured at the constant strain ε_{end} for 600 s. The combinations of ε_{max} and ε_{end} tested on the different materials using this protocol are reported in Table 22. A schematic representation of the strain history imposed as a function of time is shown in Figure 85, indicating the start of the stress-relaxation stage at time t_0.

Table 22. Combinations of maximum strain during a pre-strain cycle, ε_{max}, and final strain, ε_{end}, at the start of the stress relaxation test, for UN stress relaxation tests according to protocol TP2 for the elastomers studied.

Elastomers									
EPDM1a		*EPDM2*		*NBR*		*CR*		*NR*	
ε_{max}	ε_{end}	ε_{max}	ε_{end}	ε_{max}	ε_{end}	ε_{max}	ε_{end}	ε_{max}	ε_{end}
	0.5		0.5		0.25		0.5		0.5
	0.75		0.75		0.5		0.75		0.75
	1.0		1.0		1.0		1.0		1.0
1.0	1.5	1.0	2.0	0.5	1.5	1.0	1.5	1.0	1.5
	2.0		4.0		1.75		2.0		2.0
	2.5		5.0		-		2.5		2.5
	-		-		-		3.0		3.0
	0.5		1.0		0.25		0.5		0.5
	0.75		1.25		0.5		0.75		0.75
	1.0		1.5		0.75		1.0		1.0
1.5	1.25	2.0	2.0	1.0	1.0	2.0	1.5	2.0	1.5
	1.5		4.0		1.25		2.0		2.0
	2.0		5.0		1.5		2.5		2.5
	2.5		-		1.75		3.0		3.0
	0.5		2.0		0.5		0.5		0.5
	0.75		3.0		0.75		0.75		0.75
	1.0		3.5		1.0		1.0		1.0
2.0	1.25	4.0	4.0	1.5	1.25	2.5	1.5	2.5	1.5
	1.5		5.0		1.5		2.0		2.0
	1.75		-		1.75		2.5		2.5
	2.0		-		-		3.0		3.0
	2.5		-		-		-		-

Figure 85. Strain history imposed on specimens according to stress relaxation protocol TP2. The circle symbol indicates the start of the stress-relaxation stage, at time t_0. The maximum strain reached during the pre-deformation test protocol is denoted as ε_{max}. The final strain at the start of the stress relaxation is denoted as ε_{end}.

5.2.2.2 Results

When a loading-unloading cycle is added to the deformation history of the material as described in TP2, the relaxation response is influenced by both ε_{max} and ε_{end}. To illustrate this, the response of EPDM1a following TP2 is shown in Figure 86. Three variations of ε_{max} are represented in the figure with an offset for clarity. The relaxation stage for each condition is not shown in the diagram for clarity. Each circle indicates the different ε_{end} values at which the stress relaxation stage was started, with the corresponding stress magnitude at the beginning of the stress relaxation stage. The maximum strain during the pre-strain stage ε_{max} is also identified.
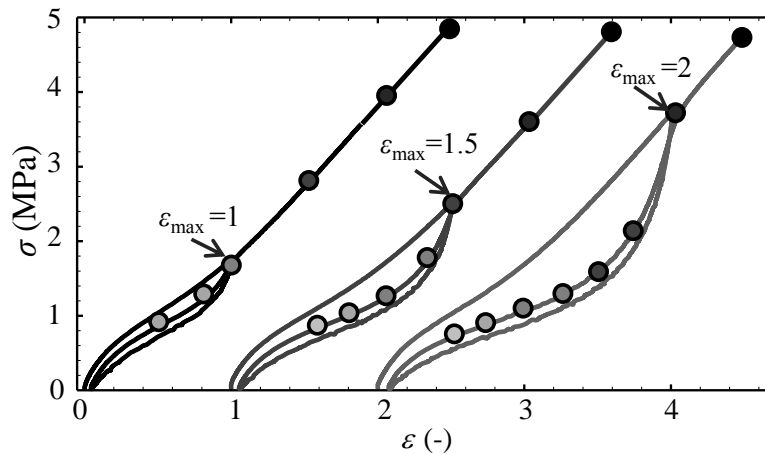
Figure 86. Nominal stress vs strain responses according to TP2 under UN testing for EPDM1a.Circles indicate the values of ε_{end} and the corresponding stress measured at which stress-relaxation measurements were started for $\varepsilon_{max}=1.0$, $\varepsilon_{max}=1.5$ (offset by $\varepsilon = 1$) and $\varepsilon_{max}=2.0$ (offset by $\varepsilon = 2$).

The stress-strain response observed prior to the stress relaxation stage exhibits the softening effect or Mullins phenomenon, as during the second loading (following a

complete cycle), there is a fall in the stress required to deform. A more detailed analysis of this phenomenon was analysed in Chapter 4.

The same normalisation of the measured stress with respect to the stress at the end of the loading ramp, σ_{end}, was determined. For the five elastomers, normalised stress relaxation plots are presented in Figure 87 (a-e), for $\varepsilon_{max} = 2$ for all materials except NBR, for which $\varepsilon_{max} = 1.5$ was used, due to the lower strength of for this material.
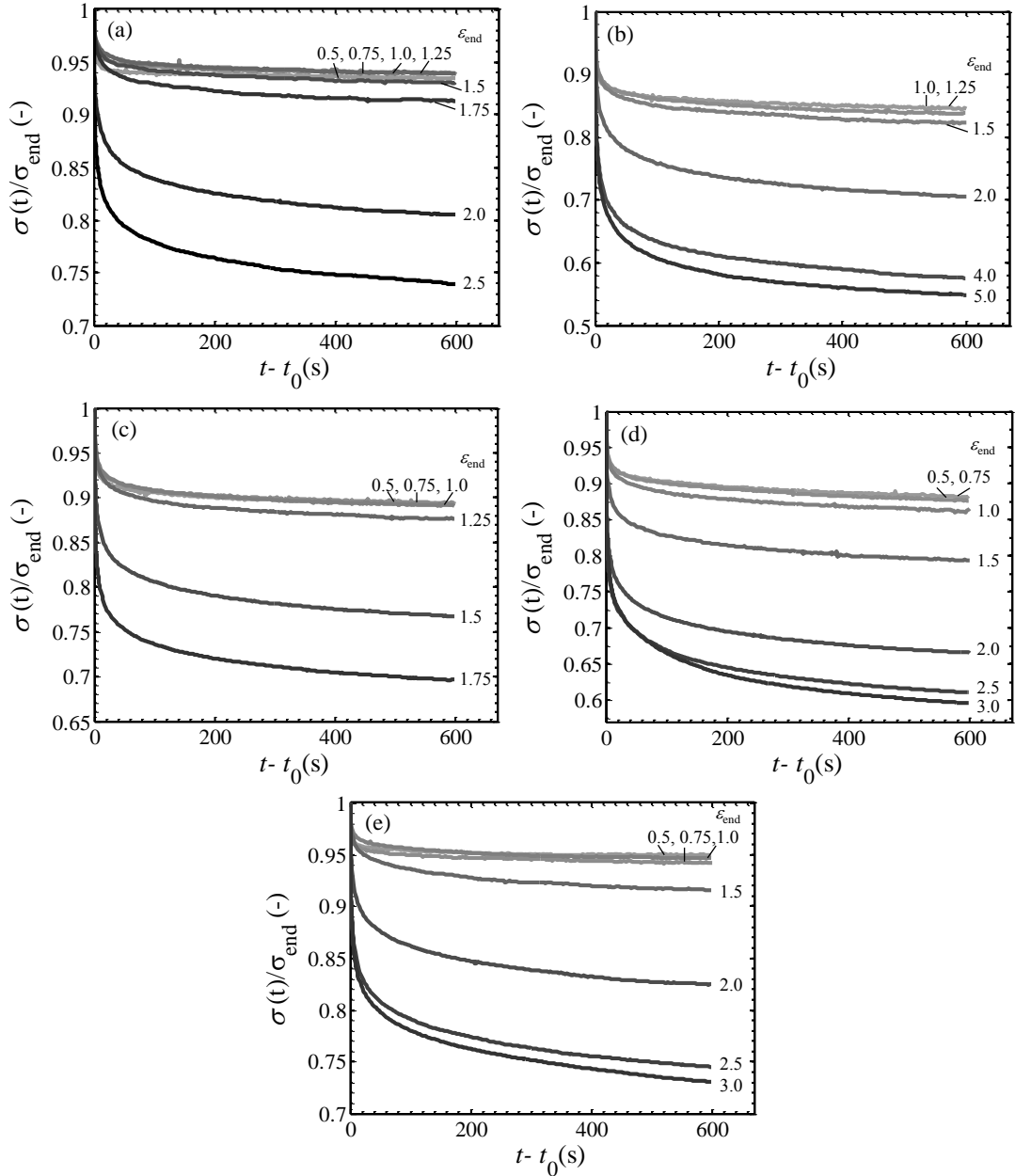
Figure 87. Normalised stress relaxation σ / σ_{end} of (a) EPDM1a, (b) EPDM2, (c) NBR, (d) CR and (e) NR specimens subjected to a load-unload cycle through to ε_{max} ($\varepsilon_{max} = 2$ for all materials with the exception of NBR where $\varepsilon_{max} = 1.5$), and reloaded to strain levels ε_{end} (indicated in the figure), according to TP2 under UN testing.

The stress relaxation responses differ clearly from those of TP1. The responses can be grouped into two cases. The first case where $\varepsilon_{end} < \varepsilon_{max}$, the fraction of stress relaxing appears independent of ε_{end}. Most specimens relax a smaller fraction of the applied stress than their counterparts tested under TP1. Each elastomer has a distinctive response of the stress relaxation process. For EPDM1a and EPDM2, the stress relaxation dependence to ε_{max} and ε_{end} is very similar. However, EPDM1a present a less fraction of stress relaxing for values where $\varepsilon_{end} < \varepsilon_{max}$. Likewise, the stress relaxation starts to deviate from this independent value when ε_{end} approximates to ε_{max}. The start of this transition differs between materials, with the lowest starting value of 1.0 for CR and the nearest to $\varepsilon_{max}=2$ for EPDM1a at $\varepsilon_{end}=1.75$. For the cases where $\varepsilon_{end} \geq \varepsilon_{max}$, there is again a strong dependence of the stress relaxation on the value of ε_{end}. The relaxation response is then identical to that observed for the same material in TP1 (Figure 82 and Figure 83). All the materials present a clear increase in the relaxation with values of ε_{end} above 2.0 (and 1.5 for NBR). The same trends were observed for the remaining ε_{max} conditions analysed, reported in Appendix F.

5.2.3 Dependence of stress relaxation on uniaxial deformation history

When the material is subjected to a strain history, the response will depend on whether the current strain exceeded or not the historical maximum. When the maximum strain, ε_{max}, during previous deformations (related to the *scragging* process) is higher than the strain at which the stress-relaxation is measured, ε_{end}, the relaxation of the material is unaffected by the deformation history. The stress-relaxation becomes linear viscoelastic, as there is no dependence of the strain in the response. However, when $\varepsilon_{end} > \varepsilon_{max}$, the stress-relaxation response is similar to that observed after a simple ramp to the same strain (TP1), depending of both the historical maximum and the current strain.

The experimental data (Figure 87) shows that an approximately fixed fraction of the stress relaxes, independently of the strain level (if ε_{end} is sufficiently smaller than ε_{max}). The fraction of stress relaxing at a given time becomes approximately independent of the *magnitude* of the applied stress. This is unexpected, as large strains are involved (above 0.5 strain). In between these two groups, there is a transition region which corresponds to a reloading strain, ε_{end}, equal to or slightly

smaller than the maximum strain reached in the first loading-unloading cycle, ε_{max}. Here the response appears to lie between these two conditions. In this region, the materials has some softening effect from the pre-strain, but the strain applied during the stress relaxation stage is still modifying the response of the material. This effect is similar to the Mullins effect observed during consecutive multicycle tests. Even though the second loading cycle will have the highest softening response, the following cycles up to the same strain will still show some softening.

A good way to capture this range of behaviour is to plot the normalised fraction of unrelaxed stress at the end of the test, $\sigma_{r,600}/\sigma_{end}$, as a function of ε_{end} for different ε_{max}. The fraction of unrelaxed stress of EPDM1a is used in Figure 88 to describe the experimental data. With no previous load history (TP1), the relaxation follows the *region (1)* and shown as $\varepsilon_{max} = \varepsilon_{end}$. When the sample is subjected to a previous strain (TP2), the response shows tow distinctive patterns. When ε_{end} is considerably smaller than $\varepsilon_{max,}$ the unrelaxed response lies in *region (2)*. The fraction of stress relaxing is constant and independent of both the reloading strain ε_{end} and the previously reached maximum strain ε_{max}. A transition *region (3)* between the two previous ones occurs when ε_{end} approaches the values of ε_{max}.
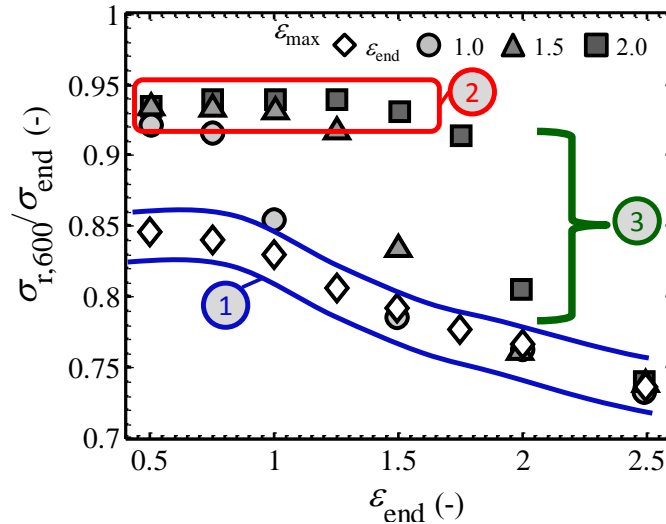
Figure 88. Fraction of unrelaxed stress $\sigma_{r,600}/\sigma_{end}$ as function of the strain during the relaxation stage ε_{end} of EPDM1a subjected to UN deformation according to TP1 ($\varepsilon_{max} = \varepsilon_{end}$) and TP2 (at different values of ε_{max} as marked in figure).

The fractions of unrelaxed stress for the rest of the elastomers are presented in Figure 89. The patterns observed may be thought of as maps of the time-dependent equivalent of the pseudo-cyclic load-unload-reload curves frequently used to

illustrate the Mullins effect.

When ε_{end} is sufficiently smaller than the previous maximum ε_{max}, the relaxed fraction lies in the *region (2)*, with an approximately constant value, independent of the reloading strain ε_{end}. What may be less apparent is that the fraction of unrelaxed stress is also independent of the value of the previously applied maximum strain, ε_{max}. The constant value in *region (2)* of unrelaxed stress seems to be an intrinsic parameter for each material. The constant fraction depends on the material type, and ranges between 0.06 and 0.12 at 600 s. These values are calculated from the average of the fraction of stress relaxing at the end of the test (t=600 s) for $\varepsilon_{end} < \varepsilon_{max}$ (without including the transition range). This is in sharp contrast to the constitutive response during loading of the rubber, which is well known to be affected by the previous maximum strain reached (i.e. see Figure 55 in Chapter 4).
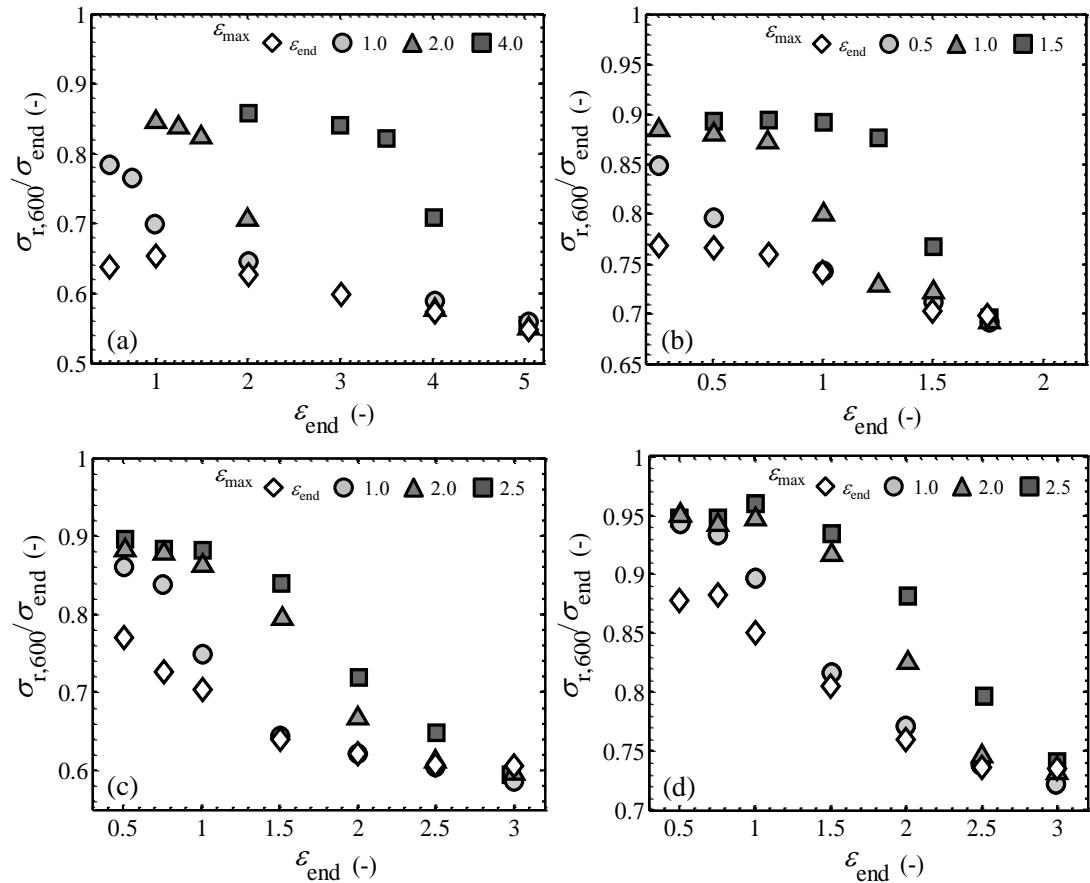
Figure 89. Fraction of unrelaxed stress $\sigma_{r,600} / \sigma_{end}$ as function of the strain during the relaxation stage ε_{end} of (a) EPDM2, (b) NBR, (c) CR and (d) NR subjected to UN deformation according to TP1 ($\varepsilon_{max} = \varepsilon_{end}$) and TP2 (at different values of ε_{max} as marked in figure).

Figure 90 shows the stress-strain response measured during the second loading, after EPDM1a was subjected to different previous maximum strains (TP2). The softening

mechanism observed is directly dependent of the strain history, as the increase of ε_{max} shows a decrease in the slope of the constitutive path compared with the mechanical response of a specimen with no strain history. However, if subsequent loadings do not reach the previous deformation, the relaxation response does not depend on the degree of softening, as was shown in the previous chapter.
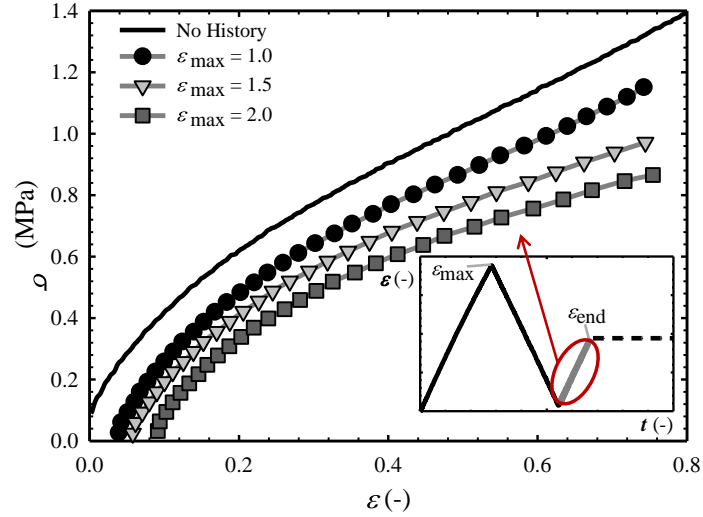
Figure 90. Stress-strain response during tensile deformation for EPDM1a following different ε_{max}

5.2.4 Empirical approach for stress relaxation dependence on strain history

The pattern emerging from the data presented (TP1 and TP2) is used to develop a simple empirical approach that is consistent with the history dependence. The relaxation process can be described as a coupled system. The system includes an elastic response contribution where a fixed fraction of the pre-strained (*scragged*) rubber network relaxes independently of the constitutive response of the network. As was presented in Chapter 4, the variation in the constitutive response of the elastic network, associated with the microstructural changes underpinning the Mullins effect, is affected by strain history (Figure 56 in Section 4.3.3).

In this section, the relaxation of the stress at a constant strain, i.e. the time-dependence, was also found to be affected by strain history. When a rubber is stretched to a deformation that is within (and not too close to) the maximum previously reached strain, the value of normalised stress relaxation converges to a constant fraction. This is independent of both, the current and historical strains. An empirical approach to evaluate the dependence of strain history on the relaxation process can be built, defining the experimental fraction as

$$\varphi_r = \frac{\sigma_{r,600}}{\sigma_{end}}$$

<div align="right">Eq. 5-1</div>

with σ_{end} and $\sigma_{r,600}$ as the stress values at the start and end of the stress relaxation stage respectively.

In order to find an empirical equation to describe the experimental behaviour, the three regions described in Figure 88 are analysed separately. On *region (1)*, when the elastomer has no deformation history, the fraction can be expressed as a linear function of the applied strain, φ_0. A parameter φ'_0 is introduced as the intercept of the fraction of unrelaxed stress of the material at zero strain. The linear response is then defined as

$$\varphi_0 = \varphi'_0 + \varepsilon.a$$

<div align="right">Eq. 5-2</div>

The value of φ_0 is proportional of the strain ε applied. The slope parameter a relates the magnitude of the dependence of the stress relaxation fraction with the strain in *region (1)*, represented as a dotted line in Figure 91. As presented in Figure 89, the trend for $\varepsilon_{max} = \varepsilon_{end}$ (TP1) is inherent to each material.
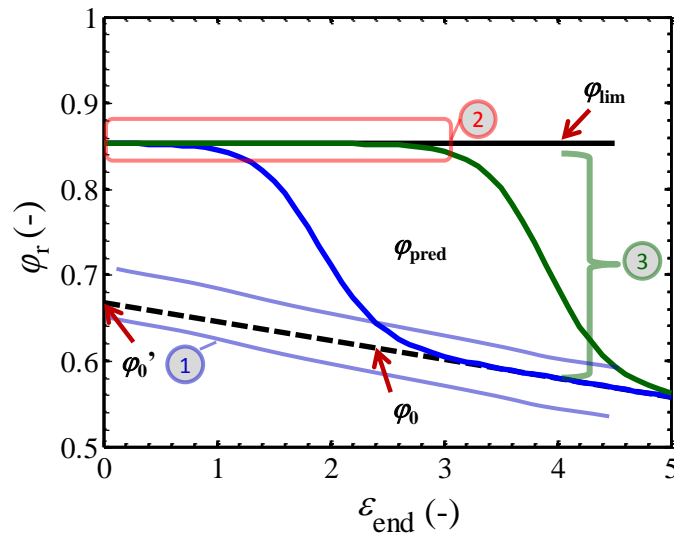
Figure 91. Empirical approach of the fraction of unrelaxed stress φ_r as function of applied strain ε_{end}. The trend φ_0 is the fraction of unrelaxed stress when no previous deformation was applied. The y-interception of the material with no history is represented by φ'_0. The constant fraction of unrelaxed stress when ε is lower than ε_{max} is defined as φ_{lim}; and φ_{pred} represents the fraction of unrelaxed stress evolution dependent on the strain.

When the influence of strain history is included (*region (2)* and *region (3)*), both the

applied strain and the maximum value from previous deformation ε_{max} have an impact on the stress relaxation, as observed in Figure 89. In this case, the fraction of unrelaxed stress φ_{pred} can be fitted to behave as

$$\varphi_{pred} = \varphi_{lim} + \left(\varphi_0 - \varphi_{lim}\right) X_\varepsilon$$

Eq. 5-3

with φ_{lim} representing the constant fraction of unrelaxed stress when $\varepsilon < \varepsilon_{max}$ in *region (2)*, shown in Figure 91, as the solid black line. The variable X_ε represents the evolution of the fraction of stress from *region (2)* to *region (1)*, expressed as

$$X_\varepsilon = 0.5\left(\tanh\left(\left[\left(\varepsilon - \varepsilon_{max}\right) + c\right]b\right) + 1\right)$$

Eq. 5-4

with the parameters b as the slope of the transition as function of the strain and c the shift of φ_{pred}. When $\varepsilon < \varepsilon_{max}$, the fraction will tend to $\varphi_{pred} \approx \varphi_{lim}$. Conversely, when $\varepsilon \geq \varepsilon_{max}$, the value will be $\varphi_{pred} = \varphi_0$. The empirical approach to the relaxation behaviour has a total of five parameters which can be calculated from the experimental data of each material, as presented in Table 23.

Table 23. Parameters of the empirical approach of the fraction of unrelaxed stress followed uniaxial tensile testing, with the error related to experimental data. φ'_0 represents the interception of the fraction of unrelaxed stress of the material at zero strain. φ_{lim} is the constant fraction of unrelaxed stress when $\varepsilon < \varepsilon_{max}$. The parameters a,b and c are fitted empirically.

	Elastomer				
Parameters	*EPDM1a*	*EPDM2*	*NBR*	*CR*	*NR*
error	0.00051	0.00386	0.00168	0.01436	0.00404
φ'_0	0.88249	0.66679	0.78997	0.77771	0.91552
φ_{lim}	0.93396	0.85288	0.88694	0.89402	0.94999
a	-0.05930	-0.02182	-0.05314	-0.06846	-0.06756
b	5.58914	1.85306	5.22706	1.50870	1.73058
c	0.09315	0.12355	0.06405	0.50261	0.23990

The fitting approach using four values of ε_{max} is compared with the experimental data presented in Figure 89 for uniaxial deformation of all five filled elastomers in Figure 92. The empirical method is in good agreement with all of the experimental data presented. This equation will allow prediction of the effect of the scragging process on the time-dependent mechanical response. The time limitation of the experimental data is a consideration to take in the analysis of the fitted parameters. Longer

relaxations times could bring more relaxation of the system and modify the empirical parameters presented.
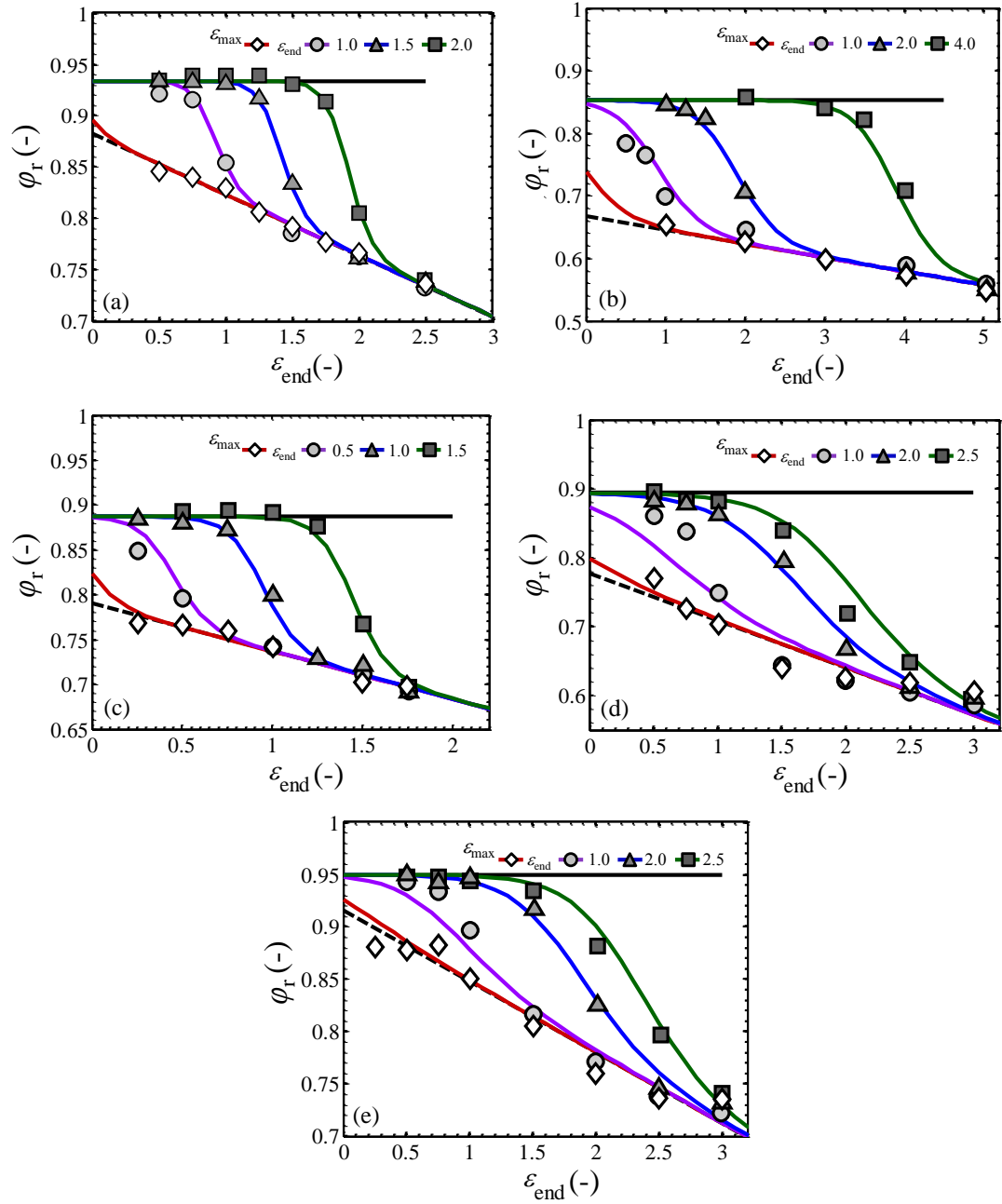
Figure 92. Comparison of experimental data (symbols) of the fraction of unrelaxed stress φ_r as function of the strain during the relaxation stage ε_{end} of (a)EPDM1a (b) EPDM2, (c) NBR, (d) CR and (e) NR subjected to UN deformation compared to the empirical approach (solid lines).

In the case of $\varepsilon_{max} = \varepsilon_{end}$ (TP1), at small values of ε_{end}, the trend deviates from the ideal no history response of φ_0, as presented in the red trend line in Figure 92. This prediction could be related with the manufacturing processing, as strain is experienced by the material during the specific manufacturing method. EPDM1a and

NR (Figure 92(a) and (c)) are processed using compression moulding; as for EPDM2, NBR and CR (Figure 92(b), (c) and (d)), a sheet rolling processing was used. The compression moulding technique applies forces equally over the entire surface area, creating a material transversely isotropic.

The sheet rolling process has a more complex system of deformations, as the force in the direction of the roll can induce anisotropy (the considerations of process-induced deformation and anisotropy will be further analysed in Chapter 6). In this approach, the two materials processed using compression moulding show a very similar trend prediction of the condition of ε_{end} with the predicted trend to the ideal response of φ_0, even a small values of ε_{end} (with nearly no deformation). However, the materials processed by sheet rolling, have a more pronounced deviation at small values of ε_{end}, possibly due to the higher deformations involved during this process.

Therefore, the initial assumption of a linear response for φ_0 with no strain history (*region (1)*) may be too simplistic. This could also explain the non-linear response of the experimental data of CR at $\varepsilon_{\text{max}} = \varepsilon_{\text{end}}$ (TP1) in Figure 92(d), especially at small values of ε_{end} (below 1.5). For this, a detailed description of the manufacturing process is needed.

The mean *error* between the fitted parameters and the experimental data is estimated in Table 23, defined as the root mean square error of all data points analysed, expressed as

$$\sqrt{\frac{1}{n}\sum_{i=1}^{n}(\varphi_{\text{r,i}} - \varphi_{\text{pred,i}})^2}$$

Eq. 5-5

This indicates a good agreement of the derived model with the experimental data. The largest error was observed at small values of ε_{end}, especially for CR. Similarly, the fit to CR showed the highest rms error value, mainly due to the poorer fit at small strains. The experimental data indicates that the mechanism of deformation of CR (Figure 92(d)) differs notably from the rest of the elastomers presented, as was also observed for its constitutive response in Chapter 4. This variation in the response brings up the importance of elastomer structure and composition in the analysis of the mechanical and time-dependence response.

5.3 Comparison of mechanism of relaxation between elastomers

The difference in the fraction of relaxation between the elastomers presented is strongly related to their formulations. The capacity of relaxation of the filled elastomer network will depend on their elastic properties and filler content. Hence they are influenced by the ability to restructure under deformation. At a fixed time, the relaxation capacity is related to the viscous response of the network.

During the characterisation of the elastomers in Chapter 3, it was found that EPDM2 has the highest filler content (60phr). A higher content of filler is known to increase the softening effect, related to the mechanism of deformation. EPDM2 presents the lowest values of φ_{lim}, which indicates a higher relaxation after subjected to a deformation history ε_{max}. The mechanism involved during deformation, allows the structure to relax at a specific period of time, showing a higher time-dependence effect on *region (2)* when $\varepsilon < \varepsilon_{\text{max}}$. This effect can be also related to the high values of permanent set of EPDM2 (Figure 57 in Section 4.4.2.4). However, in *region (1)* with no deformation history, EPDM2 is capable to deform to the highest values with the least reduction of φ_0 with strain. This can be seen by the lowest value of the parameter *a* for φ_0 between the elastomers studied (Table 23). In contrast, NR presents the highest value of φ_{lim}, which indicates less relaxation capacity when $\varepsilon < \varepsilon_{\text{max}}$ (in *region (2)*). It is important to note that NR contains the least carbon black content (30phr) studied here, highlighting the effect of the filler on the increase of the viscous response contribution. In general, the values of φ_{lim} decrease with increasing the filler content. This is just a general statement, as for a thorough comparison of the five elastomers; more information of the composition is required as each material has a different chemical structure and formulation, as investigated in Chapter 3. As no information concerning the filler is provided, only the filler content determined during characterisation is used to analyse this aspect.

The transition *region (3)* is evaluated with the parameter *b*, which represents the slope of the transition in this region in the empirical approach. EPDM1a and NBR present a steep transition, as EPDM2, CR and NR experience a slow transition. No clear evidence relates these behaviours to the composition of each material; however, the mechanism of deformation varies between elastomers. The fraction of relaxation and the viscoelastic response clearly varies depending on the elastomer formulations,

as it does with the stress-strain response in Chapter 4. However, with the present data it is not possible to distinguish which of these parameters dominate the behaviour. Although it will be reasonable to expect that the filler content may have the most predominant influence in the post strain (or post-scragging) fraction of relaxation. This reasoning seems to agree with previous publications indicating that variation in formulation such as filler content is an important factor affecting the Mullins effect [14, 29, 64].

5.4 Stress memory under uniaxial deformation

5.4.1 TP3: Memory after a load-unload cycle

5.4.1.1 Test protocol

The stress response after a complete loading-unloading cycle was analysed through test protocol TP3. Each specimen was subjected to a single loading ramp to a maximum strain, ε_{max}, and then unloaded to a strain corresponding to a force of 0.1 N ($\sigma \sim 0.04$ MPa). Stress relaxation was then measured at this constant strain for 600 s. The strain history imposed on the samples is presented in Figure 93 as function of time. The set of ε_{max} values explored is presented in Table 24. The selected range of strain evaluated for each material is according to the elongation ability before failure, analysed during characterisation (Chapter 3).
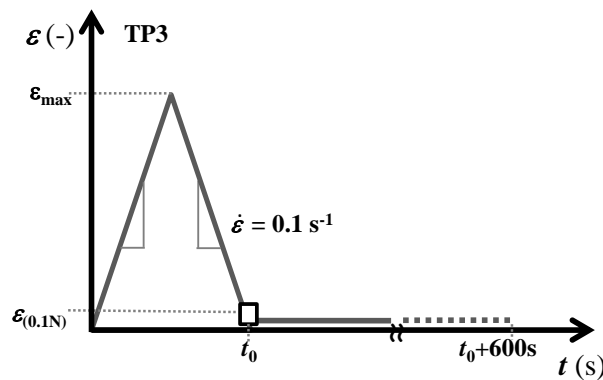

Figure 93. Strain history imposed on specimens according to stress relaxation protocol TP3. The square symbol indicates the start of the stress relaxation stage, at time t_0. The maximum strain reached during the pre-deformation test protocol is denoted as ε_{max}. The final strain at the start of the stress relaxation at 0.1N is denoted as $\varepsilon_{(0.1N)}$.

Table 24. Set of maximums strains ε_{max} explored during UN stress relaxation protocol TP3 for the elastomers studied.

	Elastomers				
	EPDM1a	*EPDM2*	*NBR*	*CR*	*NR*
	0.5	0.5	0.25	0.25	0.25
	0.75	0.75	0.5	0.5	0.5
TP3	1.0	1.0	1.0	0.75	0.75
	1.25	2.0	1.5	1.0	1.0
ε_{max}	1.5	3.0	1.75	1.25	1.25
	1.75	4.0	-	1.5	1.5
	2.0	-	-	1.75	1.75
	-	-	-	2.0	2.0

5.4.1.2 Results

This test protocol evaluates the response of the materials when they are subjected to a complete loading-unloading cycle (TP3). As a difference from the previous protocols, the specimen is unloaded to a minimum force (σ_{end} approximately 0.04 MPa) before starting the stress monitoring. A difference in the stress response is observed, as presented in the stress-strain response during pre-conditioning stage in Figure 94(a) for EPDM1a as an example. The squares symbols at the end of the unloading stage indicate the starting points of the 'stress relaxation' stage (at 0.1 N). Stress-memory, or recovery of stress after unloading can be observed, as shown in Figure 94(b) at t_0=0, defined as the starting time of the recovery stress. The data presented before t_0 shows the stress response during the pre-strain stage at different ε_{max}. When the stress relaxation starts, there is a small increase in stress, due to viscoelastic effect. For a more detailed analysis of this stage, Figure 95(a)-(e) show the stress response only during the recovery stage for each material.
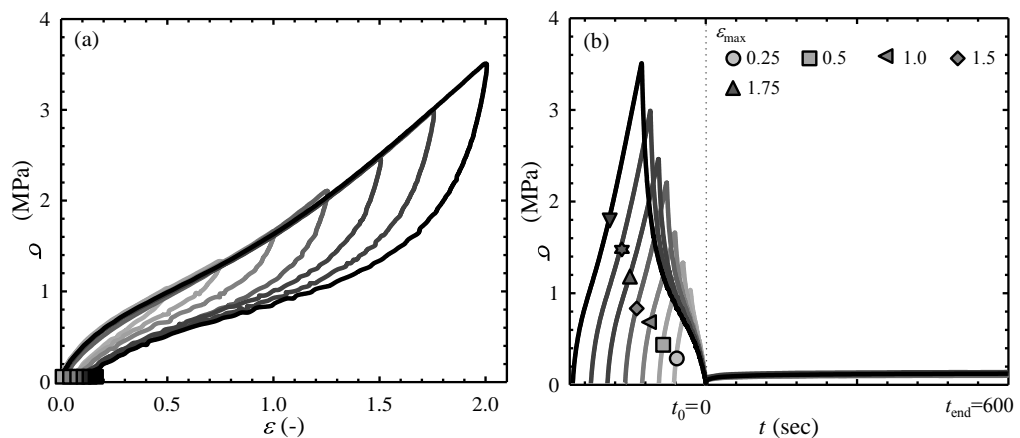
Figure 94. Nominal stress measured for EPDM1a deformed according to TP3 under UN testing. (a) Stress as a function of strain during the pre-conditioning stage. Squares indicate the specific $\varepsilon_{(0.1N)}$ at which stress-relaxation started. Relaxation stage for each condition is not represented in the diagram. (b) Stress as a function of time for varying ε_{max}. Time shifted to t_0=0 at the beginning of the stress relaxation stage. Symbols indicate ε_{max} evaluated.

The magnitude of the recovered stress is smaller for the lowest ε_{max}. For EPDM2 and CR in Figure 95 (b) and (d), the value quickly converges to constant value, independent of ε_{max}. However, the variability is not as pronounced as in TP1 and TP2 (Figure 83 Figure 84, and Figure 87). It must be pointed out that each material has a specific permanent set. In this case, the strain at which the stress memory stage starts at t_0 varies depending on ε_{max}, and increases with increasing ε_{max}.

At the beginning of the test, all the materials shows an immediate increase of the stress, related with the memory effect of an elastic material when is deformed. At small values of ε_{max}, the memory is rather instantaneous, and no more significant variation in the stress is recorded for the rest of the test. As the magnitude of ε_{max} is increased, the memory response is amplified.

There is also a difference in the strees memory behaviour between each material. EPDM1a and NR show the smallest stress recovery, up to around 0.12 MPa. NBR presents the highest memory effect, reporting 0.4 MPa at the end of the test. EPDM1a does not show noticiable variation in the stress response for ε_{max} values below 1.25. In contrast, EPDM2 and CR show no noticiable variation in the response for ε_{max} values above 2.0 and 1.25 respectivalely.
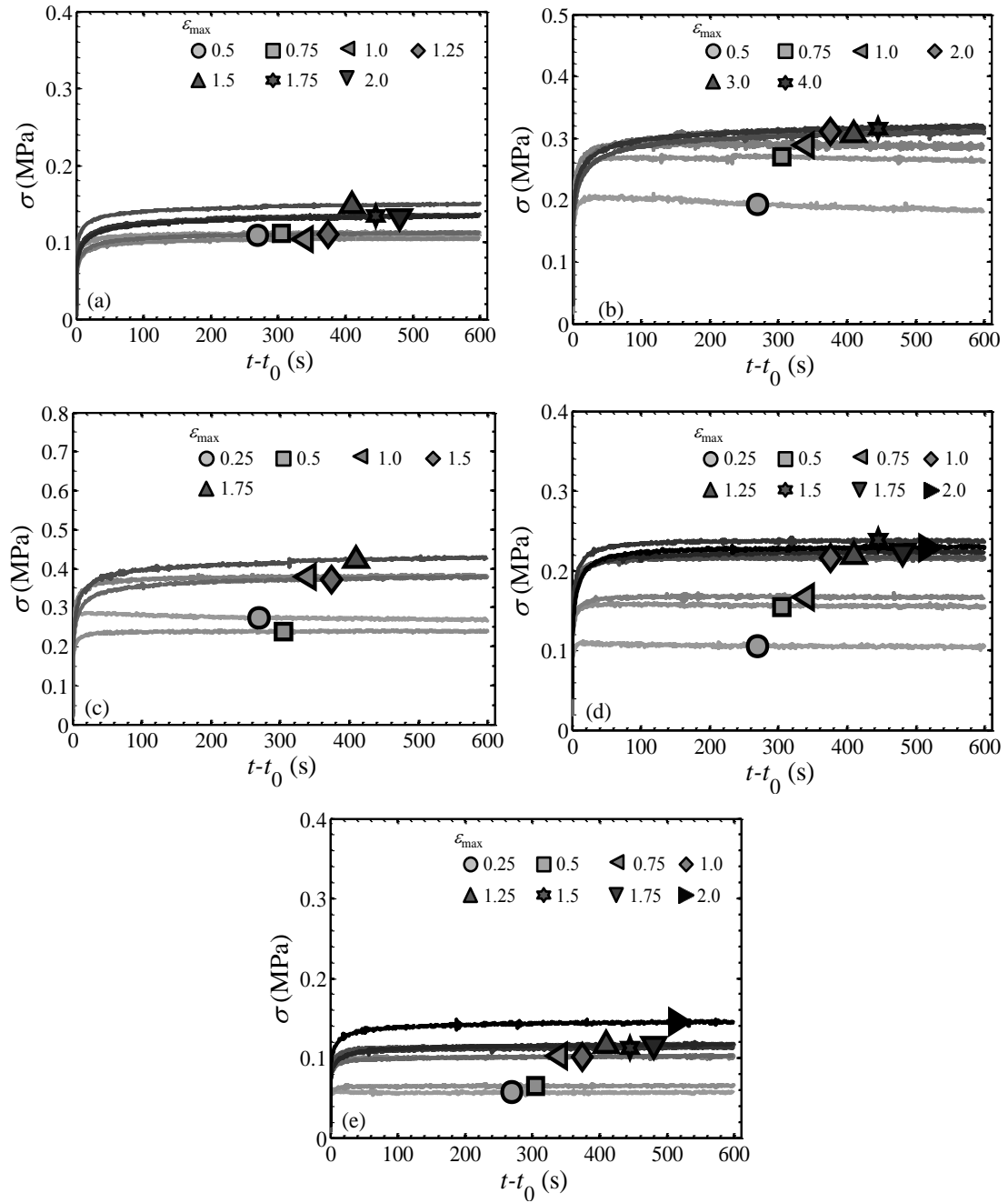
Figure 95. Stress recovery or stress-memory, σ, measured for (a) EPDM1a, (b) EPDM2, (c) NBR, (d) CR and (e) NR specimens after being subjected to a single loading-unloading cycle to ε_{max} (marked in the figure) and unloading to 0.1 N. The samples are held at constant displacement, according to TP3 under UN testing.

5.4.2 Dependence of stress memory on uniaxial deformation history

It was shown that following a complete loading-unloading cycle in the deformation history (TP3), all elastomers experience stress recovery or stress memory effects. This effect is a result of viscoelasticity, when unloading, (at $\sigma \sim 0$) there is a state of self-stress: a measure of a reaction stress to the deformation, defined as a flow stress just prior to the end of the test. Since the flow stress is rather small in all tested

materials, the stress that recovers once the flow stress has dissipated (and hence the strain) is also small. The magnitude of the recovered stress is dependent of ε_{max}. Though, it reachs a steady value of recovery at higher ε_{max} for the case of EPDM2 and CR, with no effect when ε_{max} is increased (see Figure 95(b) and (d)).

The stress at the end of the test (t=600s) as a function of ε_{max} is presented in Figure 96, to show the increase of the memory effect with ε_{max}. NBR presents the highest values of recovery, and EPDM1a and NR experience the least memory effects. Likewise, most of the materials show a tendency to a approximately constant stress response when the strain is increase. A variation in the memory response is conditioned also to the strain rate of the test. The presented data was performed at a constant rate of 0.03 s^{-1} and a modification of this condition could implicate a variation in the response mechanism. Slower strain rates could allow the material to relax during the unloading process and reduce the memory effect when the minimun load is reached. This was not considered in this work.
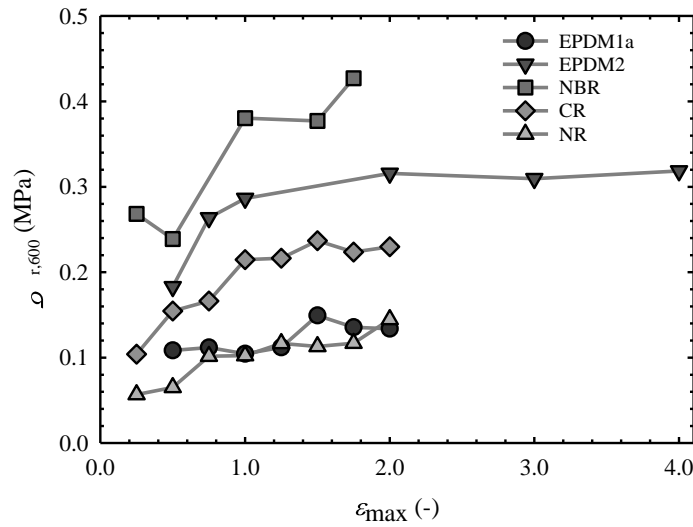
Figure 96. Stress at the end of the test $\sigma_{r,600}$ as a function of ε_{max} for all materials tested followed TP3 protocol under UN deformation.

The fact that a stress appears over time is due to the relaxation of negative or compressive flow stresses in the material which leaves behind a positive tensile elastic area. At these relatively small strains tested, the values of the stress are below 0.5 MPa. For EPDM1a, EPDM2 and NR, the difference in stress memory is less than 0.1 MPa in the range of strain evaluated for each material. The stress flow magnitude is relatively slow in these ranges of ε_{max}. For NBR and CR, a more notorious tendency of increased stress memory effect with increasing ε_{max} was observed. The

range of stress variation for the strain evaluated are approximately 0.3 MPa and 0.15 MPa for NBR and CR, respectively. It is worth to note that these two materials present the highest values of $E_{100\%}$ (6.69 ±0.03 MPa and 3.02 ±0.03 MPa) and a high stress to failure σ_f (16.90 ±1.42 MPa and 17.84 ±0.88 MPa) which is related to a higher resistance to deformation. This indicates that the stress memory response is more related to a resistance effect in the network. As analysed in Chapter 3, the chain structure of these two materials reduce the elasticity of the network, being a main factor in their high stiffness.

Even though the materials were tested at 0.1 N, the final strain after the loading-unloading $\varepsilon_{(F=0.1N)}$, is related to ε_{max}. The strain at 0.1 N, with increasing ε_{max} increases as is shown in Figure 97. This value is related to the permanent set as an effect of ε_{max}. A larger deformation history will result in a more pronounced viscoelastic response.
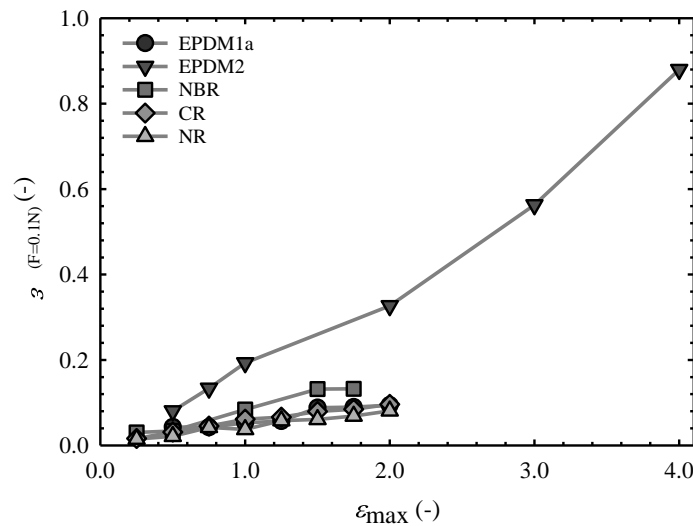
Figure 97. Remaining strain at 0.1N $\varepsilon_{(F=0.1N)}$, after TP3 testing, as function of ε_{max} applied under UN deformation for all elastomers studied.

5.5 Transition of stress relaxation to stress memory under uniaxial deformation

5.5.1 TP4: Load-partial unload history

5.5.1.1 Test protocol

Using the final protocol TP4, the material was subjected to a single loading ramp to a specified ε_{max}. During the unloading stage, the test was stopped at an intermediate

strain ε_{end}^*. The stress-relaxation measurement was then performed at this constant strain for a further 600s as it is shown in Figure 98. The combinations of ε_{max} and ε_{end}^* investigated are reported in Table 25. Only one magnitude of ε_{max} was tests in this protocol, as the variation of ε_{end}^* was the main point to evaluate in this section.
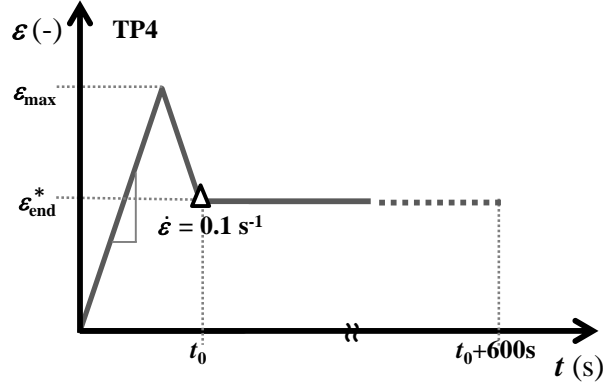
Table 25. Sets of maximum pre-strains ε_{max} and final strains ε_{end}^* investigated during stress relaxation tests following protocol TP4, for the elastomers studied.

TP4	Elastomers				
	EPDM1a	*EPDM2*	*NBR*	*CR*	*NR*
$\varepsilon_{\mathbf{max}}$	2.0	2.0	1.75	2.0	2.0
	0.5	0.5	0.5	0.25	0.25
	0.75	0.75	0.75	0.5	0.5
	1.0	1.0	1.0	0.75	0.75
	1.25	1.25	1.25	1.0	1.0
ε_{end}^*	1.5	1.5	1.5	1.25	1.25
	1.75	1.75	1.75	1.5	1.5
	2.0	2.0	-	1.75	1.75
	-	-	-	2.0	2.0

Figure 98. Strain history imposed on specimens according to stress relaxation protocol TP4. The triangle indicates the start of the stress-relaxation test, at time t_0. The maximum strain reached during the pre-deformation is denoted as ε_{max}. The final strain at the start of the stress relaxation measurements during unloading is denoted as ε_{end}^*.

5.5.1.2 Results

In test protocol TP4, the stress-relaxation (or recovery) stage is started after the samples are partially unloaded, as illustrated in Figure 99(a) for EPDM1a for $\varepsilon_{max}= 2$. The symbols indicate the starting point at each specific ε_{end}^* of the time-dependent measurements. The value of the stress at the end of the relaxation phase ($t=600$ s) is denoted as $\sigma_{r,600}$. For a better comparison between tests, the stress was normalised with respect to the stress at ε_{max}, denoted as σ_{max}.

At $\varepsilon_{end}^{*} = 2$, it is possible to observe the stress relaxation; however, at lower values, the stress relaxation and recovered is too small to be observed at this scale. When the stress normalised by σ_{max} is plotted as a function of the time, as in Figure 99(b), the relaxation (or recovery) can be observed more clearly. The stress response is dependent of the magnitude of ε_{end}^{*}. In this occasion the symbols are used in the figure as labels of the different ε_{end}^{*}.
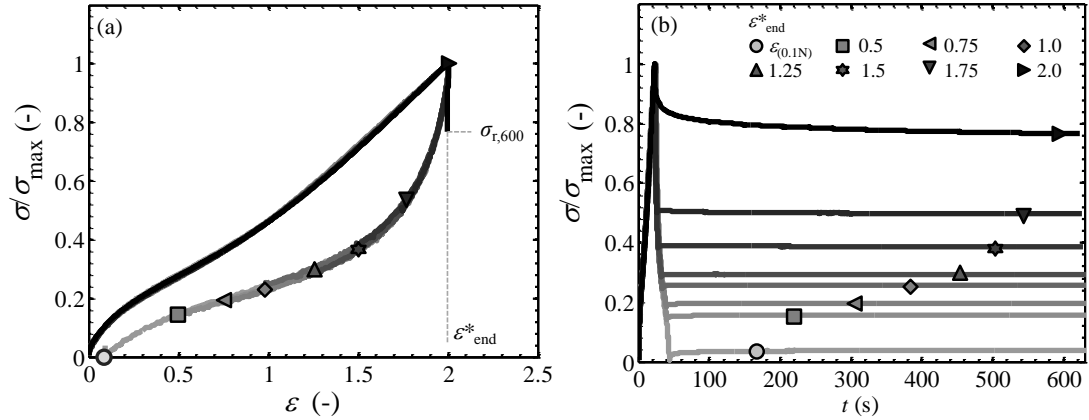
Figure 99. Stress-strain response of EPDM1a specimens deformed according to TP4 under UN testing. Normalised stress with respect to σ_{max} as a function of (a) total strain, including the relaxation stage, and (b) total time, varying ε_{end}^{*}. The symbols indicate the strain ε_{end}^{*} at which the stress-relaxation stages were started. The stress at the end of the test (t=600 s) is denoted as $\sigma_{r,600}$.

Figure 100(a-e) presents the relaxation and memory of each material for ε_{max}=2.0 (except for NBR, where ε_{max}=1.75), with the stress normalised by the value at the end of the relaxation stage, $\sigma_{r,600}$. Although this normalisation will depend of the length of the test period, it shows a clear comparison of the stress response as function of the ε_{end}^{*} during unloading. As ε_{end}^{*} increases (above 1.75 for most of the materials), a stress relaxation response is more predominant. At lower values of ε_{end}^{*}, a recovery of the stress is detected. The insets show the initial stages of the time-dependence in more detail. In this protocol, a combination of stress relaxation and memory is observed, depending on ε_{end}^{*}.
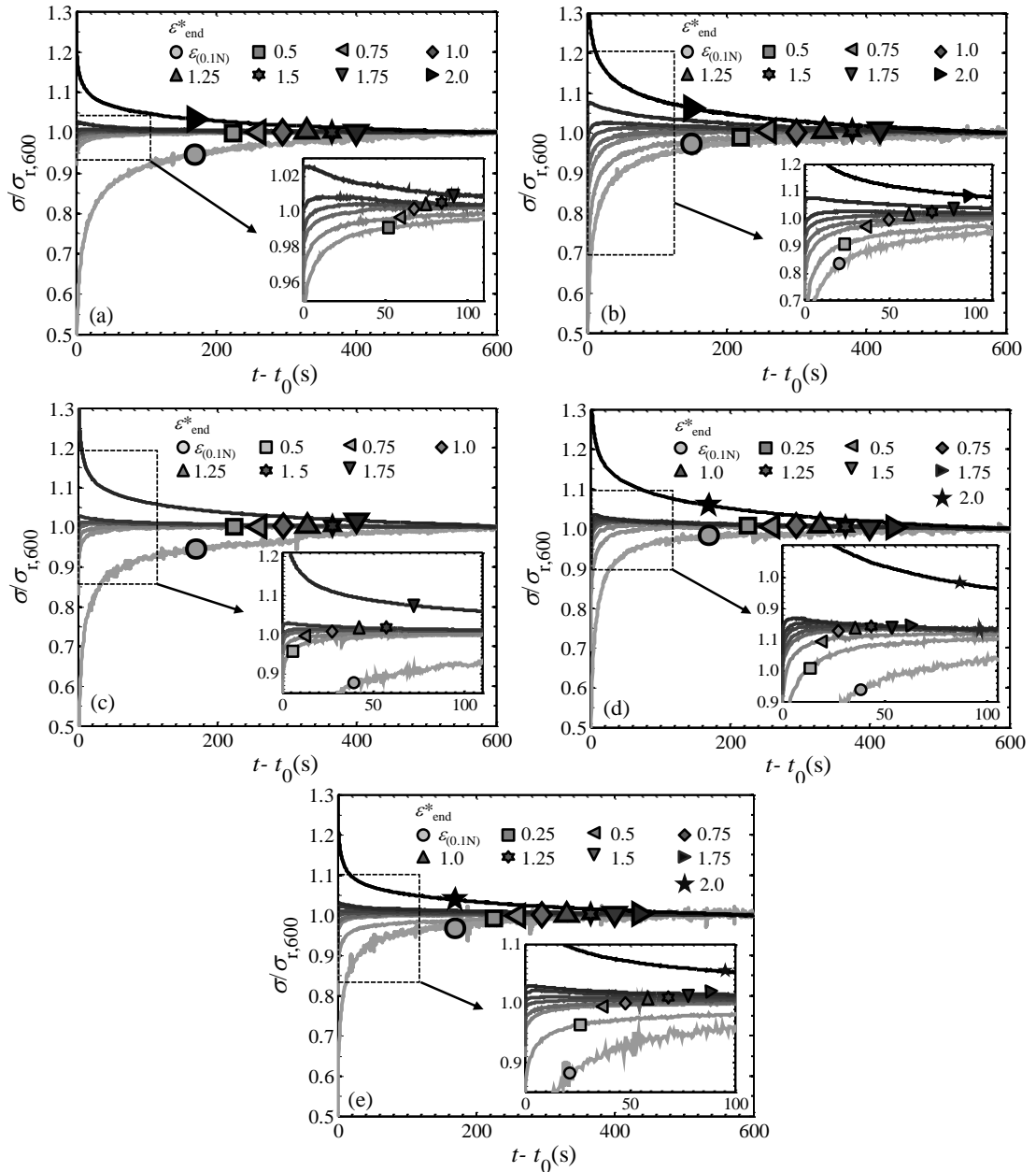
Figure 100. Stress σ normalised with the remaining stress value at the end of the relaxation test, $\sigma_{r,600}$, as a function of time for (a) EPDM1a, (b) EPDM2, (c) NBR, (d) CR and (e) NR. Specimens were subjected to a loading ramp to ε_{max}, followed by unloading to strain levels ε_{end}^{*} (marked in the figure), according to TP4 under UN testing. Symbols used as labels of each test.

For higher values of ε_{end}^{*}, stress relaxation can be observed as a drop in stress over time is observed (for example, Figure 100(a) for EPDM1a at ε_{end}^{*} above 1.5). When the specimen is unloaded to smaller strains, there is a progressive change in to a recovery effect (see insets). When the unloading reaches the minimum $\varepsilon_{(0.1N)}$, a pronounced stress recovery is observed. All the filled elastomers present the same behaviour, with a transition from stress relaxation to memory with the progression of

$\varepsilon_{\text{end}}^{*}$ to lower values.

5.5.2   Stress relaxation and memory following partial unloading

When the relaxation stage is started during unloading, stress-memory can occur even when the rubber is not fully unloaded. This might be expected by the flow process (described in Section 5.4.2), characteristic of viscoelastic materials. However, for some cases, stress-relaxation can occur even following partial unloading, in particular in the cases where $\varepsilon_{\text{end}}^{*}$ is near ε_{max}. This can be interpreted as a time- and strain-dependent relaxation process associated with the Mullins effect itself. As the material is near its previous maximum stress, this relaxation process is activated to reduce the elastic stiffness in a quasi-permanent manner that leads to the Mullins effect. In TP1, this process is visible in every test, but in TP2 it only contributes when the stress (or strain) is sufficiently large compared to a historical maximum. The strain rate could also play a role in the transition point of the strain where the response changes from relaxation to memory. This variation could be also analysed from the point of view of Tobolsky's theory of network rearrangement [77]. This would interpret stress relaxation and memory as arising from chain scission of shorter chains, together with a re-accommodation due in part to re-cross-linking. Depending on the extent of the unloading, one of these effects is predominant, leading to a transition from relaxation to memory. Apart from Tobolsky's theory, no further studies concerning this phenomenon were found.

5.6   Stress relaxation and memory under biaxial deformation.

Many of the elastomeric engineering applications can be subjected to biaxial modes of deformation such as vibration dampers, hoses and seals. Therefore, it is of importance to analyse how the time dependent behaviour changes when the material is deformed or constrained in more than one axis. The four stress relaxation protocols described in the previous sections (TP1, TP2, TP3 and TP4) were tested out on EPDM2 for equibiaxial and constant width deformations. The biaxial film tester machine used for this study allows measurement of force given on two perpendicular axes simultaneously during a stress relaxation tests. The strain combinations

examined for each test protocol for equibiaxial (EB) and constant width (CW) deformation are reported in Table 26. Higher strain values for EB and CW were not tested due to the deformation and load cell capacity of the flexible biaxial film stretcher. As EPDM2 was produced using a sheet rolling process, the direction parallel (//) to the roll was direction is aligned with axis 1, and axis 2 perpendicular to the rolling direction (⊥). For CW, the deformations were applied on axis 1and the movements were restricted on axis 2.

Table 26. Stress relaxation protocol conditions for EPDM2 followed TP1, TP2, TP3 and TP4 for EB and CW deformations. Final strain at start of relaxation stage, ε_{end}, maximum strain during pre-strain cycle, ε_{max}, and final strain during unloading, ε_{end}^{*}.

Protocols											
TP1		TP2				TP3		TP4			
EB	*CW*	*EB*		*CW*		*EB*	*CW*	*EB*		*CW*	
ε_{end}	ε_{end}	ε_{max}	ε_{end}	ε_{max}	ε_{end}	ε_{max}	ε_{max}	ε_{max}	ε_{end}^{*}	ε_{max}	ε_{end}^{*}
0.5	0.5		0.5		0.5	0.5	0.5		0.5		0.5
1.0	1.0		0.75		0.75	1.0	1.0		1.0		1.0
1.5	1.5	1.0	1.0	1.0	1.0	1.5	1.5	2.0	1.5	2.0	1.5
2.0	2.0		1.5		2.0	2.0	2.0		1.75		1.75
			0.75		0.75				2.0		2.0
			1.0		1.0						
		1.5	1.5	1.5	1.5						
			2.0		2.0						
			0.75		0.75						
			1.0		1.0						
		1.75	1.5	2.0	1.5						
			1.75		2.0						

5.6.1   Stress relaxation. TP1 and TP2

The stress relaxation and the dependence of the strain history on the mode of deformation are now examined with test protocols TP1 and TP2. Figure 101 shows the stress relaxation response on both axes for specimens of EPDM2, subjected to equibiaxial deformations according to TP1, with no previous deformation. The stress is normalised with respect to the stress at the start of the relaxation test σ_{end}, as described in Section 5.2.1.2.

As presented in Section 3.6.3, a slight difference in the stress response is expected between the axes due to the anisotropy arising from sheet rolling manufacturing process (investigated more in detail in Chapter 6). However, there is no significant difference in the relaxation process with respect to the axis. Also, there is virtually no difference in the stress relaxation process when the strain ε_{end} is increased.

Relaxations of approximately 35% at the end of the tests were measured.

Figure 101. Normalised stress relaxation σ/σ_{end} of EPDM2 specimens subjected to strain levels ε_{end} (marked in the figure and represented by the shaded color scale for each axis), according to TP1 under EB conditions. Axis 1 is parallel to the roll direction //, and axis 2 perpendicular to the rolling direction ⊥. The index illustrates the strain applied for TP1.

When the same test protocol TP1 is applied to axis 1 only, while constraining axis 2 to a constant width, CW, a variation in the stress response with respect to the axis is observed (Figure 102). For the case of axis 1, a minor increase of the relaxation is detected when ε_{end} is increased, varying from 28% to 34%. The fraction relaxing is lower than under equibiaxial strain. An equibiaxial strain induces more stress in the network as the material tries to maintain its volume. From this, the stress required to deform on both axes will increase too.
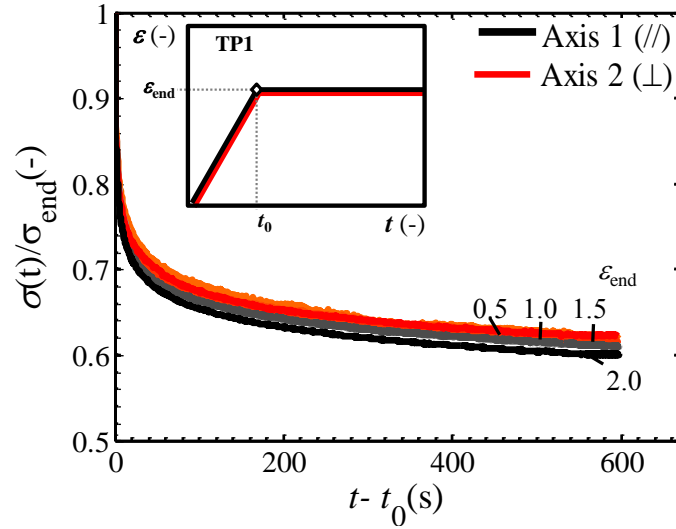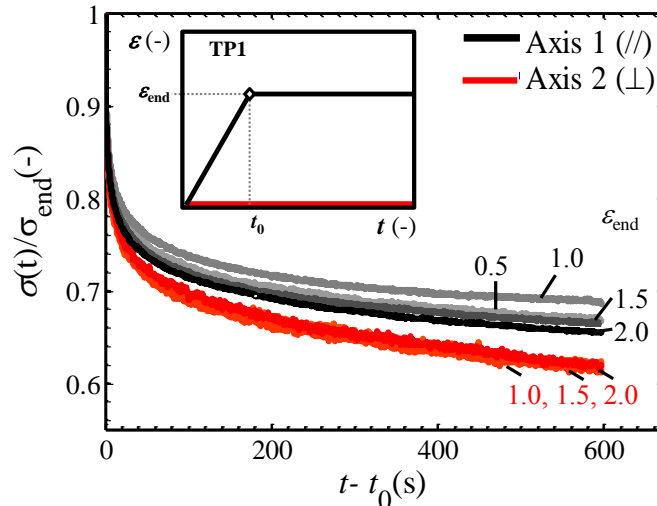

Figure 102. Normalised stress relaxing σ/σ_{end} of EPDM2 specimens subjected to strain levels ε_{end} (marked in figure and represented by the shaded color scale on each axis), according to TP1 under CW conditions. Axis 1 is parallel to the rolling direction //, and axis 2 perpendicular to the rolling direction ⊥. The inset illustrates the strain protocol for TP1.

For the restricted axis 2, perpendicular to the deformation direction, a higher stress relaxation during the time examined (600 s) compared to axis 1 is detected. The magnitude of the stress is considerably lower than the one measured in the direction of the deformation. However, the fraction of stress relaxing is higher on axis 2 than on axis 1. An almost identical relaxation response on axis 2 is detected when ε_{end} is increased. The lower values of force measured by the load cells on axis 2 give a higher noise than on axis 1, as the load recorded is considerably lower than on axis 1 (due to limitations of the load cell recording and vibration of the rig during the relaxation stage). Due to this, the value of the stress response on axis 2 for $\varepsilon_{end} = 0.5$ is not presented.

When a previous loading-unloading cycle is incorporated before the stress relaxation measurements (TP2), the effect of strain history can be examined. Figure 103 presents the stress response of EPDM2 subjected to equibiaxial deformation following TP2 for specimens subjected to $\varepsilon_{max}=1.75$. At low values of ε_{end}, the relaxation during the time examined is around 25 % of the stress at the beginning of the relaxation stage. Likewise, at strain values of 0.5 and 1.0, the relaxation response is similar during the time studied. However, when ε_{end} is approaching ε_{max} ($\varepsilon_{end}>1.5$), a higher decrease in stress is detected, of approximately 35 %, comparable to the relaxation values on TP1 (Figure 101). A slight discrepancy in the response of both axes is detected for $\varepsilon_{end} = 0.5$, especially at the beginning of the test. As ε_{end} is increased, both axes present the same response in increase of the relaxation. No major difference between the axes is observed for ε_{end} lower than ε_{max} due to the influence of the pre-strain in the relaxation response.
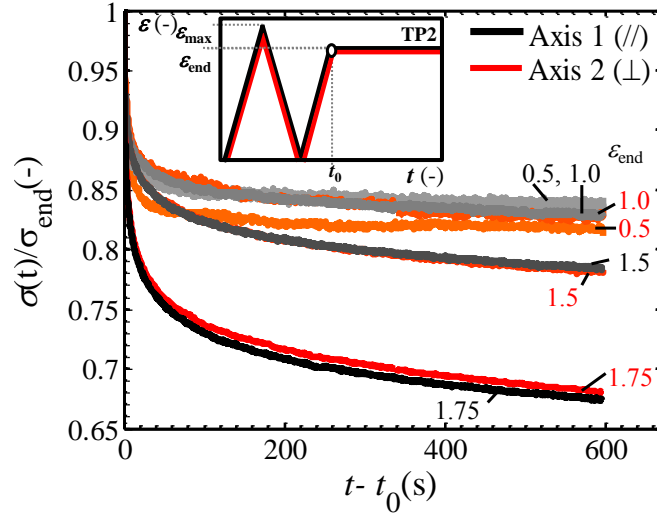
Figure 103. Normalised stress relaxing σ/σ_{end} of EPDM2 specimens subjected to a load-unload cycle through to ε_{max} =2.0 follow different strain ε_{end} levels (marked in figure and represented by the shaded color scale on each axis), according to TP2 under EB conditions. Axis 1 is parallel to the rolling direction //, and axis 2 perpendicular to the rolling direction ⊥. The inset illustrates the strain protocol for TP2

If the same TP2 test condition is examined with constant width deformation, CW, the stress relaxation response is shifted to a higher relaxation on the constant width axis 2 than in axis 1 where the deformation is applied, as presented in Figure 104 for ε_{max}=2.0. Both axes show the same ε_{end} effect for the stress relaxation with a small amount of variation for $\varepsilon_{end}<\varepsilon_{max}$ of approximately 13% for axis 1 and 25% for axis 2. However, when the ε_{end} value approaches ε_{max}, there is a noticeable increase in the stress relaxation, reaching 30% and 35% for axis 1 and 2 respectively.
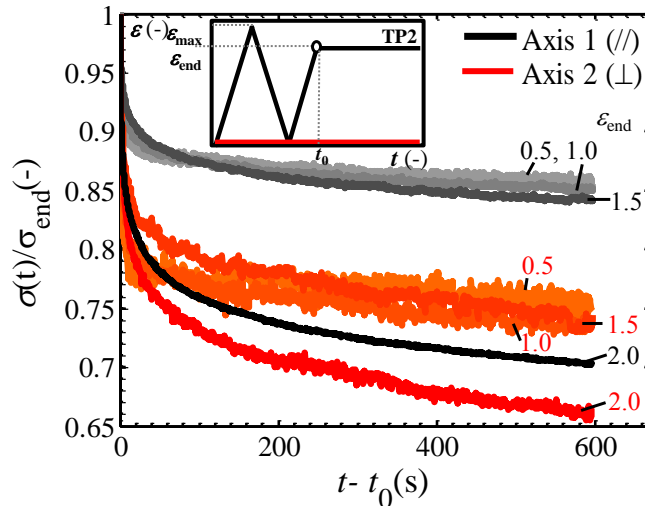

Figure 104. Normalised stress relaxing σ/σ_{end} of EPDM2 specimens subjected to strain levels ε_{end} (marked in figure and represented by the shaded color scale on each axis), according to TP2 under CW conditions. Axis 1 is parallel to the rolling direction //, and axis 2 perpendicular to the rolling direction ⊥. The index illustrates the strain protocol for TP2.

5.6.1.1   Fraction of unrelaxed stress and empirical approach

The fraction of unrelaxed stress at the end of the test (600s), $\varphi_r = \sigma_{r,600} / \sigma_{end}$, as a function of ε_{end} is analysed on each axis separately after equibiaxial deformation. The experimental data is presented in Figure 105(a-b), showing the fraction of unrelaxed stress φ_r defined previously in Section 5.2.3 for uniaxial deformation. The symbols represent the experimental data for the ε_{max} examined. The general behaviour can again be grouped as for uniaxial deformations, in three regions, as is illustrated in Figure 105(a). Both axes show the same stress response and dependence with ε_{end}. When no deformation was applied before the relaxation stage (TP1), the fraction of unrelaxed stress φ_r in *region (1)* is not affected by the increase of ε_{end}. Once the material is subjected to a previous deformation ε_{max} (TP2), if the subsequent ε_{end} is lower than ε_{max}, there is a constant φ_r, defined as *region (2)*. When ε_{end} is progressively approaching ε_{max}, the stress relaxation follows a transition form *region (2)* to *region (1)*, defined as *region (3)*. The solid lines presented in Figure 105(a-b) are from the fitting approach presented in Section 5.2.4. The only slight variation between both axes is the slope of *region (1)* as function of ε_{end} during the fitting of the model presented.

Figure 105. Fraction of unrelaxed stress φ_r of EPDM2 specimen on (a) axis 1 // and (b) axis 2 $\perp$, subjected to EB deformation according to TP1 ($\varepsilon_{max}=\varepsilon_{end}$) and TP2 (at different values of ε_{max} as marked in figure). The empirical approach is presented as solid lines.

The fraction of unrelaxed stress φ_r after 600 s for EPDM2 following constant width deformation, CW, displacing axis 1 and constraining axis 2, is presented Figure 106(a-b). The same region classification can be made for both axes as above. Axis 2 presents lower values of φ_r in *region (2)* than axis 1, and a reduction of the range of transition in *region (3)* when ε_{end} approaches ε_{max}.
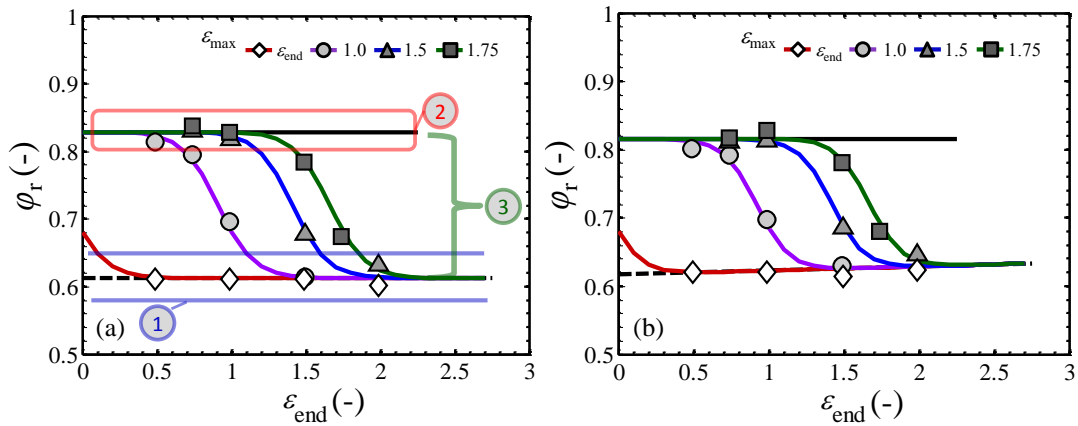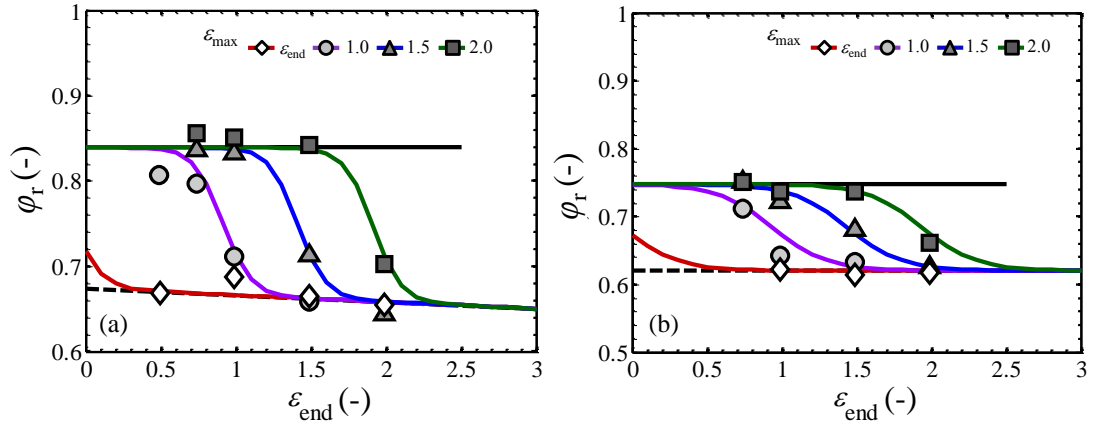
Figure 106. Fraction of unrelaxed stress φ_r of EPDM2 specimens on (a) axis 1 // and (b) axis 2 $\perp$, subjected to CW deformation according to TP1 ($\varepsilon_{max}=\varepsilon_{end}$) and TP2 (at different values of ε_{max} as marked in figure). The empirical approach is presented as solidlines.

The empirical approach developed on Section 5.2.4 for stress relaxation after uniaxial tensile deformation is implemented for the experimental data of both equibiaxial and constant width testing. The same general approach is fitted to the data, quantifying the five parameters previously described in Section 5.2.4, reported in Table 27. For comparison the values of EPDM2 after uniaxial, UN, deformation are also presented. The empirical fitting is compared to the experimental data in Figure 105(a-b) for equibiaxial deformation and in Figure 106(a-b) for constant width deformation on both axes independently.

Table 27. Parameters of the empirical approach of the fraction of stress relaxation followed equibiaxial, EB, and constant width, CW, deformation for axis 1 and 2. Parameter φ'_0 represents the interception of the fraction of unrelaxed stress of the material at zero strain, φ_{lim} is a constant fraction of unrelaxed stress when $\varepsilon < \varepsilon_{max}$. a,b and c are fitted parameters of the empirical fitting.

EPDM2	EB		CW		UN
Parameters	*Axis 1*	*Axis 2*	*Axis 1*	*Axis 2*	*Axis 1*
rms error	0.00097	0.00105	0.00483	0.00251	0.00386
φ'_0	0.61216	0.61648	0.67417	0.62000	0.66679
φ_{lim}	0.82852	0.81582	0.83918	0.74762	0.85288
a	-0.00017	0.00604	-0.00800	0	-0.02182
b	4.22137	4.64679	5.35256	2.71889	1.85306
c	0.09143	0.08205	0.09513	0.06639	0.12355

The empirical parameters are capable to describe the evolution between the three regions of relaxation. In *region (1)*, the linear relation between stress and strain of the experimental data is described very accurately, represented by a nearly constant value of $\varphi_0 \approx \varphi'_0$ as the values of the parameter a are very small. For $\varepsilon_{max}=\varepsilon_{end}$, the

fitting shows a small deviation of the ideal φ_0 (red fitted trend line) on both EB and CW testing at low values of strain. This was also observed with the uniaxial data and related with the possible strain experienced during the material processing. The error and parameters for each test quantifies the good fit of these parameters to the trend of the experimental data.

As the stress response under EB deformation is similar on both axes, it is expected that the fitting parameters for both axes will be comparable. The only exception is the parameter *a* representing the slope of the *region (1)*. This variation could be related experimentally to the initial anisotropy of EPDM2 induced by the sheet rolling process. As TP1 has no pre-strain, the response may be dependent on this anisotropy.

5.6.1.2   Stress relaxation variation on mode of deformation

The errors obtained for both modes of deformation (Table 27) are considerably low. This is due to the linear relation of φ_0, which reproduces the trend of the relaxation data better when no strain history is involved (*region (1)*) compared to the fit for UN test data. When the elastomeric network is subjected to more complicated modes of deformation such as EB and CW, the structure may experiences more directional restrictions in the deformation mechanisms than with a simple uniaxial tensile deformation.

The variation of two of the parameters evaluated, φ'_0 and φ_{lim}, with respect of the mode of deformation for EPDM2 is shown in Figure 107. The value of φ'_0 represents the ideal relaxation fraction when the material is not subjected to any previous deformation; it is expected then that φ'_0 will be the same for any mode of deformation. However, a decrease has been found for the fit to the experimental stress relaxation data after equibiaxial, EB, deformation on axis 1. A lower value of φ'_0 indicates a higher fraction of relaxation compared to the other modes of deformation. After EB deformation, the elastomer suffers two simultaneous deformation mechanisms in orthogonal directions, altering the relaxation process of the entire network structure.

For uniaxial, UN, and constant width, CW, there are similar deformations response

(as presented in Figure 46) in direction of axis 1, which results in the same value of φ'_0, independently of the reaction in the orthogonal direction. On axis 2 on CW, the value of φ'_0 indicates the relaxation as consequence of the restriction of deformation, showing a higher value of relaxing than in the axis of deformation. This is mainly due to the fact that, as this axis is not under deformation, it has more possibility to relax than in the orthogonal direction where the strain is being applied.
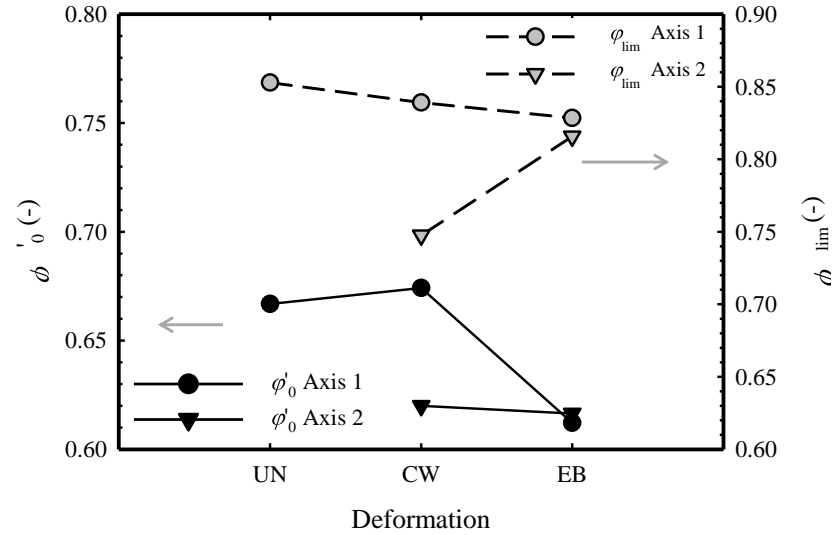
Figure 107. Parameters φ'_0 and φ_{lim} from an empirically fitted approach to experimental data, after uniaxial, UN, constant width, CW, and equibiaxial, EB, deformations. The grey arrows indicate the corresponding y-axis for each parameter.

The values of φ_{lim} represents the relaxation fraction on *region (2)* when $\varepsilon_{end} < \varepsilon_{max}$. There is a drop in this fraction when the constraints during deformation are increased, from UN to CW and EB. In this case, the deformation history and hence the deformation mechanism has altered the relaxation process, giving a slight higher relaxation capacity of the structure after the deformation history, linked also with the softening mechanism. On axis 2, as mentioned previously, the relaxation is higher when the axis is just constricted than when a strain applied. The axis only under constrain of movement gives more mobility to the chains to relax in that direction.

5.6.2 Stress memory. TP3

Stress memory effects with time are also present after equibiaxial and constant width deformations. The stress response as function of time after a complete loading-unloading cycle is shown in Figure 108, for EPDM2 especimens subjected to equibiaxial deformations. The memory effect following small strains ($\varepsilon_{max}=0.5$)

shows a recovery to ~0.2 MPa for the time examined (600s), from the starting point of approximately 0.04 MPa at the beginning of the relaxation stage. For $\varepsilon_{max}>1.0$ the recovery increases, reaching a plateau at ~0.25 MPa, approximately independent of the applied strain. Both axes show the same trend on the stress response, with a slightly higher stress recovery on axis 2. The appearance of stress memory over time is related to the relaxation of a negative (compressive) flow stress due to the previous unloading deformation that leaves behind a positive (tensile) elastic part with time. The response is similar to that analysed for uniaxial deformation on Section 5.4.

Figure 108. Recovery of stress, or stress-memory as a function of time of EPDM2 specimens subjected to a single loading-unloading cycle to ε_{max} (marked in figure and represented by the shaded color scale on each axis) and unloaded to 0.1 N according to TP3 under EB. The axis parallel to the roll direction // is denoted as Axis 1 and the one perpendicular to the rolling direction ⊥ as axis 2.

Under CW deformation only axis 1 is subjected to the loading cycle, and shows a clear recovery, as shown in Figure 109. A higher of stress memory is observed when ε_{max} is increased from 0.5 up to 2.0. In the orthogonal direction (axis 2), a less clear variation of the stress could be observed. It is interesting to notice that, even after small strains ($\varepsilon_{max} =0.5$), there is a reduced magnitude but faster recovery on axis 2, than on axis 1.
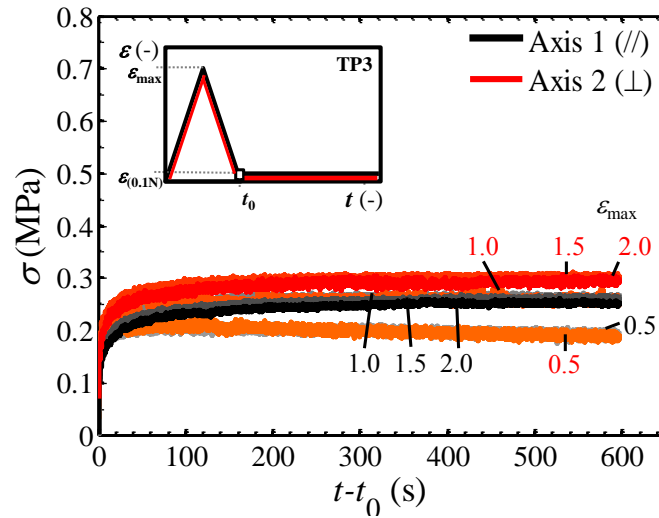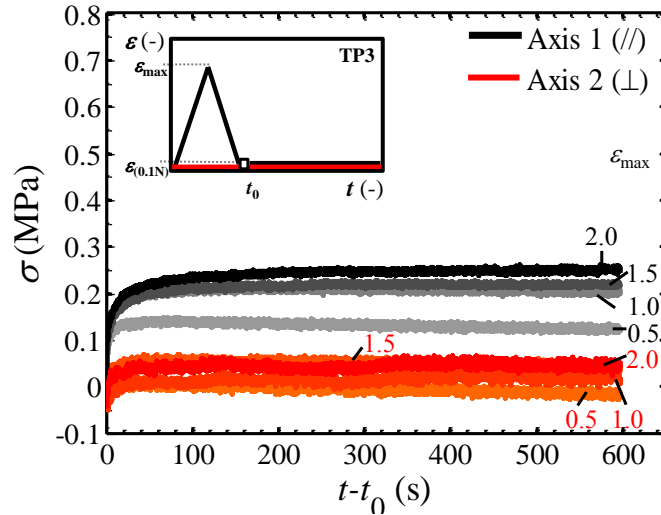
Figure 109. Recovery of stress, or stress-memory as a function of time of EPDM2 specimens subjected to a single loading-unloading cycle to ε_{max} (marked in figure and represented by the shaded color scale on each axis) and unloaded to 0.1 N according to TP3 under CW. The axis parallel to the roll direction // is denoted as Axis 1 and the one perpendicular to the rolling direction ⊥ as axis 2.

5.6.2.1 Stress memory variation with mode of deformation

The stress values at the end of the stress memory stage at t=600s, $\sigma_{r,600}$, are compared in Figure 110 for EPDM2 as a function of strain ε_{max} for the three modes of deformation The memory under UN reaches values up to ~0.31 MPa at ε_{max}=2.0, similar to the values observed under EB (~0.3 MPa) on axis 2. Axis 1 has slightly lower values, although the influence of strain is comparable to that under UN, with a tendency to converge to a constant value as the strain is increased.
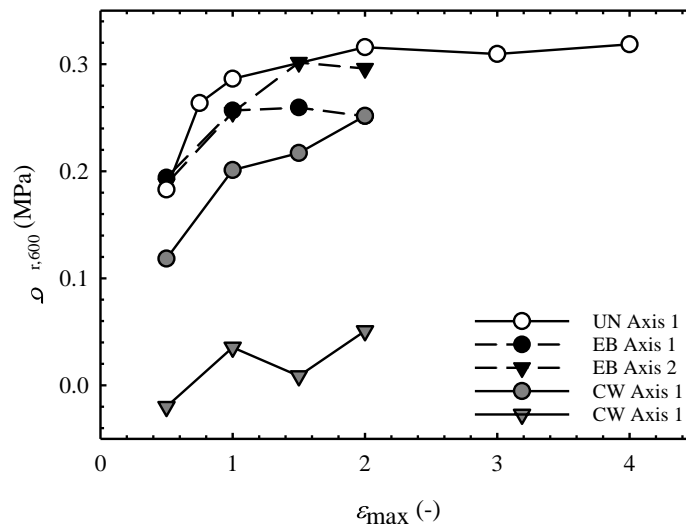
Figure 110. Stress measured at the end of the test $\sigma_{r,600}$ as a function of ε_{max} for EPDM2 tested following TP3 under UN, EB and CW modes of deformation.

For CW conditions, the values of the stress on axis 1 start lower than UN and EB

with a tendency to increase with strain up to values similar to the other modes of deformation. EPDM2 has a higher recovery at the time evaluated and hence, less permanent damage, when the material is subjected to UN deformation. The stress field on just one direction on EPDM2 may allow an easier recovery of the structure than when the specimen is restricted on two axes. It may be the case that if the relaxation response was monitored for longer for EB and CW specimens, the values could converge to the one observed for UN, although this was not verified experimentally.

5.6.3   Transition of stress relaxation to stress memory. TP4

TP4 examines the stress response when the relaxation (or recovery) stage starts during a partial unloading. Following the same conditions as with UN deformation on Section 5.5.1, the influence of EB deformation on the fraction of stress relaxation (or recovery) is presented for EPDM2 in Figure 111(a-b), for each axis respectively. There is a gradual change in the fraction of stress from relaxation to memory response, as observed during uniaxial deformation (Figure 100). When the partial unloading at the beginning of the stage ε_{end}^{*} is closer to the maximum pre-strain ε_{max}, there is a stress relaxation with time. When the strain is unloaded to lower magnitudes of ε_{end}^{*}, the material presents a transition to a stress memory response. Both axes respond with the same transition of the stress response.

Figure 111. Normalised stress relaxation $\sigma / \sigma_{r,600}$ a function of time for EPDM2 specimens subjected to a loading ramp to $\varepsilon_{max} = 2$, and unloaded to strain levels ε^*_{end} (marked in the figure), according to TP4 and EB deformation for (a) axis 1 and (b) axis 2. The axis parallel to the role direction // is denoted as Axis 1 and the one perpendicular to the role direction ⊥ as axis 2. Symbols are used to label of each test.

For CW test conditions, there is a difference between the axes, as presented in the normalised stress relaxation as function of time plotted in Figure 112(a-b), for axes 1 and 2 respectively. It is clearly noticeable the noise in the stress measurements at $\varepsilon^*_{end} = 0.5$ due to the low values of force recorded. Nonetheless, a trend in the stress response can be observed, showing a similar response to axis 1. At values of ε^*_{end} closer to ε_{max}, the material experiences stress relaxation. Whit increasing unloading, the response turns into a stress memory effect.
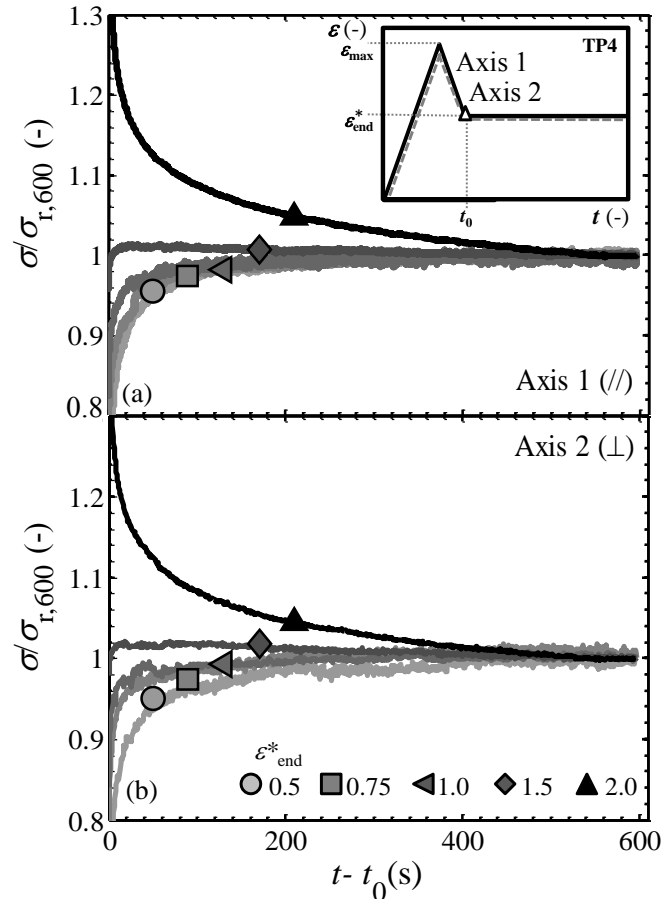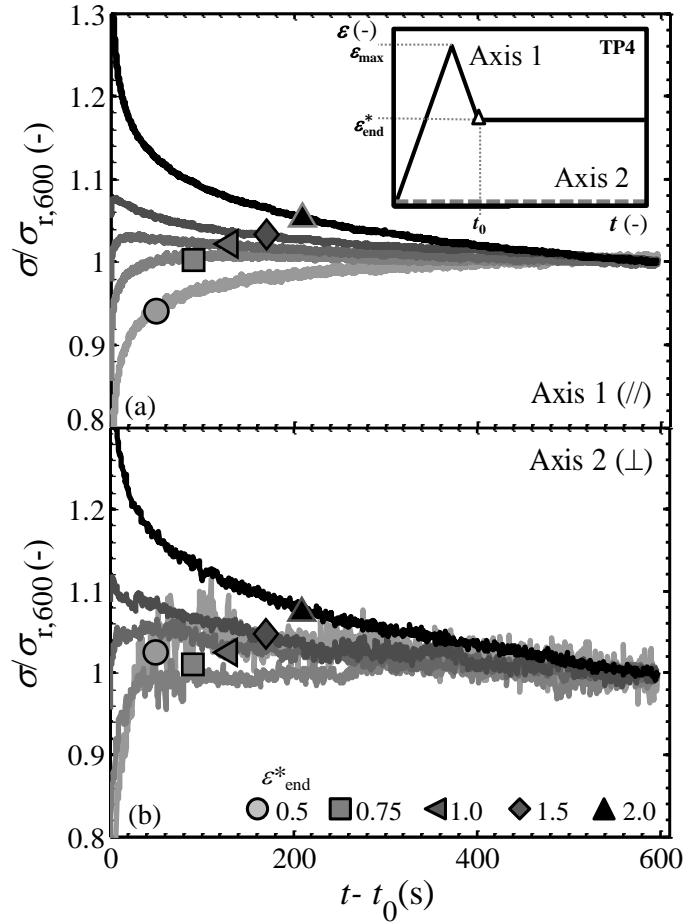
Figure 112. Normalised stress relaxation $\sigma / \sigma_{r,600}$ a function of time for EPDM2 specimens subjected to a loading ramp to $\varepsilon_{max} = 2$, and unloaded to strain levels ε_{end}^* (marked in the figure), according to TP4 and CW deformation for (a) axis 1 and (b) axis 2. The axis parallel to the role direction // is denoted as Axis 1 and the one perpendicular to the role direction ⊥ as axis 2. Symbols are used to label of each test.

5.7 Relationship between the fractions of dissipated energy and stress relaxation

As presented in Section 5.2.4, an constant value of unrelaxed stress intrinsic to each material was observed in *region (2)* of Figure 91 when the previous deformation ε_{max} is higher than ε_{end} for UN testing. This indicates that, as long as the deformation is kept below a previous maximum, the fraction of stress relaxation within a specific time interval is independent of both the applied strain and the maximum strain. The total fraction of stress relaxation after 600s, ϕ_r, can then be expressed as

$$\phi_r = 1 - \left[\sigma_{r,600} / \sigma_{end} \right]$$ Eq. 5-6

The experimental results of dissipated energy during cyclic deformation from

Chapter 4 are used compare it with ϕ_r. The values of the fraction of dissipated energy during cyclic deformation, ϕ_c (Section 4.5), when a pre-strain (ε_1) is higher than the strain in the next stage (ε_2), are recalled. It was found that when the pre-conditioning is higher than the following loading-unloading, a constant energy is dissipated, as presented in Figure 113. The values presented are focused only on the cases where $\varepsilon_1 > \varepsilon_2$ for ϕ_c and $\varepsilon_{max} > \varepsilon_{end}$ for ϕ_r under UN deformation. When the values of ϕ_r under uniaxial deformation and the fraction of energy dissipation ϕ_c are compared, an interesting similarity is found. These values are intrinsic for each elastomer, ranging between ~0.06 in NR and ~0.17 in EPDM2.

It is also particularly noteworthy that both fractions are approximately independent of both the pre-strain and current strain. It is worth reminding the reader that when pre-strain in increased, the constitutive response does depend on pre-strain, showing a higher softening phenomenon on subsequent loading following different strain histories, as presented in Figure 90 for EPDM1a.

In cyclic experiments a fixed fraction of the energy is dissipated, and in the stress-relaxation experiments a fixed fraction of the stress relaxes, independently of the constitutive response. Whereas scragging can be used to control the modulus, the dissipated fraction of energy remains unaltered provided that the range of deformation stays within the scragging strain.
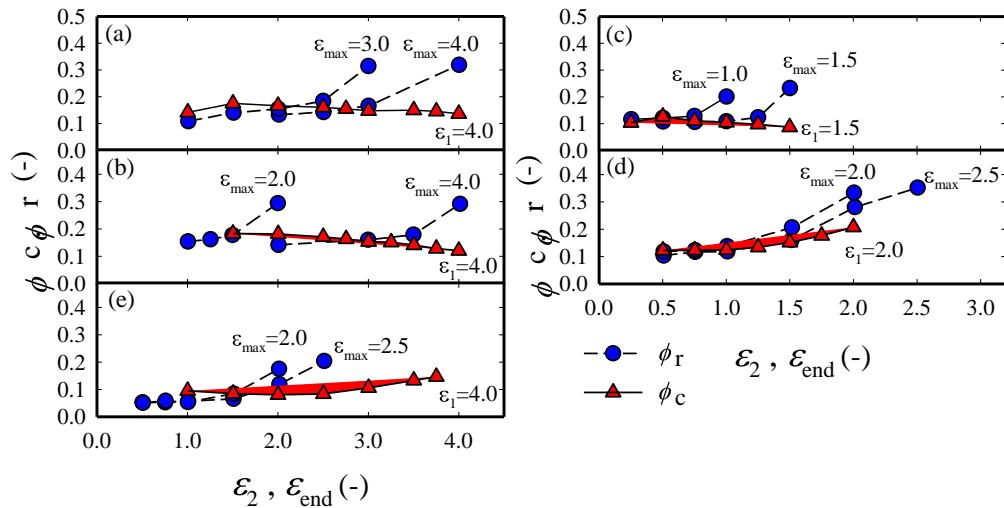
Figure 113. Fraction of stress relaxed during UN stress relaxation, ϕ_r, for $\varepsilon_{max} > \varepsilon_{end}$, and fraction of energy dissipated during UN cyclic loading, ϕ_c, as a function ε_2, for deformation $\varepsilon_2 \leq \varepsilon_1$ for (a) EPDM1b, (b) EPDM2, (c) NBR, (d) CR and (e) NR. [1]

---

[1] EPDM1b (used in Chapter 4) was used instead of the EPDM1a as examined in the rest of this chapter. Specific tests were performed for the comparison analysed in Section 5.7.

5.8   Summary

This chapter has presented new experimental measurements of stress-relaxation and stress-memory for a wide range of elastomers. Specimens were subjected to a variety of carefully constructed deformation histories protocols in order to explore the role of strain history on stress relaxation and stress memory. When stress relaxation is measured after a simple UN loading of virgin rubber (TP1), the fraction of stress relaxation was shown to be highly strain-dependent. In contrast, when the stress relaxation measurements were carried out following a loading-unloading cycle (TP2) to a strain smaller than the previously reached maximum, a constant fraction of the stress relaxation can be observed, independent of the applied strain and the previous maximum strain. This fraction varied with the different rubbers between 0.95 for NR and 0.85 for EPDM2, which indicates that this could be an intrinsic material property, related to the chain structure configuration and filled content.

This has important industrial implications since it means that the stress relaxation remains independent of scragging procedures, and that scragging may be safely used to control the modulus of rubber products without affecting the relaxation process. Maps of unrelaxed stress fraction as function of applied strain for different deformation histories were presented, and can be interpreted as time-dependent equivalents of pseudo-cyclic load-unload curves commonly used to summarise the Mullins effect (Section 5.2.3 for UN and Section 5.6.1.1 for EB and CW deformations). The transition of the stress relaxation process is described in three distinct regions, where the effects of strain history and strain during the relaxation process are related. These maps should prove useful to the community interested in predicting the relaxation of rubber products following complex strain histories, as well as to developers of constitutive models for rubber accounting for time-dependence and the Mullins effect.

The behaviour reported in this chapter has not only important implications concerning the effects of scragging on rubber viscoelasticity. The experiments have confirmed that a deformation history can have, under certain conditions, a significant and well-defined role on the determination of the time dependent response of rubber. An empirical approach was fitted to predict the stress relaxation response a function of strain history (Section 5.2.4). The method proposed, containing five parameters, shows accurate estimates of the relaxation process as a function of the stress applied

and history of the material at a given time, with a rms error of <1.4%.

Stress memory following loading-unloading cycles was investigated under UN for all five materials (TP3 in Section 5.4). It was found that the stress memory is approximately independent of the strain history. Both stress relaxation and stress memory were observed over time after a partial unloading (TP4 in Section 5.5). The use of these new test protocols has confirmed that deformation history can have a significant and well-defined role in the determination of the time-dependent response of rubber.

The deformation history dependence suggests that the degree of scragging can be safely used to tune the modulus of a rubber without affecting the viscoelastic response. Stress relaxation tests were performed for EPDM2 under EB and CW conditions and compared with UN (Section 5.6.1.2). Equibiaxial deformations resulted in lower values of stress relaxation compared to UN strain history conditions using TP2, as well as a small variation in the parameters fitted for the empirical approach (Section 5.6.1.1). Overall, the mode of deformation does not vary the stress memory and transition effects significantly.

Under EB deformation test protocols it is possible to observe an anisotropy effect due to the manufacturing process of EPDM2. A small difference is observed in both the stress relaxation and memory response between the axis parallel (axis 1) and orthogonal (axis 2) to the roll. During the first deformation (TP1) there was no significant difference in the relaxation response, but when strain history is present, axis 1 shows a minor decrease in relaxation to axis 2 (Section 5.6.1). With respect to the memory response, the recovery is higher on axis 2 (Section 5.6.2).

A comparison with the fraction of dissipated energy during cyclic deformation from Chapter 4, subjected to a series of strain histories was carried out in Section 5.7. This fraction was compared to the remaining fraction of stress during stress relaxation experiments after cyclic deformation. When the rubber is deformed within a strain envelope defined by a first strain, the fraction of relaxed energy is independent, not only of the current strain amplitude, but also of the pre-stain. It was found that the fraction of energy dissipated is very similar to the fraction of stress relaxation in stress-relaxation experiments. This suggests that this is an intrinsic parameter of each material related to the viscoelasticity of its network structure.

Chapter 6   **Anisotropy of swelling**

When an elastomer is subjected to a deformation history, the constitutive response, the energy dissipated (Chapter 4), as well as the time-dependence (Chapter 5) change as a result of deformation history. It is clear from these analyses that deformation history modifies the network structure; giving the possibility of deformation induced anisotropy. Some researchers have shown the anisotropy experienced during deformation, mainly focussed in the changes of the stress response after a deformation on uniaxial direction [90, 112]. Another aspect, often neglected during mechanical response examinations, is the anisotropy imparted during the processing stage [211]. If the material is vulcanised and processed using techniques such as sheet rolling or compression moulding (see Section 3.3), it is expected that the deformations involved during the manufacturing may lead to anisotropy in the elastomer network.

The swelling phenomenon using Flory's approach for vulcanised elastomers was conducted in this chapter to analyse how deformation history change the network structure through the average molecular weight between cross-link points. Likewise, the dimensional ratio during swelling can indicate the impact of processing methods and deformation history changes the anisotropy. This work focuses on conducting careful swelling measurements to measure the process induced anisotropy in a range of filled elastomers. Section 6.1.1 presents a detailed description of the sample preparation and swelling testing methodology for un-deformed filled-elastomer specimens.

The anisotropy of swelling due to the manufacturing process is discussed in Section 6.1.2. Section 6.2 presents the influence of deformation history in the swelling. The molecular weight through Flory's approach following uniaxial and equibiaxial tensile deformation in analysed in Section 6.2.3. Section 6.2.4 presents the experimental results of the dimensional ratio variation during swelling with respect to deformation, depending on the processing method and the deformation history. The importance of the

anisotropy examination in the mechanical response of filled elastomers is considered in Section 6.3. Finally, a summary of the findings is presented in Section 6.4.

Aspects of this chapter were presented as an oral presentation and conference article in the 9th European Conference on Constitutive Models for Rubbers held in Prague in 2015. A journal paper is being prepared to be submitted in the peer reviewed Journal Rubber Chemistry and Technology.

6.1 Swelling for un-deformed filled elastomers

6.1.1 Swelling experimental methodology

A rectangular specimen 20 mm x 20mm x 0.5mm (~0.15g) was cut from the vulcanised sheets on each material, using a straight cutter. Four swelling specimens were obtained for each condition. The mass before swelling, m_o, in the swollen state, m_s, and after drying, m_d, was recorded using a Mettler Toledo XS105 analytical balance [184]. To reduce evaporation of the solvent during measurements in the swollen state, specimens were removed from the solvent, excess cleaned from the surface with a paper towel and covered with pre-weight aluminium foil. The specimens were immersed individually in approximately 50ml of solvent in sealed glass vials. The solvents were selected to have a Hildebrand solubility parameter δ_1 similar to that of the specific elastomer δ_2 [41], as defined in the Polymer Handbook [183]. The specific solvent used for each elastomer is reported in Table 28. This similarity indicates a good solvent-polymer interaction, allowing the swelling process to occur with a lower probability of degradation of the elastomer [183]. The density of the elastomer, ρ_2, was measured in Section 3.4.1 and the density of the solvents, ρ_1, taken from the technical data sheets.

Table 28. Properties of solvents and polymers used in the swelling experiments: density of the solvent, ρ_1 ; molar volume of the solvent, V_1 ; solubility parameters for solvent, δ_1, elastomer, δ_2; density of the elastomer, ρ_2 and Huggins interaction parameter, χ .

	Elastomer				
	EPDM1b	*EPDM2*	*NR*	*NBR*	*CR*
Solvent	Toluene			Dichloro-methane	THF
ρ_1 **(g/cm^3)**	0.867			1.325	0.889
V_1 **(ml/mol)**	106.27			84.93	81.11
δ_1 **(cal/cm^3)$^{1/2}$**	8.91			9.68	9.10
ρ_2 **(g/cm^3)**	1.026 ±0.003	1.139±0.005	1.072 ±0.008	1.215±0.004	1.371 ±0.007
δ_2 **(cal/cm^3)$^{1/2}$**	8.10	8.10	8.30	10.60	9.30
χ	0.46	0.46	0.40	0.43	0.35

The Flory-Huggins parameter, χ, represents the energetic change due to the interaction between the solvent and the polymer. For polymers, a good solvent interaction is found when χ is below 0.5 [198]. Values of χ can be estimated from [183, 198]

$$\chi = 0.34 + \frac{V_1}{RT}(\delta_1 - \delta_2)^2$$

Eq. 6-1

Using the solubility parameters of each polymer and solvent selected (Table 28). The first term corresponds to a correction factor for the entropic contribution. A constant between 0.3 and 0.4 is often used for polymer-solvent solutions to reflect the additional entropy of mixing [183, 198]. The value of 0.34 was used in Eq. 6-1 based on similar studies from the literature [183, 212-214]. The second term in Eq. 6-1 corresponds to the enthalpic contribution, which includes the influence of temperature [41, 183, 215]. Similar values of χ to those reported in Table 28 has been reported previously using the same elastomer-solvent combination [38, 183, 212].

6.1.1.1   Swelling equilibrium conditions

To identify the appropriate swelling equilibrium time, T_s, 192 hour (8 days) tests at 19±1°C were carried out in which mass was monitored during the swelling stage. A specific solvent was used for each elastomer (see Table 28). Each specimen was placed in a sealed glass vial filled with approximately 50ml of the specific solvent. During the swelling stage, the specimens were kept in the dark to avoid photo-oxidation [40]. To measure the mass, each specimen was removed from the solvent and rapidly dabbed to remove any excess solvent from the surface with a paper tissue. The specimen was covered with aluminium foil to ensure that minimum evaporation of the solvent could take place during the measurement of the mass. The mean swelling ratio, defined as the ratio of the mass at time t, m_s, to the mass before swelling m_o, is shown for each elastomer in Figure 114. Four specimens were analysed for each material, with two standard errors from the mean.

The results indicate that already after 1 hour, there is little variation in the swelling ratio of the samples, and that the interaction between elastomers and solvent has reached equilibrium. A swelling time of T_s = 48 hours was selected for all experiments, as it represents a good balance between reaching equilibrium and minimising network degradation [44].
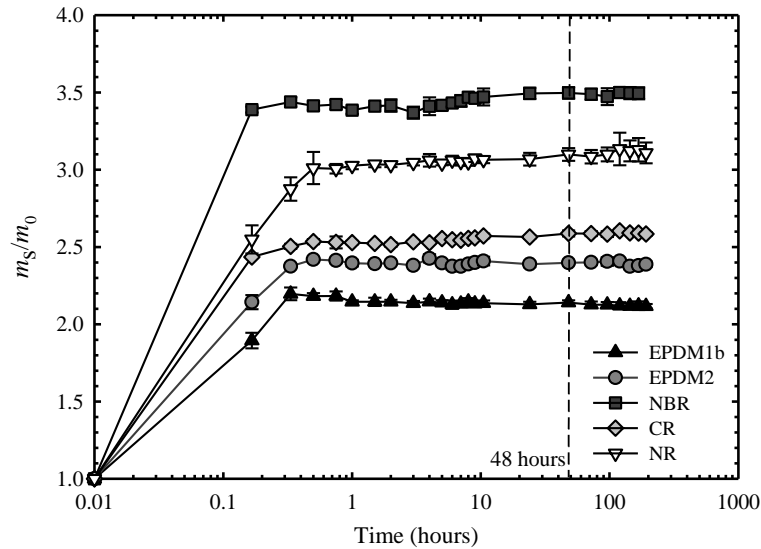
Figure 114. Mass ratio as a function of time during swelling for undeformed elastomers.

Another experiment was then derived to determine a suitable drying time, for which the solvent had completely evaporated from the specimen. After swelling four specimens for each elastomer during 48 hours, specimens were dabbed with tissue, weighted and placed in an open box to allow the evaporation of the solvent. The mass was monitored over a further 168 hours (7 days) at room temperature (19 ± 1°C). The mass ratio for the five materials is presented in Figure 115. Results indicate that, already after a few hours no significant change in weight could be recorded. It is worth noticing that after 10 hours all the materials exhibit a ratio below 1, indicating a loss of weight relative to the initial weight before the swelling stage. A drying time of $T_d =48$ hours was chosen to measure the final dried weight, m_d, for all further experiments to ensure complete evaporation of the solvent.
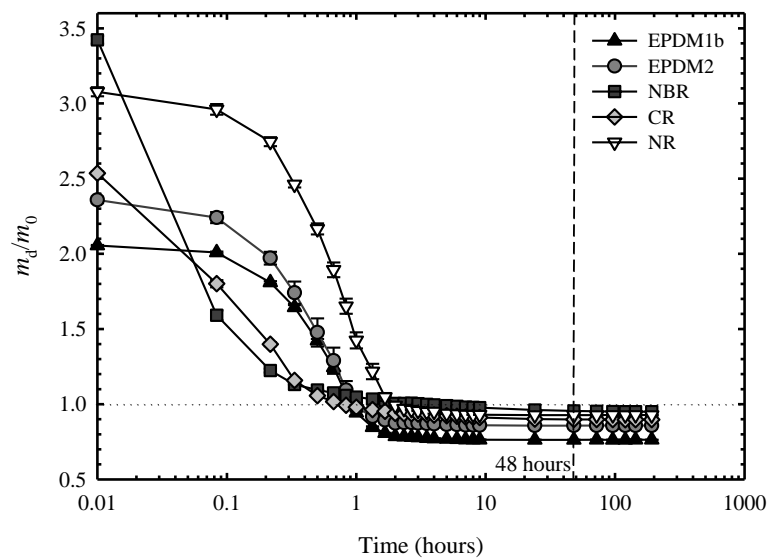
Figure 115. Mass ratio, for undeformed elastomers, as a function of time during the drying stage after swelling for 48 hours.

6.1.1.2 Linear dimensions measurements

The linear dimensions, λ, of each specimen were measured before the swelling, in the swollen state at T_s, and after drying at T_d. Using a calibrated HP Scanjet G4010 scanner system. A 1200 dpi resolution was used corresponding to a resolution of 0.0212 mm/pixel. The image was processed using a Matlab image acquisition tool (*measuretool*, see Appendix D.2). For the thickness measurement a Hildebrand rubber thickness gauge was used according to ISO 23529 [151]. To avoid evaporation of the solvent and rapid reduction of the thickness during swelling, the specimen was measured held in a glass petri dish containing the solvent, as shown in Figure 116. Special care was taken to not move the petri dish to ensure the correct calibration of the gauge before and during the measurement.

Figure 116. Measurement set up for measuring of thickness during swelling state using a Hildebrand rubber thickness gauge.

The different stages of the swelling process and the resulting dimensions measured in the experiments are schematically represented in Figure 117. For analysis of the results, the averages and standard deviations are based on a sample size of four specimens on each material. As the specimens have a square shape, a small cut was made on the two top edges to identify the length of the width dimensions.
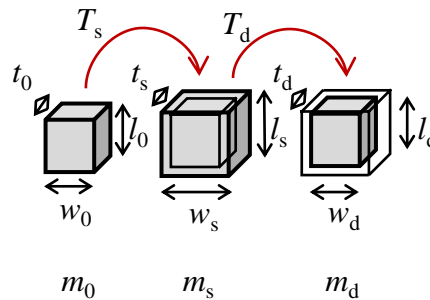
Figure 117. Uniaxial (a) and equibiaxial (b) deformation tests and subsequent linear swelling measurements.

The dimensional ratios in the swollen state λ_l, λ_w and λ_t for the length, width and thickness respectively are determined from the linear measurement ratios as

$$\lambda_l = l_s / l_d,$$
$$\lambda_w = w_s / w_d$$
$$\lambda_t = t_s / t_d$$

Eq. 6-2

with l_s and l_d as the length in the swollen and dried state, w_s and w_d the width in the swollen and dried state, and t_s and t_d the thickness in the swollen and dried state.

6.1.2   Process induced swelling anisotropy

Materials were classified as compression moulded (EPDM1b and NR) or sheet rolled (EPDM2, NBR and CR) rubbers. Swelling experiments were carried out on specimens of underformed materials and the dimensions measured to observe the swelling in each direction. Figure 118 shows the directional swelling ratios for all five materials, separated into compression-moulded and rolled rubbers.
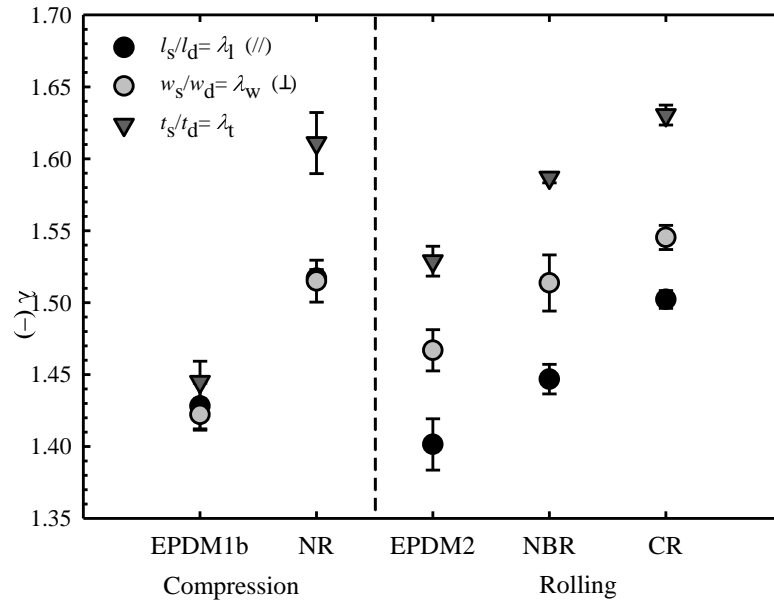
Figure 118. Dimensional ratio λ variation during swelling for rubbers manufactured by compression-moulding and rolling.

All rubbers swelled more in the thickness direction than in the other directions. The compression-moulded rubbers, EPDM1b and NR, exhibited symmetric swelling in the plane of the sheet, suggesting that these materials can be considered as transversely isotropic. EPDM1b can, in fact, be approximated as isotropic to within the experimental uncertainty, but NR presents a transvers isotropy, showing an increase of the thickness

ratio in the direction of compression. The rolled rubbers instead exhibit full anisotropy in their swelling, with different swelling ratios in each direction. The rolling direction exhibits the smallest degree of swelling.

The manufacturing process can impart a degree of anisotropy in a rubber network if some form of deformation of the chains is present during the vulcanisation process. This means that when the network is being cross-linked, the material is not in equilibrium and will relax following the removal from the mould or rolling mill. As mentioned in Section 3.3, during compression-moulding of a thin sheet, process applies a symmetric equibiaxial extension to a material during cross-linking, which will be locked in to different degrees depending on the balance between chain relaxation time and cure kinetics. Thus, if chains are stretched in the plane and compressed out of plane, the specimen will relax by expanding its thickness when removed from the mould so as to minimize its strain energy. It is evident from the anisotropy of the swelling that none of the compounded materials are completely isotropic in their post-production state, possibly due to the effect of the filler, and of the random nature of the cross-linking process. Thus, the fact that swelling is greatest in the thickness direction suggests that chains are less stretched (or more able to deform) in this direction than in the other directions. This is consistent with cross-linking taking place in a partially deformed configuration of equibiaxial extension. Figure 119 (a) describes the compression-moulding process.

In the case of rolled rubbers, typical two-roll mills will impose conditions of plane strain on a material during cross-linking. Figure 119 (b) shows a diagram of this manufacturing process. Thus, to a first approximation, chains will be more stretched in the rolling direction, undeformed in the transverse direction, and more compressed in the thickness direction when they are cross-linked. Swelling results suggest that chains are less stretched (and therefore more deformable) in the thickness direction, and more stretched (and less deformable) in the rolling direction, when compared with the transverse direction. Thus, this is also consistent with cross-linking in a planar state of deformation. In reality, the swelling following both manufacturing processes is further complicated by the presence of the filler and of the filler-rubber bonds, which may also contribute to the anisotropy as a consequence of the process.
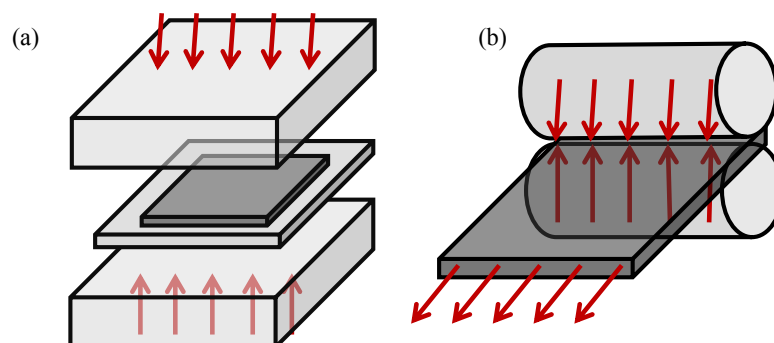
Figure 119. Representation of manufacturing process of (a) compression-moulding and (b) sheet rolling.

Analysis of specimens produced from these two simple manufacturing techniques commonly used in industry showed that, post-production there is already an initial anisotropy in the material. More complex processing techniques such as injection moulding or thermoforming could bring even more complex network orientation distributions that will modify the mechanical response during in-service deformation in specific directions.

6.1.3   Soluble fraction during swelling

When the initial weight, m_0 is compared with the dried weight, m_d, a loss of mass is found, as observed in Figure 115 with the relation below one when the sample is dried. This could be related with oils and other soluble additives included in the elastomer formulation that are dissolved in the solvent. Likewise, it could include unbounded rubber from shorter weight lengths and non-cross-linked chains. In this case, the final weight m_d represents the polymer network and other additives that have a physical interaction in the network, such as fillers. Therefore, it is more accurate to use m_d as the initial non-swelling stage to obtain a more precise approximation of the polymer network weight.

The averages of the soluble fraction, φ_s, after drying on each material are shown in Table 29. This value represents the mass lost during the swelling process, due to the solubility with the solvent. A total of 24 specimens were tested, reporting two standard variations from the mean. EPDM1b and EPDM2 contain the highest oil content, as determined in Section 3.4.4, so it was expected to observe a higher soluble fraction, as it is related to solubilisation of the oils in the solvent. However, the content of the soluble fraction after contact with the solvent is remarkable higher than the oil/plasticiser content estimated by thermogravimetry in all the materials with exception of NBR

(Table 10). This may indicate that the soluble fraction in this work is not only the oils, but also additives and unbounded carbon-black filler and unbounded polymer. No variation in φ_s was observed between the deformed and undeformed specimens.

Table 29. Average of the soluble fraction, φ_s, after swelling state for filled elastomers.

	Elastomers				
	EPDM1b	*EPDM2*	*NBR*	*CR*	*NR*
φ_s	0.242 ± 0.004	0.149 ± 0.005	0.051 ± 0.005	0.106 ± 0.002	0.074 ± 0.004

6.2 Swelling for pre-deformed filled elastomers

6.2.1 Tensile deformation methodology

6.2.1.1 Uniaxial deformation

Rubber specimens were subjected to uniaxial tensile deformation, ε_u, using an Instron 5969 tensile testing machine equipped with a 100 N load cell and an Instron counterbalanced travelling extensometer, as explained in Section 3.6.1. Dumb-bell specimens were cut from moulded or rolled sheets (with the specimen axes aligned with the rolling direction, //) using a hand-operated Wallace specimen cutting press fitted with cutter type 1BA according to BS ISO 527-2 [150]. The protocol described in Section 3.6.1.1 was used for all the specimens. Specimens were subjected to four load-unload cycles to uniaxial strain levels as presented in Table 30, at a nominal strain rate of 0.03 s^{-1} and at room temperature (20 $\pm$ 2°C). During unloading, the direction was reversed at 0.1 N to avoid buckling of the specimen. Four specimens were tested for each.

Table 30. Strain levels ε_u subjected to uniaxial tensile testing prior to swelling experiments for elastomers studied.

	Elastomers				
	EPDM1b	*EPDM2*	*NBR*	*CR*	*NR*
	1.0	1.0	0.5	0.5	0.5
	2.0	2.0	1.0	1.0	1.0
ε_u	3.0	3.0	1.25	2.0	2.0
	4.0	4.0	1.5	2.5	3.0
	4.5	5.0	1.75	2.75	3.5

6.2.1.2 Equibiaxial deformation

A second series of square specimens of approximately dimensions of 85mm x 85mm x

0.5 mm were deformed equibiaxially in tension using a Flexible Biaxial Film Tester [152], as described in Section 3.6.2.1. For rolled sheet specimens, axis 1 was aligned to the rolling direction //. Specimens were subjected to four load-unload cycles to equibiaxial strain levels, ε_{EB}, as reported in Table 31.

All test were performed at a nominal strain rate of 0.03 s^{-1} and at room temperature (20 ± 2°C). During unloading, the direction was reversed when either of the axes reached 0.1 N to avoid buckling of the specimen. A single sheet was tested for each condition, from which four specimens were cut from for subsequent swelling experiments.

Table 31. Strain levels of ε_{EB} subjected to equibiaxial tensile testing prior to swelling experiments for filled elastomers studied.

	Elastomers				
	EPDM1b	*EPDM2*	*NBR*	*CR*	*NR*
	0.5	0.5	0.5	0.5	0.5
ε_{EB}	1.0	1.0	0.75	0.75	1.0
	1.25	1.2	0.85	1.0	1.5
	1.5	2.0	1.0	1.2	1.75

In this experimental set-up, the use of the video extensometer was not possible as this requires positioning of beads to track the displacement with wet silicon. To avoid any possible contamination that could interfere in the swelling experiments, the strain measurement was determined from the grip displacement.

6.2.2   Swelling experimental methodology

A rectangular specimen 20mm x 5mm x 0.5mm (~0.15g) was cut from the central portion of each dumb-bell specimens following uniaxial deformation. For equibiaxial conditions, four square specimens 20 mm in length (~0.25g) and ~0.5mm thickness were cut from the central regions. Four swelling specimens were obtained for each deformation condition. Figure 120 illustrate the position of the specimens cut from the tensile testing specimens. The time between the deformation tests and immersion in the solvent was less than 4 hours, to standardise any recovery before immersion. The specimens were immersed individually in sealed glass vials with approximately 50ml of the solvent selected in Table 28. Following the same protocol as described in Section 6.1.1 for the un-deformed specimens, the mass before swelling, m_0, in the swollen state, m_s, and after drying, m_d was measured for each deformation condition, using the same swelling time T_s, and drying, T_d, as for un-deformed specimens (Section 6.1.1.1).

(a)   (b)
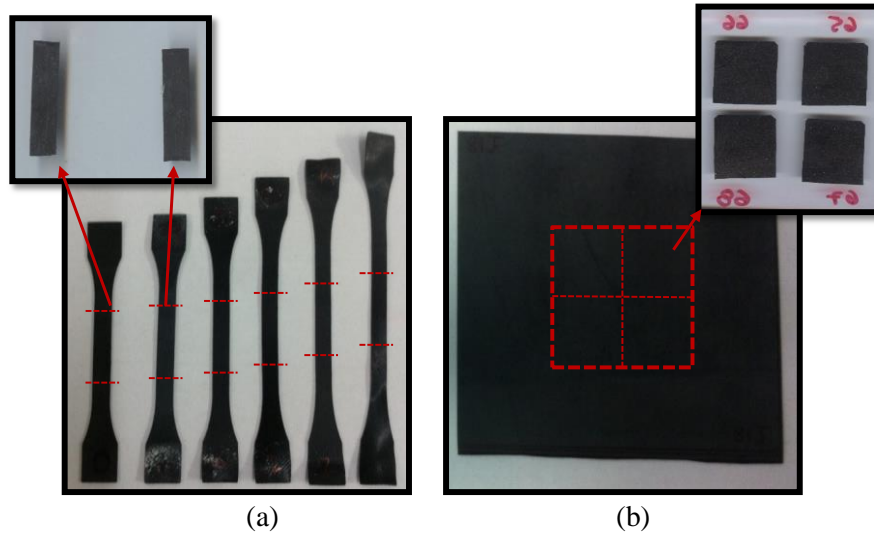
Figure 120. (a) Uniaxial and (b) equibiaxial swelling specimens cut from tensile testing specimens.

6.2.2.1 Linear dimension measurements

The linear dimensions, λ, of each specimen were measured before the swelling (after the pre-strain), in the swollen state at T_s, and after drying at T_d, as described for un-deformed specimens in Section 6.1.1.2. The different stages of deformation and the resulting dimensions measured in the swelling experiments for both uniaxial and equibiaxial deformations are schematically represented in Figure 121. For analysis of the results, the averages and standard deviations are based on a sample size of four specimens for each mode of deformation and strain ε_u and ε_{EB}.

Figure 121. Uniaxial (a) and equibiaxial (b) deformation tests and subsequent linear swelling measurements.

6.2.3   Swelling ratio followed pre-strain

The variation in the mass during the swelling state compared with the weight after dry is represented by the swelling ratio, ϕ_s, at T_s defined as the mass ratio m_s/m_d. The swelling ratio indicates the increase of the mass due to the inclusion of solvent into the polymeric network. The values of ϕ_s, for the five elastomers subjected to differe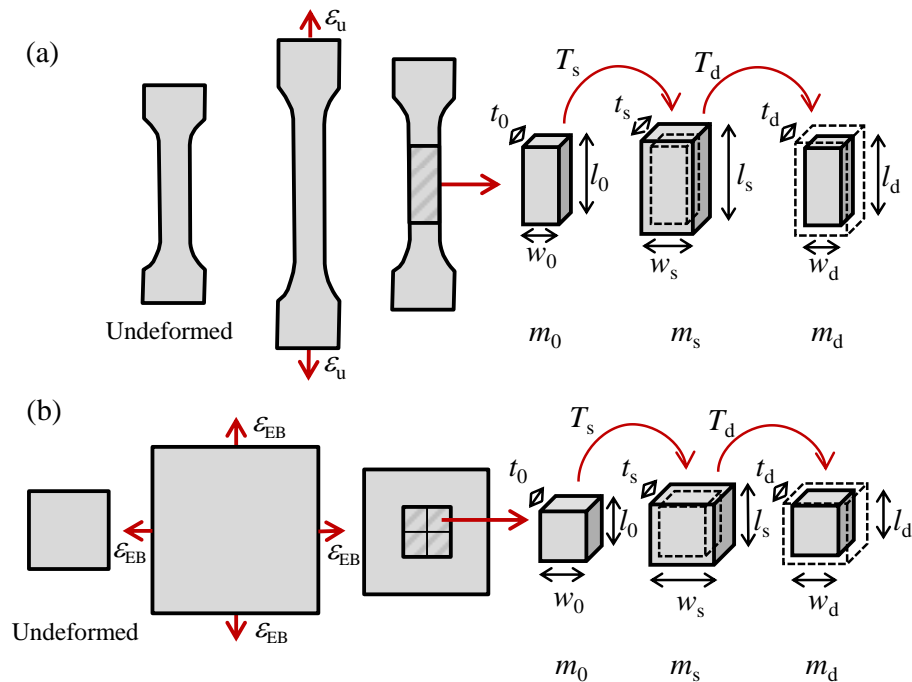nt values of pre-strain ε_u for uniaxial deformation and ε_m for equibiaxial deformation is reported in Figure 122. An increase in swelling ratio is observed with increasing deformation in all the elastomers for both ε_u and ε_m. This indicates an alteration in the network structure after deformation that allows a higher content of solvent to interact with the polymer network, thereby increasing the degree of swelling.
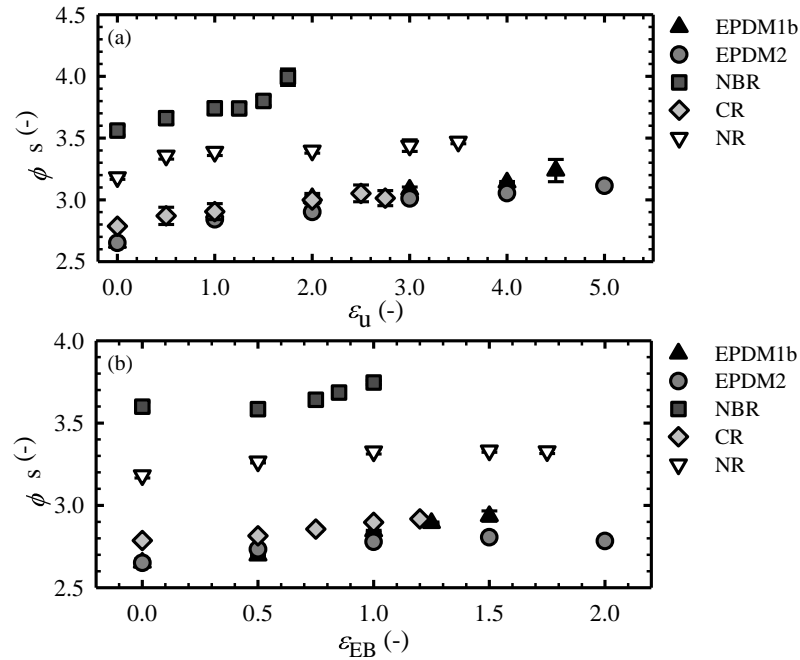
Figure 122. Swelling ratio ϕ_s for rubbers following (a) uniaxial ε_u and (b) equibiaxial ε_m deformations.

6.2.3.1   Swelling phenomenon and Flory's theory

Using Flory's approach [39, 42] detailed in Section 2.3.2, it is possible to relate swelling of the polymer network with the average molecular weight between cross-link units, M_c, of an elastomer as

$$M_c = -\frac{\rho_2 V_1(v_2^{1/3} - v_2/2)}{\ln(1-v_2)+v_2+\chi v_2^{2}} \qquad \text{Eq. 6-3}$$

with v_2 as the volume fraction of elastomer, ρ_2 the elastomer density, χ, the solubility parameter, and V_1 the molar volume of the solvent. The values of ρ_2, χ and V_1 are

constant parameters of the polymer-solvent interaction system, as given in Table 28. The volume fraction of the elastomer v_2 is defined as

$$v_2 = 1 - \frac{((m_s - m_d)/\rho_1)}{((m_s - m_d)/\rho_1) + m_d/\rho_2}$$

Eq. 6-4

Using m_d instead of m_0, the soluble fraction during swelling (Section 6.1.3) is excluded, and is not considered as part of the elastomeric network. In the case of the fillers, as they create physical interactions with the elastomer chains, they will remain in the network structure during swelling, and are accounted for as part of the network structure. The density ρ_2 refers to the density of the total composition, including the contribution of the filler.

Using Eq. 6-3, the variation in M_c can be determined as a function of the preconditioning ε_u and ε_{EB}, as is presented in Figure 123. There is a clear increase in M_c with increasing pre-deformation, for both uniaxial and equibiaxial samples. EPDM1b and EPDM2 exhibit the largest change, whereas NBR shows the smallest change when compared with the un-deformed condition. This is consistent with an overall increase in the swelling ratio with the increase in the pre-strain magnitude.

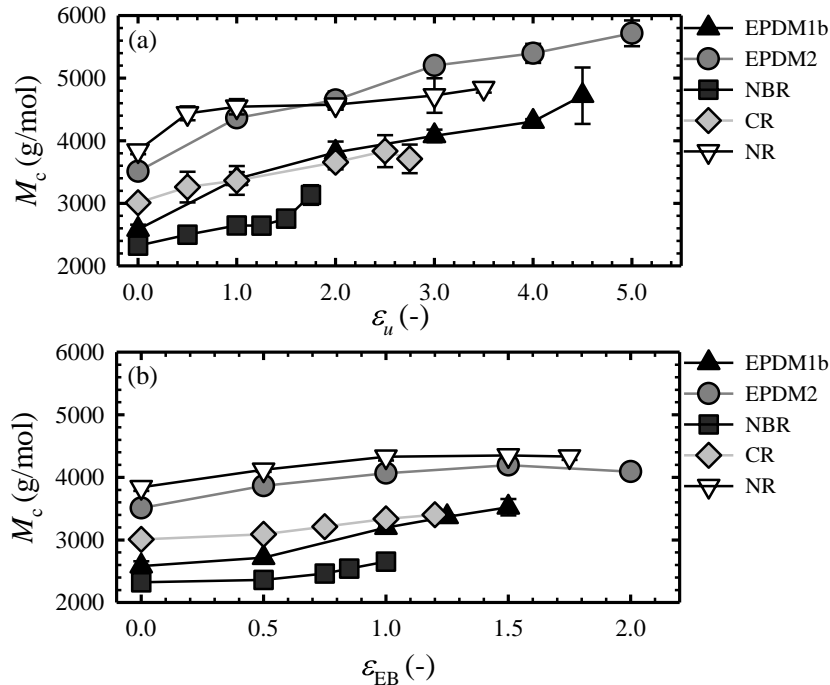Figure 123. Average molecular weight between cross-link points M_c calculated from Eq. 6-3 as a function of (a) UN and (b) EB pre-deformations.

Of the elastomers analysed, NBR contains the shortest average of chain-length between cross-links when compared with the rest of the elastomers at the un-deformed condition. This could be associated with a more vulcanised system or more compacted network

structure. A shorter average of the molecular weight is associated with a higher Young's modulus, as the elastomeric network has more cross-link points. Section 3.2.3 showed that NBR had the highest $E_{100\%}$ for NBR (6.69 ±0.03MPa). This correlates well with the results presented in this chapter. NR presented the highest values of M_c. This was also the material with the lowest values of $E_{100\%}$ (1.91 ±0.13MPa).

The variation in M_c with deformation is associated with a greater separation of the cross-link points. This behaviour can be observed for both uniaxial and equibiaxial modes of deformation. The values of M_c must be thought of as apparent values as the inclusion of the filler in the rubber network can modify the swelling capacity. Entanglements and aggregates can also be modified during the deformation, thereby allowing a higher interaction of the solvent with the network. This damage is likely to be a combination of rupture of molecular bonds in the elastomer chain and the rupture of the rubber-filler interface. The crosslink density can then be determined from the values of M_c. An increase in M_c indicates a reduction in the number of cross-link points, which means a reduction in the cross-link density (values presented in Appendix G). M_c is normalised with respect to the molecular weight between cross-links of the undeformed materials, M_{c0}, and is shown in Figure 124. EPDM1b and EPDM2 present a higher relative increase in the molecular weight when compared with NBR, CR and NR.

The data shows that following a pre-deformation, a modification in the structure of the filled elastomer allows a higher content of solvent to interact within the network. Some theories indicate that the mechanism of deformation is not associated with breakings in the chains of filler-rubber interactions [14, 108, 110]. If there is no modification of the network, it is expected then that M_c would be independent of the deformation. Nevertheless, the solvent-elastomer interaction is clearly modified after a deformation as the swelling increases with deformation. This variation could be associated with a damage in the structure, more than just a restructuring of the network.
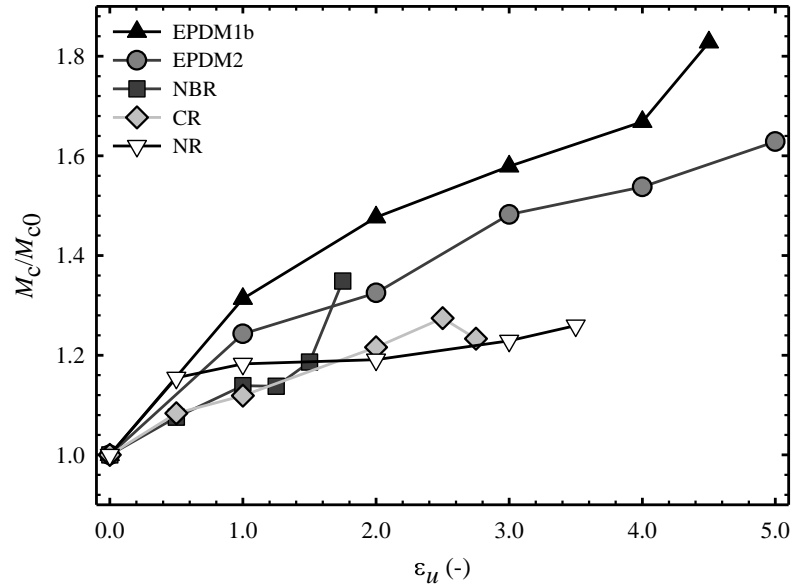
Figure 124. Normalisation of M_c with respect of the molecular weight of the undeformed material M_{c0}.

6.2.4 Deformation induced swelling anisotropy

The directional swelling ratios λ are measured for each elastomer subjected to uniaxial ε_u and equibiaxial ε_{EB} deformations. Figure 125 to Figure 129 show the directional swelling ratio as a function of pre-strain in ε_u and ε_{EB}. Following uniaxial deformation, a clear increase in the directional swelling ratio λ_l in the direction of deformation is observed for all rubbers.

EPDM2 exhibits the largest change, with an increase of λ_l of approximately 20% following uniaxial straining to ε_u of 4.5. The NBR specimens exhibit the smallest change (8%) following ε_u of 1.75. As materials have different failure strains, it is not possible to explore the same strain range with the various specimens. Changes in the directional swelling ratios in the other two dimensions are smaller in magnitude, with the different rubbers showing both increases and decreases in the swelling ratios. In the case of equibiaxial deformation, EB, there is a progressive increase in the ratios λ_l and λ_w, and a small reduction in λ_t. The equibiaxial strains tested are smaller than the uniaxial strains since the equibiaxial failure strains are smaller than the uniaxial failure strains.

Figure 125. Dimensional ratio λ variation for EPDM1b following (a) UN ε_u and (b) EB ε_{EB} pre-deformations.

Figure 126. Dimensional ratio λ variation for EPDM2 following (a) UN ε_u and (b) EB ε_{EB} pre-deformations

Figure 127. Dimensional ratio λ variation for NBR following (a) UN ε_u and (b) EB ε_{EB} predeformations.
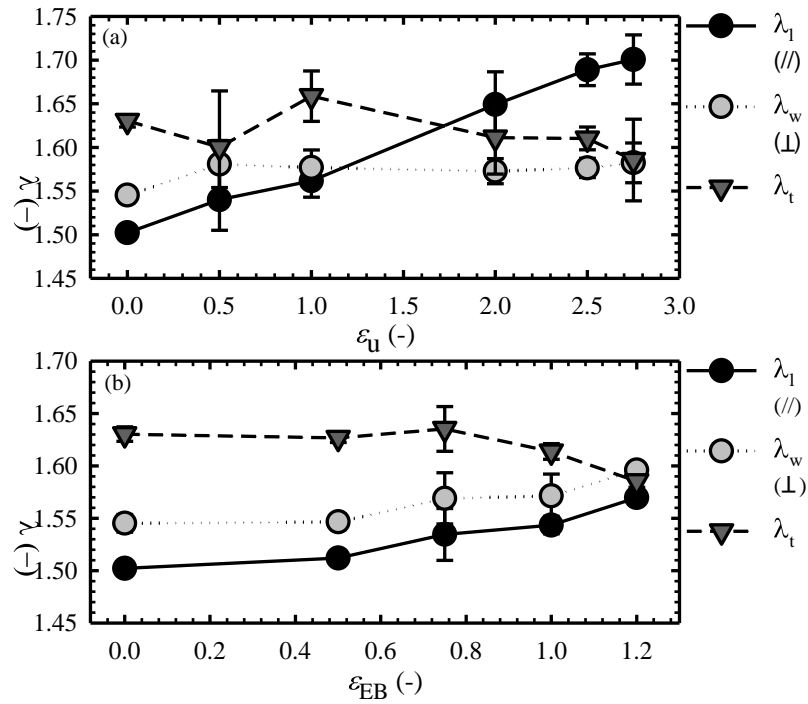
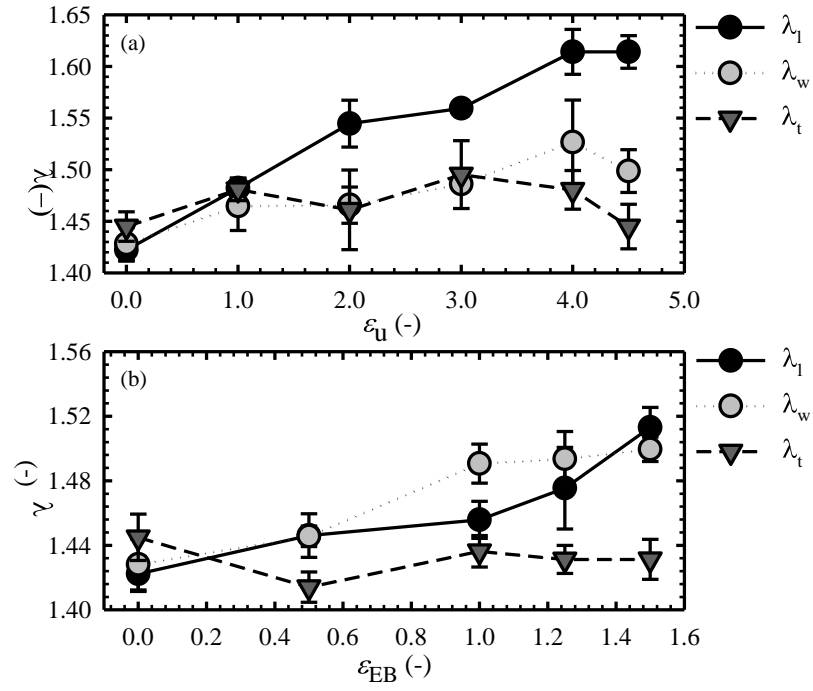Figure 128. Dimensional ratio λ variation for CR following (a) UN ε_u and (b) EB ε_{EB} deformations.
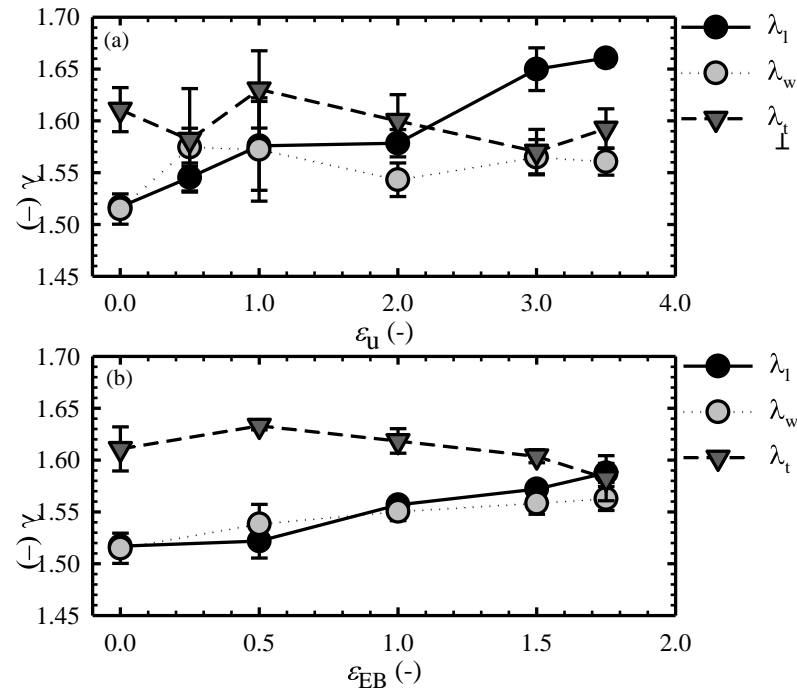
Figure 129. Dimensional ratio λ variation for NR following (a) UN ε_u and (b) EB ε_{EB} pre-deformations.
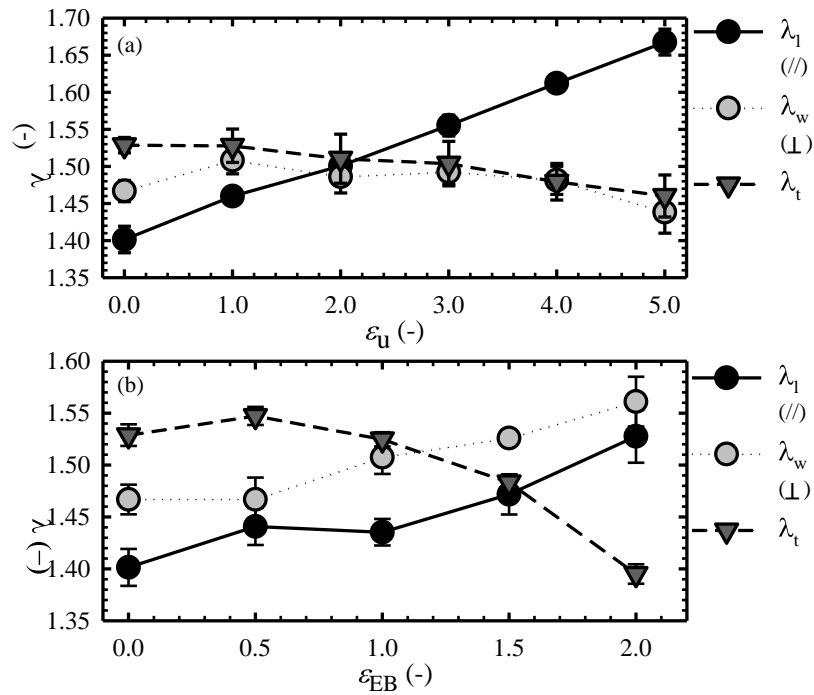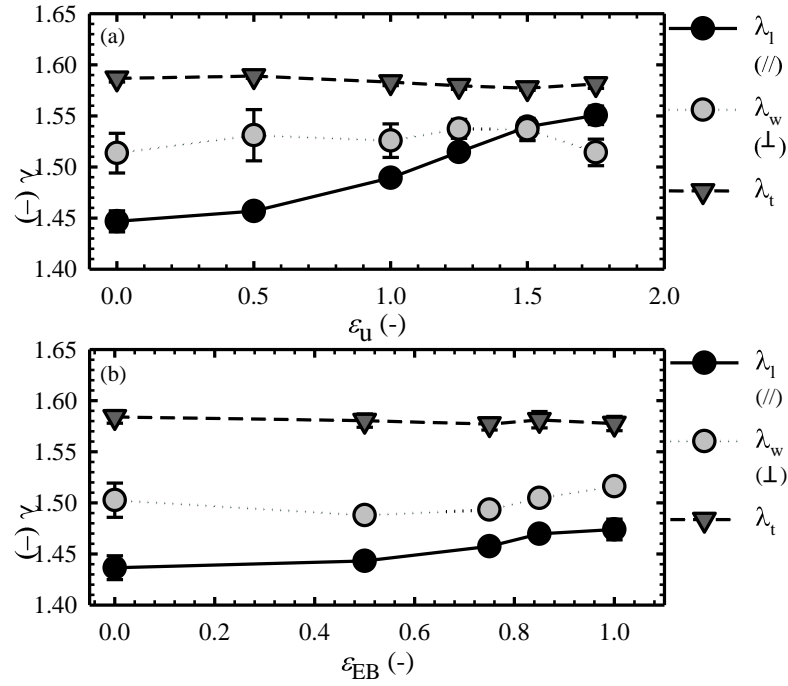
As a general trend, swelling is *increased* in the direction(s) of deformation, and either remains constant or is *reduced* in the other direction(s). This means that, to a first approximation, chains are able to lengthen more easily in a direction which has previously been stretched. This is somewhat contradictory to the undeformed swelling evidence, where swelling was smaller in the directions of deformation experienced by the manufacturing process. The key difference is that during manufacturing the cross-linking takes place in the deformed state, when chains are mobile. During deformation, the cross-linked network is stretched and possibly damaged as a consequence of the restriction of the cross-linked network.

The swollen state represents a new minimum energy state of deformation in the presence of the solvent. Therefore the swelling in each direction depends not only on the ability of chains to elongate in that particular direction, but also on the effect that the elongation has on the volume, and in turn its effect on the other directions. This is the most probable reason for the *reduction* in swelling in the directions perpendicular to the deformation. Further complexity comes from the presence of the filler, and of an interface between rubber and filler. In fact, it is generally agreed that the major contributor to the mechanical softening effect is evolution of the filler reinforcement [14].

As the swelling ratio is related to the unloaded, dried configuration, it is also connected

to the permanent change in dimensions experienced by the materials in an unswollen, dried state. All of the rubbers examined in exhibited varying degrees of permanent set, ε_{per}, as was presented in Section 4.4.2.4 . This set was the consequence of changes to the rubber network, to the filler structure, and to the interface between them. The degree of permanent set in the testing direction following uniaxial deformations (but before swelling) was shown in Figure 57 in Chapter 4. At any given strain it is greater for the EPDMs than for the other rubbers.

6.3   Discussion

Anisotropy due to deformation was reported by Mullins [67], who showed anisotropy in softening after tensile deformation of filled elastomers. When the thermodynamics of swelling was introduced by Flory, he showed that relative changes in longitudinal and transverse dimensions arose due to the difference in hydrostatic pressure, called the anisotropy of compressibility. However, the theory established an isotropic stage of swelling, and even though some extensions have been presented to account for the anisotropy [93, 216], Flory's initial equation is still a widely used technique to account the interaction of a specific elastomeric network with a solvent. The modification of the theory of swelling presented by Bruck [216] introduces the anisotropy effect on the swelling equilibrium volume ratio by identifying an independent linear deformation factor in the *x* and *y* directions. The elastic energy originally presented by Flory assumes isotropic swelling in the derivation of the free elastic energy. In the extension presented by Bruck, each direction has a linear deformation factor that is included in the swelling equation using the linear dimension measurements.

The thermodynamic interaction of an elastomer in contact with a solvent is able to give information about the structuring of the cross-linked network. [38, 46, 53]. The measure of the elastomer swelling during solvent interaction is a practical and reliable method of assessing anisotropy of the 3D network (not being restricted by the analysis on orthogonal axes on one plane), introducing the possibility of monitoring the influence of modes of deformation in the anisotropy distribution, with the rubber network as a coupled volume system. The technique can be used as a quantitative analysis of the orientation effects during processing and in-service deformation.

Flory's theory, as well as many approaches reported to account anisotropy, assumes a

uniform and isotropic network of cross-links in the rubber. However, when rubber is cross-linked in an industrial context, the flow processes that shape the component usually take place simultaneously with the cross-linking reactions and the polymer chains have insufficient time to relax. This takes place to a lesser extent in compression-moulded rubber [47], and more so in rolled rubbers and injection-moulded rubbers [211, 217-221]. When rubber is deformed, either during the scragging procedures or in service, further deviations from isotropy in the cross-linked network develop, and are readily observed in the mechanical response [14, 90, 115]. Thus, any attempt to understand the structure of vulcanised rubber products ought to reflect *both* the process-induced and the deformation-induced anisotropies of the cross-linked network.

This work investigated two commonly used techniques in the rubber industry, as the compression moulding and the sheet rolling, quantifying the anisotropy, arising due to the flow of the rubber during each specific process. Previous experimental data was presented by Blow and Demirli [92] also showed a degree of anisotropy in moulded components, and noticed a marked reduction in swelling in the direction of flow similarly to the rolled materials evaluated in this work. An increase in the cross-linking kinetics reduces the possibility of the network relaxing after flow, increasing the anisotropy in processes with substantial flow such as injection moulding. Azaar et al. [222] also showed a higher swelling ratio in the thickness direction of a compression-moulded EPDM disc specimen. Their results are in agreement with the data presented here, indicating that an elastomeric product is almost invariably anisotropic as a result of manufacture. The filler interaction during the processing of the final product is another aspect to consider in the anisotropy. The cross-link kinetics and the possible orientation of the fillers during mixing and processing of the final product can also impart anisotropy to the compound. During flow, orientation of non-spherical fillers or of sets of aggregates can also increase the anisotropy effect in the direction of the flow [92].

In addition, an elastomer certainly becomes anisotropic as a consequence of service deformations. The deformation induced anisotropy has been considered already in previous research, using the mechanical response to quantify the Mullins effect in relation with the direction of deformation [88, 115]. From these investigations, only a limited subset has started to explore the modifications needed to capture the deformation-induced anisotropy [17, 95, 112, 118, 223]. Theories such as that by

Tobolsky [77], provide a possible physical picture of the restructuring of the network through scission and new cross-links. This is one approach to dealing with the anisotropy of the network that may lead to a physical model for anisotropy. However there are, to the author's knowledge, no models including process-induced anisotropy, and all approaches generally assume an initially isotropic material.

6.4 Summary

This chapter has presented results from swelling experiments involving measurements of weight and linear dimensions in five filled elastomers subjected to different modes of deformation. Section 6.1.1 introduced the measurement methods and set-up for swelling experiments on un-deformed specimens. This detailed methodology demonstrates the possibility to monitor not only the mass, but also the dimensional ratio during the interaction of an elastomer with a solvent. Evaluating the variation of the dimensions during swelling in Section 6.1.1.2, it was found that compression-moulded rubbers are transversely isotropic after moulding; whereas, rolled rubbers exhibit anisotropy in all three directions. In all cases, swelling was largest in the thickness direction, and in rolled rubbers it was smallest in the rolling direction. This indicates that assuming a virgin isotropic condition is not the most accurate way to predict the mechanical response, as this initial condition will determine the mechanical behaviour on subsequent deformations.

Section 6.2 shows a detailed analysis of the modification of the swelling following a pre-deformation of the filled elastomer. The use of Flory's approach was used to obtain an average of the molecular weight between crosslink points, M_c. Both uniaxial and equibiaxial deformations demonstrated a clear increase in M_c with the increase in tensile deformation with respect of the average value calculated for the un-deformed materials. The analysis of the measurements of linear swelling ratios presented following different degrees of uniaxial and equibiaxial deformations was presented in Section 6.2.4, confirming that deformation also contributes to the anisotropy. Swelling increases with the direction of deformation for both uniaxial and biaxial deformations. This is consistent with a picture of deformation-induced damage to the polymer network. This is a new approach in the analysis of the manifestation of the Mullins effect using swelling, in order to identify damage in the structure influenced by a previous

deformation. The measurement of the dimensional ratio during swelling is strong evidence of the anisotropy present in the network structure. The results demonstrate a good use of this technique to analyse changes of the molecular structure as a consequence of deformation. Section 6.3 summaries the implications of the swelling technique and the results presented to analyse the process induced and deformation induced anisotropy.

Chapter 7   **Conclusions**

This thesis has sought to provide new experimental evidence concerning the Mullins effect in filled elastomers, from the point of view of energy dissipation, viscoelasticity and swelling. The influence of deformation history on the modification of the constitutive response has been the focus of the work. Five commercial cross-linked filled elastomers were analysed in order to obtain a broad perspective of the range of mechanical responses that can be expected in commercial rubbers.

This chapter summarises the most significant findings of this thesis. The wider implications of the outcomes are discussed in Section 7.1, followed by the major conclusions of the chapters presented in the main body of this thesis in Section 7.2. Finally, recommendations for future work are presented in Section 7.3.

7.1   Summary of results

The elastomers investigated in this thesis are in common use across a number of industries, including automotive, aerospace and construction. The differences in their chemical structure, composition and vulcanisation process allowed some correlation between the material type and the different mechanisms of deformation. These elastomers exhibit a wide variations in their mechanical properties, representing a general picture of the in-service behaviour of filled elastomers in industry. The use of a range of polymers is in contrast to most research previously reported in literature, where the use of one or two elastomers is more typical for laboratory analysis purposes only.

As it is for the typical commercial elastomers, the composition was not provided. Thus, a series of experiments aimed to characterise was presented in Chapter 1, highlighting the main differences between them. The main focus was the chemical structure, filler

content and vulcanisation process. Techniques such as DSC and TGA (Section 3.4.3 and Section 3.4.4) were able to give some information about the composition. The lowest T_g's were reported for EPDM1a-b (-51.95±1.77 °C), EPDM2 (-52.08±1.55 °C) and NR (-57.03±0.76°C). A lower T_g is related to a higher elasticity under mechanical deformation, due to chains configurational rearrangements of the chains. Through the Shore A° hardness measurement (Section 3.4.2) it was found that the lowest H reported was for the EPDM's (54-55 Shore A°) and NR (55 Shore A°). The thermal analysis using TGA provided information about the content on each elastomer, especially the carbon black filler content, an important element in the mechanical response and softening effect. The highest content of carbon black was reported for EPDM2 with 34.53±0.33% and the lowest content for NR with 21.88±0.24%. Further analysis of the fracture surface by SEM and the energy dispersive spectrometry provided qualitative details of the filler morphology and other additives on each compound.

The observations reported during the thermal and physical characterisation were compared with the mechanical properties studied during uniaxial and biaxial deformations (Section 3.6). EPDM1, EPDM2 and NR can be subjected to uniaxial deformations above 500% before failure, more than twice than those of NBR (194.60 ±8.05%) and CR (317.95 ±12.81%). This is consistent with the results of T_g and hardness presented for these materials.

Chapter 4 analysed the deformation history in relation with the Mullins effect and the energies stored and dissipated during deformation (Chapter 4). An extensive set of testing protocols was derived to enable further understanding of the mechanical behaviour, and to evaluate the relationship between energy and deformation history. The history of the material was found to be an important factor to consider on both the constitutive response and the energies stored and dissipated during deformation. The constitutive response followed uniaxial tensile deformation was first analysed as a function of the strain history (Section 4.4.2). As expected, the stress response is modified by the previous maximum deformation in every elastomer. On the other side, when a specimen is subjected to tensile deformation under constant width condition on one axis, the variation in the stress response, when deforming along the perpendicular axis, is not significantly different than during a simple uniaxial deformation. However, if the material is subjected to equibiaxial deformation, the deformation is restricted due to the simultaneous constraints, increasing also the stress required to deform (Section

4.4.3). The maximum deformation is reduced to almost half between uniaxial and equibiaxial tensile deformation.

From the constitutive response, the energies stored and dissipated during deformation were evaluated as a function of deformation history (Section 4.5). The energy map created for each material, indicates a linear relationship between the energy stored during the stretching process and the energy dissipated. This proportionality is independent of strain levels, but different for first stretching and for repeated stretching within a given envelope. When the applied stretch starts to approach the previous maximum, a transition from these two limits is perceived. The change in mode of deformation was found to generate the same energy distribution, reporting the same energy map evolution, independently of whether the elastomer was deformed uniaxially, equibiaxially or at a constant width (Section 4.5.3). To the author's knowledge, this is the first time this has been observed in this range of materials. This new approach for the energy evaluation represents a good technique to study strain energy as a function of history.

A modelling approach was introduced in Section 4.6, to capture the transition of the energy fraction ϕ_c, incorporating the physical description based on a hard (filler) and soft (rubber) phase conversion, initially used by Mullins [15]. The filled elastomer is represented as a coupling of phases, with an initial fraction of hard phase $\theta_h = \xi . \eta$, responsible for the softening effect. The modification of the hard phase is represented by reduction of ξ; representing the pull-out under deformation, to be included into the soft phase. This approach gives a good qualitative representation of both, the constitutive response and energy dissipation as a function of the deformation history.

The viscoelastic behaviour of filled elastomers was investigated in Chapter 5 through stress relaxation experiments with a focus on the influence of previous deformation history on the time-dependent response. These results were achieved through a combination of new experimental test protocols for stress-relaxation and stress-memory. Specimens were subjected to a variety of carefully constructed deformation histories (Section 5.1.3) in order to shed light on the underlying mechanisms of time-dependent stress evolution.

When stress relaxation followed a simple uniaxial loading ramp, TP1 (no strain history), the fraction of stress relaxing after a fixed time was found to be highly strain-dependent

(Section 5.2), increasing with the strain amplitude. When the stress relaxation stage is carried out following a prior strain cycle (TP2), the response depends on both the current, ε_{end}, and previous strain, ε_{max}. When $\varepsilon_{end} < \varepsilon_{max}$, an approximately constant fraction of the stress relaxes. However, when ε_{end} approaches the previous ε_{max} an increase in relaxation is observed, as with a simple loading ramp. The deformation history modifies the structure of the network, reducing the relaxing capacity in subsequent deformations below the historical maximum. This demonstrates the impact of techniques such as the scragging not only in the stress-strain response, but also in the relaxing process of the material. If the material is subjected to a complete loading-unloading cycle (TP3 in Section 5.4), stress memory is observed. This recovery is almost independent of strain history. When the elastomer is subjected to a loading following a partial unloading (TP4 in Section 5.5), a transition between stress relaxation and stress memory occurs, depending on the strain level.

The same testing protocols were also examined under equibiaxial and constant width deformation in Section 5.6. A modification in the stress response of the material, especially during the simple loading ramp (TP1) was observed. The relaxation was found independent of the variation of ε_{end}, in contrast with the dependence observed in uniaxial testing. The rest of the protocols showed a similar stress response with an increase in the stress relaxation fraction when the material is subjected to equibiaxial deformation.

Maps of the unrelaxed stress fraction as a function of the applied strain for different histories were generated for each material using the experimental data from TP1 and TP2 (Section 5.2.3). They show a transition of the fraction of unrelaxed stress, dependent of both the strain applied and the strain history. These maps could prove useful to the community interested in predicting the relaxation of filled rubber products following complex strain histories. An empirical function was suggested to describe the fraction of stress relaxing with only five parameters (Section 5.2.4). The function provides values in a good agreement with the experimental findings.

Swelling of filled elastomers during solvent interaction was employed to investigate both the process-induced and deformation-induced anisotropy in Chapter 6. It was shown that the two manufacturing methods studied, i.e. compression moulding and sheet rolling, imparted a different initial anisotropy in the materials (Section 6.1). The compression moulded rubbers, EPDM1 and NR, were shown to be transversely

isotropic in the plane of the sheet after moulding. The sheet-rolled elastomers, EPDM2, NBR and CR, were found to be fully anisotropic.

The swelling technique also showed the anisotropy induced by deformation history (Section 6.2). Measurements of linear swelling ratios in rubbers following different degrees of uniaxial and equibiaxial deformations confirm that deformation also contributes to evolving anisotropy. The increase of swelling ratio with deformation is consistent with a picture of deformation-induced damage to the network. The novelty of this study in analysing linear swelling ratios provided new experimental evidence for anisotropy of rubber, both after manufacture and after deformation.

7.2   Conclusions

The work undertaken set out to investigate different manifestations of the Mullins effect. An extensive set of tests focused on the strain history and mode of deformation was developed to provide insight into the mechanism of deformation related to energy dissipation, time-dependence and network anisotropy. An understanding of how these features affected the mechanical response and the softening mechanism was presented, allowing a better understanding, and contributing to improve the prediction of the constitutive response following given strain histories on filled elastomers. The main novel findings of the research are detailed below.

7.2.1   Energy storage and dissipation

∗   The determination of the energy stored and dissipated during cyclic loading confirmed the link to deformation history. Simulating the process of scragging, it was found that, as long as the strain history is higher than the current strain, the dissipated fraction of energy in cyclic loadings remains relatively constant, independent of the strain. However, exceeding the previous maximum strain levels leads to a variation in the energy dissipation, dependent of both current and history strain, as represented in the energy maps generated for each material. The fraction of energy dissipated was shown to be intrinsic for each of the filled elastomers composition studied.

∗   A physical model describing the network structure as a combination of hard and

soft phases was qualitatively able to reproduce the energy trends found experimentally. The Edwards-Vilgis version of the model is capable of describing the evolution of the hard phase as a function of the strain applied, simulating the softening process with deformation.

7.2.2   Viscoelasticity

*   A new set of test protocols were developed for the analysis of the stress relaxation and stress memory following different deformation histories. Evidence of the influence of deformation history was found in the stress relaxation response. When stress relaxation follows a uniaxial loading ramp in virgin rubber, the fraction of stress relaxing is highly strain-dependent. Instead, when stress relaxation is carried out following a prior load-unload cycle (to a strain smaller than the previous maximum), a constant fraction of the stress relaxes, independent of both the applied strain and the previous maximum strain.

*   Maps of unrelaxed fraction as a function of applied strain at a given time for different histories were generated for each filled elastomer. They can be interpreted as the time-dependent equivalent of pseudocyclic load-unload curves commonly used to summarise the Mullins effect. These maps, together with an empirical equation suggested to describe them, should prove useful for the prediction of stress relaxation in filled elastomer products following complex strain histories.

*   Following load-unload cycles, stress memory instead of relaxation was observed. The memory was found to be approximately independent of strain history. If the deformation is interrupted after a partial unloading, either stress relaxation or stress memory can be observed, depending on the maximum strain and the final strain. The predominant effect will be attributed to the condition of the strain history.

7.2.3   Swelling

*   Linear swelling measurements were used to determine anisotropy in virgin and pre-deformed rubbers. The approach employed for this technique allowed examination of the influence of manufacturing process and of deformation hisotory through the measurement of the linear dimensions in the swollen state.

*   Widely used manufacturing process techniques such as compression moulding and

sheet rolling impart an initial anisotropy in the network structure. Compression moulding processes show transverse isotropy in the plane of moulding. Sheet rolling technique result in full anisotropy in the three principal axes.

∗   When elastomers are subjected to tensile deformation, the variation in the linear swelling along the axis of deformation indicates a noticeable modification of the network. The change in linear swelling along the three directions is evidence for coupling of the network.

7.3   Recommendations for future work

This work has presented a simple modelling approach to predict the influence of previous deformation on the energy dissipation. Further developments of the model could bring about a more detailed and quantitative prediction of not only the energy dissipation, but also the constitutive response. Aspects such as permanent set, detailed finite extensibility criteria and stress flow variation were neglected in this first approach. Further adjustments to the model accounting these aspects could bring a more truthful prediction of the material behaviour.

The results presented using the swelling technique proved that anisotropy arises not just following deformation, but also during the manufacturing process. This is an important consideration when using experimental data to develop modelling approaches. This remains to be addressed through a 3D model capable of capturing the anisotropy. Research has started to include deformation induced anisotropy in the modelling of the constitutive response [90, 112, 224]. However, this is still at a very early stage and most authors consider a fully isotropic material as a starting point. This would be a worthy topic for further research.

References

[1]T. Vijayaram, 'A technical review on rubber', *International Journal on Design and Manufacturing Technologies,* vol. 3, p. 13, 2009.

[2]L. R. G. Treloar, 'General physical properties of rubber', in *The Physics of Rubber Elasticity*, 3rd Edition: OUP Oxford, 2005.

[3]N. McCrum, C. P. Buckley, and C. B. Bucknall, *Principles of Polymer Engineering*, 2nd Edition Britain: Oxford Science Publications, 1997.

[4]G. Holden, 'Elastomers, Thermoplastic', in *Encyclopedia of Polymer Science and Technology*. vol. 6, J. P. Queslel and J. E. Mark, 3rd Edition: John Wiley & Sons, pp. 63-88, 2004.

[5]R. J. Young, *Introduction to Polymers*, 2nd Edition. United States of America: CRC Press, 1991.

[6]J. P. Queslel and J. E. Mark, 'Elasticity, Rubber- like', in *Encyclopedia of Polymer Science and Technology*. vol. 2, J. P. Queslel and J. E. Mark, 3rd Edition: John Wiley & Sons, pp. 216-252, 2004.

[7]D. J. Khols and G. Beaucage, 'Rational design of reinforced rubber', *Current Opinion in Solid State and Materials Sciense,* vol. 6, pp. 183-194, 2002.

[8]L. B. Tunnicliffe, Particulate Reinforcement of Elastomers at Small Strains, Doctor of Philosophy, The School of Engineering and Materials Science, Queen Mary University of London, 2015.

[9]J. L. Leblanc, 'Rubber–filler interactions and rheological properties in filled compounds', *Progress in Polymer Science,* vol. 27, pp. 627-687, 2002.

[10]   J. Fröhlich, W. Niedermeier, and H.-D. Luginsland, 'The effect of filler–filler and filler–elastomer interaction on rubber reinforcement', *Composites Part A: Applied Science and Manufacturing,* vol. 36, pp. 449-460, 2005.

[11]   C. Blow and C. Hepburn, *Rubber technology and manufacture*, 2nd Edition. England: Plastics and Rubber Institute, 1982.

[12]   H. Bouasse and C. Z., 'Sur le courbes de traction du caoutchouc vulcanise', *Annales de la faculté des sciences de Toulouse 2e série,* vol. 5, p. 28, 1903.

[13]   L. Mullins and M. Tobin, 'Theoretical model for the elastic behavior of filler-reinforced vulcanized rubbers', *Proceedings of the Third Rubber Technology Conference.,* p. 15, 1956.

[14]   J. Diani, B. Fayolle, and P. Gilormini, 'A review on the Mullins effect', *European Polymer Journal,* vol. 45, pp. 601-612, 2009.

[15]   A. G. Mullins, 'Softening of rubber by deformation', *Rubber Chemistry and Technology,* vol. 42, pp. 339-362, 1969.

[16]   J. G. R. Kingston and A. H. Muhr, 'Effect of scragging on parameters in viscoplastic model for filled rubber', *Plastics, Rubber and Composites,* vol. 40, pp. 161-168, 2011.

[17]   R. W. Ogden and D. G. Roxburgh, 'A pseudo-elastic model for the Mullins effect in filled rubber', *Proceedings of the Royal Society of London Series a-Mathematical Physical and Engineering Sciences,* vol. 455, pp. 2861-2877, 1999.

[18]   D. Hanson, M. Hawley, R. Houlton, K. Chitanvis, P. Rae, E. B. Orler, and D. Wrobleski, 'Stress softening experiments in silica-filled polydimethylsiloxane provide insight into a mechanism for the Mullins effect', *Polymer,* vol. 46, pp. 10989-10995, 2005.

[19]   M. Kluppel and J. Schramm, 'A generalized tube model of rubber elasticity and stress softening of filler reinforced elastomer systems', *Macromolecular Theory and Simulations,* vol. 9, pp. 742-754, 2000.

[20]   N. Gent, *Engineering with Rubber. How to Design Rubber Components.*, 1st Edition. United States: Hanser Publishers, 1992.

[21]   B. P. Grady and S. L. Cooper, 'Thermoplastic Elastomers', in *Science and Technology of Rubber*, J. Mark, B. Erman, and F. Eirich, Second Edition United States: Academic Press, Inc., 1994.

[22]   C. Harper, *Handbook of Plastic, Elastomers and Composites.*, 4th Edition. McGraw Hill 2004.

[23]   J. G. Drobny, *Handbook of thermoplastic elastomers*. United States of America: William Andrew Publishing, 2007.

[24]   V. Jha, Carbon Black Filler. Reinforcement of Elastomers, Doctor of Philosophy, Department of Materials, Queen Mary, University of London, London, 2008.

[25]   S. Anil, 'A review on rubber compound mixing in Banbury mixer at tire industries', *International Journal of Engineering Research and Reviews,* vol. 2, pp. 106-109, 2014.

[26]   B. Rodgers, W. Waddel, and W. Klingensmith, 'Rubber Compounding ', in *Encyclopedia of Polymer Science and Technology.* vol. 11, J. P. Queslel and J. E. Mark, 3rd Edition: John Wiley & Sons, pp. 612-670, 2004.

[27]   A. I. Medalia and G. Kraus, 'Reinforcement of Elastomers by Particulate Fillers', in *Science and Technology of Rubber*, J. Mark, B. Erman, and F. Eirich, Second Edition United States: Academic Press, Inc., 1994.

[28]   Y. Fukahori, 'New progress in the theory and model of carbon black reinforcement of elastomers', *Journal of Applied Polymer Science,* vol. 95, pp. 60-67, 2005.

[29]   J. S. Bergstrom and M. C. Boyce, 'Large strain time-dependent behavior of filled elastomers', *Mechanics of Materials,* vol. 32, pp. 627-644, 2000.

[30]   N. Rattanasom, T. Saowapark, and C. Deeprasertkul, 'Reinforcement of natural rubber with silica/carbon black hybrid filler', *Polymer Testing,* vol. 26, pp. 369-377, 2007.

[31]   T. A. Vilgis, 'Time scales in the reinforcement of elastomers', *Polymer,* vol. 46, pp. 4223-4229, 2005.

[32]   A. V. Chapman and M. Porter, 'Sulphur vulcanisation chemistry', in *Natural Rubber Science and Technology*, A. D. Roberts, United States of America: Oxford Univeristy Press, 1988.

[33]   B. G. Crowther, P. M. Lewis, and C. Metherell, 'Compounding', in *Natural Rubber Science and Technology*, A. D. Roberts, United States of America: Oxford Univeristy Press, 1988.

[34]   C. S. L. Baker, 'Non-sulphur vulcanisation', in *Natural Rubber Science and Technology*, A. D. Roberts, United States of America: Oxford Univeristy Press, 1988.

[35]   A. Y. Coran, 'Vulcanization', in *Science and Technology of Rubber*, J. Mark, B. Erman, and F. Eirich, United States: Academic Press, Inc., 1994.

[36]   N. H. H. Shuhaimi, N. S. Ishak, N. Othman, H. Ismail, and S. Sasidharan, 'Effect of different types of vulcanization systems on the mechanical properties of natural rubber vulcanizates in the presence of oil palm leaves-based antioxidant', *Journal of Elastomers and Plastics,* vol. 46, pp. 747-764, 2013.

[37]   M. Van Duin, 'Chemistry of EPDM cross-linking', *KGK. Kautschuk, Gummi, Kunststoffe,* vol. 55, pp. 150-156, 2002.

[38]   L. R. G. Treloar, 'Swelling Phenomena', in *The Physics of Rubber Elasticity*: OUP Oxford, 2005.

[39]   P. J. Flory, 'Thermodynamics of high polymer solutions', *The Journal of Chemical Physics,* vol. 10, pp. 51-61, 1942.

[40]   G. Gee, 'The interaction between rubber and liquids. IX. The elastic behaviour of dry and swollen rubbers', *Transactions of the Faraday Society,* vol. 42, pp. 585-598, 1946.

[41]   J. F. Rabek, *Experimental methods in polymer chemistry: physical principles and applications*: Wiley, 1980.

[42]   P. J. Flory, *Principles of Polymer Chemistry*. USA: Ithaca: Cornell University Press, 1953.

[43]   P. J. Flory and J. Rehner, 'Statistical Mechanics of Cross-Linked Polymer Networks II. Swelling', *The Journal of Chemical Physics,* vol. 11, p. 521, 1943.

[44]   J. L. Valentín, J. Carretero-González, I. Mora-Barrantes, W. Chassé, and K. Saalwächter, 'Uncertainties in the Determination of Cross-Link Density by Equilibrium Swelling Experiments in Natural Rubber', *Macromolecules,* vol. 41, pp. 4717-4729, 2008.

[45]   G. Gee and L. R. G. Treloar, 'The interaction between rubber and liquids. 1. A thermodynamical study of the system rubber-benzene', *Transactions of the Faraday Society,* vol. 38, pp. 147-165, 1942.

[46]   G. Gee, 'Physics and chemistry of swelling and shrinking ', *Nature,* vol. 158, pp. 571-572, 1946.

[47]   L. R. G. Treloar, 'The swelling of cross-linked amorphous polymers under strain', *Transactions of the Faraday Society,* vol. 46, pp. 783-789, 1950.

[48]   L. R. G. Treloar, 'The Equilibrium Swelling of Cross-Linked Amorphous Polymers', vol. 200, pp. 176-183, 1950.

[49]   P. J. Flory and B. Erman, 'Theory of elasticity of polymer networks. 3', *Macromolecules,* vol. 15, pp. 800-806, 1982.

[50]   P. J. Flory, 'Theory of elasticity of polymer networks. The effect of local constraints on junctions', *The Journal of Chemical Physics,* vol. 66, pp. 5720-5729, 1977.

References

[51]   K. Saalwächter, W. Chassé, and J.-U. Sommer, 'Structure and swelling of polymer networks: insights from NMR', *Soft Matter,* vol. 9, pp. 6587-6593, 2013.

[52]   H. M. James and E. Guth, 'Theory of the Increase in Rigidity of Rubber during Cure', *The Journal of Chemical Physics,* vol. 15, pp. 669-683, 1947.

[53]   M. Braden, D. Latham, and M. P. Patel, 'Observations on the swelling of cross-linked poly(dimethylsiloxane) networks by solvents', *European Polymer Journal,* vol. 41, pp. 3069-3071, 2005.

[54]   A. F. Blanchard, 'Elasticity theory and crosslinking of reinforced rubber', *Journal of Applied Polymer Science,* vol. 67, pp. 119-129, 1998.

[55]   S. Schlögl, M.-L. Trutschel, W. Chassé, G. Riess, and K. Saalwächter, 'Entanglement Effects in Elastomers: Macroscopic vs Microscopic Properties', *Macromolecules,* vol. 47, pp. 2759-2773, 2014.

[56]   C. P. Buckley, 'Experimental methods for rubberlike solids', in *Mechanics and Thermomechanics of Rubberlike Solids*. vol. 32, Vienna: Springer, 2004.

[57]   V. M. Litvinov and P. A. M. Steeman, 'EPDM-Carbon Black Interactions and the Reinforcement Mechanisms, as Studied by Low-Resolution 1H NMR', *Macromolecules,* vol. 32, pp. 8476-8790, 1999.

[58]   G. Heinrich and T. A. Vilgis, 'Contribution of Entanglements to the Mechanical Properties of Carbon Black Filled Polymer Networks ', *Macromolecules,* vol. 26, pp. 1109-1119, 1993.

[59]   Y. Zhang, S. Ge, B. Tang, T. Koga, M. H. Rafailovich, J. C. Sokolov, D. G. Peiffer, Z. Li, A. J. Dias, K. O. McElrath, M. Y. Lin, S. K. Satija, S. G. Urquhart, H. Ade, and D. Nguyen, 'Effect of Carbon Black and Silica Fillers in Elastomer Blends', *Macromolecules,* vol. 34, pp. 7056-7065, 2001.

[60]   F. Clement, L. Bokobza, and L. Monnerie, 'On the mullins effect in silica filled polydimethylsiloxane networks', *American Chemical Society- Rubber Division,* vol. 74, pp. 847-870, 2001.

[61]   A. Kato, Y. Ikeda, R. Tsushi, Y. Kokubo, and N. Kojima, 'A new approach to visualizing the carbon black/natural rubber interaction layer in carbon black-filled natural rubber vulcanizates and to elucidating the dependence of mechanical properties on quantitative parameters', *Colloid and Polymer Science,* vol. 291, pp. 2101-2110, 2013.

[62]   L. B. Tunnicliffe, A. G. Thomas, J. J. C. Busfield, and A. S. Farid, 'The effect of fillers on crosslinking, swelling and mechanical properties of peroxide-cured rubbers', *Proceedings European Conference on Constitutive Models for rubber VII,* vol. 8, pp. 563-568, 2013.

[63]   L. B. Tunnicliffe, A. G. Thomas, and J. J. C. Busfield, 'Energy losses at small strains in filled rubbers', *Constitutive Models for Rubber VII,* p. 63, 2011.

[64]   S. Cantournet, R. Desmorat, and J. Besson, 'Mullins effect and cyclic stress softening of filled elastomers by internal sliding and friction thermodynamics model', *International Journal of Solids and Structures,* vol. 46, pp. 2255-2264, 2009.

[65]   Y. Merckel, J. Diani, M. Brieu, P. Gilormini, and J. Caillard, 'Effect of the microstructure parameters on the mullins softening in carbon-black filled styrene-butadiene rubbers', *Journal of Applied Polymer Science,* vol. 123, pp. 1153-1161, 2012.

[66]   Z. H. Li, 'Effects of carbon blacks with various structures on vulcanization and reinforcement of filled ethylene-propylene-diene rubber', *Express Polymer Letters,* vol. 2, pp. 695-704, 2008.

[67]   L. Mullins, 'Effect of stretching on the properties of rubber', *Journal of Rubber Research,* vol. 16, p. 22, 1947.

[68]   L. Mullins and N. Tobin, 'Stress softening in rubber vulcanizates. Part I. Use of a strain amplification factor to describe the elastic behavior of filler reinforced vulcanized rubber', *Journal of Applied Polymer Science,* vol. 9, pp. 2993-3009, 1965.

[69]   J. A. C. Harwood and A. R. Payne, 'Stress softening of natural rubber vulcanisates', *Journal of Applied Polymer Science,* vol. 10, pp. 315-325, 1966.

[70]   F. Bueche, 'Molecular basis for the Mullins effect', *Journal of Applied Polymer Science,* vol. 4, pp. 107-114, 1960.

[71]   L. Mullins, 'Permanent Set in Vulcanized Rubber', *Rubber Chemistry and Technology,* vol. 22, pp. 1036-1044, 1949.

[72]   A. Dorfmann and R. W. Ogden, 'A constitutive model for the Mullins effect with permanent set in particle-reinforced rubber', *International Journal of Solids and Structures,* vol. 41, pp. 1855-1878, 2004.

[73]   S. R. Rickaby and N. H. Scott, 'Transversely isotropic cyclic stress-softening model for the Mullins effect', *Proceedings of the Royal Society A: Mathematical, Physical and Engineering Science,* 2012.

[74]   C. P. Buckley, D. S. A. De Focatiis, and C. Prisacariu, 'Unravelling the mysteries of cyclic deformation in thermoplastic elastomers', *Constitutive Models for Rubber VII,* pp. 3-10, 2011.

[75]   A. Dorfmann and F. Q. Pancheri, 'A constitutive model for the Mullins effect with changes in material symmetry', *International Journal of Non-Linear Mechanics,* vol. 47, pp. 874-887, 2012.

[76]   R. Andrews, A. Tobolsky, and E. Hanson, 'The theory of permanent set at elevated temperatures in natural and synthetic rubber vulcanizates', *Journal of Applied Physics,* vol. 17, pp. 352-361, 1946.

[77]   A. Tobolsky and R. Andrews, 'Systems manifesting superposed elastic and viscous behavior', *The Journal of Chemical Physics,* vol. 13, pp. 3-27, 1945.

[78]   V. S. Papkov and Y. K. Godovskii, 'Energy investigation of the softening of siloxane rubbers', *Polymer Mechanics,* vol. 11, pp. 329-333, 1975.

[79]   H. Lorenz and M. Klüppel, 'Microstructure-based modelling of arbitrary deformation histories of filler-reinforced elastomers', *Journal of the Mechanics and Physics of Solids,* vol. 60, pp. 1842-1861, 2012.

[80]   D. S. A. De Focatiis, F. Abraham, and C. P. Buckley, 'Multi-axial viscoelastic deformation of carbon-black filled EPDM rubber', *Constitutive Models for Rubber VI,* pp. 187-192, 2010.

[81]   H. Pouriayevali, Y. B. Guo, and V. P. W. Shim, 'A constitutive description of elastomer behaviour at high strain rates - A strain-dependent relaxation time approach', *International Journal of Impact Engineering,* vol. 47, pp. 71-78, 2012.

[82]   M. S. H. Fatt and X. Ouyang, 'Integral-based constitutive equation for rubber at high strain rates', *International Journal of Solids and Structures,* vol. 44, pp. 6491-6506, 2007.

[83]   T. Dalrymple, J. Choi, and K. Miller, 'Elastomer rate-dependence: A testing and material, modeling methodology', in *172nd Technical Meeting of the Rubber Division of American Chemical Society, Cleveland*, 2007.

[84]   K. Yamaguchi, A. G. Thomas, and J. J. Busfield, 'Stress relaxation, creep and set recovery of elastomers', *International Journal of Non-Linear Mechanics,* vol. 68, pp. 66-70, 2015.

[85]   T. Tada, K. Urayama, T. Mabuchi, K. Muraoka, and T. Takigawa, 'Nonlinear stress relaxation of carbon black-filled rubber vulcanizates under various types of deformation', *Journal of Polymer Science Part B-Polymer Physics,* vol. 48, pp. 1380-1387, 2010.

[86]   S. Farzaneh, J. Fitoussi, A. Lucas, W. Bocquet, and A. Tcharkhtchi, 'Shape memory effect and properties memory effect of polyurethane', *Journal of Applied Polymer Science,* vol. 125, 2013.

[87]   J. G. R. Kingston, 'The effect of scragging strain on the dynamic mechanical properties of filled rubber', *Journal of Rubber Research,* vol. 11, pp. 1-12, 2008.

[88]   G. Machado, G. Chagnon, and D. Favier, 'Experimental observation of induced anisotropy of the Mullins effect in particle-reinforced silicone rubber', *Constitutive Models for Rubber VI,* pp. 511-515, 2010.

[89]   Y. Merckel, M. Brieu, J. Diani, and J. Caillard, 'A Mullins softening criterion for general loading conditions', *Journal of the Mechanics and Physics of Solids,* vol. 60, pp. 1257-1264, 2012.

[90]   G. Machado, G. Chagnon, and D. Favier, 'Induced anisotropy by the Mullins effect in filled silicone rubber', *Mechanics of Materials,* vol. 50, pp. 70-80, 2012.

[91]   W. A. Gurney and V. E. Gough, 'Moulding Anisotropy', *Rubber Chemistry and Technology,* vol. 20, pp. 863-878, 1947.

[92]   C. M. Blow, H. B. Demirli, and D. W. Southwart, 'Anisotropy in Molded Nitrile Rubber', *Rubber Chemistry and Technology,* vol. 48, pp. 236-245, 1975.

[93]   L. R. G. Treloar, 'Volume changes and mechanical anisotropy of strained rubbers', *Polymer,* vol. 10, pp. 279-289, 1969.

[94]   C. Nah, G.-B. Lee, C. Lim, J.-H. Ahn, and A. Gent, 'Swelling of Rubber under Nonuniform Stresses and Internal Migration of Swelling Liquid When the Stresses Are Removed', *Macromolecules,* vol. 44, pp. 1610-1614, 2011.

[95]   A. B. Chai, E. Verron, A. Andriyana, and M. R. Johan, 'Mullins effect in swollen rubber: Experimental investigation and constitutive modelling', *Polymer Testing,* vol. 32, pp. 748-759, 2013.

[96]   A. B. Chai, A. Andriyana, E. Verron, and M. R. Johan, 'Mechanical characteristics of swollen elastomers under cyclic loading', *Materials & Design,* vol. 44, pp. 566-572, 2013.

[97]   A. Andriyana, A. B. Chai, E. Verron, and M. R. Johan, 'Interaction between diffusion of palm biodiesel and large strain in rubber: Effect on stress-softening during cyclic loading', *Mechanics Research Communications,* vol. 43, pp. 80-86, 2012.

[98]   G. Berselli, G. Vassura, M. Pellicciari, and R. Vertechy, *Hyperelastic modeling of rubber-like photopolymers for additive manufacturing processes*: INTECH Open Access Publisher, 2011.

References

[99]   M. Rubinstein and S. Panyukov, 'Elasticity of Polymer networks', *Macromolecules,* vol. 35, p. 17, 2002.

[100]   R. Everaers, 'Constrained fluctuation theories of rubber elasticity: General results and an exactly solvable model', *The European Physical Journal B-Condensed Matter and Complex Systems,* vol. 4, pp. 341-350, 1998.

[101]   R. W. Ogden, 'Elasticity and inelasticity of rubber', in *Mechanics and Thermomechanics of Rubberlike Solids.,* United Kingdom: Springer, pp. 135-185, 2004.

[102]   R. W. Ogden, G. Saccomandi, and I. Sgura, 'Fitting hyperelastic models to experimental data', *Computational Mechanics,* vol. 34, pp. 484-502, 2004.

[103]   R. W. Ogden, 'Stress softening and residual strain in the azimuthal shear of pseudo-elastic circular cylindrical tube', *International Journal of Non-Linear Mechanics,* vol. 36, pp. 477-487, 2001.

[104]   H. Qi and M. C. Boyce, 'Constitutive model for stretch-induced softening of the stress-stretch behavior of elastomeric materials', *Journal of the Mechanics and Physics of Solids,* vol. 52, pp. 2187-2205, 2004.

[105]   M. C. Boyce and E. M. Arruda, 'Constitutive models of rubber elasticity: A review', *Rubber Chemistry and Technology,* vol. 73, pp. 504-523, 2000.

[106]   S. R. Rickaby and N. H. Scott, 'A cyclic stress softening model for the Mullins effect', *International Journal of Solids and Structures,* vol. 50, pp. 111-120, 2013.

[107]   S. R. Rickaby and N. H. Scott, 'A model for the Mullins effect during multicyclic equibiaxial loading', *Acta Mechanica,* vol. 224, pp. 1887-1900, 2013.

[108]   P. D'Ambrosio, D. De Tommasi, D. Ferri, and G. Puglisi, 'A phenomenological model for healing and hysteresis in rubber-like materials', *International Journal of Engineering Science,* vol. 46, pp. 293-305, 2008.

[109]   D. Besdo and J. Ihlemann, 'A phenomenological constitutive model for rubberlike materials and its numerical applications', *International Journal of Plasticity,* vol. 19, pp. 1019-1036, 2003.

[110] D. Besdo and J. Ihlemann, 'Properties of rubberlike materials under large deformations explained by self-organizing linkage patterns', *International Journal of Plasticity,* vol. 19, pp. 1001-1018, 2003.

[111] J. Diani, M. Brieu, J. M. Vacherand, and A. Rezgui, 'Directional model for isotropic and anisotropic hyperelastic rubber-like materials', *Mechanics of Materials,* vol. 36, pp. 313-321, 2004.

[112] J. Diani, M. Brieu, and J. M. Vacherand, 'A damage directional constitutive model for Mullins effect with permanent set and induced anisotropy', *European Journal of Mechanics A-Solids,* vol. 25, pp. 483-496, 2006.

[113] Y. Merckel, J. Diani, M. Brieu, and J. Caillard, 'Constitutive modeling of the anisotropic behavior of Mullins softened filled rubbers', *Mechanics of Materials,* vol. 57, pp. 30-41, 2013.

[114] R. Dargazany and M. Itskov, 'A network evolution model for the anisotropic Mullins effect in carbon black filled rubbers', *International Journal of Solids and Structures,* vol. 46, pp. 2967-2977, 2009.

[115] M. Itskov, E. Haberstroh, A. E. Ehret, and M. C. Vohringer, 'Experimental observation of the deformation induced anisotropy of the mullins effect in rubber', *KGK Kautschuk Gummi Kunststoffe,* vol. 59, p. 4, 2006.

[116] N. Suzuki, M. Ito, and F. Yatsuyanagi, 'Effects of rubber/filler interactions on deformation behavior of silica filled SBR systems', *Polymer,* vol. 46, pp. 193-201, 2005.

[117] M. Takayanagi, S. Minami, and S. Uemura, 'Application of equivalent model method to dynamic rheo-optical properties of crystalline polymer', *Journal of Polymer Science Part C-Polymer Symposium,* p. 113, 1964.

[118] S. Goktepe and C. Miehe, 'A micro-macro approach to rubber-like materials. Part III: The micro-sphere model of anisotropic Mullins-type damage', *Journal of the Mechanics and Physics of Solids,* vol. 53, pp. 2259-2283, 2005.

[119] S. Govindjee and J. Simo, 'A Micro-Mechanically Based Continuum Damage Model for Carbon Black-Filled Rubbers Incorporating Mullins Effect', *Journal of the Mechanics and Physics of Solids,* vol. 39, pp. 87-112, 1991.

[120] B. Meissner and L. Matejka, 'Description of the tensile stress-strain behavior of filler-reinforced rubber-like networks using a Langevin-theory-based approach. Part I', *Polymer,* vol. 41, pp. 7749-7760, 2000.

[121] N. Bhatnagar, R. Bhardwaj, P. Selvakumar, and M. Brieu, 'Development of a biaxial tensile test fixture for reinforced thermoplastic composites', *Polymer Testing,* vol. 26, pp. 154-161, 2007.

[122] G. Palmieri, M. Sasso, G. Chiappini, and D. Amodio, 'Mullins effect characterization of elastomers by multi-axial cyclic tests and optical experimental methods', *Mechanics of Materials,* vol. 41, pp. 1059-1067, 2009.

[123] M. Sasso, G. Palmieri, G. Chiappini, and D. Amodio, 'Characterization of hyperelastic rubber-like materials by biaxial and uniaxial stretching tests based on optical methods', *Polymer Testing,* vol. 27, pp. 995-1004, 2008.

[124] L. R. G. Treloar, 'Strains in an inflated rubber sheet, and the mechanism of bursting', *Rubber Chemistry and Technology,* vol. 17, pp. 957-967, 1944.

[125] J. Li, D. Mayau, and V. Lagarrigue, 'Constitutive model dealing with damage due to cavity growth and the Mullins effect in rubber-like materials under triaxial loading', *Journal of the Mechanics and Physics of Solids,* vol. 56, pp. 953-973, 2008.

[126] J. Li, D. Mayau, and F. Song, 'A constitutive model for cavitation and cavity growth in rubber-like materials under arbitrary tri-axial loading', *International Journal of Solids and Structures,* vol. 44, pp. 6080-6100, 2007.

[127] C. Galliot and R. Luchsinger, 'Uniaxial and biaxial mechanical properties of ETFE foils', *Polymer Testing,* vol. 30, pp. 356-365, 2011.

[128] J. Day and K. Miller. Axel Products, Inc, Equibiaxial stretching of elastomeric sheets, an analytical verification of experimental technique, 2000.

[129] D. S. A. De Focatiis and S. Kelly, A mechanism for large strain biaxial testing of materials,1,501,599.3., UK Patent, 2014.

[130] D. S. A. De Focatiis and S. Kelly, 'A novel mechanism for large strain biaxial tensile testing of polymeric materials using uniaxial test machines', in *16th International Conference on the Deformation, Yield and Fracture of Polymers*, 2015, pp. 257-260.

[131] R. Lombardi, K. Schneider, C. Kipscholl, S. Cotugno, P. Straffi, G. Mensitieri, and G. Heinrich, 'Experimental investigation and constitutive modeling of a filled rubber under dynamic multi-axial loading conditions', presented at the RubberCon 2014. Advanced Engineering and Materials Developments, Manchester, UK., 2014.

[132] B. Kim, S. B. Lee, J. Lee, S. Cho, H. Park, S. Yeom, and S. H. Park, 'A comparison among Neo-Hookean model, Mooney-Rivlin model, and Ogden model for chloroprene rubber', *International Journal of Precision Engineering and Manufacturing,* vol. 13, pp. 759-764, 2012.

[133] J. E. Mark, *Polymer Data Handbook*: Oxford University Press, 1999.

[134] A. Ciesielski, *An introduction to rubber technology*: iSmithers Rapra Publishing, 1999.

[135] B. S. Institution, 'BS 2751:2001. General purpose acrylonitrile-butadiene rubber compounds. Specification'. United Kingdom: BSI, p. 12, 2001.

[136] B. S. Institution, 'BS 2752:2003. Chloroprene rubber compounds. Specification'. United Kingdom: BSI, p. 10, 2003.

[137] D. S. A. De Focatiis, 'Tooling for near net-shape compression moulding of polymer specimens', *Polymer Testing,* vol. 31, pp. 550-556, 2012.

[138] B. S. Institution, 'BS 7619:2010 Rubber, vulcanised or thermplastic: Determination of indetation hardness.', in *Part 1: Durometer method (shore hardness).* United Kingdom: BSI, p. 22, 2010.

[139] B. S. Institution, 'BS 1154:2003. Natural rubber compounds. Specifications.'. United Kingdom: BSI, p. 12, 2003.

[140] T. Hatakeyama and F. Quinn, 'Fundamentals and applications to polymer science', *Thermal Analysis,* 1994.

[141] B. S. Institution, 'BS ISO 11357-2:2013. Plastics: Differential scanning calorimetry (DSC)', in *Part 2: Determination of glass transition temperature and glass transition step height*. United Kingdom: British Standard Institution, p. 16, 2010.

[142] M. Ginic-Markovic, N. Roy Choudhury, M. Dimopoulos, D. R. G. Williams, and J. Matisons, 'Characterization of elastomer compounds by thermal analysis', *Thermochimica Acta,* vol. 316, pp. 87-95, 1998.

[143] M. J. Loadman, *Analysis of rubber and rubber-like polymers*, 4th The Netherlands: Kluer Academic Publishers, 1998.

[144] J. J. Maurer, 'Application of Differential Thermal Analysis and Thermogravimetric Analysis to Elastomer Systems', *Rubber Chemistry and Technology,* vol. 42, pp. 110-158, 1969.

[145] A. K. Sircar and T. G. Lamond, 'Total Thermal Analysis of NBR Vulcanizates', *Rubber Chemistry and Technology,* vol. 51, pp. 647-654, 1978.

[146] A. K. Sircar, 'Analysis of elastomer vulcanizate composition by TG-DTG techniques', *American Chemical Society- Rubber Division,* 1991.

[147] R. W. Smith, 'Microscopy of rubber products', *Rubber Chemistry and Technology,* vol. 75, pp. 511-526, 2002.

[148] M. Flamm, J. Spreckels, T. Steinweger, and U. Weltin, 'Effects of very high loads on fatigue life of NR elastomer materials', *International Journal of Fatigue,* vol. 33, pp. 1189-1198, 2011.

[149] L. C. Sawyer, D. T. Grubb, and G. F. Meyers, 'Polymer microscopy: characterization and evaluation of materials': Springer, Berlin, 2008.

[150] B. S. Institution, 'BS ISO 527-2:2012. Plastics: Determination of tensile properties', in *Part 2: Test conditions for moulding and extrusion plastics*. Geneva: BSI, p. 20, 2012.

[151]   B. S. Institution, 'BS ISO 23529:2010. Rubber: General procedures for preparing and conditioning test pieces for physical test methods'. United Kingdom: BSI, p. 26, 2010.

[152]   C. P. Buckley and D. M. Turner, *Application of flexible biaxial testing in the development of constitutive models for elastomers*. Leiden: A a Balkema Publishers, 1999.

[153]   A. M. Adams, C. P. Buckley, and D. P. Jones, 'Biaxial hot drawing of poly(ethylene terephthalate): measurements and modelling of strain-stiffening', *Polymer,* vol. 41, pp. 771-786, 2000.

[154]   C. Gerlach, C. P. Buckley, and D. P. Jones, 'Development of an Integrated Approach to Modelling of Polymer Film Orientation Processes', *Chemical Engineering Research and Design,* vol. 76, pp. 38-44, 1998.

[155]   C. P. Buckley, D. C. Jones, and D. P. Jones, 'Hot-drawing of poly(ethylene terephthalate) under biaxial stress: application of a three-dimensional glass—rubber constitutive model', *Polymer,* vol. 37, pp. 2403-2414, 1996.

[156]   J. Chiu, 'Polymer characterization by coupled thermogravimetry-gas chromatography', *Analytical Chemistry,* vol. 40, pp. 1516-1520, 1968.

[157]   J. J. Maurer, *Status of Thermal Analysis: Proceedings of a Symposium on the Current Status of Thermal Analysis Held at Gaithersburg, Maryland, April 21-22, 1970*: U. S. National Bureau of Standards, 1970.

[158]   M. Huang, L. B. Tunnicliffe, A. G. Thomas, and J. J. C. Busfield, 'The glass transition, segmental relaxations and viscoelastic behaviour of particulate-reinforced natural rubber', *European Polymer Journal,* vol. 67, pp. 232-241, 2015.

[159]   S. Amanuel, A. N. Gaudette, and S. S. Sternstein, 'Enthalpic relaxation of silica–polyvinyl acetate nanocomposites', *Journal of Polymer Science Part B: Polymer Physics,* vol. 46, pp. 2733-2740, 2008.

[160] E. Denardin, D. Samios, P. Janissek, and G. De Souza, 'Thermal Degradation of Aged Chloroprene Rubber Studied by Thermogravimetric Analysis', *Rubber Chemistry and Technology,* vol. 74, pp. 622-629, 2001.

[161] Mettler-Toledo. Mettler-Toledo AG, TGA of chloroprene rubber, Switzerland, 2009.

[162] N. Okubo, Y. Nishiyama, F. Klein, and J. Rivas. Separated determination of carbon black in chloroprene Rrubber by simulation of heating rate conversion, Japan.

[163] N. V. Schwartz and D. W. Brazier, 'Observations on the thermogravimetric oxidation of carbon blacks in vulcanizates', *Thermochimica Acta,* vol. 26, pp. 349-359, 1978.

[164] W. E. Mahmoud, S. A. Mansour, M. Hafez, and M. A. Salam, 'On the degradation and stability of high abrasion furnace black (HAF)/acrylonitrile butadiene rubber (NBR) and high abrasion furnace black (HAF)/graphite/acrylonitrile butadiene rubber (NBR) under cyclic stress–strain', *Polymer Degradation and Stability,* vol. 92, pp. 2011-2015, 2007.

[165] H. Ismail and H. C. Leong, 'Curing characteristics and mechanical properties of natural rubber/chloroprene rubber and epoxidized natural rubber/chloroprene rubber blends', *Polymer Testing,* vol. 20, pp. 509-516, 2001.

[166] V. Pistor, F. G. Ornaghi, R. Fiorio, and A. J. Zattera, 'Thermal characterization of oil extracted from ethylene–propylene–diene terpolymer residues (EPDM-r)', *Thermochimica Acta,* vol. 510, pp. 93-96, 2010.

[167] A. El-Wakil and A. El-Megeed, 'Effect of calcium carbonate, Sillitin N85 and carbon black fillers on the mechanical and electrical properties of the EPDM', *Journal of Engineering & Applied Sciences,* vol. 6, 2011.

[168] G. Narsimhan, 'Thermal decomposition of calcium carbonate', *Chemical Engineering Science,* vol. 16, pp. 7-20, 1961.

[169]   H. Nabil, H. Ismail, and A. R. Azura, 'Thermal stability and aging characteristics of (natural rubber)/(waste ethylene-propylene-diene monomer terpolymer) blends', *Journal of Vinyl and Additive Technology,* vol. 20, pp. 99-107, 2014.

[170]   X. Hu, Y. Li, and X. Liu, 'Experimental Studies of Thermal Aging Effects on the Tensile and Tearing Fracture Behavior of Carbon Black Filled Rubbers', in *ICF13*, 2013.

[171]   H. Khajehsaeid, J. Arghavani, and R. Naghdabadi, 'A hyperelastic model for rubber like material', *European Journal of Mechanics a-Solids,* vol. 38, pp. 144-151, 2013.

[172]   H. R. Ahmadi, J. Kingston, and A. Muhr, 'Dynamic properties of filled rubber-Part I: simple model, experimental data and simulated results', *Rubber Chemistry and Technology,* vol. 81, p. 18, 2008.

[173]   P. Y. Le Gac, M. Broudin, G. Roux, J. Verdu, P. Davies, and B. Fayolle, 'Role of strain induced crystallization and oxidative crosslinking in fracture properties of rubbers', *Polymer,* vol. 55, pp. 2535-2542, 2014.

[174]   N. Candau, C. Gauthier, L. Chazeau, and J.-M. Chenal, 'New insights about strain-induced crystallization of natural rubber thanks to in situ X-rays measurements during uniaxial cyclic deformation at high velocity', *Constitutive Models for Rubber VII,* vol. 6893, p. 39, 2011.

[175]   K. Brüning, K. Schneider, and G. Heinrich, 'Deformation and orientation in filled rubbers on the nano- and microscale studied by X-ray scattering', *Journal of Polymer Science Part B: Polymer Physics,* vol. 50, pp. 1728-1732, 2012.

[176]   J. T. Baumann, 'Rubber Components. Guide for Design Engineers'.

[177]   C. P. Buckley, C. Prisacariu, and C. Martin, 'Elasticity and inelasticity of thermoplastic polyurethane elastomers: Sensitivity to chemical and physical structure', *Polymer,* vol. 51, pp. 3213-3224, 2010.

[178]   A. D. Drozdov and N. Dusunceli, 'Unusual mechanical response of carbon black-filled thermoplastic elastomers', *Mechanics of Materials,* vol. 69, pp. 116-131, 2014.

[179]   D. De Tommasi, G. Puglisi, and G. Saccomandi, 'A micromechanics-based model for the Mullins effect', *Journal of Rheology,* vol. 50, pp. 495-512, 2006.

[180]   B. Meissner, 'Theory of bound rubber', *Rubber Chemistry and Technology,* vol. 48, pp. 810-818, 1975.

[181]   J. L. Leblanc, 'A molecular explanation for the origin of bound rubber in carbon black filled rubber compounds', *Journal of Applied Polymer Science,* vol. 66, pp. 2257-2268, 1997.

[182]   J. L. Leblanc, 'Elastomer–filler interactions and the rheology of filled rubber compounds', *Journal of Applied Polymer Science,* vol. 78, pp. 1541-1550, 2000.

[183]   J. Brandrup, E. H. Immergut, and E. A. Grulke, *Polymer Handbook*, 4th. United States of America: John Wiley and Sons, INC, 1990.

[184]   Metler Toledo, Excellence Analytical Balances. Operating Instructions. XS Models: Part 1, Switzerland, 2012.

[185]   S. Mueller, E. W. Llewellin, and H. M. Mader, 'The rheology of suspensions of solid particles', *Proceedings of the Royal Society of London A: Mathematical, Physical and Engineering Sciences,* 2009.

[186]   W. Pabst, 'Fundamental considerations on suspension rheology', *Ceramics Silikaty,* vol. 48, pp. 6-13, 2004.

[187]   H. Ahmadi and A. Muhr, 'Dynamic properties of filled rubber. Part II: physical basis of contributions to the model', *Rubber Chemistry and Technology,* vol. 84, pp. 24-40, 2011.

[188]   H. M. Smallwood, 'Limiting Law of the Reinforcement of Rubber', *Rubber Chemistry and Technology,* vol. 18, pp. 292-305, 1945.

[189] E. Guth, 'Theory of Filler Reinforcement. II', *Rubber Chemistry and Technology,* vol. 23, pp. 635-643, 1950.

[190] H. S. Chen and A. Acrivos, 'The effective elastic moduli of composite materials containing spherical inclusions at non-dilute concentrations', *International Journal of Solids and Structures,* vol. 14, pp. 349-364, 1978.

[191] L. R. G. Treloar, 'Cross-Linking and Modulus', in *The Physics of Rubber Elasticity*: OUP Oxford, 2005.

[192] J. Queslel and J. Mark, 'Molecular interpretation of the moduli of elastomeric polymer networks of known structure', in *Analysis/Networks/Peptides*: Springer, pp. 135-176, 1984.

[193] B. Omnès, S. Thuillier, P. Pilvin, Y. Grohens, and S. Gillet, 'Effective properties of carbon black filled natural rubber: Experiments and modeling', *Composites Part A: Applied Science and Manufacturing,* vol. 39, pp. 1141-1149, 2008.

[194] J. Boylan, 'Carbon. Graphite Materials', *Materials World,* vol. 4, 1996.

[195] A. Limited. (2015, September). *Carbon-Graphite Materials*.

[196] M. O. Marlowe. Nucleonics Laboratory. General Electric Company, Elastic properties of three grades of fine grained graphite to 2000°C, California, USA, 1970.

[197] L. J. Fetters, D. J. Lohse, and R. H. Colby, 'Chain Dimensions and Entanglement Spacings', in *Physical Properties of Polymers Handbook*, J. Mark: Springer New York, pp. 447-454, 2007.

[198] L. H. Sperling, *Introduction to physical polymer science*: John Wiley & Sons, 2005.

[199] P. J. Flory, 'Spatial Configuration of Macromolecular Chains', *Science,* vol. 188, pp. 1268-1276, 1975.

[200] J. Vohlídal, 'Mean-Square End-to-End Distance and Characteristic Ratio of Polyvinylene (Polyacetylene) Chains of Various Configurations', *Macromolecular Chemistry and Physics,* vol. 207, pp. 224-230, 2006.

[201] S. F. Edwards and T. A. Vilgis, 'The effect of entanglements in rubber elasticity', *Polymer* vol. 27, 1986.

[202] S. F. Edwards and T. A. Vilgis, 'The tube model theory of rubber elasticity', *Rep. Prog. Phys,* vol. 51, pp. 243-297, 1988.

[203] J. D. Ferry, *Viscoelastic properties of polymers*: John Wiley & Sons, 1980.

[204] S. F. Edwards and K. K. Muller-Nedebock, 'Entanglements in polymers: II. Networks', *Journal of Physics A: Mathematical,* vol. 32, pp. 3301-3320, 1999.

[205] J. W. Alistair, 'Stress relaxation and compression set behaviour of thermoplastic elastomers in sealing applications', *Thermoplastic Elastomers,* vol. III, p. 14, 1991.

[206] P. Tuckner, 'Compression stress relaxation test comparisons and development', *SAE Technical Paper. SAE World Congress,* 2000.

[207] H. M. Osman, S. A. A. Ghani, T. M. Madkour, and A. R. Mohamed, 'Stress relaxation in carbon black loaded butyl rubber', *Journal of Applied Polymer Science,* vol. 77, pp. 1067-1076, 2000.

[208] S. Siouris, B. Shaw, and C. Wilson, 'Method for the evaluation of elastomeric seals by compression stress relaxation', *Polymer Testing,* vol. 32, pp. 1299-1305, 2013.

[209] A. N. Gent, 'Relaxation processes in vulcanized rubber. I. Relation among stress relaxation, creep, recovery, and hysteresis', *Journal of Applied Polymer Science,* vol. 6, pp. 433-441, 1962.

[210] V. A. Fernandes and D. S. A. De Focatiis, 'The role of deformation history on stress relaxation and stress memory of filled rubber', *Polymer Testing,* vol. 40, pp. 124-132, 2014.

[211] H. Lavebratt and B. Stenberg, 'Anisotropy in injection-molded ethylene-propylene-diene rubbers. Part I', *Polymer Engineering and Science,* vol. 34, pp. 905-912, 1994.

[212] P. C. Hiemenz and T. P. Lodge, *Polymer chemistry*: CRC press, 2007.

[213]   R. F. Blanks and J. Prausnitz, 'Thermodynamics of polymer solubility in polar and nonpolar systems', *Industrial & Engineering Chemistry Fundamentals,* vol. 3, pp. 1-8, 1964.

[214]   G. Wypych, *Handbook of solvents*: ChemTec Publishing, 2001.

[215]   J. A. Emerson, D. T. Toolan, J. R. Howse, E. M. Furst, and T. H. Epps III, 'Determination of solvent–polymer and polymer–polymer Flory–Huggins interaction parameters for poly (3-hexylthiophene) via solvent vapor swelling', *Macromolecules,* vol. 46, pp. 6533-6540, 2013.

[216]   S. D. Bruck, 'Extension of the Flory-Rehner Theory of Swelling to an Anisotropic Polymer System', *Journal of research of the National Bureau of Standards,* pp. 485-488, 1961.

[217]   M. A. Wheelans, 'Injection moulding on rubber', *Rubber Chemistry Technology,* vol. 57, pp. 1023-1043, 1978.

[218]   H. Lavebratt and B. Stenberg, 'Anisotropy in injection-moulded styrene-butadiene rubbers.Part 2: discs delaminated by water-jet cutting techniques', *Plastics, Rubber and Composites Processing and Applications,* vol. 20, pp. 15-24, 1993.

[219]   H. Lavebratt and B. Stenberg, 'Anisotropy in injection-moulded styrene-butadiene rubbers. part 1', *Plastics, Rubber and Composites Processing and Applications,* vol. 20, pp. 3-13, 1993.

[220]   H. Lavebratt, B. Stenberg, and P. E. Werner, 'Orientation effects in injection-moulded rubber materials studied by X-ray scattering', *Polymer,* vol. 34, pp. 1109-1113, 1993.

[221]   H. Lavebratt and B. Stenberg, 'Anisotropy in injection-molded ethylene-propylene-diene rubbers. Part II: Disks delaminated by a water-jet cutting technique', *Polymer Engineering and Science,* vol. 34, pp. 913-920, 1994.

[222]   K. Azaar, I. D. Rosca, and J. M. Vergnaud, 'Anisotropic swelling of thin EPDM rubber discs by absorption of toluene', *Polymer,* vol. 43, pp. 4261-4267, 2002.

[223] J. Diani, M. Brieu, and P. Gilormini, 'Observation and modeling of the anisotropic visco-hyperelastic behavior of a rubberlike material', *International Journal of Solids and Structures,* vol. 43, pp. 3044-3056, 2006.

[224] M. H. Shariff, 'Direction dependent orthotropic model for Mullins materials', *International Journal of Solids and Structures,* vol. 51, pp. 4357-4372, 2014.

Appendices

Appendix A.   Strain video tracking for biaxial tensile testing

A.1   Biaxial video strain measurement and correlation with grip displacement

All biaxial tests using the FBFT were performed controlling the displacement of the grips. For a more accurate measurement in the centre of the specimen, a video recording technique was implemented for mostly all biaxial tests, excluding the swelling tests.

The video strain measurement consisted in tracking four beads positioned in the centre of the specimen. The LabView interface allows measuring the difference in position between the beads, according to the movement of each axis. Figure 130– 123 shows the relation between the strain measured by the grips displacement and the strain from the video measurements. The deformation presented in the figure is the maximum deformation made for each elastomers studied under EB and CW deformation. No more than 15% difference between the strains is measured for any material. A monitoring of the relation between the displacement of the grips and the video recorded can be made during each test. The LabView interface was designed to measure in real time the difference between both measurements. A difference of more than 20% can indicate possible slipping at the grips or error during the tracking of the beads.

The results presented in Chapter 4 and Chapter 5 for equibiaxial and constant width tensile testing deformation are reported using the video strain. For the case of the Chapter 6, no beads were placed due to the subsequent swelling tests.
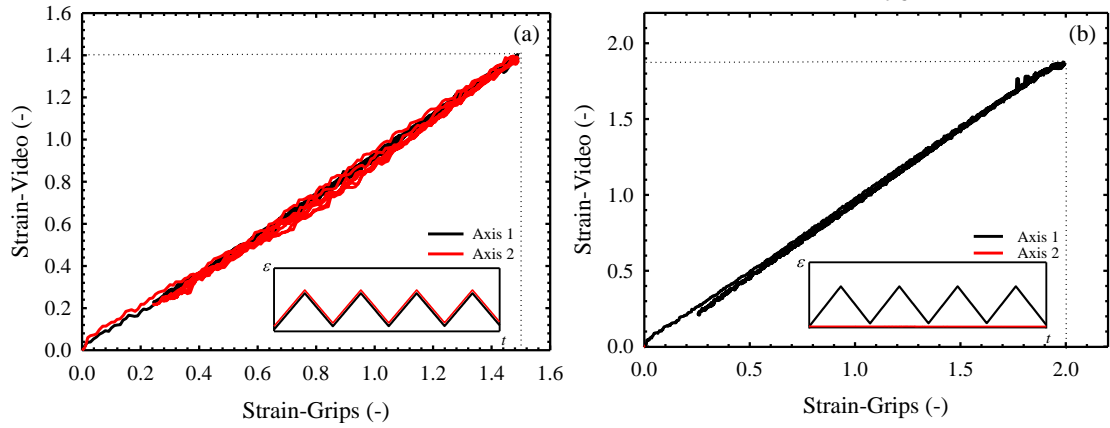
Figure 130. Relation between strain measured by grip displacement and strain form video tracking for EPDM1 under (a) EB and (b) CW cyclic deformation
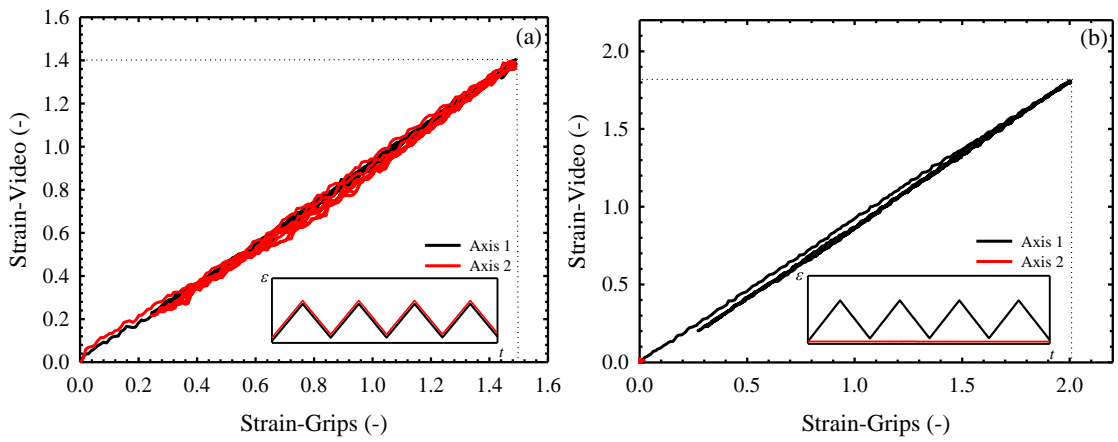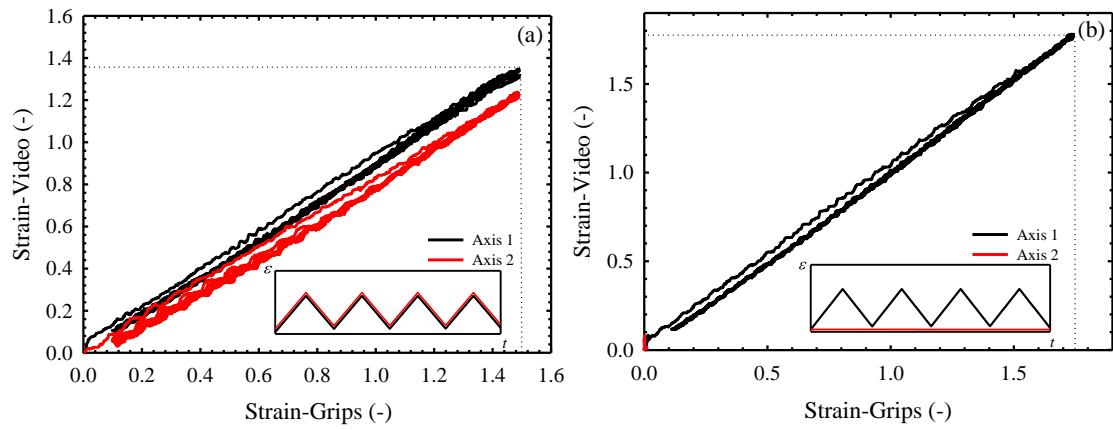

Figure 131. Relation between strain measured by grip displacement and strain form video tracking for EPDM2 under (a) EB and (b) CW cyclic deformation
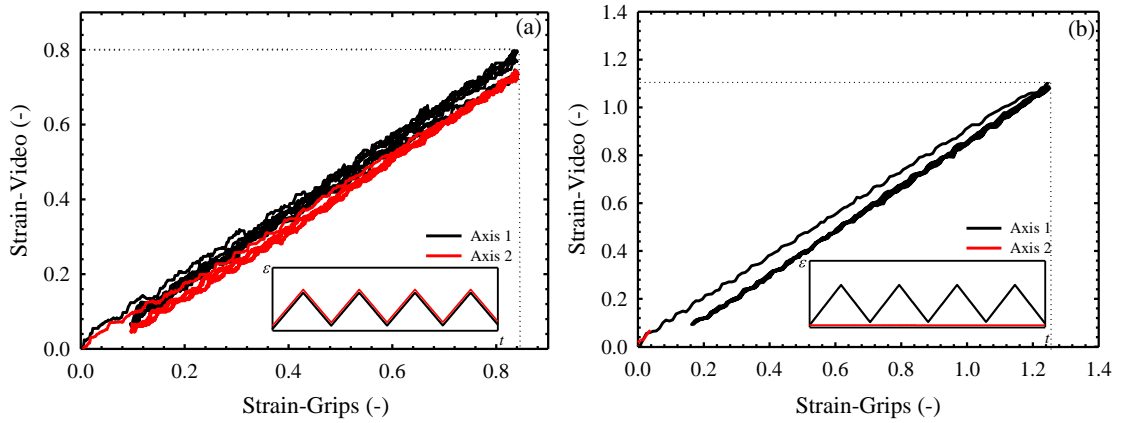
Figure 132. Relation between strain measured by grip displacement and strain form video tracking for NBR under (a) EB and (b) CW cyclic deformation
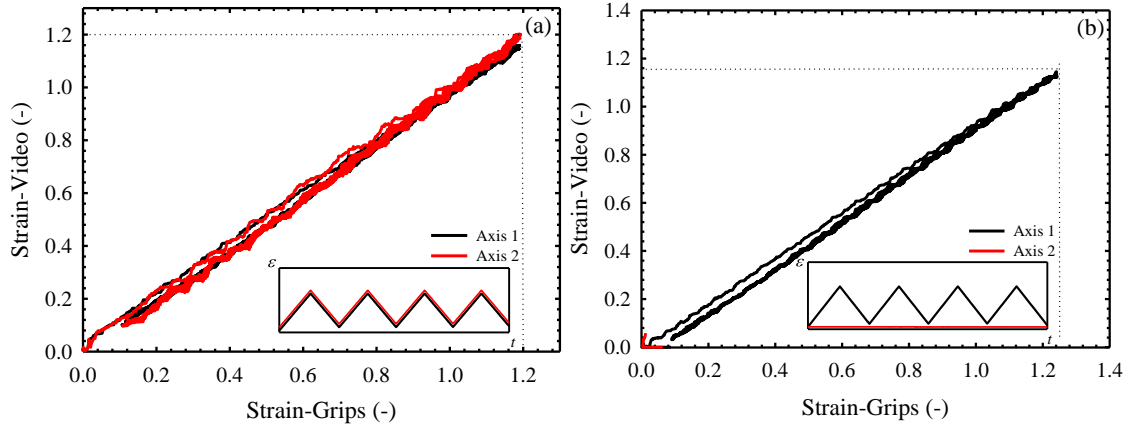
Figure 133. Relation between strain measured by grip displacement and strain form video tracking for CR under (a) EB and (b) CW cyclic deformation

Figure 134. Relation between strain measured by grip displacement and strain form video tracking for NR under (a) EB and (b) CW cyclic deformation

A.2 Digital Image Correlation for FBFT

To ensure a homogeneous deformation throughout the specimen, Digital Image Correlation (DIC) was used on a sample of EPDM2 with a speckle pattern created with white paint (Figure 131).
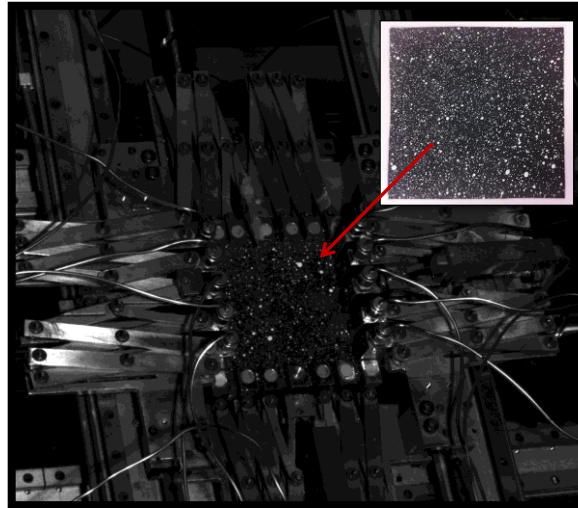
Figure 135. Video tracking Digital Image Correlation (DIC) set-up of a sample of EPDM2 with a speckle pattern.

Both equibiaxial and constant width of deformation was tested to measure the displacement on both axes. Due to the large deformation subjected, above strains of 1.0 the points presented a big amount of distortion, losing the possibility to measure the displacement. As presented for EPDM1 under equibiaxial deformation (Figure 132), the software starts to lose points at around 0.5 strain. However, the displacement on both axes indicates a homogeneous deformation up to this point.
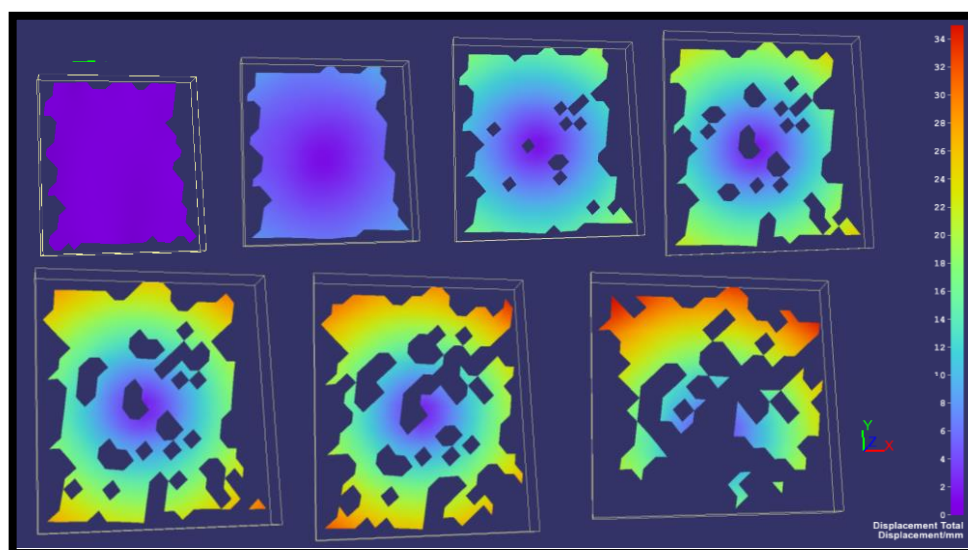
Figure 136. Displacement measurement using Digital Image Correlation (DIC) for a EPDM2 specimen subjected to equibiaxial deformation.

The strain measurement during constant width deformation allowed a more extensive

tracking of the specimen. Figure 133 presents the strain measurement using DIC technique for a EPDM2 specimen subjected to a strain up to 1.5 and constant width deformation on axis 2. As axis 2 does not show any significant displacement, only axis 1 is presented. In this case, the major distortion of the speckle pattern starts after a strain of 0.7. Values near 1.5 were able to be recorded. A homogeneous strain distribution is present under constant with deformation.
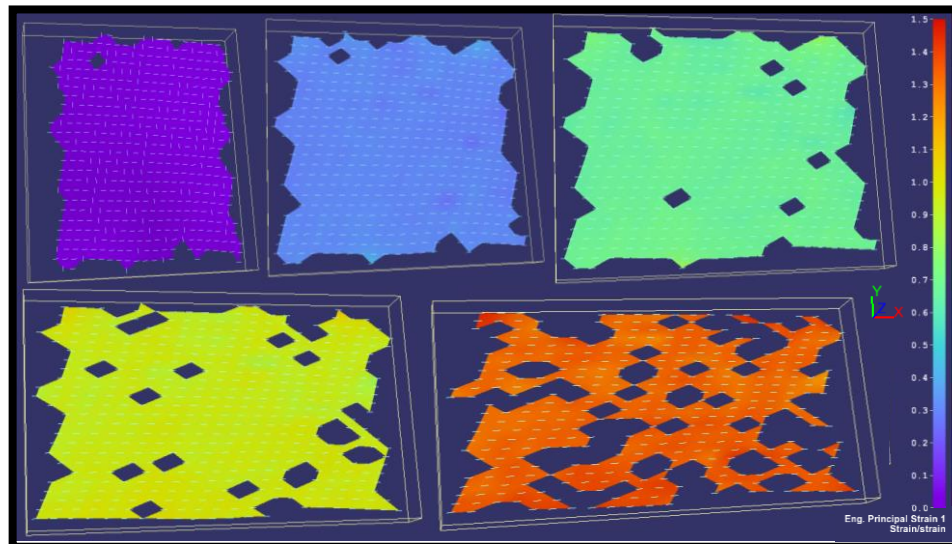
Figure 137. Strain measurement using Digital Image Correlation (DIC) for a EPDM2 specimen subjected to constant width deformation.

Appendix B. Constitutive response under different modes of deformation

B.1   Pseudo-cyclic constitutive response under different modes of deformation.

The cyclic stress-strain response during pseudo-cyclic deformation for EPDM2, NBR and CR under uniaxial, equibiaxial and constant width deformation are presented in Figure 138 to Figure 140 respectively.
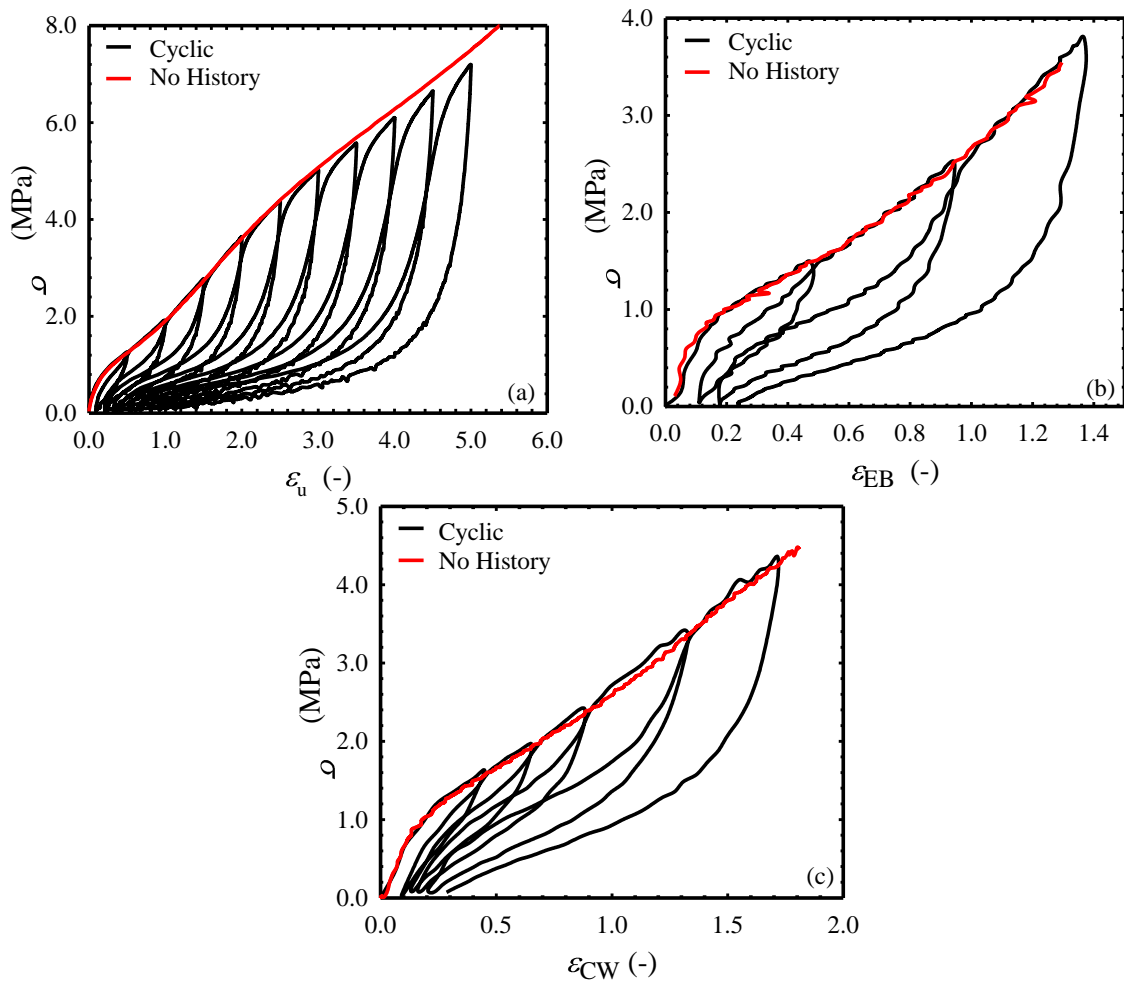
Figure 138. Pseudo-cyclic stress-strain response of EPDM2 increasing maximum strain on subsequent cycles.(a) UN, (b) EB (only showing axis 1//) and (c) CW restriction on axis 2 ⊥.
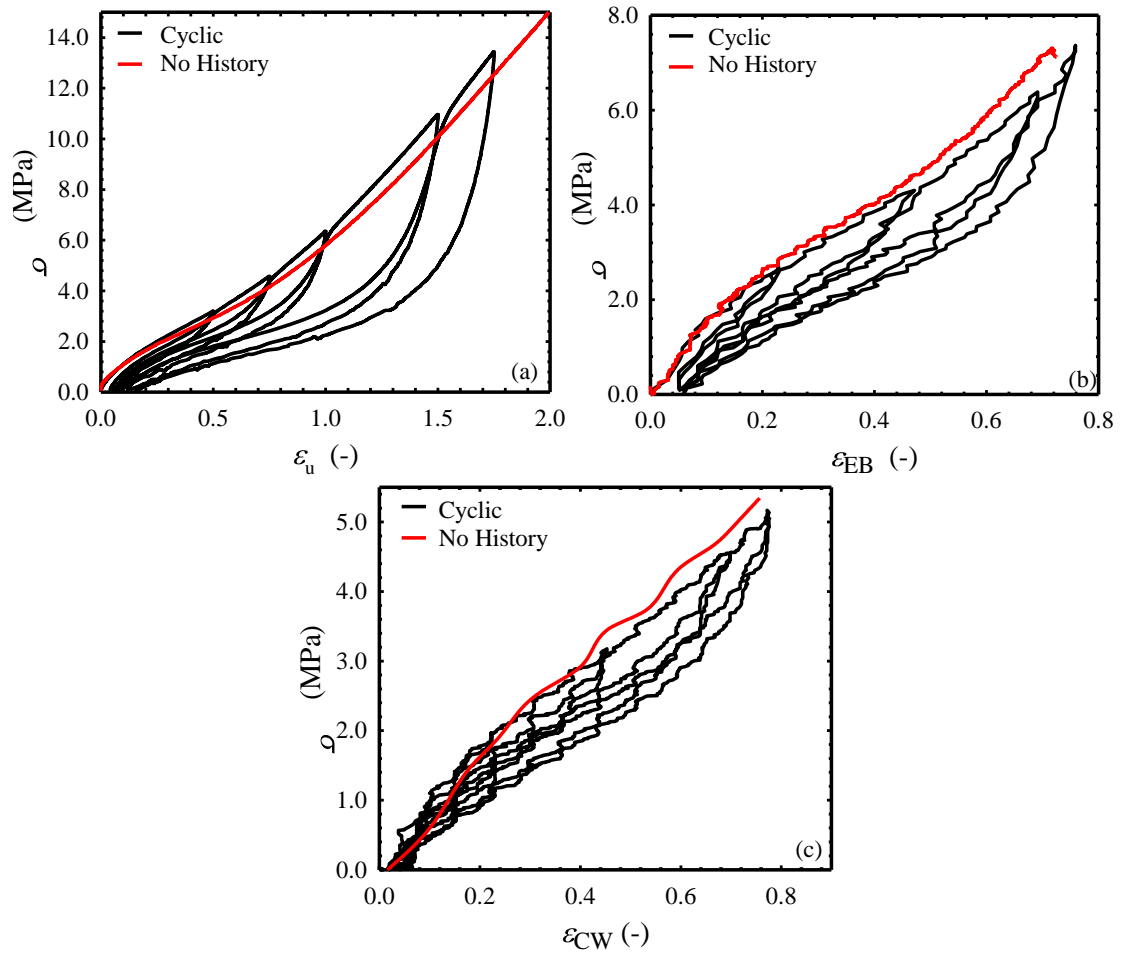
Figure 139. Pseudo-cyclic stress-strain response of NBR increasing maximum strain on subsequent cycles.(a) UN, (b) EB (only showing axis 1//) and (c) CW restriction on axis 2 ⊥.
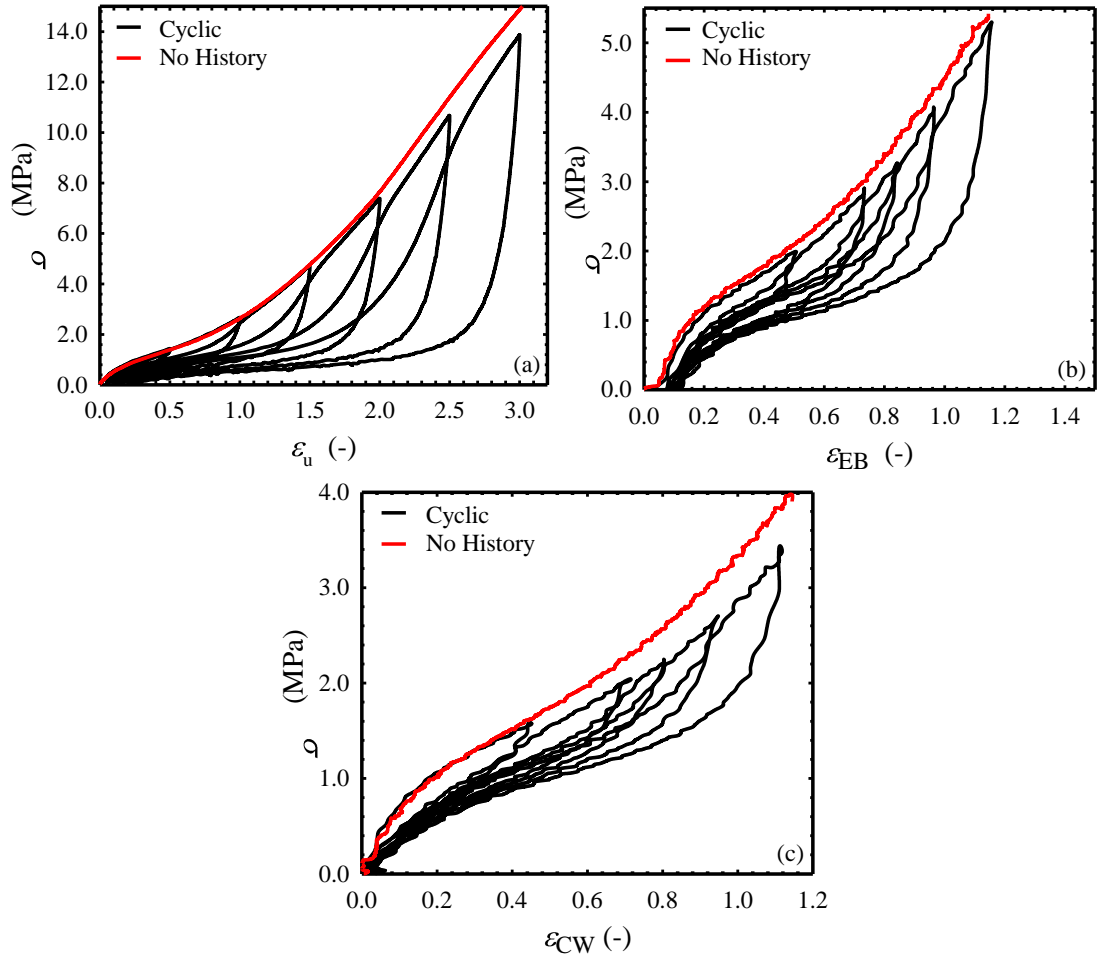
Figure 140. Pseudo-cyclic stress-strain response of CR increasing maximum strain on subsequent cycles.(a) UN, (b) EB (only showing axis 1//) and (c) CW restriction on axis 2 ⊥.

B.2 Uniaxial cyclic deformation response after pre-strain $\varepsilon_1 > \varepsilon_2$

The stress response as a function of strain in presented in Figure 141 to Figure 144 for EPDM2, NBR, CR and NR following cyclic deformations with the condition of $\varepsilon_1 > \varepsilon_2$.
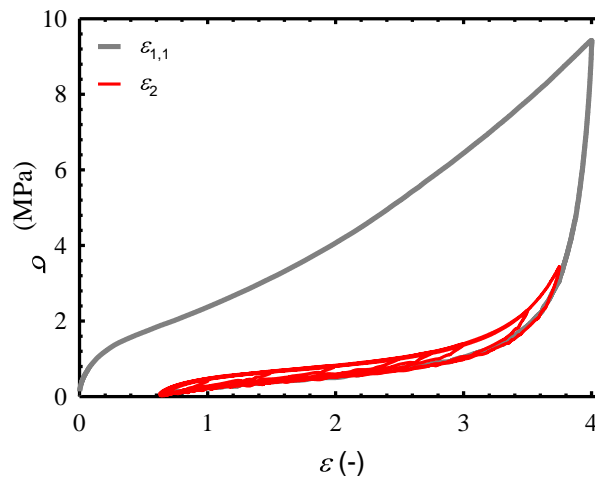
Figure 141. Uniaxial cyclic deformation response after pre-strain $\varepsilon_1 = 4.0$ and variation of $\varepsilon_2 < \varepsilon_1$ for EPDM2.
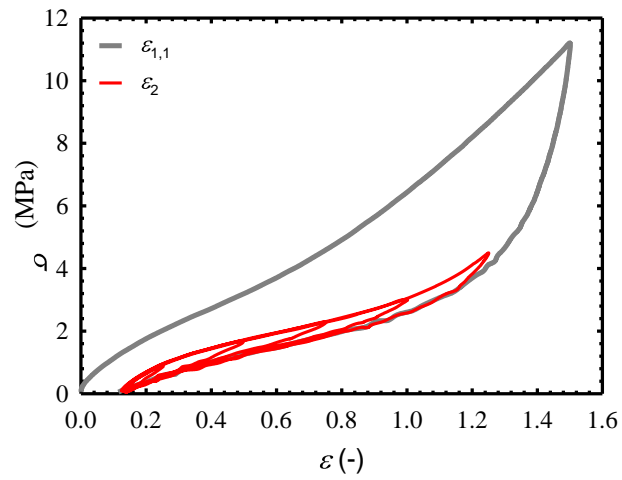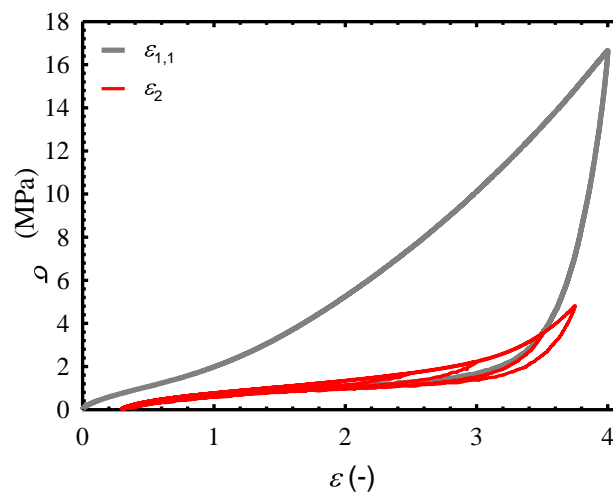
Figure 142. Uniaxial cyclic deformation response after pre-strain $\varepsilon_1=4.0$ and variation of $\varepsilon_2<\varepsilon_1$ for NBR.
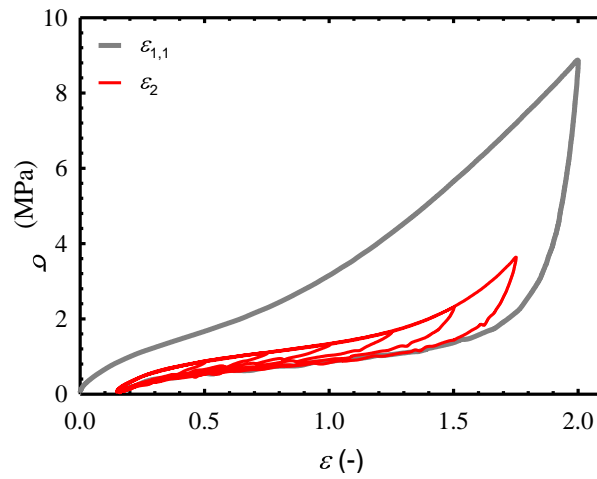
Figure 143. Uniaxial cyclic deformation response after pre-strain $\varepsilon_1=4.0$ and variation of $\varepsilon_2<\varepsilon_1$ for CR.

Figure 144. Uniaxial cyclic deformation response after pre-strain $\varepsilon_1=4.0$ and variation of $\varepsilon_2<\varepsilon_1$ for NR.

B.3   Energy dissipation under uniaxial strain

The work input (during the loading stage) as a function of the strain at different combinations of ε_1 and ε_2 is presented in Figure 145 for EPDM2, NBR, CR and NR respectively.
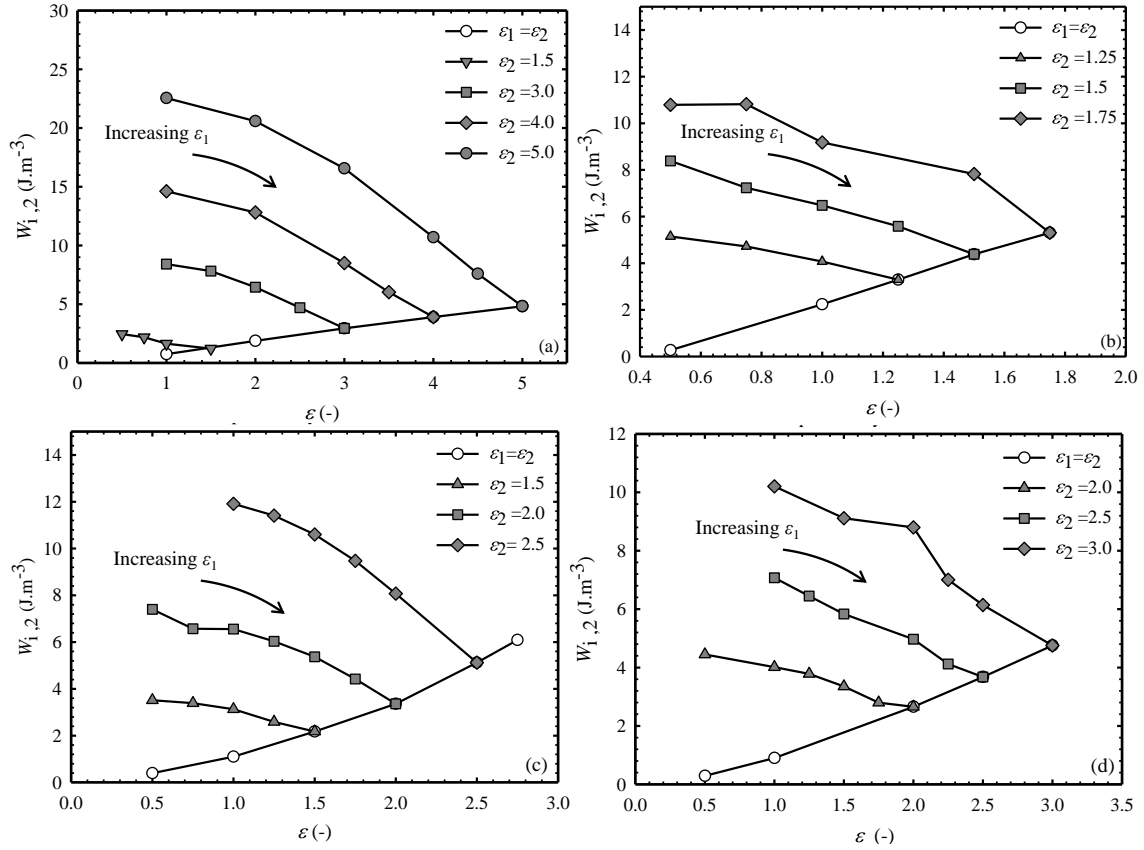

Figure 145. Work input at second stage loading $W_{i,2}$ under variation of ε_2 after ε_1 stage. (a) EPDM2, (b) NBR, (c) CR and (d) NR.

B.4   Energy dissipation under different modes of deformation

The fraction of energy dissipated ϕ_c as a function of the work input W_i, is presented in Figure 146. The energy required to deform during uniaxial, equibiaxial and constant width are reported for comparison for EPDM2, NBR, CR and NR.
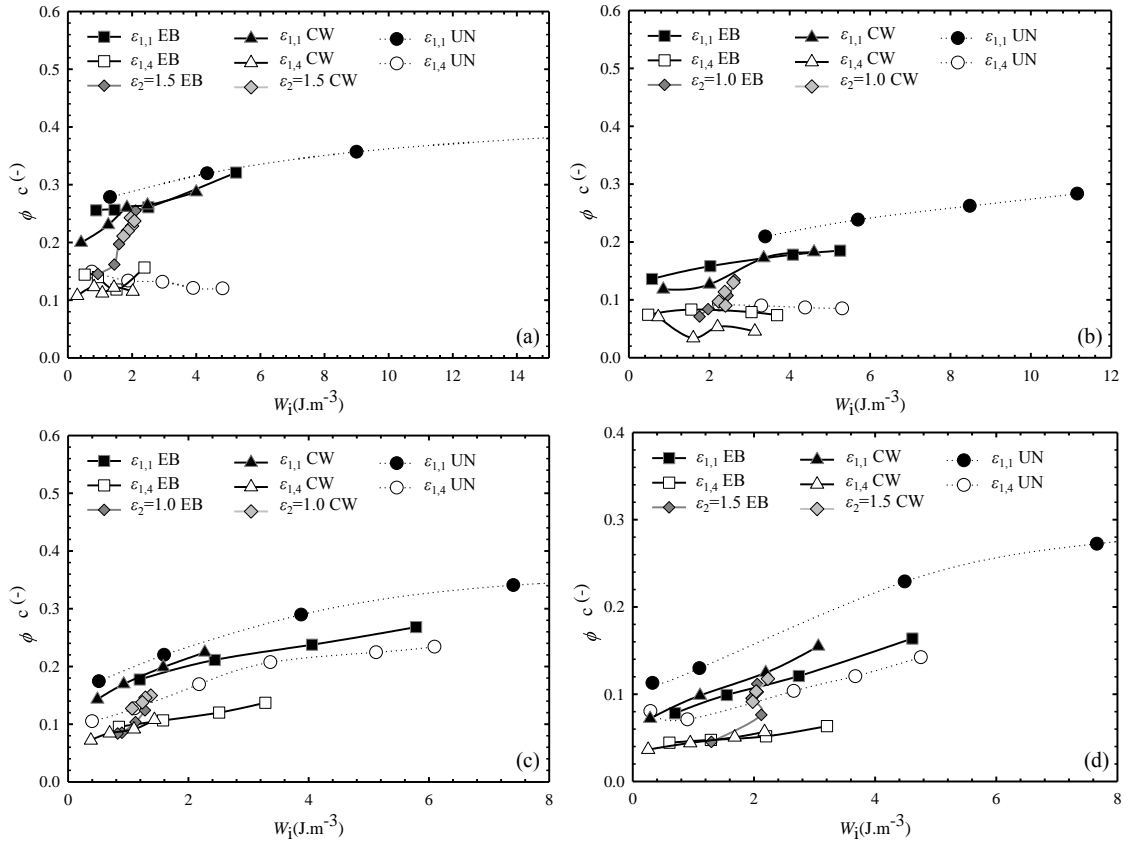
Figure 146. Comparison of the fraction of energy dissipated ϕ_c versus work input W_i under UN, EB and CW tensile testing, varying ε_1 and ε_2. (a) EPDM2, (b) NBR, (c) CR and (d) NR.

Appendix C.   Repeatability statistical analysis.

With the knowledge that each material should follow the same stress-strain response during the first loading stage, every set of tests for every material was compared during the first loading. The range between 0.1-0.5 strains was chosen for the repeatability criteria on each deformation tests. From the mean measurements, a test under the same loading condition is considered valid and repeatable when the deviation in stress is less than 10% for UN deformation and 15% for EB and CW testing (due to higher noise in the data). The mean is calculated from the whole set of data on each deformation conditions. Each material was analysed independently as well as every mode of deformation (UN, EB and CW).

An example is presented in Figure 147 for EPDM1 for 20 UN tensile tests used for work presented in Chapter 4. The first loading stress-strain response up to 0.5 strain is presented in order to illustrate the variation range. Data exceeding the 10% condition was discarded and repeated if needed.
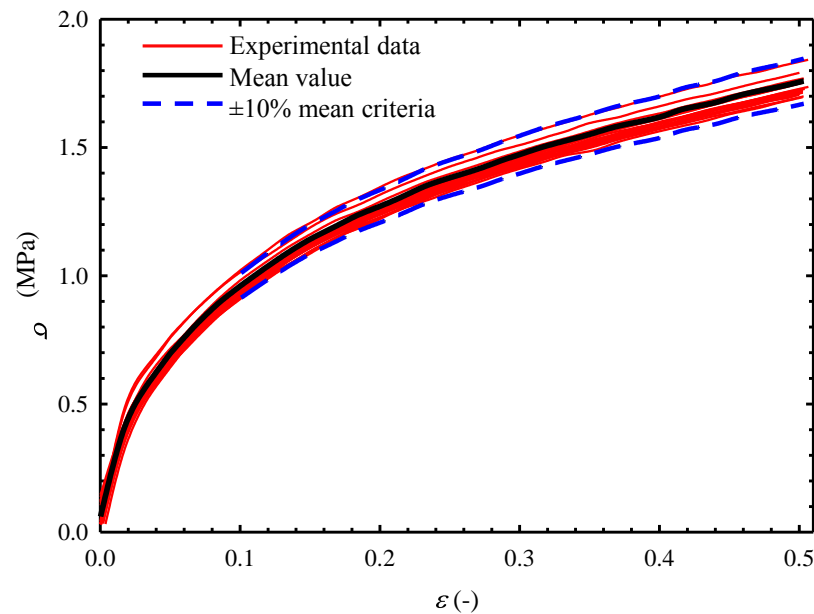

Figure 147. Stress-strain response under UN deformation up to 0.5 strain for analysis of repeatability EPDM1.

Appendix D.   Image processing in Matlab

The image processing to measure the specimens dimensions and swelling process was carried out in Matlab®. This technique was used for measurements of the width for uniaxial tensile testing experiments and the width and length dimensions of specimens subjected to swelling conditions were measured as illustrated in the following description. The same methodology was applied on both conditions. A calibrated HP Scanjet G4010 scanner system was used to record a 1200 DPI resolution image. This image is then processed using the Matlab image acquisition tool. The *measuretool* tool was used to calibrate the image length (mm)/pixel. A calibration of 47.24 Pixel/mm was used to measure the width. In order to avoid error during calibration, every image processed was scanned with a ruler to calibrate every image independently. Each distance was measured with a drawing of the edge angle to ensure an orthogonal measure on each section.

D.1   Uniaxial tensile testing specimens

For uniaxial tensile testing specimens, an example of specimen measurement is shown in Figure 148. Three width measurements were recorded in the middle of the specimens to get the average.
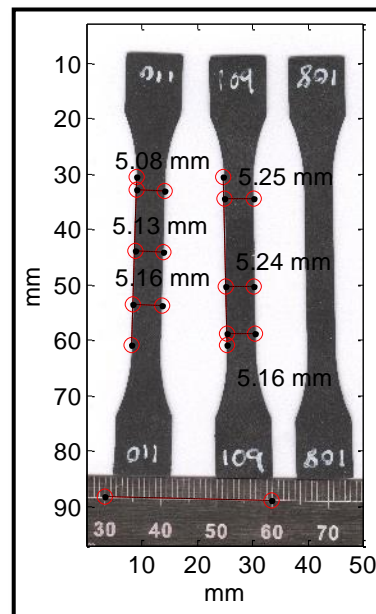

Figure 148. Width measurement example using Matlab image processing for uniaxial tensile testing specimen.

D.2 Swelling specimens

The measurement of the linear swelling ratios λ_l and λ_w were recorded using the *measuretool* tool for all tested specimens. Figure 149(a) shows an example of one set of biaxial specimens after swelling. As for equibiaxial swelling the initial dimensions of width and length were similar, a small cut on the top corners was made to identify the sample position. Three measurements on each dimension were recorded to calculate the average. Special consideration was taken for NBR specimens due to rapid evaporation of the solvent. During T_s stage, the specimen was scanned while placed in a glass petri dish with the specific solvent, as shown in Figure 149(b).

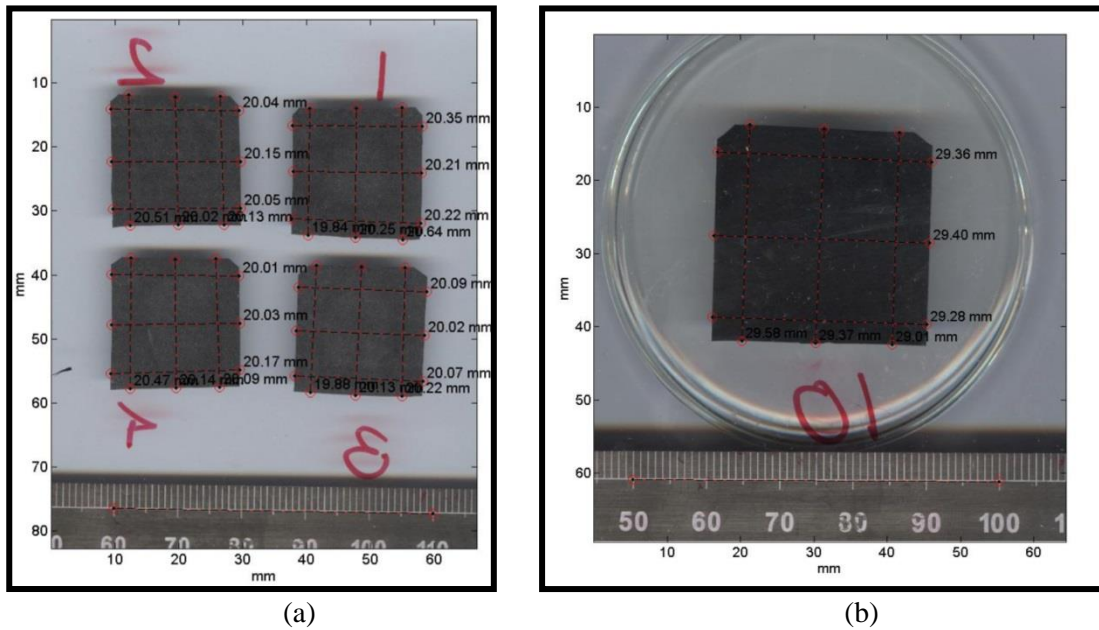(a)   (b)

Figure 149. Width and length measurement using Matlab image processing for specimens under swelling conditions. (a) Specimens placed directly to the scanner. (b) Specimen scanned submerged in the solvent.

Appendix E. Edwards-Vilgis Tube theory

The Edwards-Vilgis tube theory defines the strain energy function as a combination of energies related with the density of slip-links and cross-linking points. The single chain is described to be arranged as in a tube created by neighbouring chains. The constraints coming from the entanglements and cross-linking points will made the chain to respond to a deformation by moving in reptile way, surrounded by the limitation of the tube. The general strain energy function of the Edward-Vilgis [201, 202, 204] theory is presented as

$$W_{EV} = W_{EVc} + W_{EVs}$$
<div align="right">Eq. E- 1</div>

where the first term represents the energy function associated to the cross-link density of the system

$$W_{EVc} = \frac{1}{2} N_c k_B T \left(\frac{\left(1-\alpha^2\right)\lambda_1^2 + \left(1-\alpha^2\right)\lambda_2^2 + \left(1-\alpha^2\right)\lambda_3^2}{1-\alpha^2\left(\lambda_1^2 + \lambda_2^2 + \lambda_3^2\right)} + \ln\left(1-\alpha^2\left(\lambda_1^2 + \lambda_2^2 + \lambda_3^2\right)\right) \right)$$
<div align="right">Eq. E- 2</div>

where N_c is the cross-link density, k_B the Boltzmann constant, T the temperature λ_i as the stretches in the three dimensions and α as the chain extensibility. The second term is associated with the slip-link density as

$$W_{EVs} = \frac{1}{2} N_s k_B T \left\{ \frac{\lambda_1^2\left(1-\eta\right)\left(1-\alpha^2\right)}{\left(1+\eta\lambda_1^2\right)\left(1-\alpha^2\left(\lambda_1^2 + \lambda_2^2 + \lambda_3^2\right)\right)} + \ln\left(1+\eta\lambda_1^2\right) + \frac{\lambda_2^2\left(1-\eta\right)\left(1-\alpha^2\right)}{\left(1+\eta\lambda_2^2\right)\left(1-\alpha^2\left(\lambda_1^2 + \lambda_2^2 + \lambda_3^2\right)\right)} + \right.$$
$$\left. \dots\ln\left(1+\eta\lambda_2^2\right) + \frac{\lambda_3^2\left(1-\eta\right)\left(1-\alpha^2\right)}{\left(1+\eta\lambda_3^2\right)\left(1-\alpha^2\left(\lambda_1^2 + \lambda_2^2 + \lambda_3^2\right)\right)} + \ln\left(1+\eta\lambda_3^2\right) + \ln\left(1-\alpha^2\left(\lambda_1^2 + \lambda_2^2 + \lambda_3^2\right)\right) \right\}$$
<div align="right">Eq. E- 3</div>

with N_s as the slip-link density and η as the slip-link mobility factor. By assuming a main contribution of the cross-link points, the energy function can be reduced to $W_{EV} = W_{EVc}$. The cross-link density N_c can be replaced by the shear modulus [191] as

$$G = N_s k_B T$$
<div align="right">Eq. E- 4</div>

Under uniaxial deformation the stretches can be defines as a function of λ_1 as

$$\lambda_1, \lambda_2 = \frac{1}{\sqrt{\lambda_1}}, \lambda_3 = \frac{1}{\sqrt{\lambda_1}}$$
<div align="right">Eq. E- 5</div>

The stress can be derived from the $\sigma_1 = \frac{\partial W_{EVc}}{\partial \lambda_1}$, getting the stress under uniaxial deformation as

$$\sigma = \frac{1}{2}\left\{ \frac{G\alpha^2\lambda_1^2\left(-2\alpha^2\lambda_1 + \frac{2\alpha^2}{\lambda_1^2}\right)}{\left(-\alpha^2\lambda_1^2 + \frac{2\alpha^2}{\lambda_1^2} + 1\right)^2} - \frac{G\alpha^2\lambda_1}{\left(-\alpha^2\lambda_1^2 + \frac{2\alpha^2}{\lambda_1^2} + 1\right)} + \frac{G\alpha^2\left(-2\alpha^2\lambda_1 + \frac{2\alpha^2}{\lambda_1^2}\right)}{\left(-\alpha^2\lambda_1^2 + \frac{2\alpha^2}{\lambda_1^2} + 1\right)^2\lambda_1}\dots \right.$$

$$\frac{G\alpha^2}{\left(-\alpha^2\lambda_1^2 + \frac{2\alpha^2}{\lambda_1^2} + 1\right)^2\lambda^2} - \frac{1}{2}\frac{G\lambda_1^2\left(-2\alpha^2\lambda_1 + \frac{2\alpha^2}{\lambda_1^2}\right)}{\left(-\alpha^2\lambda_1^2 + \frac{2\alpha^2}{\lambda_1^2} + 1\right)^2} + \frac{G\lambda^2}{\left(-\alpha^2\lambda_1^2 + \frac{2\alpha^2}{\lambda_1^2} + 1\right)}\dots$$

$$\left. -\frac{G\left(-2\alpha^2\lambda_1 + \frac{2\alpha^2}{\lambda_1^2}\right)}{\left(-\alpha^2\lambda_1^2 + \frac{2\alpha^2}{\lambda_1^2} + 1\right)^2\lambda_1^2} - \frac{G}{\left(-\alpha^2\lambda_1^2 + \frac{2\alpha^2}{\lambda_1^2} + 1\right)^2\lambda_1^2}\frac{1}{2}\frac{G\alpha^2\left(2\lambda_1 + \frac{2}{\lambda_1^2}\right)}{\left(1 - \alpha^2\left(\lambda_1^2 + \frac{2}{\lambda_1^2}\right)\right)} \right\}$$

Eq. E- 6

Appendix F.   Stress relaxation response under TP2

The remaining test conditions varying ε_{max} are presented in Figure 150 to Figure 149, showing the normalised stress relaxation σ / σ_{end} as a function of time, followed TP2 for all the filled elastomers evaluated.
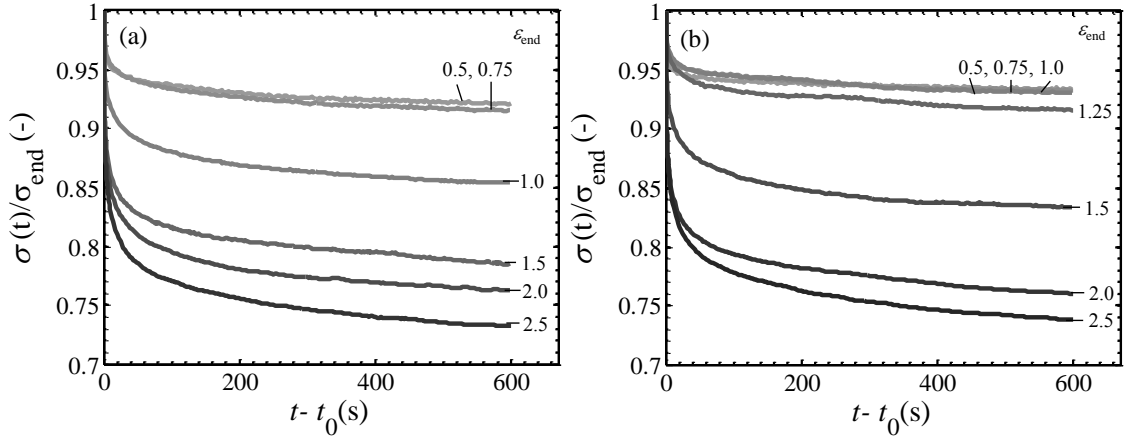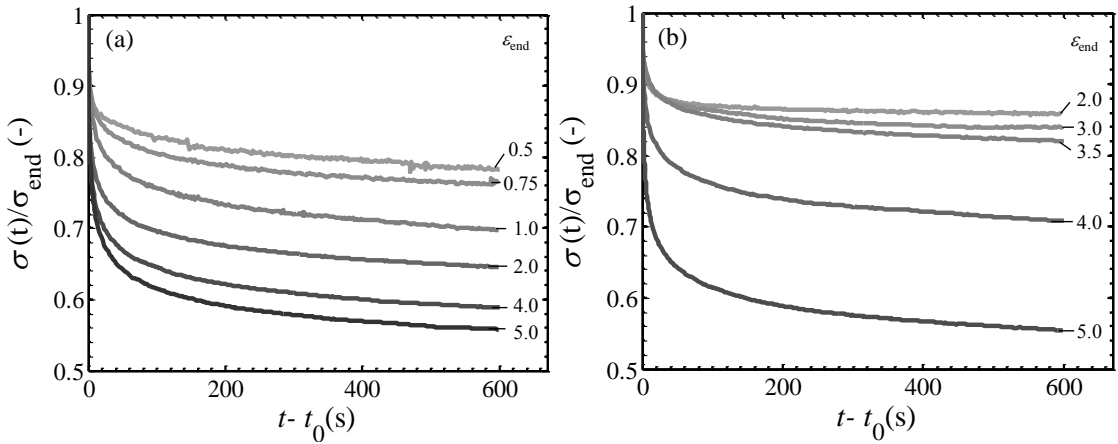

Figure 150 Normalised stress relaxation σ / σ_{end} of EPDM1a specimens subjected to a load-unload cycle through to (a) $\varepsilon_{max} = 1.0$ and (b) $\varepsilon_{max} = 1.5$ and reloaded to strain levels ε_{end} (indicated in the figure), according to TP2 under UN testing.

Figure 151 Normalised stress relaxation σ / σ_{end} of EPDM2 specimens subjected to a load-unload cycle through to (a) $\varepsilon_{max} = 1.0$ and (b) $\varepsilon_{max} = 4.0$ and reloaded to strain levels ε_{end} (indicated in the figure), according to TP2 under UN testing.
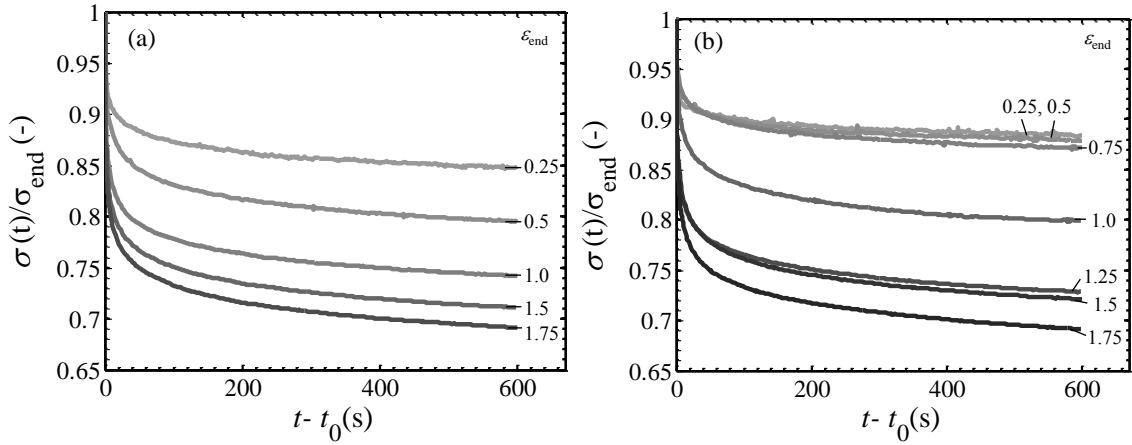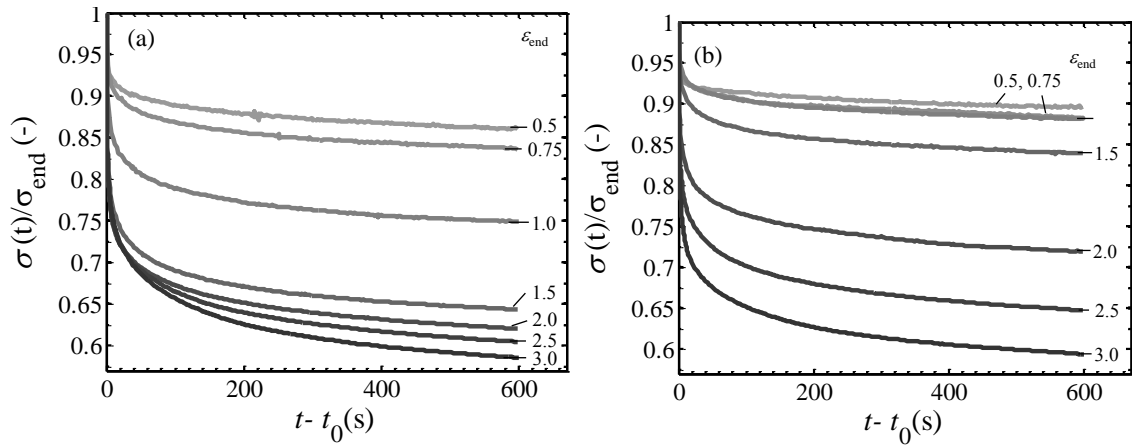
Figure 152 Normalised stress relaxation σ/σ_{end} of NBR specimens subjected to a load-unload cycle through to (a) ε_{max} =0.5 and (b) ε_{max} = 1.0 and reloaded to strain levels ε_{end} (indicated in the figure), according to TP2 under UN testing.
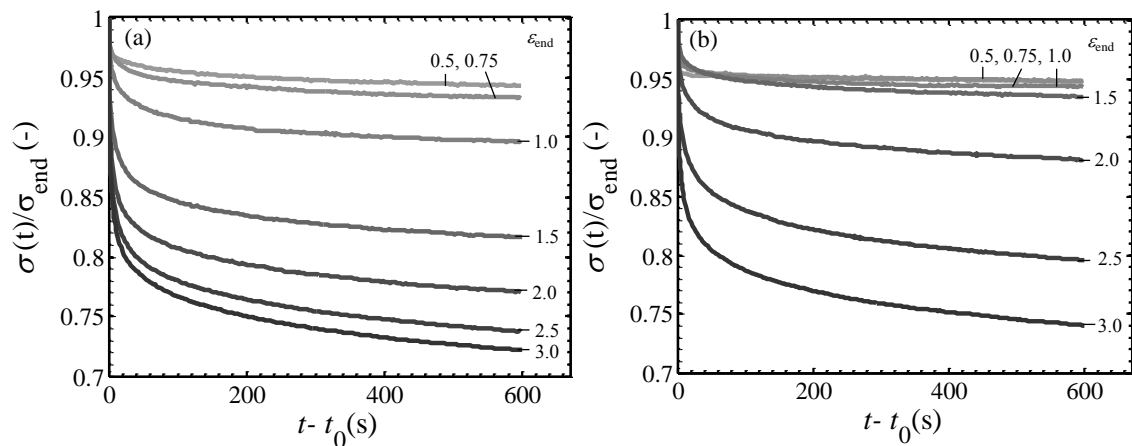

Figure 153 Normalised stress relaxation σ/σ_{end} of CR specimens subjected to a load-unload cycle through to (a) ε_{max} =1.0 and (b) ε_{max} = 2.5 and reloaded to strain levels ε_{end} (indicated in the figure), according to TP2 under UN testing.

Figure 154 Normalised stress relaxation σ/σ_{end} of NR specimens subjected to a load-unload cycle through to (a) ε_{max} =1.0 and (b) ε_{max} = 2.5 and reloaded to strain levels ε_{end} (indicated in the figure), according to TP2 under UN testing.

Appendix G.   Crosslink density calculation

The affine description of network elasticity can be used to define an apparent crosslink density υ_c, as [38, 44]

$$\upsilon_c = \frac{1}{2M_c}$$

Eq A7-1

The molecular weight is directly connected with the crosslink density of the material. As it is expected υ_c decreases with deformation (Figure 155). A similar tendency of reduction of υ_c is noticed for both uniaxial and equibiaxial deformations.
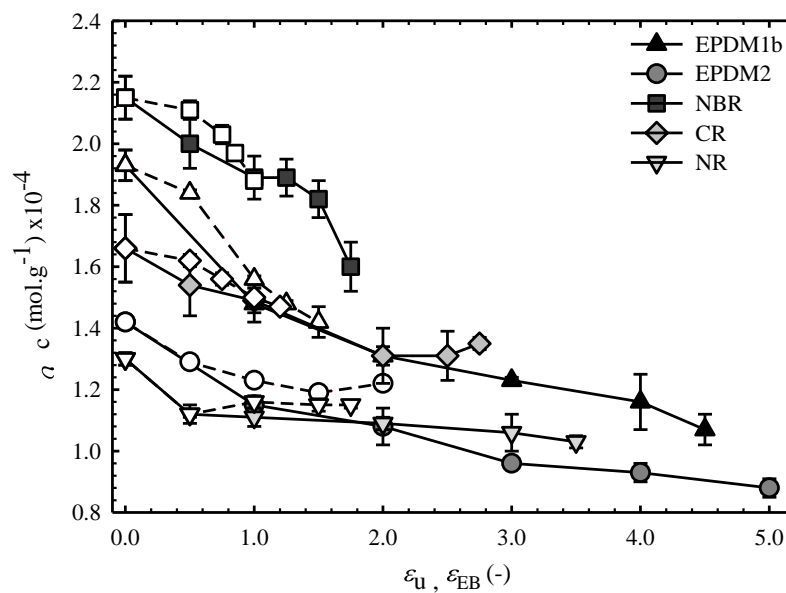

Figure 155.Apparent crosslink density υ_c calculated from swelling experiments for filled elastomers varying previous tensile strains under ε_u for UN (filled symbols) and ε_{EB} for EB (white symbols).